Retrospective Cost Adaptive Control of Uncertain Hammerstein Systems

by

Jin Yan

A dissertation submitted in partial fulfillment
of the requirements for the degree of
Doctor of Philosophy
(Aerospace Engineering)
in the University of Michigan
2013

Doctoral Committee:

Professor Dennis S. Bernstein, Chair
Professor Pierre Tshimanga Kabamba
Professor Ilya Vladimir Kolmanovsky
Professor Huei Peng

If we are facing in the right direction, all we have to do is keep on walking.

– Zen Proverb

嚴瑾

Yán Jǐn

To Mom and Dad,

whose tremendous sacrifices provided me with good opportunities,

and whose efforts and accomplishments are a continual inspiration.

In memory of Grandma, Fudi Wu (1933-2006),

for her unconditional love and support.

ACKNOWLEDGMENTS

I would like to express thanks to all those who helped make this research effort such an enjoyable and fulfilling learning experience. I extend my most sincere gratitude to my advisor, Professor Dennis Bernstein, whose endless patience, perpetual encouragement, and brilliant feedback were crucial to keeping me focused and on schedule. I was constantly inspired by his enthusiasm towards research and his ability to uncover the most important and useful aspects of many problems. Special thanks also go to Professor Ilya Kolmanovsky, whom I have had the privilege of learning from and working with during my graduate education. I was impressed by his knowledge and diligence, and his modest character has made a positive impact on my understanding of a scholar. Throughout my career, I will always strive to emulate the qualities of these two people.

I would also like to thank the other members on my dissertation committee. In particular, I would like to thank Professor Anouck Girard for agreeing to serve on my committee as a proxy. On the saturation work presented in Chapter III, I benefited from the advice, comments, and suggestions of Professor Huei Peng. I have long admired the excellent teaching technique and vast theoretical insight of Professor Pierre Kabamba, and I also had the pleasure of being a GSI for his course on Linear System Theory.

I owe my gratitude to all of my Professors throughout my entire academic career. I am especially indebted to Professor Dennis Bernstein for giving me my first opportunity to conduct research as a junior undergraduate student, and opening the doors

for me to this wonderful world. I would also like to specially thank Professor Alec Gallimore for his tutelage and support as my undergraduate advisor. Thank you to Professor Jing Sun, Professor Johan Schouken and Professor Rik Pintelon at Vrije Universiteit Brussel, Professor Ilya Kolmanovsky, Professor Pierre Kabamba, Professor Domitilla Del Vecchio, Professor Kim Winick, Professor Jessy Grizzle, Professor Jim Freudenberg, and Professor Kenn Oldham for your superlative instruction which exposed me to control systems as a graduate student.

I owe much appreciation to all my fellow colleagues in Bernstein Research Group for stimulating discussions and great friendship. Particularly, I would like to thank Dogan Sumer, Jesse Hoagg, Anthony D'Amato, Mario Santillo, Mohammad Aljanaideh, Asad Ali, Khaled Aljanaideh, Bojana Drincic, Jiapeng Zhong, Adam Brzezinski, Harish Palanthandalam-Madapusi, and Alexey Morozov as well as Sara Spangelo, Justin Jackson, Ali Nasir, Uros Kalabic, and Rohit Gupta from FDC student group.

A special thanks to all my good friends here, especially Xiaoning Jin, Dianyun Zhang, Wu Xiao, Shuyu Wang, Li Jiang, Shiming Duan, Haoyun Fu, Jie Zhu, Wei Chen, Hao Yu, Congzhen Qiao, Zhoujie Lyu, Caoxie Zhang, Xinfan Lin, Zhekang Du, Hai Wang, Yi Chen, Zheng Wu, Jiaer Zhang, Jian Zhang, Jie Wang, Xun Liu, Chang Liu, Xianke Lin, Shinuo Weng, Min Zhu, Yunjiao Cai, Shifang Li, Jingjing Li, and Weitao Duan whose companionship made my stay in Ann Arbor truly colorful. They will always be close and dear to me.

Finally, none of this would have been possible without the love and support of my family, whom I cannot possibly thank enough. They have always been my true source of inspiration and perspective. Thank you my beloved parents, my Grandparents, as well as my cousins Yawen and Yufei.

The author would like to acknowledge that this work was funded from the National Science Foundation, the United States Air Force, Department of Defense, and the Zonta International Organization Amelia Earhart Fellowship.

TABLE OF CONTENTS

LIST OF FIGURES

Figure

ABSTRACT

Retrospective Cost Adaptive Control of Uncertain Hammerstein Systems

by

Jin Yan

Chair: Dennis Bernstein

This dissertation extends retrospective cost adaptive control (RCAC) by broadening its applicability to nonlinear systems. Specifically, we consider command following and disturbance rejection for uncertain Hammerstein systems.

All real-world control systems must operate subject to constraints on the allowable control inputs. We use convex optimization to perform the retrospective input optimization, provided the saturation levels are known. The use of convex optimization bounds the magnitude of the retrospectively optimized input and thereby influences the controller update to satisfy the control bounds. We demonstrate this technique on illustrative numerical examples involving single and multiple inputs. In particular, this technique is applied to a multi-rotor helicopter with constraints on the total thrust magnitude and inclination of the rotor plane.

We develop RCAC for uncertain Hammerstein systems with odd, even, or arbitrary nonlinearities by constructing auxiliary nonlinearities to account for the nonmonotonic input nonlinearities. The purpose of the auxiliary nonlinearities is to ensure that RCAC is applied to a Hammerstein system with a globally nondecreasing composite input nonlinearity. We assume that the linear plant is either asymptoti-

cally stable or minimum-phase, and only one Markov parameter of the linear plant is known. The input nonlinearity is uncertain. The required modeling information for the input nonlinearity includes the intervals of monotonicity as well as values of the nonlinearity that determine overlapping segments of the range of the nonlinearity within each interval of monotonicity. In addition, we prove that the auxiliary nonlinearities preserve the range of the original nonlinear system and the composite input nonlinearity is globally nondecreasing.

Although RCAC is able to tune the linear controller to the command signal and nonlinear characteristics of the plant, the ability of the linear controller to produce accurate command following is limited by the distortion introduced by the nonlinearities. The linear controller structure of RCAC is replaced by a NARMAX (nonlinear ARMAX) controller structure, where the basis functions in the NARMAX controller are chosen by the user, and the controller coefficients appear linearly. To account for the case in which the input nonlinearity is uncertain, we investigate the performance of retrospective cost adaptive NARMAX control (RCNAC) in the case of uncertainty. In particular, we determine the minimal modeling information about the input nonlinearity that RCANC requires; once this information is known, an approximate input nonlinearity, called the ersatz nonlinearity, can be used by RCANC for adaptation.

CHAPTER I

Introduction

1.1 Motivation and Goals

Stabilization, command following, and disturbance rejection for a plant whose dynamics are uncertain and unknown can be challenging and difficult in many applications. For example, the airplane usually flies in the normal flight envelope, where aerodynamic models of the aircraft are available from wind-tunnel data. However, aircraft flight control under failure or damage conditions is demanding due to complex and unknown physics. Under these circumstances, the airplane flies outside the wind-tunnel data envelope, where the highly nonlinear aerodynamic models obtained by extrapolating the wind-tunnel test data are uncertain and inaccurate. Therefore, control applications for safety-critical flight systems require that the controller maintain the performance in the absence of either accurate aerodynamic models or predictable changes in the environment. Additional applications include automotive engine control with process parameter variations caused by production deviations, variations of external conditions, and aging; power systems with failure in the generator, transmission line, or distribution network; high-precision pointing systems with actuator and sensor nonlinearities; process control for food, oil, and wastewater; and biomedical applications to cardiovascular systems, where the cardiac outputs partially depend on the patient's unpredictable "states" (e.g., level of exercise, emotion, and posture). In

the area of endocrine systems composed of a continuous glucose sensor and an insulin infusion pump, the insulin is used to cancel the glucose rise from eating or to recover from an elevated hyperglycemic state. The design of a controller that can regulate or alter the insulin dosing in response to the time-varying glucose levels can be difficult and challenging. Therefore, from safety considerations, those applications call for a technique that is able to adapt to unknown and unpredictable changes.

Numerous design methods are commonly used in feedback control problems, ranging from classical control to modern control. For example, as shown in Figure 1.1, the controller inputs u are processed to produce plant outputs y. The controller design goal is to choose the input $u(t)$ such that the output $y(t)$ satisfies certain performance requirements.

Figure 1.1: Schematic of the system.

Model-based control techniques rely on the accuracy of the mathematical model of the plant. An exact plant model with same initial conditions and inputs u produces the same outputs y as the plant. However, in many applications, the physics of the systems may not be well understood. Under these circumstances, an exact mathematical model of the plant is not only costly but may be impossible to obtain as well. Furthermore, for some models of biological systems that are highly nonlinear, time-varying, and infinite dimensional, even if the exact plant model is available, this plant model cannot be used directly for control design. The difficulty in obtaining reliable models motivates the need to consider the case where the nonlinear systems are *uncertain*, and to develop a control technique for nonlinear systems that can adapt to imperfect models and unknown changes.

Linearization and model order reduction techniques [1] are used to obtain simpli-

fied models. For continuous time systems, the linearization can be either based on Taylor expansion of the nonlinear function around operating points or achieved by model fitting methods applied to experimental data. On the other hand, model order reduction techniques replace the original large scale system with a much smaller one, yet neglect the nonlinear effects that are outside the frequency range of interests.

An adaptive controller uses simplified models to tune itself to the actual plant characteristics in order to overcome uncertainty in the model or unexpected changes in the environment. Therefore, this simplified model containing *limited* model information is crucial for adaptive control. Hence, the motivation for this dissertation is to find the minimal but essential prior modeling information of the plant required by a control law in order to achieve a specified level of performance. Thus, the goals of this dissertation are to find answers to the following two questions:

- *What must be modeled and what is the minimal prior modeling information required by an adaptive control law to achieve desired performance for an uncertain nonlinear system?*

- *The ability of the linear controller to produce accurate command following is limited by the distortion introduced by the nonlinearities in the model. Can we develop a technique to reduce this distortion?*

1.2 Technical Approach and Impact

The design of autopilots for high-performance aircraft has motivated an intense research activity in adaptive control in the 1950s. Model reference adaptive control (MRAC) was proposed in [2, 3], where the sensitivity method and the MIT rule were used to design the adaptive laws. In this case, the objective is to force an unknown plant to follow the output of a known reference model. An adaptive pole placement control law was proposed by Kalman in [4]. In addition, adaptive control has attracted

growing interest since the 1960s. State space techniques and stability theory based on Lyapunov method were introduced in [5, 6, 7, 8, 9, 10, 11, 12, 13, 14]. Adaptive control with rich literature for the design, analysis, stability, and applications is presented in [15, 16, 17, 18, 19, 20, 21]. Widely invoked assumptions in adaptive control are passivity [22] and that plant is minimum-phase or stably invertible [11, 23]; these assumptions are restrictive for practical applications and approaches to relax them have been aproposed in the prior literature. With these challenges in mind, this work focuses on retrospective cost adaptive control (RCAC), which is a direct digital control approach that is applicable to linear plants that are possibly MIMO, nonminimum phase (NMP), and unstable as shown in [24, 23, 25, 26, 27, 28, 29, 30]. RCAC relies on knowledge of Markov parameters and, for NMP open-loop-unstable plants, estimates of the NMP zeros. This information can be obtained from either analytical modeling or system identification, see [31].

RCAC was developed for linear systems; the extension of RCAC in this dissertation broadens its applicability to nonlinear systems. If the nonlinear system is uncertain, then adaptive control may be useful for learning the characteristics of the nonlinearity online. Adaptive inversion control with uncertain input nonlinearities and linear dynamics is considered in [32, 33, 34]. However, many practical nonlinearities, such as saturation, deadzone, preload, and relay, are not one-to-one and onto, and thus are not *invertible*. Therefore, in this dissertation, we make no attempt to identify or invert the nonlinear plant.

All real-world control systems must operate subject to constraints on the allowable control inputs. The work presented in this dissertation uses convex optimization to perform the retrospective input optimization [35], provided the saturation levels are known. The use of convex optimization bounds the magnitude of the retrospectively optimized input and thereby influences the controller update to satisfy the control bounds. We demonstrate this technique on illustrative numerical examples involving

single and multiple inputs.

A nonlinear plant may be uncertain except for its ranges and intervals of its argument on which it is increasing or decreasing. RCAC with auxiliary nonlinearities, which capture the essential features of the uncertain nonlinearities for use by the adaptive control algorithm, is then applied in place of the uncertain nonlinearity to construct a globally nondecreasing nonlinear system. Numerical results provide evidence for the effectiveness of this technique.

Although RCAC is able to tune the linear controller to the command signal and nonlinear characteristics of the plant, the ability of the linear controller to produce accurate command following is limited by the distortion introduced by the nonlinearities. The linear controller structure of RCAC is replaced by a NARMAX (nonlinear ARMAX) controller structure, where the basis functions in NARMAX controller are chosen by the user, and the controller coefficients appear linearly. To account for the case in which the input nonlinearity is uncertain, we investigate the performance of Retrospective Cost Adaptive NARMAX Control (RCANC) in the case of uncertainty. In particular, we determine the minimal modeling information about the input nonlinearity that RCANC requires; once this information is known, an approximate input nonlinearity, called the ersatz nonlinearity, can be used by RCANC for adaptation.

The research to address the effects of uncertain nonlinear systems based on limited modeling information of the plant extends the applicability and reliability of RCAC to many applications. Examples such as aerospace, automotive, power network, and biomedical system (mentioned above) can benefit from this technique.

1.3 Problem Definition

1.3.1 Plant Models

The objective of this dissertation is to extend the applicability of RCAC to nonlinear systems. Nonlinear dynamic systems can be approximated by nonlinear block-structured models. Specifically, plants with input nonlinearities (Hammerstein systems), plants with output nonlinearities (Wiener systems), and plants with both input and output nonlinearities (Hammerstein-Wiener systems), are considered. The nonlinear block-oriented models are shown in Figure 1.2, where $\mathcal{N}(\cdot)$ represents a deadzone, signum function, hysteresis, saturation, or other nonlinearities, and G represents a linear dynamic plant. Throughout the dissertation, we consider Hammerstein systems, in which the control input is transformed by a nonlinearity before being applied to a linear plant.

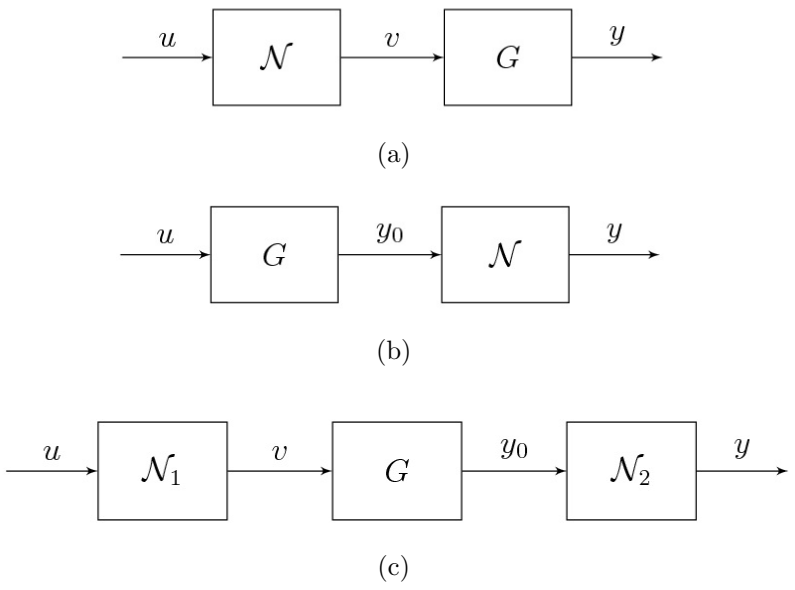

Figure 1.2: Block-structured nonlinear models. (a) Hammerstein systems, (b) Wiener Systems, and (c) Hammerstein-Wiener systems.

1.3.2 Input Nonlinearities

In this section, we present four types of input nonlinearities that are ubiquitous in mechanical, hydraulic, and magnetic systems, namely, deadzone, signum function, hysteresis, and saturation.

Deadzone and signum function are static and memoryless. Deadzone describes the system's insensitivity to small signals. In heating-cooling systems, deadzone nonlinearity prevents simultaneous heating and cooling, and a signum function represents on-off operation. In addition to memoryless nonlinearities, hysteresis and saturation may depend on states or control inputs and are, in fact, dynamic. Smart actuators, such as devices based on piezoelectric and magnetostrictive materials, use electrical energy to realize large strains and forces. These devices enable control technology for a wide range of new applications but are challenging, however, due to the fact that these materials are hysteretic. The play operator or the generalized Prandtl-Ishlinskii model are used to represent hysteresis in the system [36].

1.3.2.1 Deadzone

The deadzone function is given by

$$y(u) = \begin{cases} f_1(u), & \text{if} \quad u > b_r, \\ 0, & \text{if} \quad -b_l \leq u \leq b_r, \\ f_2(u), & \text{if} \quad u < -b_l. \end{cases} \tag{1.1}$$

where $b_l, b_r \in \mathbb{R}$, $f_1 : \mathbb{R} \to \mathbb{R}$, and $f_2 : \mathbb{R} \to \mathbb{R}$. Figure 1.3 shows the output of (1.1) for $b_r = 1$, $b_l = 2$, $f_1(u) = u - 1$, and $f_2(u) = u + 2$.

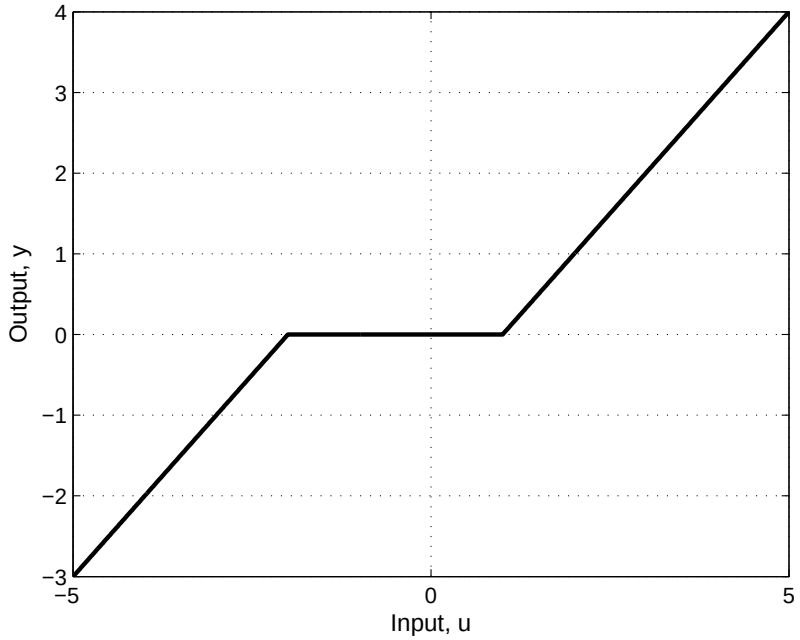

Figure 1.3: Output of (1.1) for $b_r = 1$, $b_l = 2$, $f_1(u) = u - 1$, and $f_2(u) = u + 2$.

1.3.2.2 Signum Function

The signum function is given by

$$y(u) = \frac{1}{2}[\text{sign}(u - u_r) + \text{sign}(u + u_l)], \tag{1.2}$$

where $u_l, u_r \in \mathbb{R}$. Note that y can assume only the values -1, 0, and 1, which represents on-off operation. Figure 1.4 shows the output of (1.2) for $u_r = 1$ and $u_l = 2$.

1.3.2.3 Play Operator

Let the input $u(k) \in \mathbb{R}$ be a piecewise monotone continuous function for $k \in [0, m]$, and let the initial state of the play operator be $x(u(0)) = x_0$. The output of the play

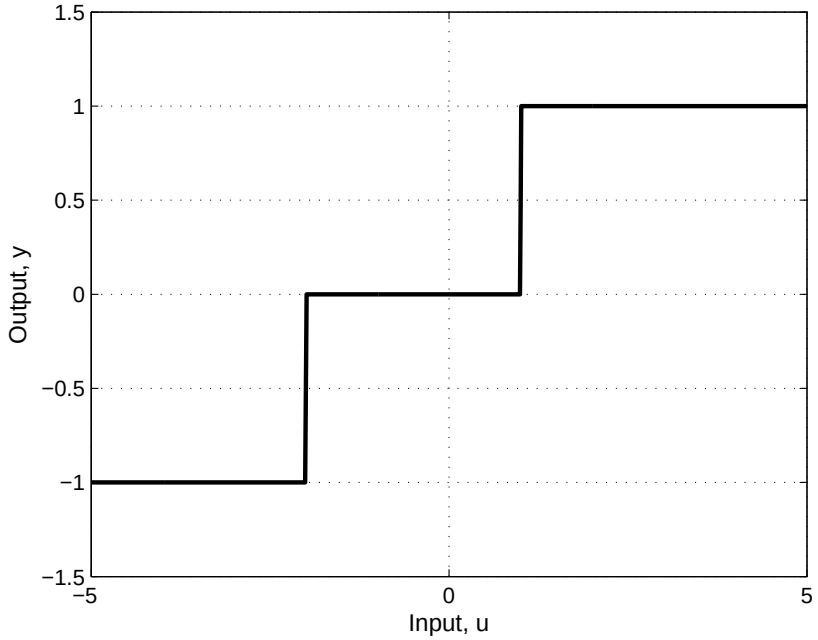

Figure 1.4: Output of (1.2) for $u_r = 1$ and $u_l = 2$.

operator for $k \in [1, m]$ is defined as

$$x\big(u(k)\big) = \max\Big(u(k) - r, \min\Big(u(k) + r, x\big(u(k-1)\big)\Big)\Big), \tag{1.3}$$

where the threshold r determines the width of the play operator. Figure 1.5 shows the output of the play operator (1.3) for $r = 2, 4, 6$.

1.3.2.4 Prandtl-Ishlinskii Model

The Prandtl-Ishlinskii (PI) model is a rate-independent hysteresis model with nonlocal memory. This model is based on superposition of N play operators with thresholds r_i, $i = 1, \ldots, N$. Let the input $u(k)$ be as above, and let the initial state of the i-th play operator be $x_i(u(0)) = x_{0i}$. The output of the i-th play operator at

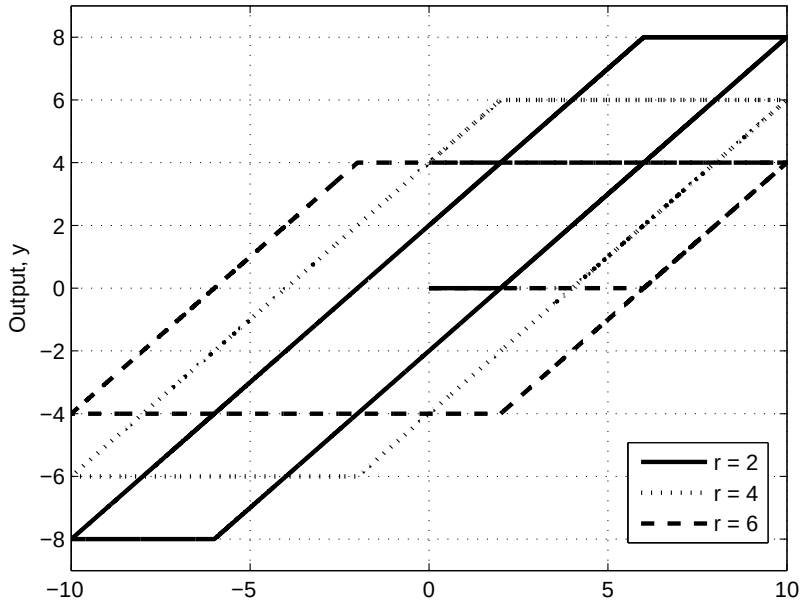

Figure 1.5: Output of the play operator (1.3) for $r = 2, 4, 6$.

step k, for $k \in [1, m]$ is defined as

$$x_i\big(u(k)\big) = \max\Big(\gamma(u(k)) - r_i, \min\Big(\gamma(u(k)) + r_i, x_i\big(u(k-1)\big)\Big)\Big), \tag{1.4}$$

where $\gamma : \mathbb{R} \to \mathbb{R}$ is a continuous increasing odd envelope function. Choosing the trivial envelope function $\gamma(v) = v$ gives the most commonly used form of the PI model. The output of the PI model at step k is defined as

$$y(k) = q\gamma(u(k)) + \sum_{i=1}^{N} p(r_i) x_i(u(k)), \tag{1.5}$$

where q is a positive constant and $p(f)$ is a positive density function [36]. An example of the PI model is shown in Figure 1.6 with parameters $N = 100$, $r_j = 0.01j$ for $j = 1, \ldots, N$, $p(r) = 0.5e^{-0.5r}$, $q = 0.5$, $\gamma(v) = 5\tanh(0.05v)$, and $u(k) = 9.4\sin(\omega t) + 6.9\cos(2.3\omega t)$, $\omega = 0.001$. The nonlocal memory of this model is represented by the minor loops, which correspond to input reversals.

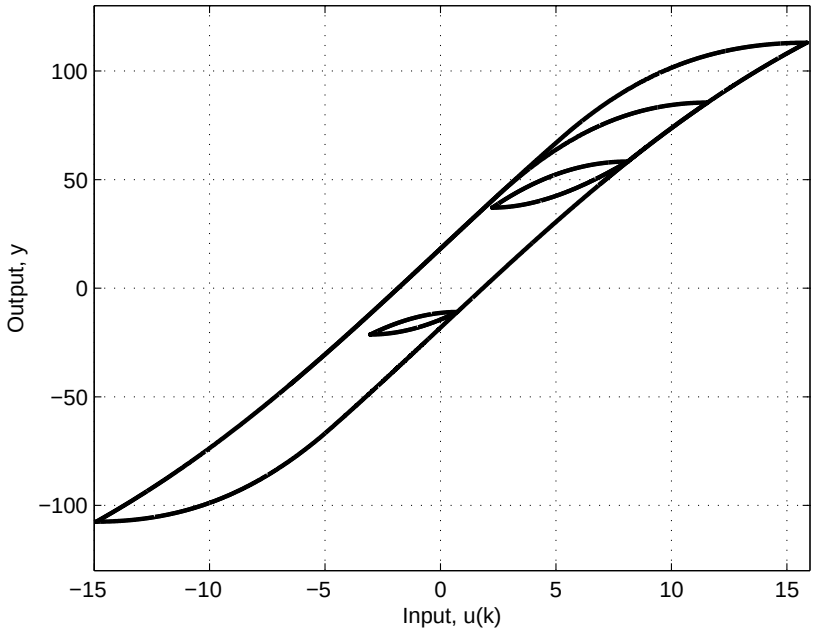

Figure 1.6: Output of the PI model (1.4), (1.5) with $N = 100$, $r_j = 0.01j$ for $j = 1, \ldots, N$, $p(r) = 0.5e^{-0.5r}$, $q = 0.5$, $\gamma(v) = 5\tanh(0.05v)$, and $u(k)9.4\sin(\omega t) + 6.9\cos(2.3\omega t)$, $\omega = 0.001$. The minor loops shown in the figure correspond to input reversals and represent nonlocal memory.

1.3.2.5 Saturation

The saturation input nonlinearity is a function $\mathrm{Sat} : \mathbb{R}^{l_u} \to \mathcal{U}$, where $\mathcal{U} \subseteq \mathbb{R}^{l_u}$ is the control constraint set. We assume that the function "Sat" is onto, that is, $\mathrm{Sat}(\mathbb{R}^{l_u}) = \mathcal{U}$. In particular, if $\mathcal{U}$ is rectangular, then

$$\mathrm{Sat}(u) = \begin{bmatrix} \mathrm{sat}_{a_1,b_1}(u_1) \\ \vdots \\ \mathrm{sat}_{a_{l_u},b_{l_u}}(u_{l_u}) \end{bmatrix}, \tag{1.6}$$

where $u = [u_1 \ \cdots \ u_{l_u}]^{\mathrm{T}} \in \mathcal{U} = [a_1, b_1] \times \cdots \times [a_{l_u}, b_{l_u}]$ and $\mathrm{sat} : \mathbb{R} \to [a, b]$ is defined as

$$\mathrm{sat}_{a,b}(u) = \begin{cases} a, & \text{if} \quad u < a, \\ u, & \text{if} \quad a \leq u \leq b, \\ b, & \text{if} \quad u > b. \end{cases} \tag{1.7}$$

An example of (1.7) is shown in Figure 1.8, where $a = -1$ and $b = 2$. Note that for MIMO systems, if $\mathcal{U}$ is rectangular, then Sat is a *decentralized saturation function* as shown in Figure 1.8, that is, the ith output depends only on the ith component of the input. Although decentralized saturations are the most common input nonlinearities in control system design, the results presented in Chapter III also apply to a larger class of centralized saturation nonlinearities.

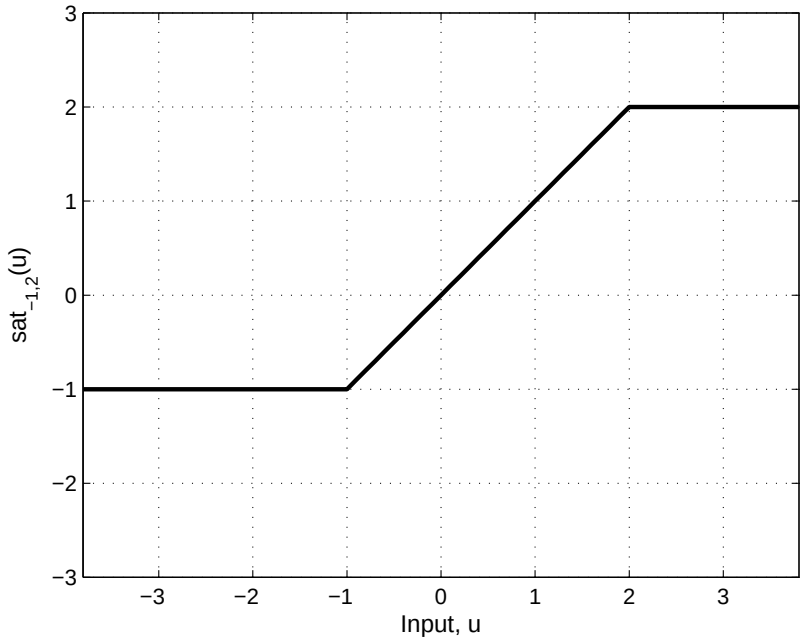

Figure 1.7: Output of (1.7), where $a = -1$ and $b = 2$.

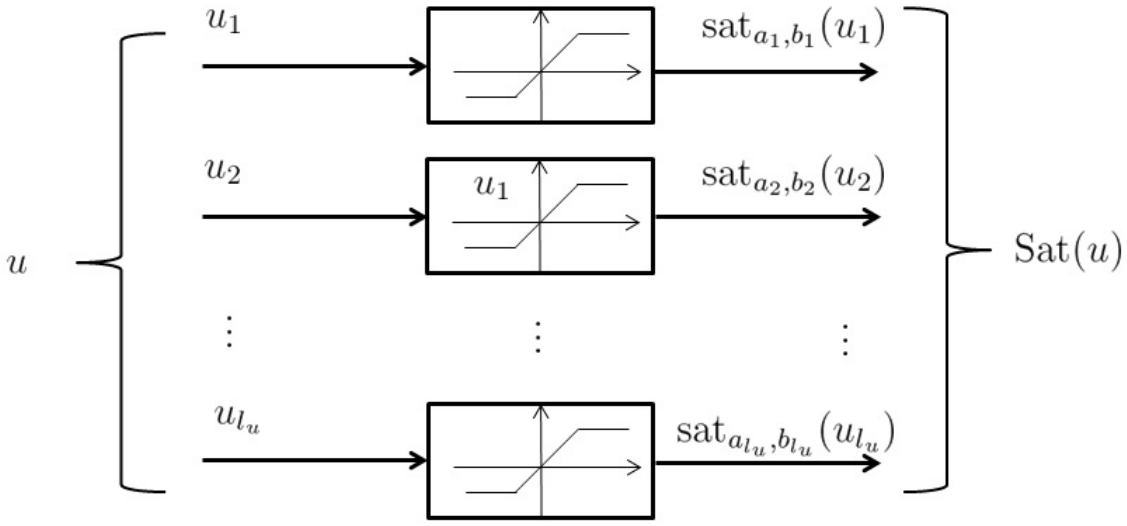

Figure 1.8: The decentralized saturation nonlinearities.

1.3.2.6 Other Nonlinearities

Many complex types of nonsmooth nonlinearities, can be interpreted as combinations of these four elementary nonlinear characteristics, and nonmonotonic input nonlinearities are discussed in Chapter IV.

1.4 Dissertation Outline

The remainder of this dissertation is organized as follows.

Chapter II Linear Retrospective Cost Adaptive Control Summary

In Chapter II, we apply retrospective cost adaptive control (RCAC) developed in [23, 25] to a linear plant with deadzone and hysteresis nonlinearities. The hysteresis is modeled with the play operator, Prandtl-Ishlinskii model, or modified Prandtl-Ishlinskii model. Initially, the system with hysteresis is controlled with RCAC having knowledge of the exact locations of the nonminimum-phase zeros of the plant. Then, the system is controlled with RCAC when the locations of the nonminimum-phase

zeros are determined through least-squares identification of the linear plant with hysteresis.

Next, we consider command-following and disturbance-rejection problems for a diesel engine model. The engine is a multi-input, multi-output system, where the transfer function of the linearized diesel engine model from EGR valve percent open to the intake manifold pressure is nonminimum phase. We demonstrate that RCAC is effective for both the linearized and nonlinear engine systems provided that two Markov parameters of the linearized engine plant model are known, either analytically or through system identification. For the command-following and disturbance-rejection problems, we consider the case when the disturbance is harmonic but otherwise unknown, and while the command signal is harmonic and known but no advance knowledge of its spectrum is assumed to be available.

Finally, we consider a command-following problem for the uncertain electromagnetically controlled oscillator (ECO). We assume that an estimate of the first Markov parameter of the discretized and linearized plant is known, but RCAC does not require knowledge of the inertia, damping, or stiffness of the plant. In this case, a setpoint feedback path is used to stabilize the unstable ECO at the commanded equilibria.

Chapter III Retrospective Cost Adaptive Control with Convex Saturation Constraints Summary

Chapter III begins the main topic of this dissertation. All real-world control systems must operate subject to constraints on the allowable control inputs. However, the method of the unconstrained adaptive control algorithm presented in Chapter II cannot be extended to the system with a saturation input nonlinearity. To account for the saturation constraint, we use convex optimization to minimize the quadratic retrospective cost function. The use of convex optimization bounds the magnitude of the retrospectively optimized input and thereby influences the controller update

to satisfy the control bounds. This technique is applied to a multi-rotor helicopter with constraints on the total thrust magnitude and inclination of the rotor plane. In particular, we formulate the multi-input constrained retrospective cost function as a second-order cone optimization (SOCP) problem. With this approach, RCAC is shown to adapt to these constraints.

The original contribution of Chapter III is the development of a constrained retrospective-cost-based adaptive controller. We demonstrate this technique on illustrative numerical examples involving single and multiple inputs. In the case of multiple control inputs, it is usually the case for optimal PID controller to assume that individual control inputs are subject to independent saturation. However, in many applications, a saturation constraint may affect multiple control inputs. The proposed control algorithm is able to deal with the problems in which multiple control inputs may be subject to *dependent* saturation constraints, where the dependency is assumed to be unknown.

Chapter IV Retrospective Cost Adaptive Control with Auxiliary Nonlinearities Summary

To further develop retrospective-cost-based adaptive control for uncertain Hammerstein systems, the results of Chapter IV generalize the results of Chapter II and Chapter III to uncertain Hammerstein systems with possibly non-monotonic input nonlinearities. We assume that only one Markov parameter of the linear plant is known and that the input nonlinearity is uncertain. The required modeling information for the input nonlinearity includes the intervals of monotonicity as well as values of the nonlinearity that determine overlapping segments of the range of the nonlinearity within each interval of monotonicity.

A novel feature of the adaptive control algorithms developed in Chapter IV of this dissertation is the use of auxiliary nonlinearities. The purpose of the auxiliary nonlin-

earities is to ensure that RCAC is applied to a Hammerstein system with a globally nondecreasing composite input nonlinearity. In particular, if the input nonlinearity is not nondecreasing, then an auxiliary blocking nonlinearity $\mathcal{N}_{\mathrm{b}}$, an auxiliary sorting nonlinearity $\mathcal{N}_{\mathrm{s}}$, and an auxiliary reflection nonlinearity $\mathcal{N}_{\mathrm{r}}$ are used to create a composite nonlinearity $\mathcal{N} \circ \mathcal{N}_{\mathrm{r}} \circ \mathcal{N}_{\mathrm{s}} \circ \mathcal{N}_{\mathrm{b}}$ that is nondecreasing, thus preserving the signs of the Markov parameters of the linearized system. An additional auxiliary saturation nonlinearity $\mathcal{N}_{\mathrm{sat}}$, which is used to tune the transient response of the closed-loop system, may depend on estimates of the range of the input nonlinearity and the gain of the linear dynamics.

The original contribution of Chapter IV is the construction of auxiliary nonlinearities to modify RCAC to deal with the input nonlinearities, which could be odd, even, or arbitrary, as well as monotonic or non-monotonic. In addition, we have proved that the auxiliary nonlinearities preserve the range of the original nonlinear system and construct a globally nondecreasing composite input nonlinearity.

Chapter V Retrospective Cost Adaptive NARMAX Control with Ersatz Nonlinearities Summary

The results of Chapter V present an unconventional approach to nonlinear output feedback control of Hammerstein systems by using adaptive control to directly update the gains of a NARMAX controller. A NARMAX model is a discrete-time ARMAX system in which the past output and inputs appear as arguments of basis functions. These functions are chosen by the user, and the controller coefficients appear linearly. The constraint that the controller coefficients appear linearly implies that the basis functions are fixed a priori and thus cannot be modified as part of the adaptation process. We numerically demonstrated that RCANC can improve the command-following performance for the Hammerstein systems over the linear controller structure for compensating performance distortion caused by the input

nonlinearity.

The original contribution of Chapter V is the modification of the adaptation mechanism to include a nonlinear adaptation mechanism. This modification ensures that the retrospective optimization accounts for the presence of the input nonlinearity. To account for the case in which the input nonlinearity is uncertain, we investigate the performance of RCNAC control in the case of uncertainty. In particular, we determine the minimal modeling information about the input nonlinearity that RCANC requires; once this information is known, an approximate input nonlinearity, called the ersatz nonlinearity, can be used by RCANC for adaptation.

CHAPTER II

Linear Retrospective Cost Adaptive Control

In this chapter, we apply retrospective cost adaptive control (RCAC) developed in [23, 25] to a linear plant with deadzone and hysteresis nonlinearities. The hysteresis is modeled with the play operator, Prandtl-Ishlinskii model, or modified Prandtl-Ishlinskii model. Initially, the system with hysteresis is controlled with RCAC having knowledge of the exact locations of the nonminimum-phase zeros of the plant. Then, the system is controlled with RCAC when the locations of the nonminimum-phase zeros are determined through least-squares identification of the linear plant with hysteresis. Next, we consider command-following and disturbance-rejection problems for a diesel engine model. The engine is a multi-input, multi-output system, where the transfer function of the linearized diesel engine model from EGR valve percent open to the intake manifold pressure is nonminimum phase. We demonstrate that RCAC is effective for both the linearized and nonlinear engine systems provided that two Markov parameters of the linearized engine plant model are known, either analytically or through system identification. For the command-following and disturbance-rejection problems, we consider the case when the disturbance is harmonic but otherwise unknown, and while the command signal is harmonic and known but no advance knowledge of its spectrum is assumed to be available. Finally, we consider a command-following problem for the uncertain electromagnetically controlled

oscillator (ECO). We assume that an estimate of the first Markov parameter of the discretized and linearized plant is known, but RCAC does not require knowledge of the inertia, damping, or stiffness of the plant. In this case, a setpoint feedback path is used to stabilize the unstable ECO at the commanded equilibria.

The work on hysteresis is in collaboration with Bojana Drincic, and the results on the diesel engine and uncertain ECO are published in [37, 38].

2.1 Retrospective Cost Adaptive Controller

In this section, we briefly review the retrospective cost adaptive control algorithm developed in [23, 25]. This adaptive controller is effective in the presence of the hysteresis. Furthermore, this adaptive controller is effective for command following where the spectrum of the commands is unknown.

2.1.1 Problem Formulation

Consider the multi-input, multi-output (MIMO) discrete-time system

$$x(k+1) = Ax(k) + Bu(k) + D_1 w(k), \tag{2.1}$$

$$y(k) = Cx(k) + D_2 w(k), \tag{2.2}$$

$$z(k) = E_1 x(k) + E_0 w(k), \tag{2.3}$$

Where $x(k) \in \mathbb{R}^n$, $y(k) \in \mathbb{R}^{l_y}$, $z(k) \in \mathbb{R}^{l_z}$, $u(k) \in \mathbb{R}^{l_u}$, $w(k) \in \mathbb{R}^{l_w}$, and $k \geq 0$. Our goal is to develop an adaptive output feedback controller under which the performance variable z is minimized in the presence of the exogenous signal w. We assume that (A, B) is stabilizable, (A, C) and (A, E_1) are detectable, and the measurements of y and z are available for feedback. If the command signal is included as a component of y, then the adaptive controller has a feedforward architecture.

Consider the ARMAX representation of (2.1) and (2.3),

$$z(k) = \sum_{i=0}^{n} -\alpha_i z(k-i) + \sum_{i=0}^{n} \beta_i u(k-i) + \sum_{i=0}^{n} \gamma_i w(k-i), \tag{2.4}$$

where $\alpha_1, \cdots, \alpha_n \in \mathbb{R}$, $\beta_1, \cdots, \beta_n \in \mathbb{R}^{l_z \times l_u}$, and $\gamma_1, \cdots, \gamma_n \in \mathbb{R}^{l_z \times l_w}$, and the relative degree d is defined as the smallest non negative integer i such that the ith Markov parameter $H_i \triangleq E_1 A^{i-1} B \in \mathbb{R}^{l_z \times l_u}$ and $H_d = \beta_d$, if $i > 0$, or $H_0 \triangleq E_2$ if $i = 0$.

2.1.2 Controller Construction

We construct a strictly proper time series controller $u(k)$ of order n_c to formulate an adaptive control algorithm for (2.1)–(2.3). The controller $u(k)$ is given by

$$u(k) = \sum_{i=1}^{n_c} M_i(k) u(k-i) + \sum_{i=1}^{n_c} N_i(k) y(k-i), \tag{2.5}$$

where, for all $i = 1, \cdots, n_c$, $M_i(k) \in \mathbb{R}^{l_u \times l_u}$ and $N_i(k) \in \mathbb{R}^{l_u \times l_u}$. The control (2.5) can be expressed as

$$u(k) = \theta(k)\phi(k), \tag{2.6}$$

where the controller gain matrix

$$\theta(k) \triangleq \left[\begin{array}{cccccc} N_1(k) & \cdots & N_{n_c}(k) & M_1(k) & \cdots & M_{n_c}(k) \end{array} \right] \in \mathbb{R}^{l_u \times n_c(l_u + l_y)}, \tag{2.7}$$

and the regressor vector $\phi(k)$ is given by

$$\phi(k) \triangleq \begin{bmatrix} y(k-1) \\ \vdots \\ y(k-n_c) \\ u(k-1) \\ \vdots \\ u(k-n_c) \end{bmatrix} \in \mathbb{R}^{n_c(l_u+l_y)}. \tag{2.8}$$

Next, defining $\hat{\Theta} \triangleq \mathrm{vec}\hat{\theta} \in \mathbb{R}^{n_c l_u(l_y+l_u)}$ and $\Theta(k) \triangleq \mathrm{vec}\theta(k) \in \mathbb{R}^{n_c l_u(l_y+l_u)}$, the retrospective performance vector $\hat{z}(\hat{\theta}, k)$ is given by

$$\begin{aligned} \hat{z}(\hat{\Theta}, k) &= z(k) + \sum_{i=d}^{\nu} \Phi_i^{\mathrm{T}}(k)[\hat{\Theta} - \Theta(k-i)] \\ &= z(k) - \sum_{i=d}^{\nu} \Phi_i^{T}(k)\Theta(k-i) + \Psi^{\mathrm{T}}(k)\hat{\Theta}, \end{aligned} \tag{2.9}$$

where, for $i = d, \ldots, \nu$,

$$\Phi_i(k) \triangleq \phi(k-i) \otimes \bar{\beta}_i^{\mathrm{T}} \in \mathbb{R}^{(n_c l_u(l_y+l_u))\times l_z},$$

where $\otimes$ represents the Kronecker product, and $\nu > d, \hat{\theta} \in \mathbb{R}^{l_u \times (n_c(l_y+l_u))}$ is an optimization variable used to derive the adaptive law, and the selection matrix coefficients $\bar{\beta}_d, \ldots, \bar{\beta}_\nu$ is discussed in [25], and

$$\Psi(k) \triangleq \sum_{i=d}^{\nu} \Phi_i(k). \tag{2.10}$$

Note that $\hat{z}(\hat{\Theta}, k)$ does not need either the information of the open-loop zeros nor the transfer functions from the exogenous signal w to z. However, when w represents a command, then w can be viewed as an additional measurement y, and thus the

controller has feedforward action.

Next, define the cumulative retrospective cost function

$$J(\hat{\Theta},k) \triangleq \frac{1}{2}\sum_{i=0}^{k}\lambda^{k-i}\hat{z}^{\mathrm{T}}(\hat{\Theta},i)R\hat{z}(\hat{\Theta},i)+\frac{1}{2}(\Theta(k)-\Theta(0))^{\mathrm{T}}Q(\Theta(k)-\Theta(0)), \quad (2.11)$$

where $\lambda \in (0,1]$, and $R \in \mathbb{R}^{l_z \times l_z}$, and $Q \in \mathbb{R}^{(n_c l_u(l_y+l_u))\times(n_c l_u(l_y+l_u))}$ are positive definite. $J(\hat{\Theta},k)$ is minimized by the adaptive law

$$\Theta(k+1) = \Theta(k) - P(k)\Psi(k)\times[\lambda R^{-1}+\Psi^{\mathrm{T}}(k)P(k)\Psi(k)]^{-1}z_{\mathrm{R}}(k), \quad (2.12)$$

$$P(k+1) = \frac{1}{\lambda}P(k) - \frac{1}{\lambda}P(k)\Psi(k)\times[\lambda R^{-1}+\Psi^{\mathrm{T}}(k)P(k)\Psi(k)]^{-1}\Psi^{\mathrm{T}}(k)P(k), \quad (2.13)$$

where $P(0) = Q^{-1}, \Theta(0) \in \mathbb{R}^{n_c l_u(l_y+l_u)}$. Finally, the cumulative retrospective cost adaptive control law is thus given by (2.12), (2.13), and

$$u(k) = \theta(k)\phi(k) = \mathrm{vec}^{-1}(\Theta(k))\phi(k). \quad (2.14)$$

2.2 Examples of Adaptive Control of Linear Systems with Deadzone Input Nonlinearity

We apply the linear retrospective cost adaptive (RCA) control algorithm developed in [23] to linear systems with deadzone input nonlinearities. Consider the linear plant

$$G(\mathbf{z}) = \frac{(z-0.5)(z-0.9)}{(z-0.7)(z-0.5-\jmath 0.5)(z-0.5+\jmath 0.5)} \quad (2.15)$$

with the deadzone input nonlinearity with $f_1(u) = u, f_2(u) = u$ in (1.1), which is not one-to-one but onto. Note that $d = 1$ and $H_d = 1$. We consider the sinusoidal command $r(k) = \sin(\Omega_1 k)$, where $\Omega_1 = \pi/5$ rad/sample. We set $n_{\mathrm{c}} = 10$, $P_0 =$

$0.01I_{2n_c}$, $\eta_0 = 0$, and $\tilde{\mathcal{H}} = H_1$, and we vary the deadzone thresholds b_l and b_r in (1.1). The time history of z with $b_l = b_r = 5$, 10, and 20 is shown in Figure 2.1, Figure 2.2, and Figure 2.3, respectively. In all three cases, RCAC is able follow the command due to fact that it provides the gains of u in (2.14) needed to drive z to a small value.

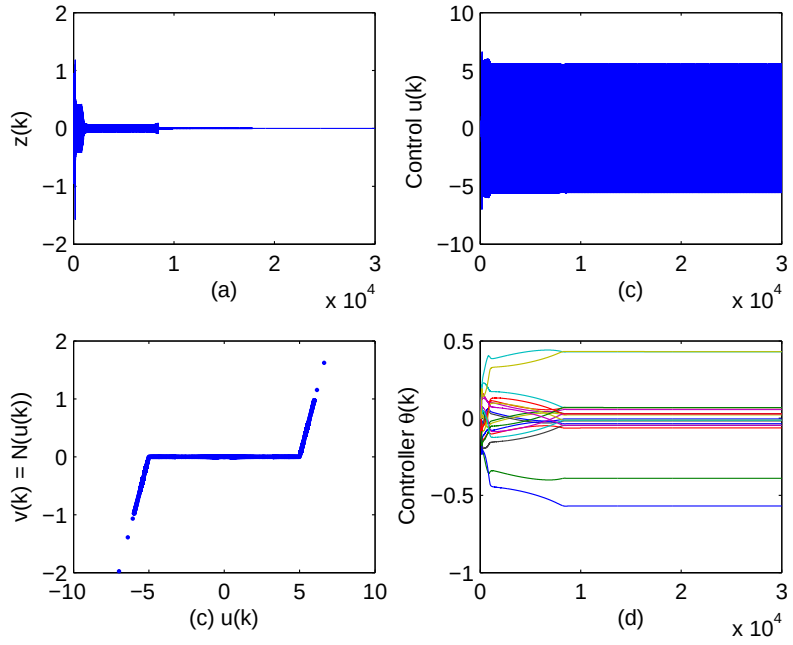

Figure 2.1: Closed-loop response of the plant (2.15) with the sinusoidal command $r(k) = \sin(\Omega_1 k)$, where $\Omega_1 = \pi/5$ rad/sample. Deadzone is modeled by (1.1) with $f_1(u) = u$, $f_2(u) = u$, and $b_l = b_r = 5$.

2.3 Examples of Adaptive Control of Linear Systems with Hysteretic Input Nonlinearity

We apply the retrospective cost adaptive (RCA) control algorithm developed in [23]. The definitions and notations of [23] are used in applying this algorithm to nonminimum-phase systems with hysteretic input nonlinearities. RCA control is applied to command following and disturbance rejection where the spectra of the commands and disturbances are unknown and the commands are not measured.

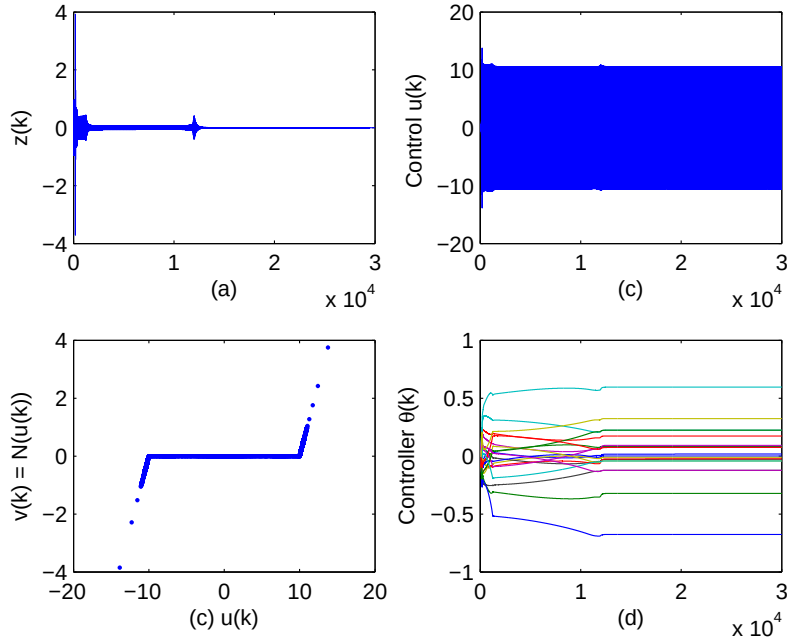

Figure 2.2: Closed-loop response of the plant (2.15) with the sinusoidal command $r(k) = \sin(\Omega_1 k)$, where $\Omega_1 = \pi/5$ rad/sample. Deadzone is modeled by (1.1) with $f_1(u) = u$, $f_2(u) = u$, and $b_l = b_r = 10$.

2.3.1 Architecture and Parameters

The system architecture is shown in Figure 2.4, where RCAC is in a feedback loop with a two-input two-output plant. The hysteretic nonlinearity is in the feedback loop and has the control signal as the input. This configuration can be interpreted as an approximation of a hysteretic actuator. We test the system with either a first- or second-order linear plant. The hysteresis is modeled by a play operator or by the Prandtl-Ishlinskii model.

The numerator coefficients $\bar{\beta}_d, \ldots, \bar{\beta}_\nu$ of the linear plant (see [23]) are obtained in two different ways, and the results of these two strategies are compared. Initially we assume that the linear plant is known, and we use the numerator coefficients. Next, we assume that the plant and the hysteretic nonlinearity are both unknown, and we use off-line least-squares identification to find these coefficients. In this case,

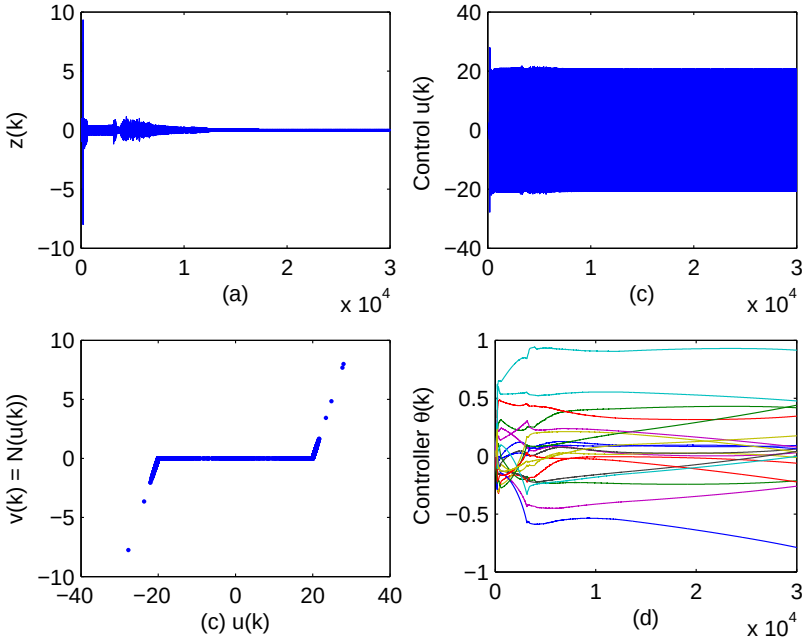

Figure 2.3: Closed-loop response of the plant (2.15) with the sinusoidal command $r(k) = \sin(\Omega_1 k)$, where $\Omega_1 = \pi/5$ rad/sample. Deadzone is modeled by (1.1) with $f_1(u) = u$, $f_2(u) = u$, and $b_l = b_r = 20$.

we obtain a linear approximation of the hysteresis and the linear plant.

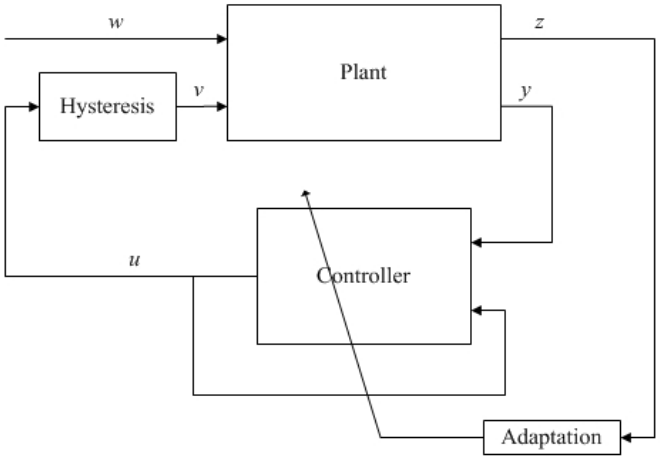

Figure 2.4: Schematic of the system architecture.

2.3.2 Simulations With Exact Plant Information

In this section we assume that the plant is exactly known and we use the numerator coefficients of the linear plant as the required modeling data $\bar{\beta}_d, \ldots, \bar{\beta}_\nu$. In all of the examples the controller is turned on at time step $k = 100$.

Example 2.3.1. *First-order plant, step command with play operator.* For the minimum-phase stable plant $G_1 = \frac{1}{z-0.5}$, we consider a command-following problem with the step command $w(k) \equiv 10$. Initially, we run the simulation without the hysteresis block and let the response reach steady state. Then we save the gain matrix θ and insert the hysteresis block into the loop. We model the hysteresis with a play operator of width $r = 1$. We use the saved gain matrix as a feedback gain instead of the adaptive controller to demonstrate the degradation in the performance in presence of hysteresis. Finally, we turn on the adaptive controller with the hysteresis nonlinearity in the loop to demonstrate that the performance is recovered. The closed-loop response is shown in Figure 2.5. ■

Example 2.3.2. *First-order plant, unit step command with PI model.* We consider the plant and input as in Example 2.3.1, but model the hysteresis by the Prandtl-Ishlinskii model (1.4), (1.5) with $N = 10$, $r_j = 0.5j$ for $j = 1, \ldots, N$, $p(r) = 0.5e^{-0.5r}$, $q = 0.5$, $\gamma(v) = 5\tanh(0.05v)$. The closed-loop response is shown in Figure 2.6. ■

Example 2.3.3. *First-order plant, sinusoidal command with play operator.* In this example, we use the plant G_1 in Example 2.3.1 with the sinusoid command $w(k) = 10\sin\omega k$, where $\omega = \pi/6$ rad/sample. The hysteresis is modeled by a play operator with width $r = 5$. We first let the system run without the hysteresis. Then we save the controller gains and switch off the adaptive controller. We add the play operator to the system and use the saved gains in a feedback controller. The performance of the system degrades significantly. Finally, we turn the adaptive

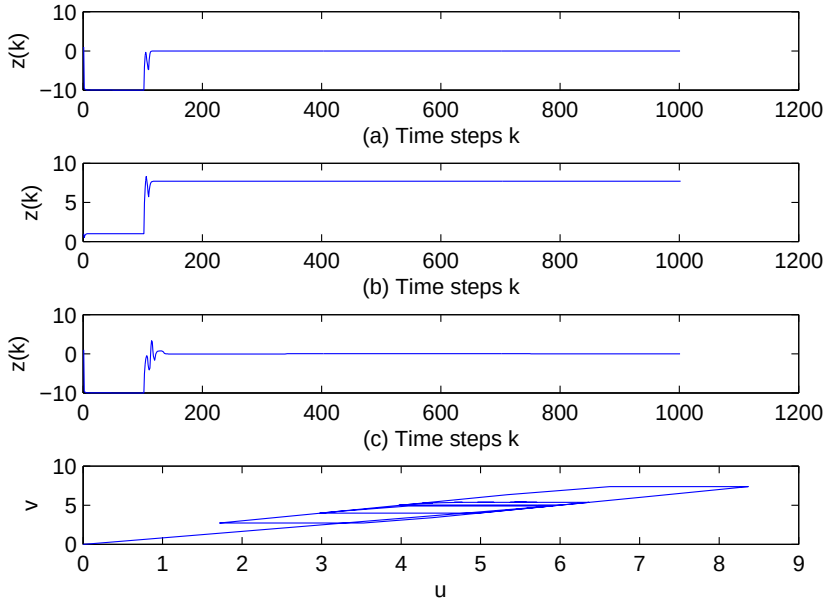

Figure 2.5: Closed-loop response to a step command $w(k) \equiv 10$ of the plant $G_1 = \frac{1}{z-0.5}$. (a) shows the response with no hysteresis present. (b) shows the response with hysteresis and without the adaptive controller, using the steady state gains that the adaptive controller converged to in (a). (c) shows the response with the adaptive controller turned on and hysteresis present. u is the input of the hysteresis, and v is the output of the hysteresis.

controller on with the hysteresis present and recover the performance. The closed-loop response is shown in Figure 2.7. ■

Example 2.3.4. *First-order plant, sinusoidal command with PI model.* We consider the plant G_1 and input from Example 2.3.3, but model the hysteresis in the system by a PI model (1.4), (1.5) with $N = 10$, $r_j = 0.5j$ for $j = 1, \ldots, N$, $p(r) = 0.5e^{-0.5r}$, $q = 0.5$, $\gamma(v) = 5\tanh(0.05v)$. The closed-loop response is shown in Figure 2.8. ■

Example 2.3.5. *Second-order plant with NMP zero, step input with play operator.* Consider the 2nd-order nonminimum phase stable plant with low damping $G_{\text{2NMP}} = \frac{z-1.5}{(z+0.8)(z-0.9)}$ and consider the step command $w(k) \equiv 10$. We model the hysteresis with

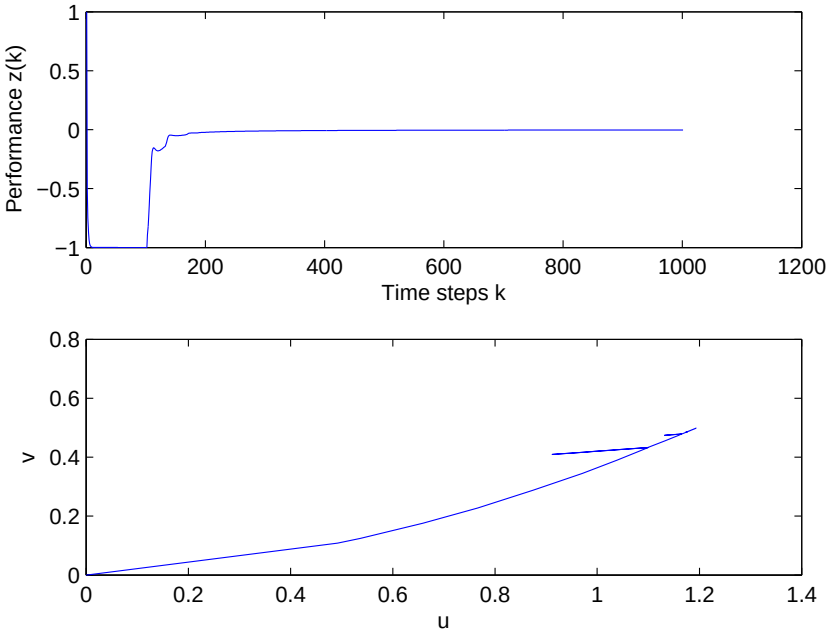

Figure 2.6: Closed-loop response of the plant $G_1 = \frac{1}{z-0.5}$ to the unit step input. The PI model of hysteresis has parameters $N = 10$, $r_j = 0.5j$ for $j = 1, \ldots, N$, $p(r) = 0.5e^{-0.5r}$, $q = 0.5$, $\gamma(v) = 5\tanh(0.05v)$.

a play operator of width $r = 1$. We follow the same procedure outlined in Example 2.3.1. The closed-loop response is shown in Figure 2.9. ■

Example 2.3.6. *Second-order plant with NMP zero, step command with PI.* We use the plant $G_{2\text{NMP}}$ and input from Example 2.3.5. The hysteresis is modeled by the PI model with parameters $N = 100$, $r_j = 0.05j$ for $j = 1, \ldots, N$, $p(r) = 0.5e^{-0.5r}$, $q = 0.5$, and $\gamma(v) = 5\tanh(0.05v)$. The closed loop response of the system is shown in Figure 2.10. ■

Example 2.3.7. *Second-order plant with NMP zero, sinusoidal command with play operator.* We use the plant $G_{2\text{NMP}}$ with the sinusoidal command $w(k) = 10\sin\omega k$, where $\omega = \pi/6$ rad/sample. Hysteresis is modeled by the play operator with width $r = 1$. We use the procedure outlined in Example 2.3.3. The closed-loop response is shown in Figure 2.11. ■

Example 2.3.8. *Second-order plant with NMP zero, sinusoidal command with*

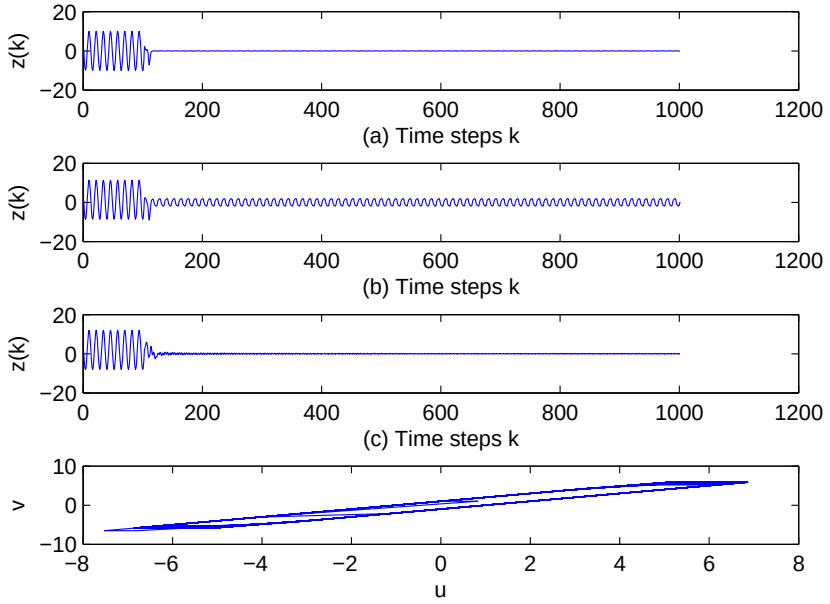

Figure 2.7: Closed-loop response of the of the plant $G_1 = \frac{1}{z-0.5}$ with the command $w(k) = 10\sin\omega k$, $\omega = \pi/6$ rad/sample. (a) shows response without hysteresis. (b) shows the response with the steady-state adaptive controller gains obtained in (a) and hysteresis present. (c) shows the performance with hysteresis present and the adaptive controller turned on.

PI. We use the plant and input from Example 2.3.7. Hysteresis is modeled by a PI model with parameters $N = 100$, $r_j = 0.05j$ for $j = 1, \ldots, N$, $p(r) = 0.5e^{-0.5r}$, $q = 0.5$, and $\gamma(v) = 5\tanh(0.05v)$. The closed loop response of the system is shown in Figure 2.12. In this case, the controller cannot compensate for the nonlinearity of the PI model and command following is not achieved. ■

Example 2.3.9. *Third-order plant with NMP zeros, sinusoidal command with play.* In this example we test RCAC with NMP plants of order higher than 2. The plant is $G_{3\text{NMP}} = \frac{z^2-2.2z+1.85}{(z-0.3)(z+0.8)(z-0.9)}$, hysteresis is modeled by a play operator with width $r = 1$. The command is as in Example 2.3.8. The closed loop response of the system is shown in Figure 2.13. ■

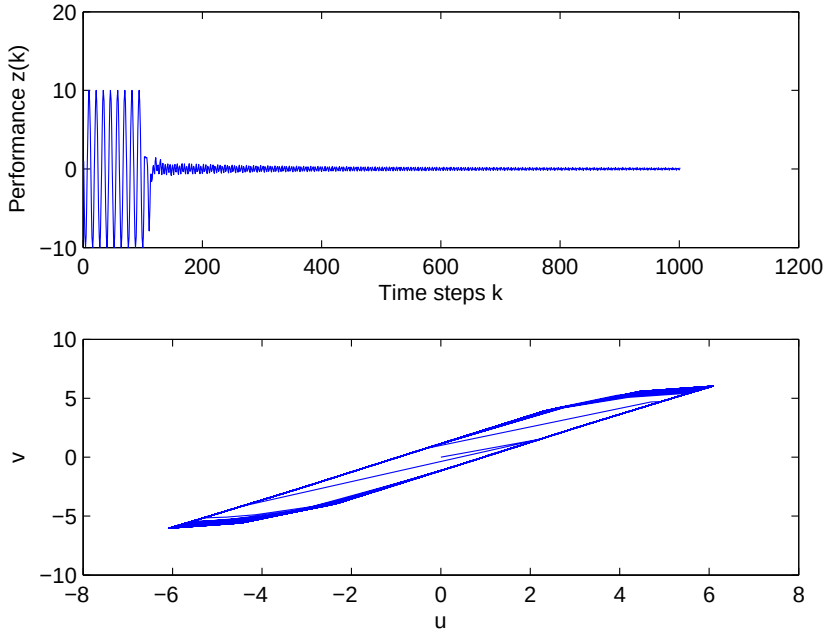

Figure 2.8: Closed-loop response of the plant $G_1 = \frac{1}{z-0.5}$ with the PI model of hysteresis with parameters $N = 10$, $r_j = 0.5j$ for $j = 1, \ldots, N$, $p(r) = 0.5e^{-0.5r}$, $q = 0.5$, $\gamma(v) = 5\tanh(0.05v)$ and command $w(k) = 10\sin\omega k$, $\omega = \pi/6$ rad/sample.

2.3.3 Simulations with Off-Line ID

In this section we consider the more realistic case in which the only way to identify the plant would be in cascade with the hysteresis nonlinearity. We present the results of simulations in which the coefficients $\bar{\beta}_d, \ldots, \bar{\beta}_\nu$ are found through least-squares identification (ID) of the hysteresis and plant. This method yields a linear approximation of the system. The numerator coefficients of the linear approximation are used in the controller algorithm. A white noise signal is applied as the input u to the hysteresis block. The output of the hysteresis block v is used as the input to the plant. The output of the plant z and the input to the hysteresis u are used for the ID. The location of poles and zeros with the second order minimum-phase (MP) plant $G_{2\text{MP}} = \frac{z-0.5}{(z-0.2)(z+0.1)}$ is shown in Figures 2.14 (a) and (b), respectively, for three levels of standard deviation of the input noise u. The location of poles and zeros with

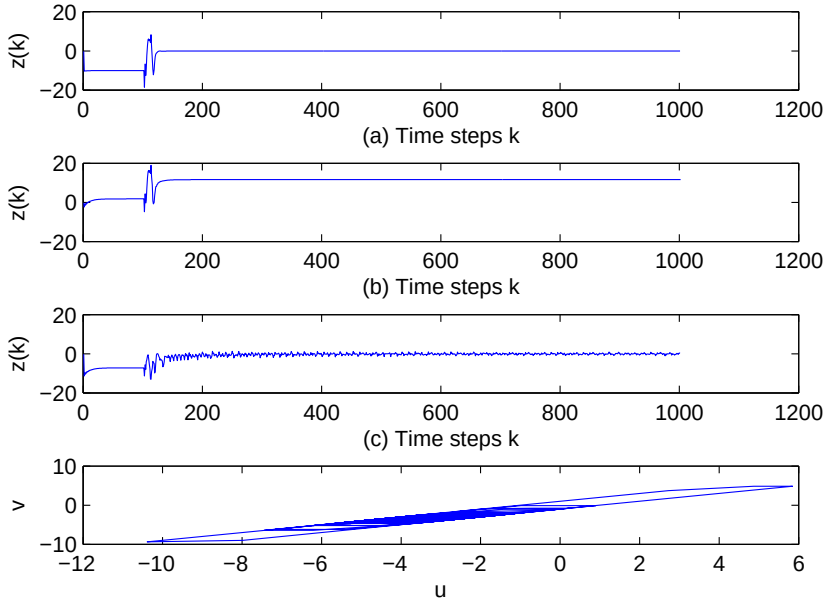

Figure 2.9: Closed-loop response to the step command $w(k) \equiv 10$ of the stable nonminimum-phase plant $G_{2\text{NMP}} = \frac{z-1.5}{(z+0.8)(z-0.9)}$. (a) shows the response with no hysteresis present. (b) shows the response with hysteresis and with adaptive controller turned off, the steady-state gains from (a) are used in the feedback loop. (c) shows the response with adaptive controller turned on and hysteresis present. u is the input of the hysteresis, and v is the output of the hysteresis.

the second-order NMP plant $G_{2\text{NMP}}$ is shown in Figures 2.14 (c) and (d), respectively, for three levels of standard deviation of the input noise u. In all cases, it is assumed that the order of the system is 5 with relative degree 1. The figures show that this ID technique gives a good approximation of the NMP zero in the system even though it may not capture the poles or minimum phase zeros accurately. This is consistent with the results of [39].

In all of the following examples the identification was done with zero-mean white noise input u with standard deviation 3.

Example 2.3.10. *First-order plant, step command with play operator.* We consider the first-order stable plant G_1, and model the hysteresis with the play operator

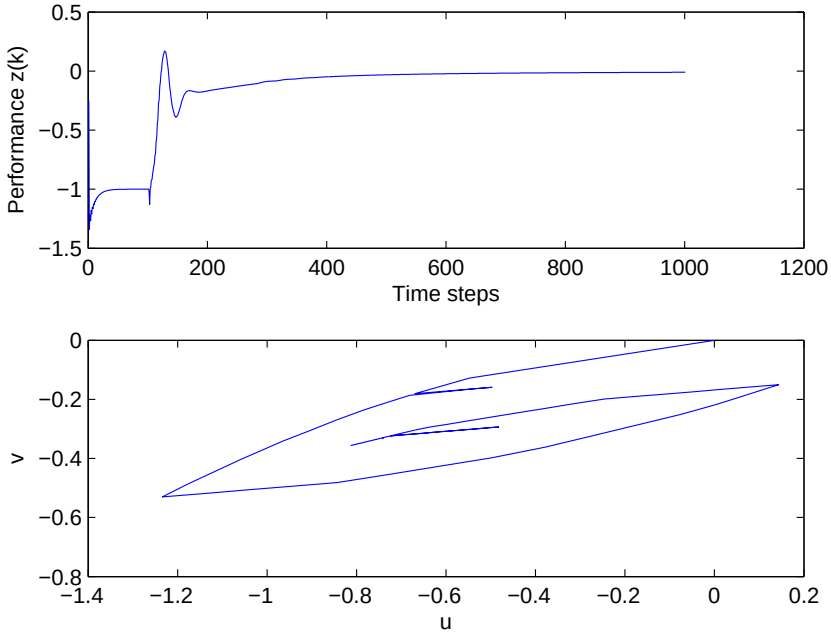

Figure 2.10: Closed-loop response of the of the plant $G_{\text{2NMP}} = \frac{z-1.5}{(z+0.8)(z-0.9)}$ with the unit step command. Hysteresis is modeled by a PI model with parameters $N = 100$, $r_j = 0.05j$ for $j = 1, \ldots, N$, $p(r) = 0.5e^{-0.5r}$, $q = 0.5$, and $\gamma(v) = 5\tanh(0.05v)$.

with $r = 1$. The coefficients $\bar{\beta}_d, \ldots, \bar{\beta}_\nu$ are obtained through a least-squares identification. We assume that the plant order is $n = 3$ with relative degree $d = 1$. The pole-zero map of the identified plant is shown in Figure 2.15(a). The closed-loop response with adaptive controller is shown in Figure 2.15(b).

Example 2.3.11. *First-order plant, sinusoidal command with play operator.* We consider the plant G_1, and $\bar{\beta}$ coefficients and the hysteresis model from Example 2.3.10, and set the input to a sinusoidal signal $w(k) = 10\sin\omega k$, where $\omega = \pi/6$ rad/sample. The closed-loop response with adaptive controller is shown in Figure 2.16. ■

Example 2.3.12. *First-order plant, sinusoidal command with PI model.* We consider the plant, input, and $\bar{\beta}$ coefficients as in Example 2.3.11, but use the PI model of hysteresis with parameters $N = 100$, $r_j = 0.05j$ for $j = 1, \ldots, N$, $p(r) = 0.5e^{-0.5r}$,

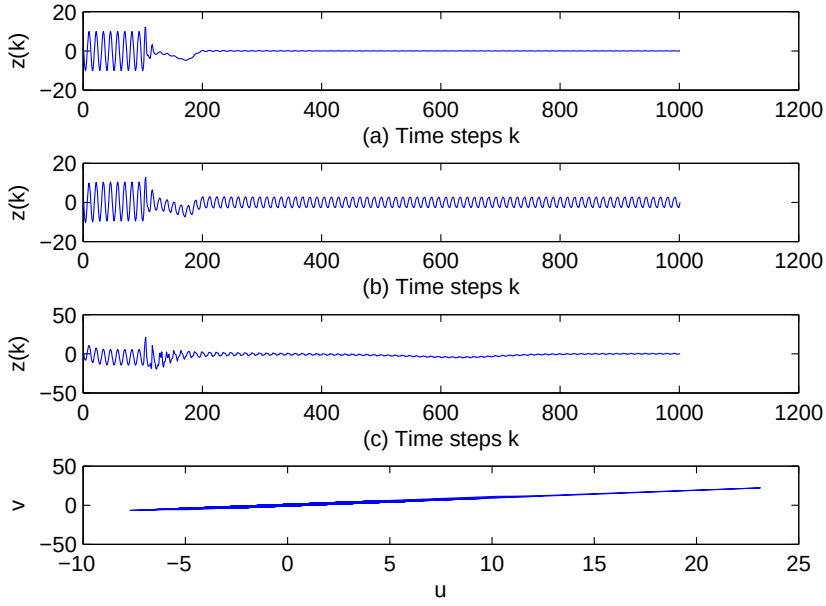

Figure 2.11: Closed-loop response of the plant $G_{\text{2NMP}} = \frac{z-1.5}{(z+0.8)(z-0.9)}$ with the command $w(k) = 10\sin\omega k$, $\omega = \pi/6$ rad/sample. The response without hysteresis is shown in (a). (b) shows the response with the steady-state adaptive controller gains in a feedback loop and hysteresis present. Performance with hysteresis present and RCAC is shown in (c).

$q = 0.5$, and $\gamma(v) = 5\tanh(0.05v)$. The closed-loop response with adaptive controller is shown in Figure 2.17. ■

Example 2.3.13. *Second-order plant with MP zero, step command with play operator.* We consider the second order plant G_{2MP}, and model the hysteresis with the play operator with $r = 1$. The coefficients $\bar{\beta}_d, \ldots, \bar{\beta}_\nu$ are obtained through a least-squares ID method. We assume that the plant order is $n = 5$ with relative degree $d = 1$. The pole-zero map of the identified plant is shown in Figure 2.18(a). The closed-loop response with adaptive controller is shown in Figure 2.18(b). ■

Example 2.3.14. *Second-order plant with MP zero, sinusoidal command with play operator.* We consider the plant G_{2MP}, and $\bar{\beta}$ coefficients and hysteresis model from Example 2.3.13, but set the input to a sinusoidal signal $w(k) = 10\sin\omega k$, where

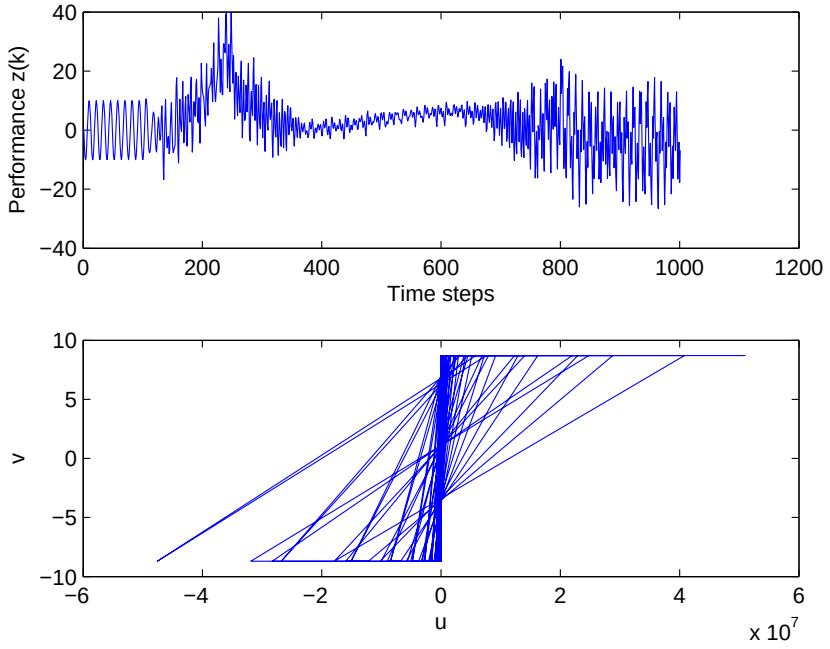

Figure 2.12: Closed-loop response of the of the plant $G_{\text{2NMP}} = \frac{z-1.5}{(z+0.8)(z-0.9)}$ with command $w(k) = 10\sin\omega k$, $\omega = \pi/6$ rad/sample. Hysteresis is modeled by a PI model with parameters $N = 100$, $r_j = 0.05j$ for $j = 1, \ldots, N$, $p(r) = 0.5e^{-0.5r}$, $q = 0.5$, and $\gamma(v) = 5\tanh(0.05v)$. This is an example of hysteretic nonlinearity that cannot be compensated by RCAC.

$\omega = \pi/6$ rad/sample. The closed-loop response with adaptive controller is shown in Figure 2.19. ■

Example 2.3.15. *Second-order plant with NMP zero, step command with play operator.* We consider the step response of the second order stable plant with one nonminimum-phase zero $G_{\text{2NMP}} = \frac{z-1.5}{(z+0.8)(z-0.9)}$, and model the hysteresis with the play operator with $r = 1$. The coefficients $\bar{\beta}_d, \ldots, \bar{\beta}_\nu$ are obtained through least-squares ID. For ID, we assume that the plant order is $n = 5$ with relative degree $d = 1$. The pole-zero map of the identified plant is shown in Figure 2.20(a). The closed-loop response with adaptive controller is shown in Figure 2.20(b). ■

Example 2.3.16. *Second-order plant with NMP zero, step command with PI model.* We consider the plant G_{2NMP} and input as in Example 2.3.15. We model the

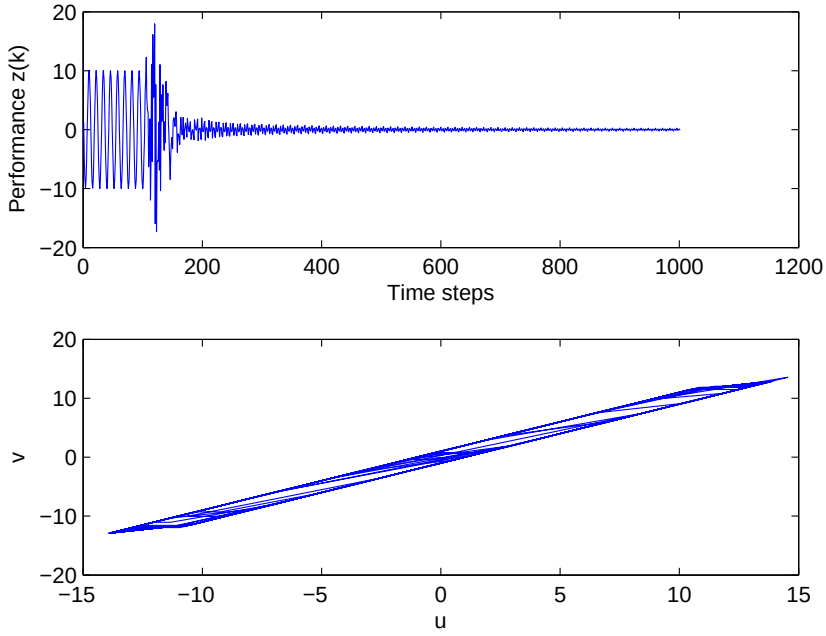

Figure 2.13: Closed-loop response of the of the plant $G_{\text{3NMP}} = \frac{z^2-2.2z+1.85}{(z-0.3)(z+0.8)(z-0.9)}$ with command $w(k) = 10\sin\omega k$, $\omega = \pi/6$ rad/sample. Hysteresis is modeled by the play operator with $r = 1$.

hysteresis with a PI model with parameters $N = 100$, $r_j = 0.05j$ for $j = 1, \ldots, N$, $p(r) = 0.5e^{-0.5r}$, $q = 0.5$, and $\gamma(v) = 5\tanh(0.05v)$. We use the least-squares ID to get the $\bar{\beta}$ coefficients and for ID we assume that the system order is 10 with relative degree 1. The pole zero map of the plant from the ID is shown in Figure 2.21(a). The closed-loop response is shown in Figure 2.21(b). ■

Example 2.3.17. *Second-order plant with NMP zero, sinusoidal command with play operator.* We consider the plant G_{2NMP}, but model the hysteresis with a play operator with $r = 1$ and set the input to a sinusoidal signal $w(k) = 10\sin\omega k$, where $\omega = \pi/6$ rad/sample. The closed-loop response with the fifth order plant is shown in Figure 2.22. ■

Example 2.3.18. *Second-order plant with NMP zero, sinusoidal command with PI model.* We consider the plant and input from Example 2.3.17. We model the hysteresis with a PI model with parameters $N = 100$, $r_j = 0.05j$ for $j = 1, \ldots, N$,

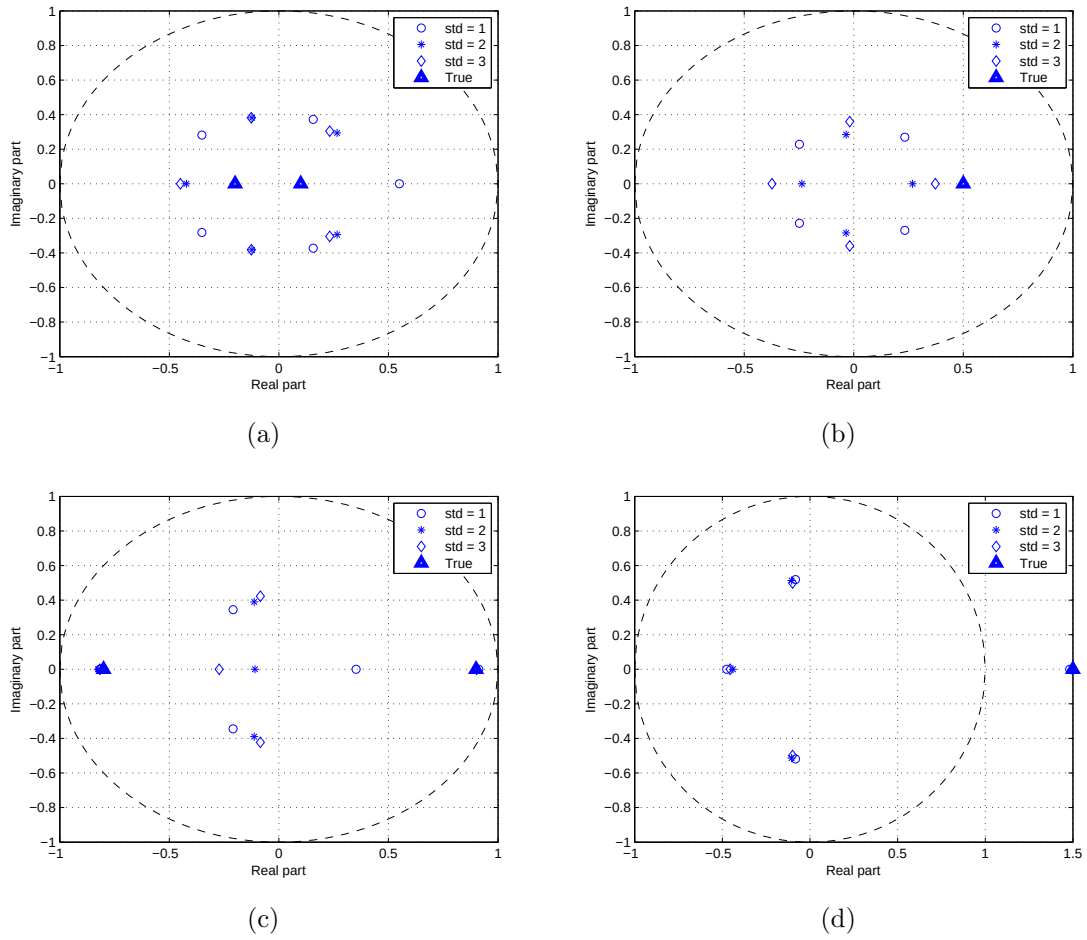

Figure 2.14: Locations of poles and zeros obtained through the identification with three levels of standard deviation of input noise. (a) and (b) show the poles and the zeros, respectively, of the plant $G_{2\text{MP}} = \frac{z-0.5}{(z-0.2)(z+0.1)}$. (c) and (d) show the poles and the zeros, respectively, of the plant $G_{2\text{NMP}} = \frac{z-1.5}{(z+0.8)(z-0.9)}$. In all cases it is assumed that the order of the system is 5 with relative degree 1.

$p(r) = 0.5e^{-0.5r}$, $q = 0.5$, and $\gamma(v) = 5\tanh(0.05v)$. The closed-loop response with the assumed tenth order plant is shown in Figure 2.23. ■

Example 2.3.19. *Third-order plant with NMP zero, sinusoidal command with play operator.* We consider the third order plant $G_{3\text{NMP}}$ and input as in Example 2.3.18. We model the hysteresis with the play operator with $r = 1$. The coefficients $\bar{\beta}_d, \ldots, \bar{\beta}_\nu$ are obtained through a least-squares ID method. For ID, we assume that

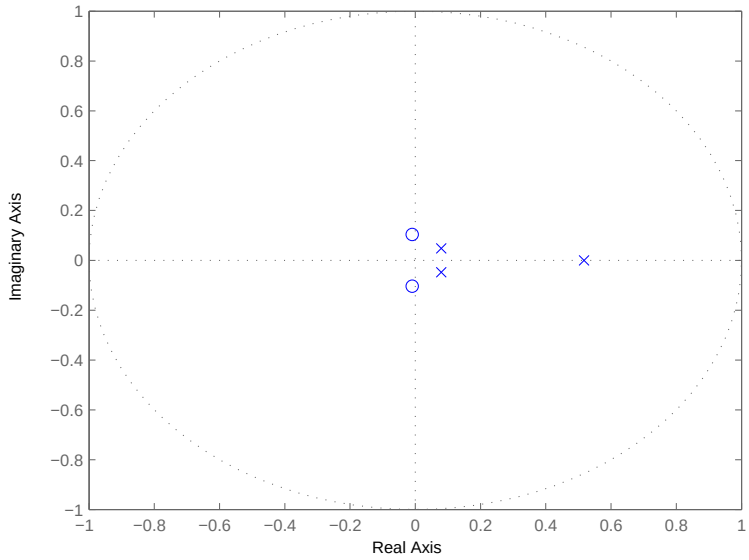

(a)

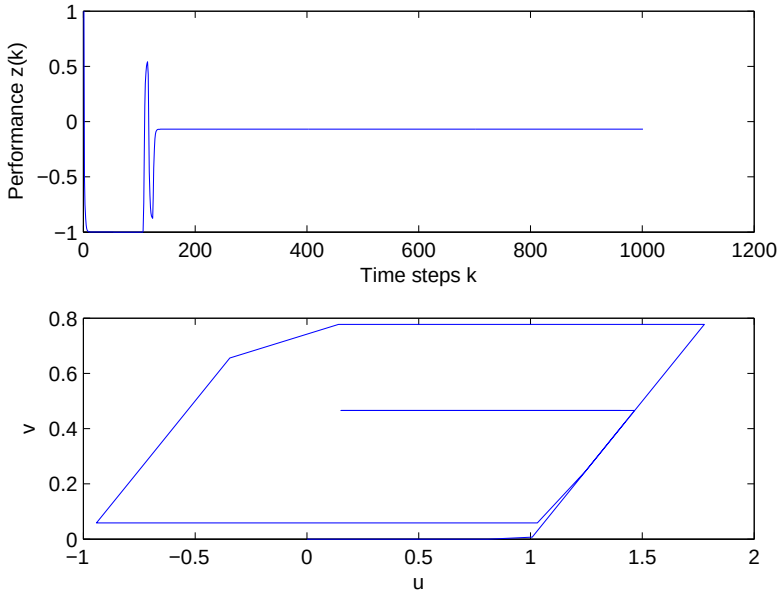

(b)

Figure 2.15: Closed-loop response of the first order plant G_1 with controller coefficients obtained from ID and hysteresis modeled by play operator with $r = 1$. (a) shows the pole-zero map of the identified third order plant. (b) shows the closed loop response. The plant order is assumed to be 3 with relative degree 1.

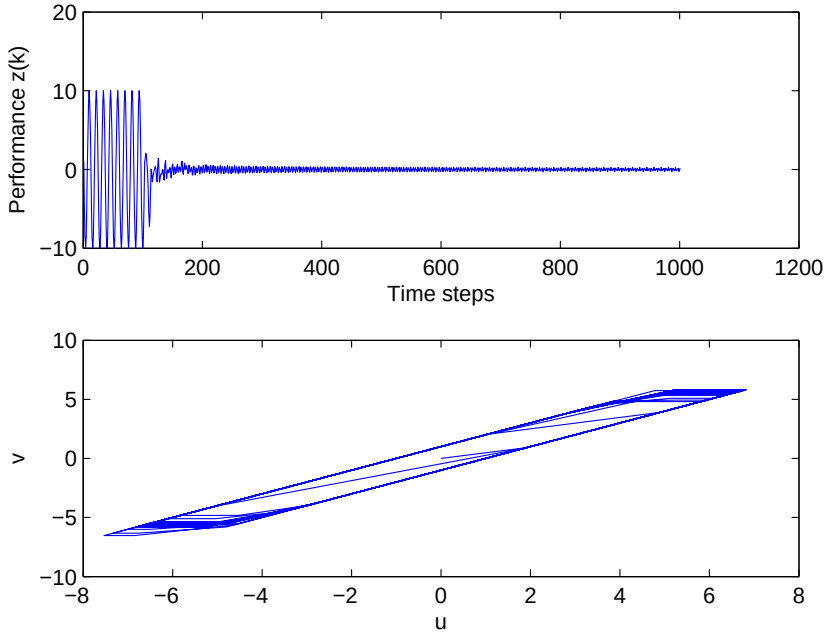

Figure 2.16: Closed-loop response of the first order plant G_1 with controller coefficients obtained from ID with hysteresis modeled by a play operator with $r = 1$. The command input is $w(k) = 10 \sin \omega k$, where $\omega = \pi/6$ rad/sample. For ID, the plant order is assumed to be 3 with relative degree 1.

the plant order is $n = 5$ with relative degree $d = 1$. The pole-zero map of the identified plant is shown in Figure 2.24(a). The closed-loop response with adaptive controller is shown in Figure 2.24(b). ■

2.3.4 Sensitivity to Hysteresis Width

We consider the minimum-phase first-order stable plant $G_1 = \frac{1}{z-0.5}$, and use the play operator to represent the input hysteresis. We consider a command-following problem with either the unit step input $w(k) \equiv 1$ or the sinusoid input $w(k) = 10 \sin \omega k$, where $\omega = \pi/6$ rad/sample. We simulate the system and consider the steady-state performance error $z(k)$ for various values of the play width r. The steady-state performance error, normalized by the open-loop steady-state error, is shown in Figure 2.25. For a sinusoidal command, the performance is more sensitive

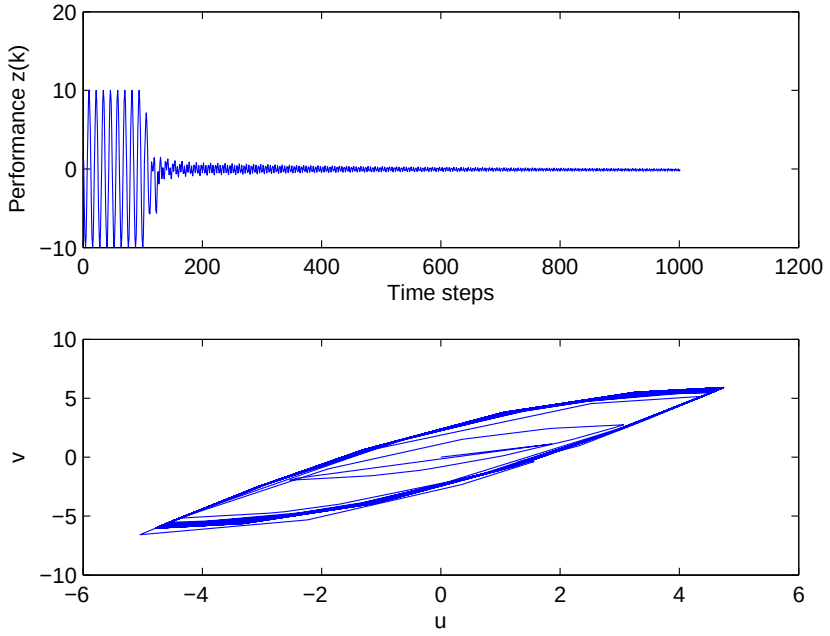

Figure 2.17: Closed-loop response of the first order plant G_1 with controller coefficients obtained from ID with PI hysteresis model. The command input is $w(k) = 10 \sin \omega k$, where $\omega = \pi/6$ rad/sample. The plant order is assumed to be 5 with relative degree 1.

to the width of the hysteresis than for the unit step command. When the ratio of $\frac{z_{ss}}{z_{ol}}$ is equal to 1, the performance of the closed-loop system is the same as the open-loop system. The normalized error $\frac{z_{ss}}{z_{ol}}$ is less than 30% for $\frac{r}{u_{ss}} \leq 1$. Note that the control problem becomes more challenging as we increase the width of the play operator, which results in larger steady-state control input u_{ss}. In particular, for $\frac{r}{u_{ss}} = 2$, Figure 2.26 compares the steady state control input u_{ss} with and without hysteresis.

2.3.5 Summary

In this section we tested the RCAC possibility of command tracking in nonminimum phase systems with a hysteretic input nonlinearity. RCAC is used in all the scenarios. The hysteresis is modeled with the play operator or the Prandtl-Ishlinskii model. The RCA controller requires the knowledge of the NMP zeros in the system in order to function properly. The system was simulated in two different scenarios.

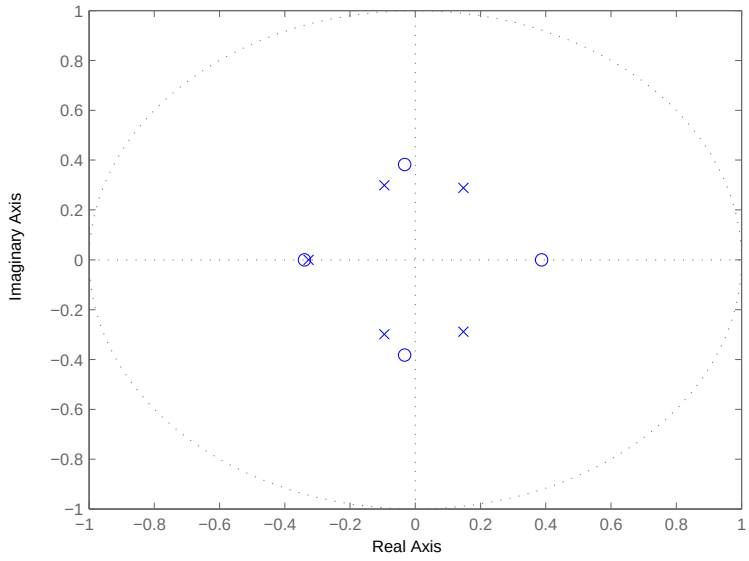

(a)

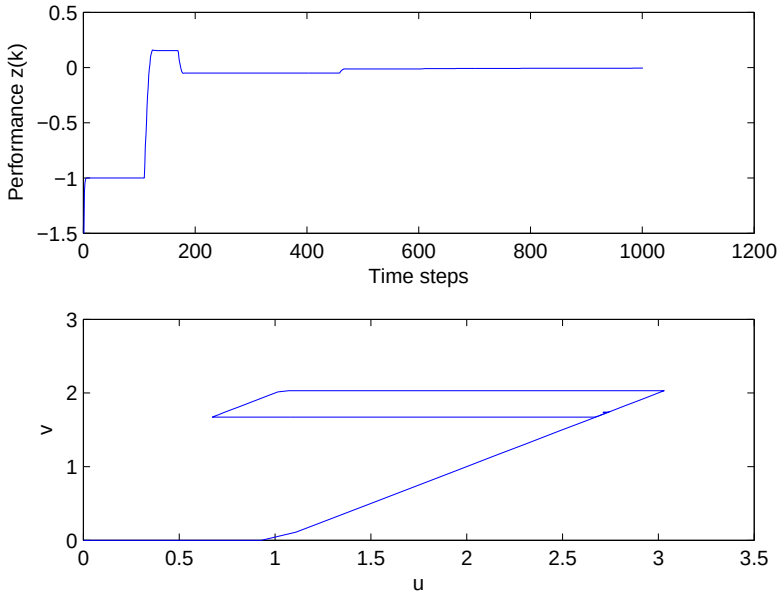

(b)

Figure 2.18: Closed-loop response of the second order plant $G_{2\mathrm{MP}}$ with one minimum-phase zero and controller coefficients obtained from ID. (a) shows the pole-zero map of the identified fifth order plant. (b) shows the closed loop response. The plant order is assumed to be 5 with relative degree 1.

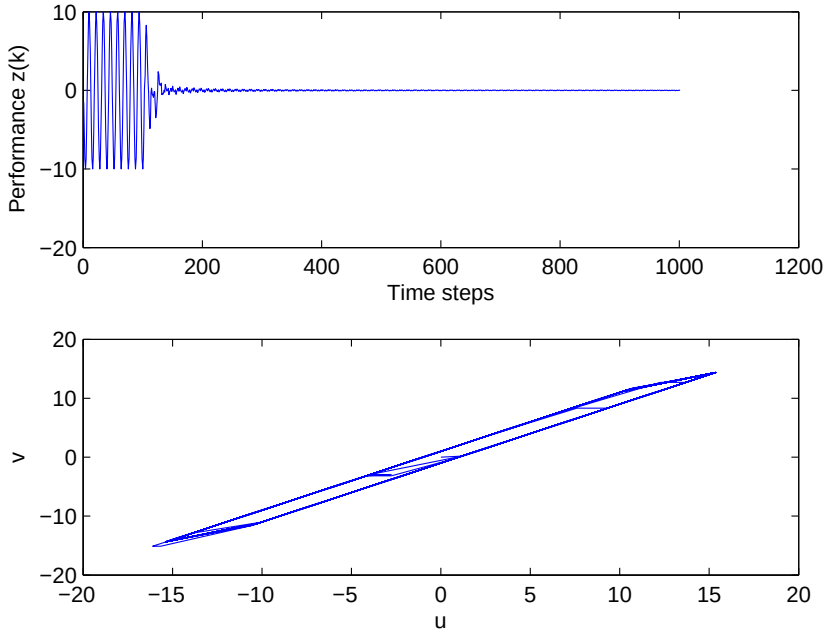

Figure 2.19: Closed-loop response of the second order plant $G_{2\text{MP}}$ with one minimum-phase zero and with controller coefficients obtained from ID. The command input is $w(k) = 10 \sin \omega k$, where $\omega = \pi/6$ rad/sample.

First, we assumed that the plant and the location of the NMP zeros were exactly known. Then, the NMP zeros were determined through a least-squares identification of the hysteresis and the plant. In both cases, and for steps and sinusoidal commands, RCAC was able to follow the reference command.

2.4 Examples of Adaptive Control of the Air and EGR Flow System in a Diesel Engine

In contrast to spark-ignition engines, diesel engines use compression to initiate ignition and achieve high fuel efficiency. According to [40], diesel engines presently account for more than 50% of all new car sales in Europe. However, diesel engines present various challenges in practice, primarily with regard to emissions [41]. Motivated by this challenge, we consider a control problem for a turbocharged diesel

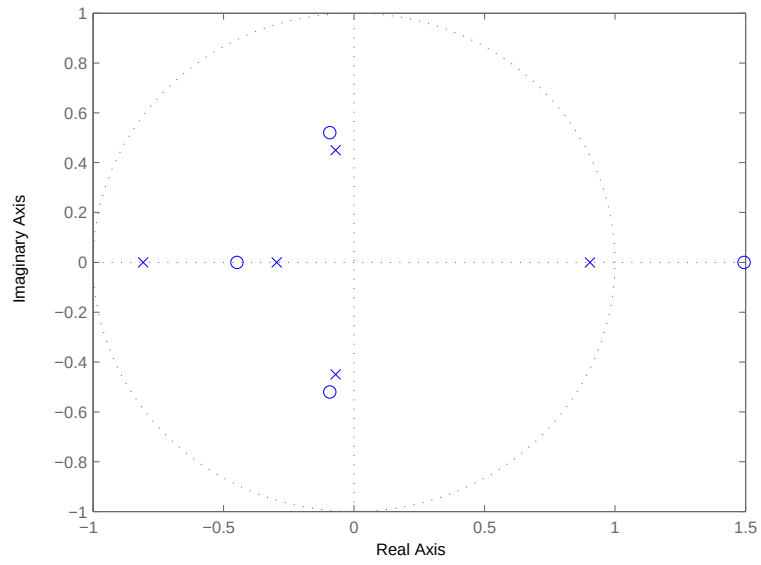

(a)

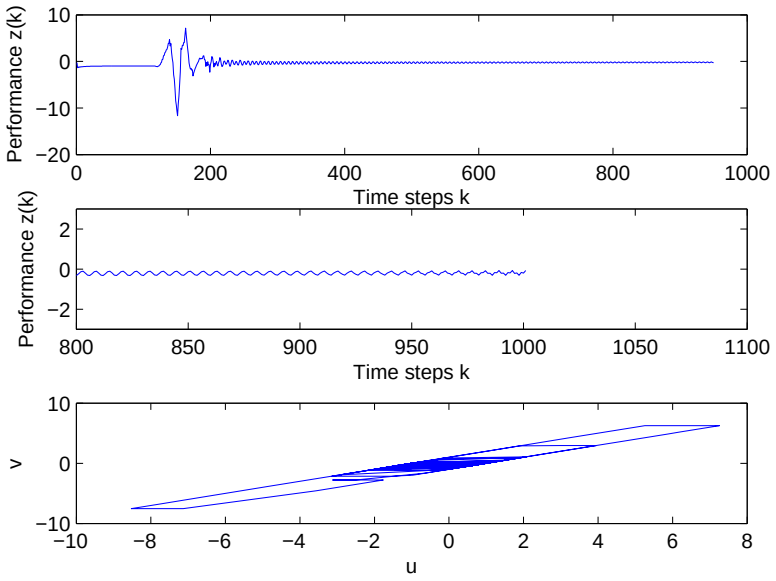

(b)

Figure 2.20: Closed-loop response of the second order plant with nonminimum-phase zero $G_{\text{2NMP}} = \frac{z-1.5}{(z+0.8)(z-0.9)}$ with controller coefficients obtained from ID and unit step command. (a) shows the pole-zero map of the identified fifth order plant. (b) shows the performance $z(k)$ and the hysteresis in the system. For ID, the plant order is assumed to be 5 with relative degree 1.

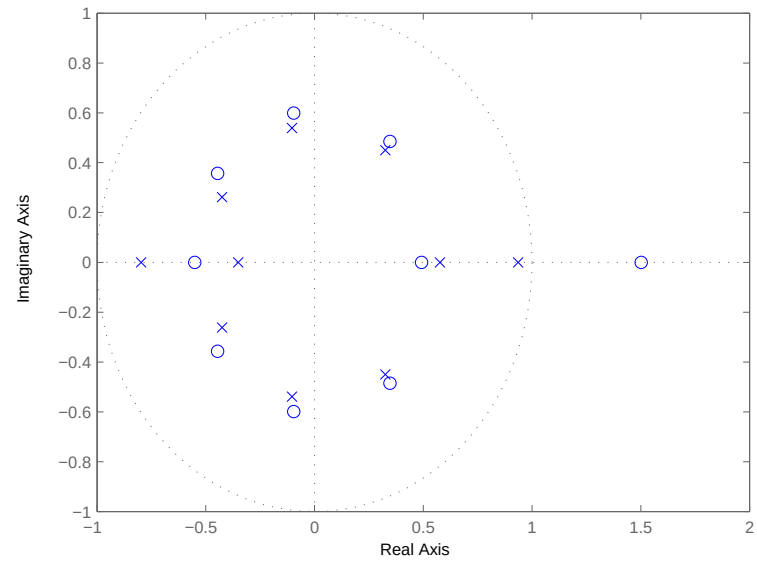

(a)

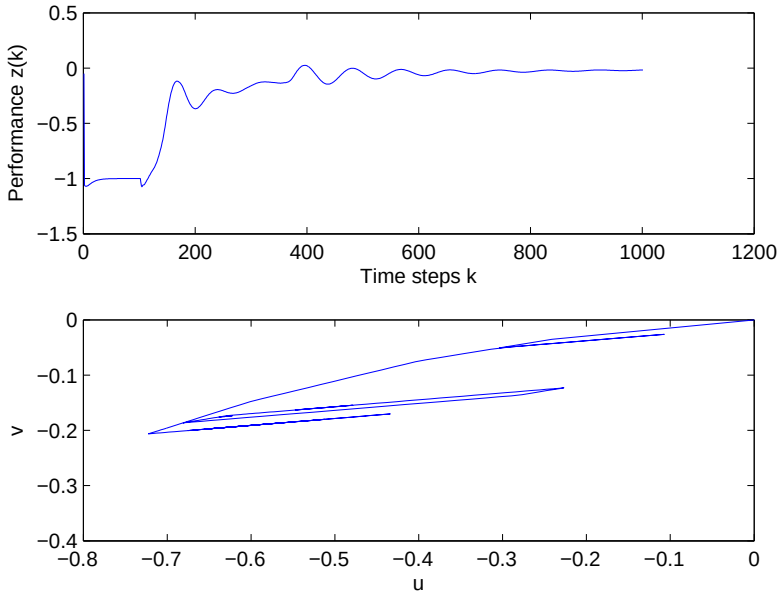

(b)

Figure 2.21: Closed-loop response of the second order plant G_{2NMP} to a unit step input with controller coefficients obtained from ID. The hysteresis is modeled with a PI model with parameters $N = 100$, $r_j = 0.05j$ for $j = 1, \ldots, N$, $p(r) = 0.5e^{-0.5r}$, $q = 0.5$, and $\gamma(v) = 5\tanh(0.05v)$. (a) shows the pole-zero map of the identified tenth order plant. (b) shows the closed loop response.

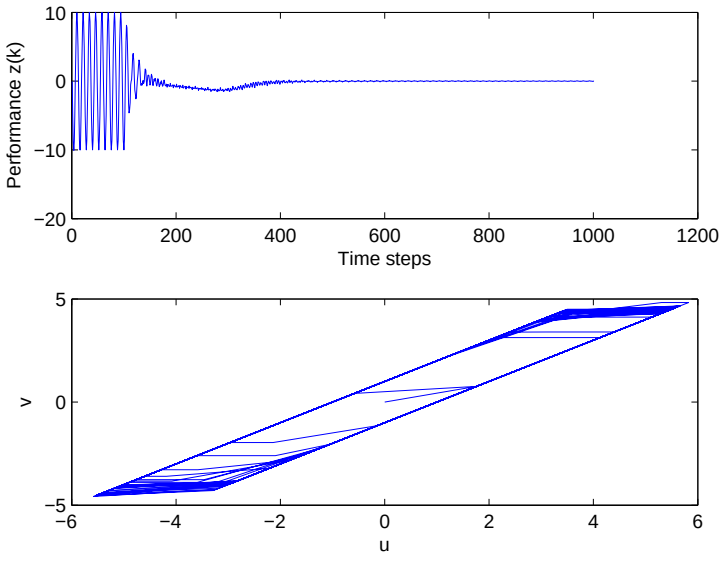

Figure 2.22: Closed-loop response of the second order plant $G_{2\text{NMP}}$ with one NMP zero and with controller coefficients obtained from ID. The command input is $w(k) = 10 \sin \omega k$, where $\omega = \pi/6$ rad/sample.

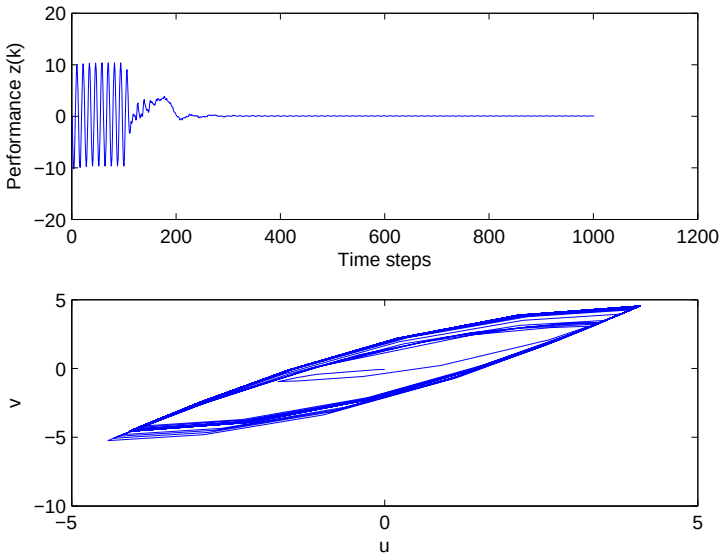

Figure 2.23: Closed-loop response of the second order plant $G_{2\text{NMP}}$ with one NMP zero and with controller coefficients obtained from ID. The hysteresis is modeled with a PI model with parameters $N = 100$, $r_j = 0.05j$ for $j = 1, \ldots, N$, $p(r) = 0.5e^{-0.5r}$, $q = 0.5$, and $\gamma(v) = 5 \tanh(0.05v)$. The command input is $w(k) = 10 \sin \omega k$, where $\omega = \pi/6$ rad/sample.

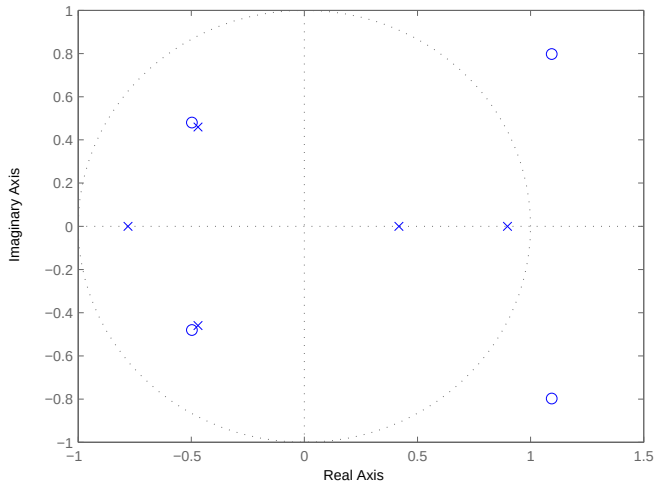

(a)

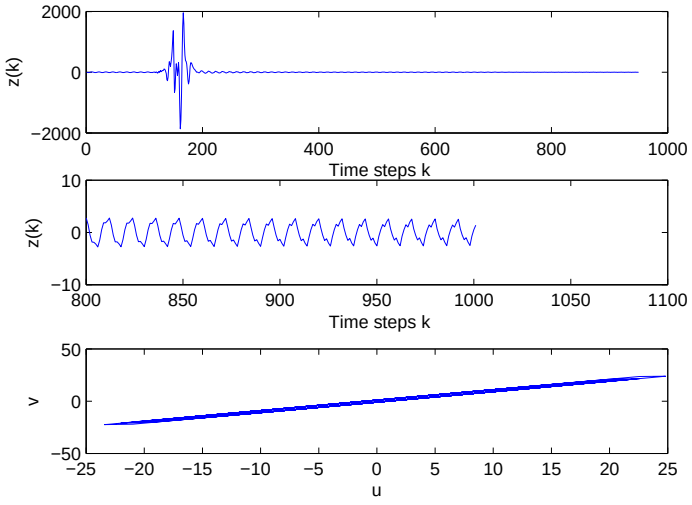

(b)

Figure 2.24: Closed-loop response of the third order plant with two nonminimum-phase zeros $G_{\text{3NMP}} = \frac{z^2-2.2z+1.85}{(z-0.3)(z+0.8)(z-0.9)}$ with controller coefficients obtained from ID. The plant order is assumed to be 5 with relative degree 1. We model the hysteresis with a play operator with $r = 1$ and set the input to a sinusoidal signal $w(k) = 10 \sin \omega k$, where $\omega = \pi/6$ rad/sample. (a) shows the pole-zero map of the identified fifth order plant. (b) shows the performance $z(k)$ and the hysteresis in the system. Comparing to Figure 2.13, the large transient in this figure is due to identification error.

engine (Figure 2.27) with Exhaust Gas Recirculation (EGR) valve, EGR throttle, and Variable Geometry Turbocharger (VGT) actuation. The turbocharger increases

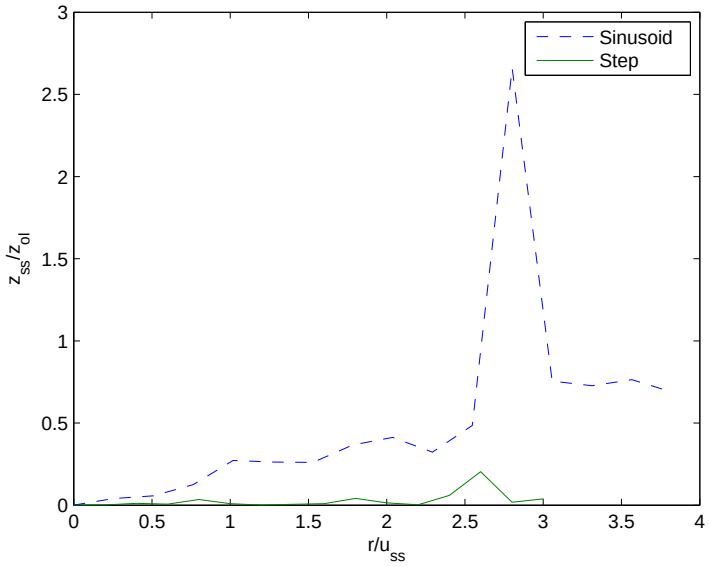

Figure 2.25: Normalized performance error for various values of hysteresis width. z_{ss} is the steady-state value of the system with hysteresis and the adaptive controller, z_{ol} is the error of the open-loop system with same hysteresis, r is the width of the play operator, and u_{ss} is the steady-state control input to the system without hysteresis. Note that for a sinusoid command input, the response is sensitive to the ratio $\frac{r}{u_{ss}} = 2.6$.

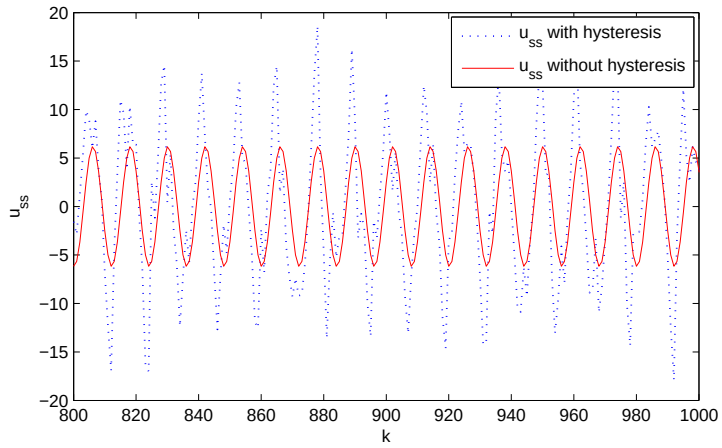

Figure 2.26: For $\frac{r}{u_{ss}} = 2$ in Figure 2.25, we stimulate the steady state control input u_{ss} corresponding to the systems with and without hysteresis. Note that when hysteresis is present, the adaptive controller compensates for the deadzone by producing a larger control amplitude.

engine air flow by utilizing the energy of the exhaust gas. The variable-geometry actuator changes the effective flow area of the turbine as well as the angle at which the flow is directed at the turbine blades. The EGR valve and EGR throttle are used to recirculate a fraction of the burnt gas in the exhaust back to the engine cylinders in order to reduce the emission of nitrogen oxides. For background on modeling and control of diesel engines, see [42]. Several prior approaches to controlling diesel engines with EGR and VGT actuation are discussed in the survey article [43].

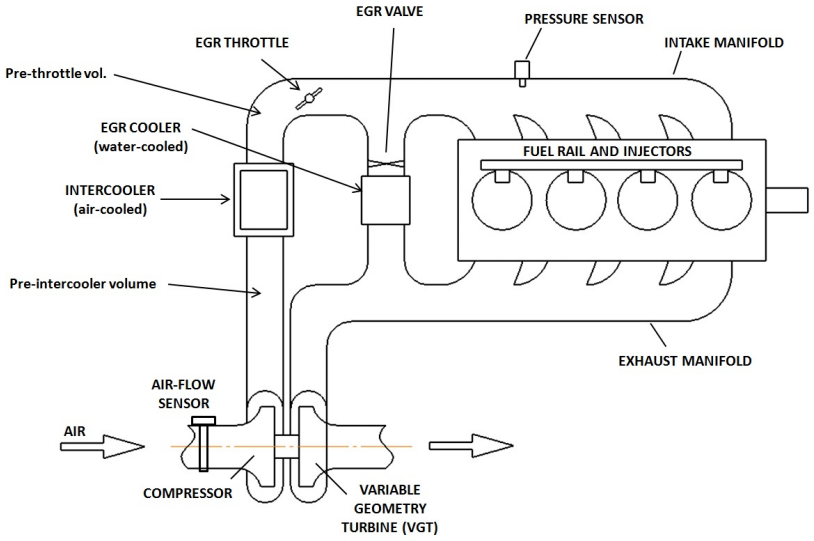

Figure 2.27: Schematics of a typical diesel engine.

The goal of the present example is to develop a controller to track setpoints in the intake manifold pressure (MAP) and EGR rate. The EGR rate is defined as the percent ratio of flow through the EGR valve to the flow through the engine cylinders. The setpoints depend on operating conditions of the engine and driver inputs. The setpoint map is determined during engine calibration in order to reduce fuel consumption and emissions. The control inputs are VGT percent closed, EGR throttle percent closed, and EGR valve percent open. To ensure good vehicle drivability and performance, the control objectives are to achieve fast tracking of the intake manifold pressure setpoint with small overshoot. In addition, zero steady-state error is

desirable for both EGR rate and intake manifold pressure outputs.

To develop a controller that achieves these objectives, we consider a mean-value model with ten states, including pressure, density, and burnt-gas fraction in the intake manifold; pressure, density, and burnt-gas fraction in the exhaust manifold; as well as turbocharger speed, pre-throttle pressure, EGR cooler temperature, and exhaust manifold heat transfer state. While the open-loop dynamics are stable, they are known to be nonlinear. In addition, the linearized model possesses a nonminimum-phase zero in one of the input-output channels [42].

To control the diesel air-flow system, we apply retrospective-cost adaptive control (RCAC) to the linearized model. RCAC is a discrete-time approach to adaptive stabilization, command following, and disturbance rejection for systems that are SISO or MIMO and possibly nonminimum phase [23, 25, 26, 27]. The modeling information that RCAC requires consists of Markov parameters of the plant transfer function from the control input to the performance variables. For SISO systems, a single Markov parameter typically provides sufficient modeling information, even for nonminimum-phase plants [30, 29]. The Markov parameters provide a finite-impulse-response (FIR) approximation of the plant that is used for controller update. In some cases, a more efficient approximation can be constructed based on frequency-domain data; the robustness of RCAC to uncertainty in these data is discussed in [44]. From an identification perspective, RCAC provides guidance on the plant modeling information needed for adaptive control and the required accuracy of that modeling data.

In the present example we apply RCAC to the linearized mean-value model, and we consider a command-following problem involving intake manifold pressure and EGR rate check. Since the plant has two outputs and three inputs, RCAC requires two Markov parameters, which are obtained from the linearized state space model. In practice, these data could be obtained using system identification techniques [31]. To demonstrate the operation of the closed-loop system, we simulate the RCAC

controller with a model linearized at a chosen operating point. We also demonstrated that RCAC is able to follow step commands for the nonlinear diesel engine model, provided two Markov parameters of the linearized engine plant model are known.

2.4.1 Application to Turbocharged Diesel Engines

To apply RCAC to a turbocharged diesel engine, we control VGT percent closed V, EGR throttle percent closed $E_{\rm t}$, and EGR valve percent open $E_{\rm v}$ using measurements of the intake manifold pressure $P_{\rm i}$ and an estimate of the EGR rate $E_{\rm r}$. The Markov parameters are based on the state-space matrices of the linearized diesel engine model.

We linearize the nonlinear engine model at engine speed of 1671 RPM. For the linearized diesel engine, the discrete state-space form of the model with a sample time $T_{\rm s} = 0.01$ sec is given by

$$\tilde{x}(k+1) = \tilde{A}\tilde{x}(k) + \tilde{B}\tilde{u}(k) + \tilde{D}_1\tilde{w}(k), \tag{2.16}$$

$$\tilde{y}(k) = \tilde{C}\tilde{x}(k) + \tilde{D}\tilde{u}(k), \tag{2.17}$$

$$\tilde{z}(k) = \tilde{r}(k) - \tilde{y}(k), \tag{2.18}$$

where $\tilde{x} \triangleq \left[\begin{array}{cccccccccc} P_{\rm i} & P_{\rm e} & \omega_{\rm tc} & P_{\rm p} & T_{\rm d} & \rho & C_{\rm m} & \rho_{\rm e} & F_{\rm i} & F_{\rm e} \end{array}\right]^{\rm T}$, $\tilde{u} \triangleq \left[\begin{array}{ccc} V & E_{\rm t} & E_{\rm v} \end{array}\right]^{\rm T}$, $\tilde{y} \triangleq \left[\begin{array}{cc} P_{\rm i} & E_{\rm r} \end{array}\right]^{\rm T}$, $\tilde{r}$ is the vector of the commands, and $\tilde{w}$ is the unknown disturbance. The states are intake manifold pressure $P_{\rm i}$ (kPa), exhaust manifold pressure $P_{\rm e}$ (kPa), turbo rotational speed $\omega_{\rm tc}$, prethrottle manifold pressure $P_{\rm p}$ (kPa), EGR cooler temperature $T_{\rm d}$, intake manifold density ρ (kg/m^3), exhaust heat transfer state $C_{\rm m}$, exhaust manifold density $\rho_{\rm e}$ (kg/m^3), intake manifold burnt gas fraction $F_{\rm i}$, and exhaust manifold burnt gas fraction $F_{\rm e}$. The inputs are VGT percent closed V, EGR throttle percent closed $E_{\rm t}$, and EGR valve percent open $E_{\rm v}$, while the available measurements are $P_{\rm i}$ and $E_{\rm r}$. The matrices $\tilde{A} \in \mathbb{R}^{10\times10}$, $\tilde{B} \in \mathbb{R}^{3\times10}$, $\tilde{C} \in \mathbb{R}^{2\times10}$, and $\tilde{D} \in \mathbb{R}^{2\times3}$ are given by (2.19)-(2.20). Note that all the eigenvalues of $\tilde{A}$ are within the unit circle,

$$\tilde{A} = \left[\begin{array}{cccccccccc}
0.1962 & 0.0437 & 0.0033 & 0.1305 & 0.0024 & 0.7039 & 0.0011 & -0.1524 & -0.0098 & -0.0000 \\
0.0271 & 0.2926 & 0.0005 & 0.0860 & -0.0050 & 13.4343 & 0.0182 & 28.5360 & -0.2668 & -0.0014 \\
1.5911 & 1.9022 & 0.9702 & 1.2428 & -0.0018 & 23.8505 & 0.0427 & -30.0380 & -0.3285 & -0.0012 \\
0.1861 & 0.0403 & 0.0034 & 0.1236 & 0.0022 & 0.6248 & 0.0010 & -0.1527 & -0.0083 & -0.0000 \\
0.0667 & 1.9737 & 0.0001 & 0.0456 & 0.3653 & 1.0430 & 0.0487 & -390.9750 & -0.3967 & -0.0015 \\
-0.0059 & -0.0001 & 0.0000 & 0.0012 & -0.0000 & 0.9401 & -0.0000 & 0.0055 & -0.0000 & -0.0000 \\
2.4830 & 0.0724 & -0.0022 & -0.2249 & 0.0083 & -344.6835 & 0.3690 & -1.0773 & -12.2236 & -0.0934 \\
-0.0001 & -0.0019 & 0.0000 & 0.0004 & -0.0000 & 0.0887 & -0.0000 & 0.9196 & 0.0003 & 0.0000 \\
0.0005 & 0.0002 & -0.0000 & -0.0002 & 0.0000 & 0.0023 & 0.0000 & 0.0017 & 0.9412 & 0.0122 \\
0.0003 & 0.0000 & -0.0000 & -0.0001 & 0.0000 & -0.0533 & 0.0000 & -0.0000 & 0.1646 & 0.8275
\end{array}\right], \tag{2.19}$$

$$\tilde{B} = \left[\begin{array}{ccc}
0.0246 & -0.0061 & 0.0438 \\
0.6297 & -0.0021 & -0.1892 \\
-1.2203 & 0.0120 & -0.1701 \\
0.0206 & 0.0022 & 0.0391 \\
0.2814 & -0.0009 & -0.0846 \\
-0.0000 & -0.0001 & -0.0001 \\
0.0262 & 0.0053 & 0.0670 \\
0.0027 & -0.0000 & -0.0008 \\
0.0001 & 0.0000 & 0.0002 \\
0.0000 & 0.0000 & 0.0000
\end{array}\right], \tilde{C} = \left[\begin{array}{cccccccccc}
1.0000 & 0 & 0 & 0 & 0 & 0 & 0 & 0 & 0 & 0 \\
-0.8792 & 0.8687 & -0.0284 & 5.3820 & 0.0337 & 0 & 0 & 0 & 0 & 0
\end{array}\right],$$

$$\tilde{D} = \left[\begin{array}{ccc} 0 & 0 & 0 \\ 0 & 0 & 0.7219 \end{array}\right]. \tag{2.20}$$

---

and thus the linearized diesel engine plant is asymptotically stable. However, the transfer function of the linearized engine model from E_{v} to E_{r} is nonminimum phase at all operation points.

Since the linearized model is exactly proper, that is, $\tilde{D}$ in (2.17) is nonzero, we add a unit delay to the output $\tilde{y}(k)$ such that $y(k) = \tilde{y}(k-1)$, and therefore the first two nonzero Markov parameters used to implement (2.14) in RCAC are $H_1 \triangleq \tilde{C}\tilde{B}$ and $H_2 \triangleq \tilde{C}\tilde{A}\tilde{B}$. RCAC generates a control signal $u(k)$ that attempts to minimize the performance variable $\tilde{z}(k)$, which is the command-following error based on the intake manifold pressure and EGR rate. We assume that measurements of only $\tilde{z}(k)$ are available for feedback. We initialize the adaptive control gains to zero, that is, $\theta(0) = 0$, and we choose the controller order $n_{\mathrm{c}} = 12$ and the covariance matrix $P(0) = 10^{-3} I_{5n_{\mathrm{c}}}$. These values are found by trial and error. Furthermore, since the linearized model is nonminimum phase, we choose the regularization $\eta(k) = z^{\mathrm{T}}(k)z(k)$ [25] and $R_2 = \left[\begin{array}{ccc} 0 & 0 & 0 \\ 0 & 0 & 0 \\ 0 & 0 & 1 \end{array}\right]$ for the input from EGR E_{v} to E_{r}. Finally we do not use a forgetting factor in the adaptive controller, that is, $\lambda = 1$. Figure 2.28 and

2.29 show the time history of the intake manifold pressure $P_{\rm i}$ and EGR rate $E_{\rm r}$ in response to step commands. The numerical results show the ability of RCAC to make the outputs $P_{\rm i}$ and $E_{\rm r}$ follow the commands, while Figure 2.30 shows the time history of the control inputs V, $E_{\rm t}$, and $E_{\rm v}$ from RCAC. Note that zero steady-state tracking errors are achieved for both the intake manifold pressure and EGR rate outputs with satisfactory transient behavior. However, as shown in Figure 2.30(b), the adaptive controller uses large control signals in the EGR throttle percent closed ($E_{\rm t} \in (-580, 520)$), that exceeds the actuator range of travel ($E_{\rm t} \in [0, 100]$). We note that the controller does not use the EGR valve extensively, which is reasonable given that at this operating point the pressure drop across the EGR valve is small and throttle authority is essential for following the commands.

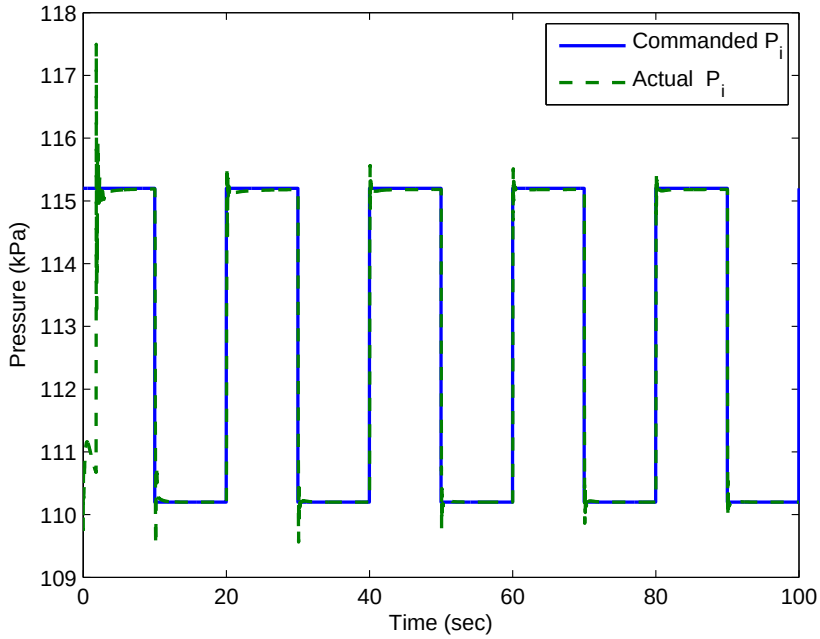

Figure 2.28: *Command following for the linearized diesel engine model:* Intake manifold pressure $P_{\rm i}$ in response to step changes in the setpoint. Note that zero steady-state tracking error is achieved for the intake manifold pressure outputs.

Next, we implement the adaptive controller with saturated outputs. To do this, we

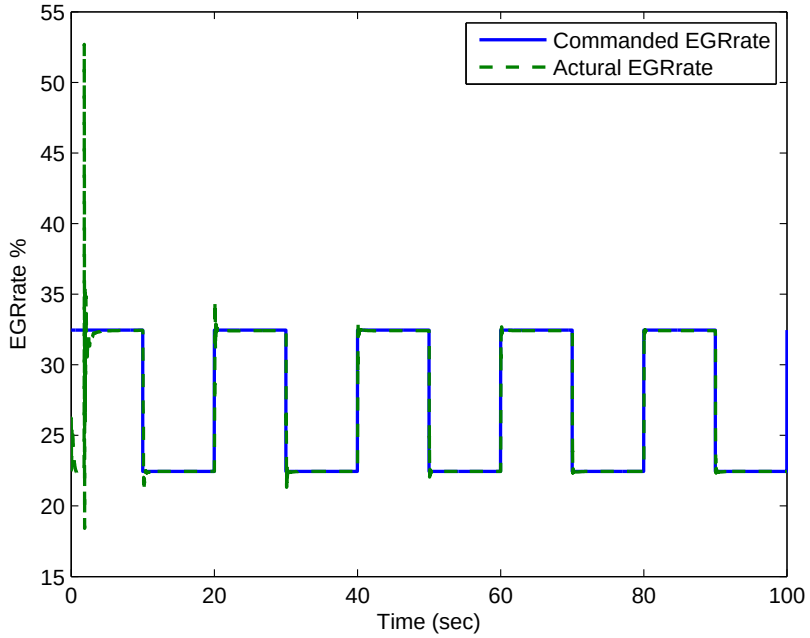

Figure 2.29: *Command following for the linearized diesel engine model:* EGR rate E_{r} in response to step changes in the setpoint. Note that zero steady-state tracking error is achieved for EGR rate.

set three different saturation levels based on the trim conditions of the control inputs V, E_{t}, and E_{v}. In particular, we choose $\eta(k) = z^{\mathrm{T}}(k)z(k), n_{\mathrm{c}} = 12, P(0) = 10^{-4}I_{5n_{\mathrm{c}}}$, R_2 as above, and initialize the control gains to zero. Figures 2.31 and 2.32 show that the output of the linearized model follows the step commands; however, the transient response is degraded due to the limits imposed on the control inputs. Figure 2.33 shows the time history of the control inputs V, E_{t}, and E_{v}. Note that, in this case, all the control signals are within the admissible range, that is, between 0 and 100 percent.

Next, we consider a disturbance rejection problem, where the control objective is to drive z to zero in the presence of the sinusoidal disturbance $w(k) = 0.01\sin(0.25\pi k)$, whose frequency, phase, and amplitude are unknown to the controller. We assume that the first two nonzero Markov parameters are known, but no other information about the system is assumed to be known. Figure 2.34 shows that RCAC rejects the

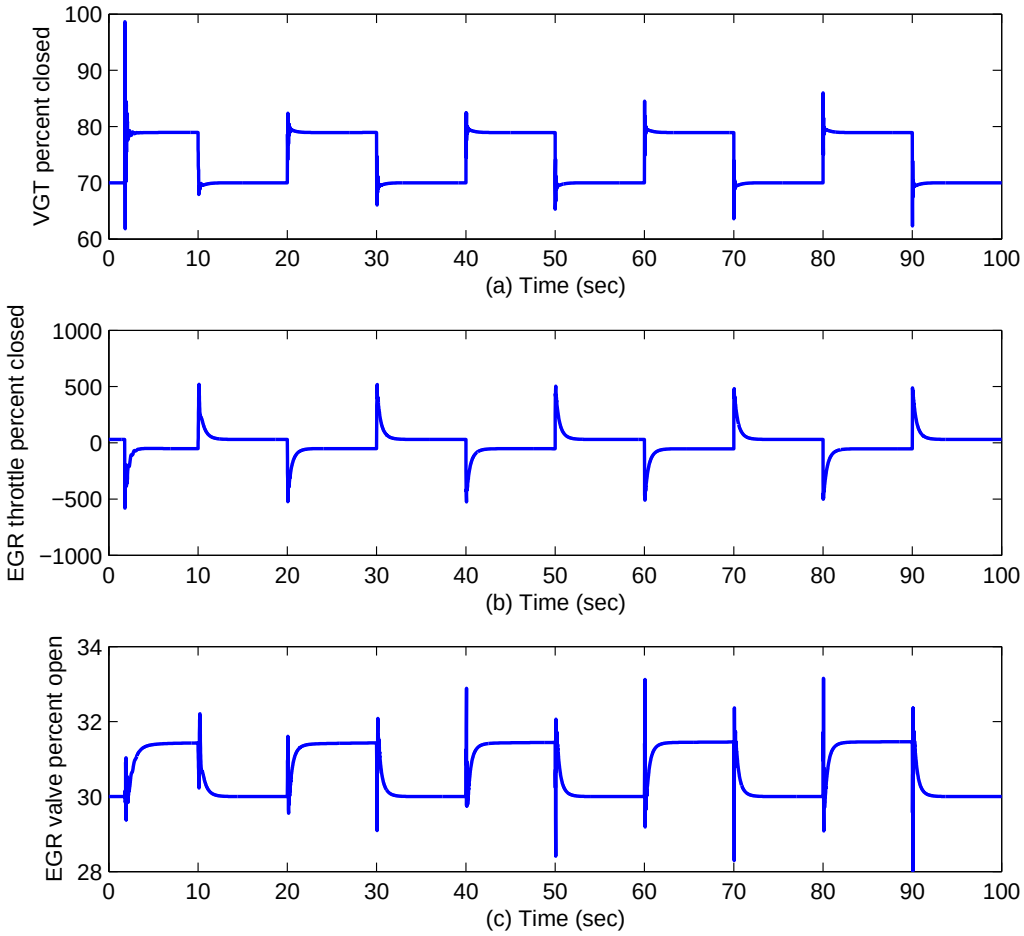

Figure 2.30: Control inputs VGT percent closed V (a), EGR throttle percent closed E_{t} (b), and EGR valve percent open E_{v} (c) corresponding to the closed-loop response shown in Figure 2.28 and Figure 2.29. Note that in this case, the adaptive controller uses large control authority in the EGR throttle percent closed ($E_{\mathrm{t}} \in (-580, 520)$), which exceeds the limits $E_{\mathrm{t}} \in [0, 100]$.

disturbance and drives z to zero.

Finally, we include preliminary results where we apply RCAC to the nonlinear diesel engine system. The first two nonzero Markov parameters $H_1 = \tilde{C}\tilde{B}$ and $H_2 = \tilde{C}\tilde{A}\tilde{B}$ of the linearized diesel engine (2.19)-(2.20) are used as the only model information for the nonlinear engine plant for the controller. We implement the RCAC controller with saturated outputs, and we set three different saturation levels based on

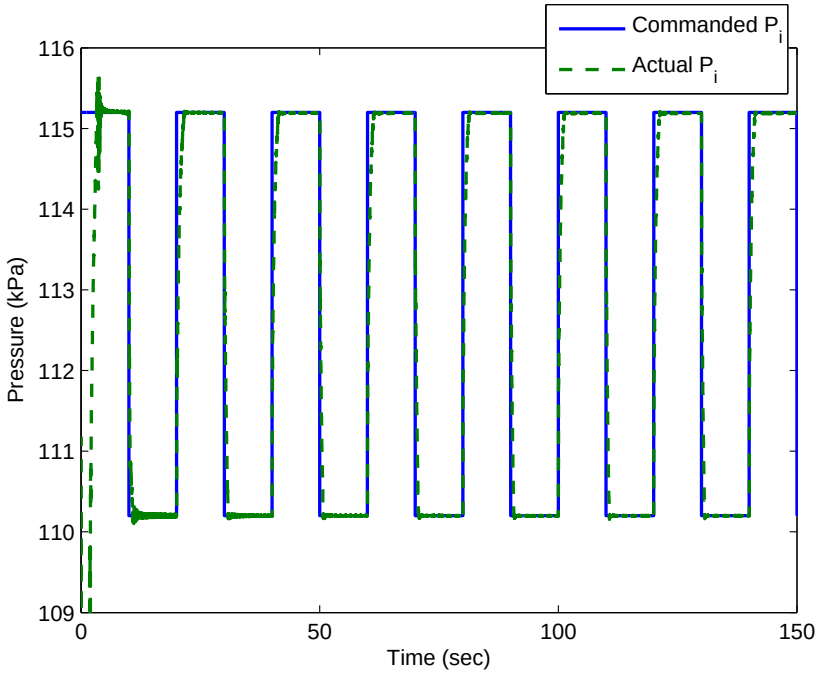

Figure 2.31: *Command following for the linearized diesel engine model*: Intake manifold pressure $P_{\rm i}$ in response to step commands. Note that zero steady-state tracking error is achieved for the intake manifold pressure outputs. In this case, where the control signals are saturated, the transient response is degraded relative to Figure 2.28.

the trim conditions of the control inputs V, E_t and $E_{\rm v}$. Measurements of only $z(k)$ are available for feedback. In particular, we choose $\eta(k) = 0.01, n_{\rm c} = 12, P(0) = 10^{-3} I_{5n_{\rm c}}$, R_2 as above, and initialize the control gains to zero. Figures 2.35(a) and 2.35(b) show that the output of the nonlinear diesel model follow the step commands. Figures 2.35(c), (d), and (e) show the time history of the control inputs V, $E_{\rm t}$, and $E_{\rm v}$. Note that, since we saturate the RCAC control, all of the control outputs are within the admissible range, that is, between 0 and 100 percent.

2.4.2 Summary

In this example, we considered command-following and disturbance-rejection problems for a diesel engine. RCAC was used with limited modeling information, namely, the first two nonzero Markov parameters of the linearized plant. The problem is chal-

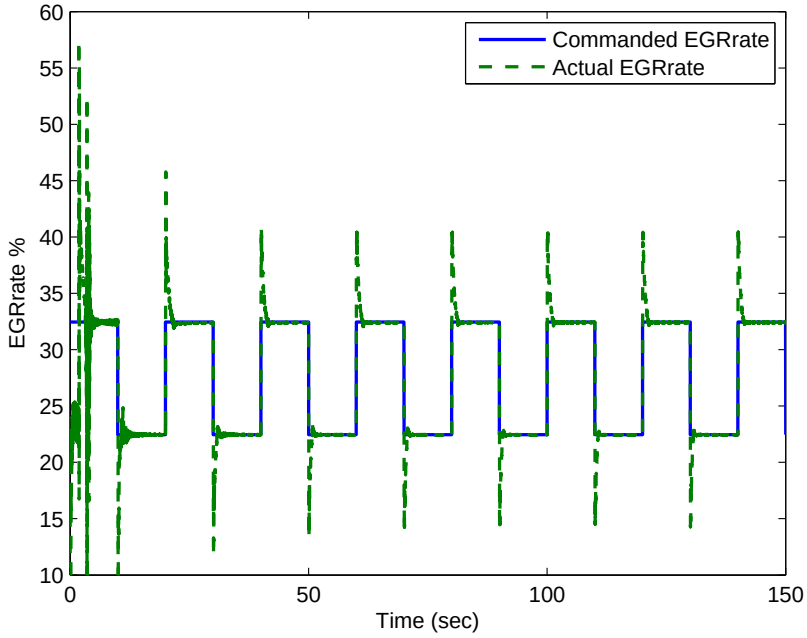

Figure 2.32: *Command following for the linearized diesel engine model:* EGR rate E_{r} in response to steps in the setpoint. Note that zero steady-state tracking error is achieved for EGR rate. In this case, where the control signals are saturated, the transient response is worse than the response in Figure 2.29.

lenging as the engine exhibits nonminimum phase characteristics. First, we assumed there is no bound on the control inputs. Then, we considered the more realistic case where we saturate the control outputs using physical bounds. In both cases, RCAC was able to follow the reference commands. Finally, we demonstrated disturbance rejection for disturbances with unknown spectra. Future research will focus on robustness of RCAC to uncertainty in the Markov parameters as well as completing the development of RCAC for the full operating range of the diesel engine based on the nonlinear model.

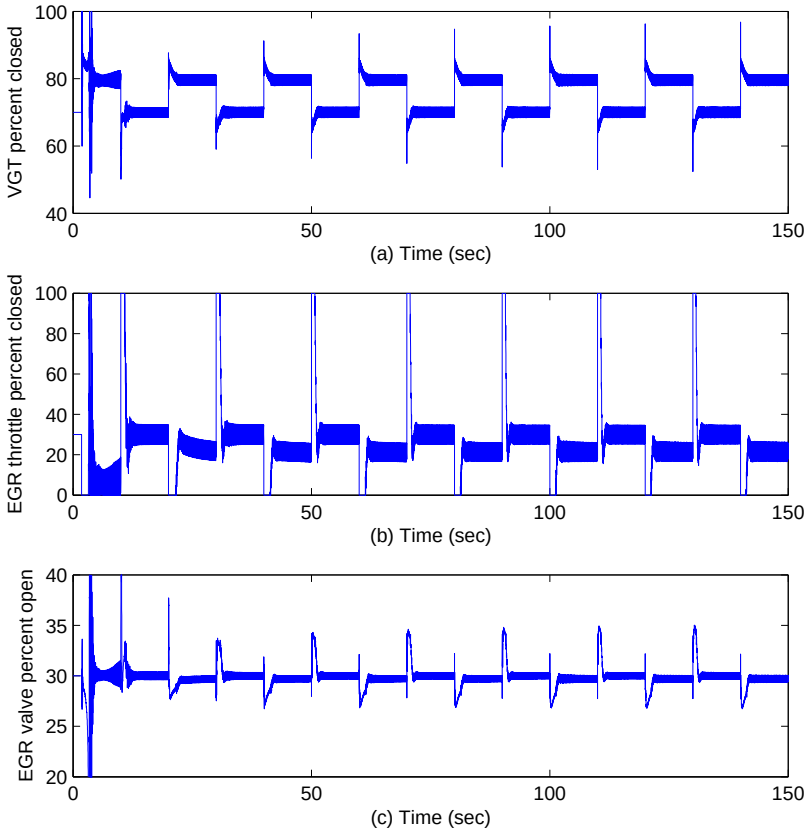

Figure 2.33: Control inputs VGT percent closed V (a), EGR throttle percent closed E_{t} (b), and EGR valve percent open E_{v} (c) corresponding to the closed-loop response shown in Figures 2.31 and 2.32. Note that in this case, all of the control signals are within the admissible range, that is, between 0 and 100. Compared with Figure 2.30, the response is degraded due to the limits imposed on the control input E_{t} and high gains of the controllers. Note that E_{v} to P_i is of nonminimum-phase.

2.5 Examples of Setpoint Control of the Uncertain Electromagnetically Controlled Oscillator

Inverse square laws are ubiquitous in physics, for example, in gravitational, electromagnetic, and electrostatic fields. Electromagnetic and electrostatic fields are widely used as a means of actuation. When applied over a fixed gap, electromagnetic actuation is easy to manage; this is the basis of rotary motors. When applied over a variable

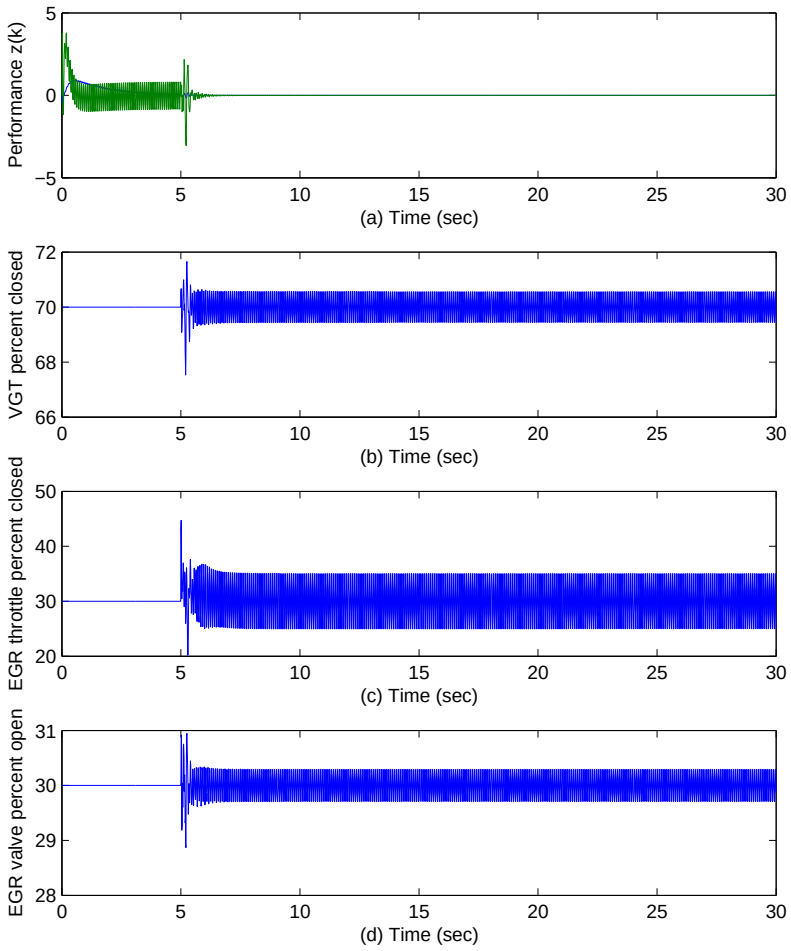

Figure 2.34: *Disturbance rejection for the linearized diesel engine model:* The adaptive control uses knowledge of the first two nonzero Markov parameters to reject a sinusoidal disturbance acting on the linearized engine model. The frequency, phase, and amplitude of the disturbance are assumed to be unknown. The adaptive control is turned on after 5 seconds and drives the performance z (a) to zero. Time history of control inputs VGT percent closed V, EGR throttle percent closed E_{t}, and EGR valve percent open E_{v} are shown in (b), (c), and (d), respectively.

gap, however, electromagnetic actuation can be challenging to work with. The electromagnetically levitated ball is a staple of control labs [45]. However, the restoring force in this case is uniform gravity and thus is independent of displacement. If, however, the restoring force is provided by a stiffness, then the restoring force depends

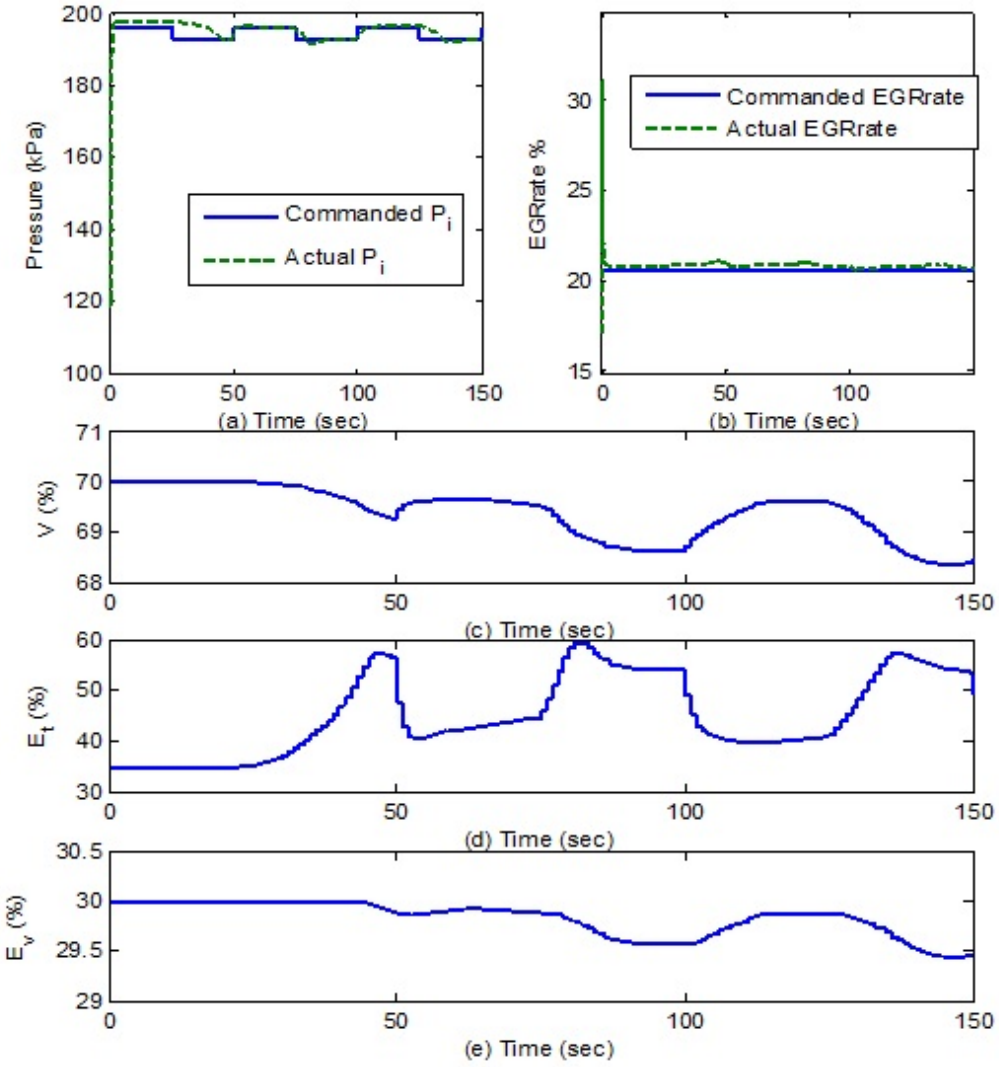

Figure 2.35: *Command following for the nonlinear diesel engine model:* (a) shows the intake manifold pressure $P_{\rm i}$ in response to a step command. (b) shows the EGR rate $E_{\rm r}$ in response to a step command. Figures 2.35(c), (d), and (e) show the time history of the control inputs V, $E_{\rm t}$, and $E_{\rm v}$. Note that, since we saturated the RCAC controller, all the control outputs are within the admissible range, that is, between 0 and 100 percent.

on the displacement, and this dependence leads to extremely challenging dynamics. We call this system the *electromagnetically controlled oscillator* (ECO).

Control of the ECO is considered in [46, 47, 48, 49, 50, 51] with applications to

linear motors in [52]. As shown in [50], the presence of the stiffness leads to unstable equilibria; in fact, for a linear spring, all equilibria beyond one-third of the initial gap are unstable, and these equilibria become increasingly unstable as the gap increases. In addition, as shown in Figure 2.38, for each equilibrium current, the ECO has two equilibria; consequently, the domain of attraction and transient response of the adaptive controller can lead to convergence to the "wrong" equilibrium. Another complicating factor is the fact that the applied force is proportional to the square of the current, which introduces a quadratic input nonlinearity [53]. A consequence of this quadratic nonlinearity is the fact that the electromagnetic force is able to pull but not push (assuming a nonmagnetic target mass) and thus the actuation is one-sided. The same observations apply to electrostatic actuation, which is used in MEMS devices [54, 55] and flexible antennas [56, 57].

The goal of the present example is to develop a control law for the ECO that is applicable to the case in which the mass, damping, and stiffness parameters are uncertain and, in addition, does not use detailed knowledge of the quadratic dependence on current and the inverse-quadratic dependence on the distance between the mass and the electromagnet. This goal is motivated by the realistic situation in which estimates of these parameters are uncertain due to measurement, identification, and calibration errors. Consequently, we do not attempt to invert the input nonlinearities as in [50].

The approach that we take in the present example is based on retrospective cost adaptive control (RCAC). RCAC is a direct digital control approach that requires minimal modeling information about the plant. RCAC was developed for linear systems, but is extended in [58, 59] to the case of Hammerstein systems with uncertain memoryless input nonlinearities. For the ECO we modify the approach of [58] to account for the fact that, for each equilibrium current, the ECO has two equilibria. Consequently, the domain of attraction and transient response of the adaptive

controller can lead to convergence to the "wrong" equilibrium. To counteract this possibility, we introduce a setpoint feedback path to assist RCAC in reaching the desired equilibrium as the position command increases and thus the mass is moved farther into the unstable region.

2.5.1 Equations of Motion and Equilibria of the ECO

Consider the ECO shown in Figure 2.36, where m is the mass, i is the manipulated input current to the electromagnet, $c > 0$ is the damping constant, and $k > 0$ is the spring constant. The displacement $q = 0$ corresponds to the position of the mass where the spring is relaxed, and ℓ is the gap between the electromagnet and the relaxed position of the mass. The dynamics of the oscillator are given by

$$m\ddot{q} + c\dot{q} + kq = \frac{\varepsilon i^2}{(\ell - q)^2}, \tag{2.21}$$

which can be written as

$$\begin{bmatrix} \dot{q} \\ \ddot{q} \end{bmatrix} = A_{\mathrm{c}} \begin{bmatrix} q \\ \dot{q} \end{bmatrix} + B_{\mathrm{c}} \frac{\varepsilon i^2}{(\ell - q)^2}, \tag{2.22}$$

where

$$A_{\mathrm{c}} \triangleq \begin{bmatrix} 0 & 1 \\ -\frac{k}{m} & -\frac{c}{m} \end{bmatrix}, \quad B_{\mathrm{c}} \triangleq \begin{bmatrix} 0 \\ \frac{1}{m} \end{bmatrix}. \tag{2.23}$$

The parameter ε is a force constant needed to render (2.21) dimensionally correct. For simplicity, we assume $\varepsilon = 1$ N-m^2/A^2.

Next, let $q_{\mathrm{eq}} \in (0, \ell)$ denote the desired equilibrium of the ECO. The corresponding

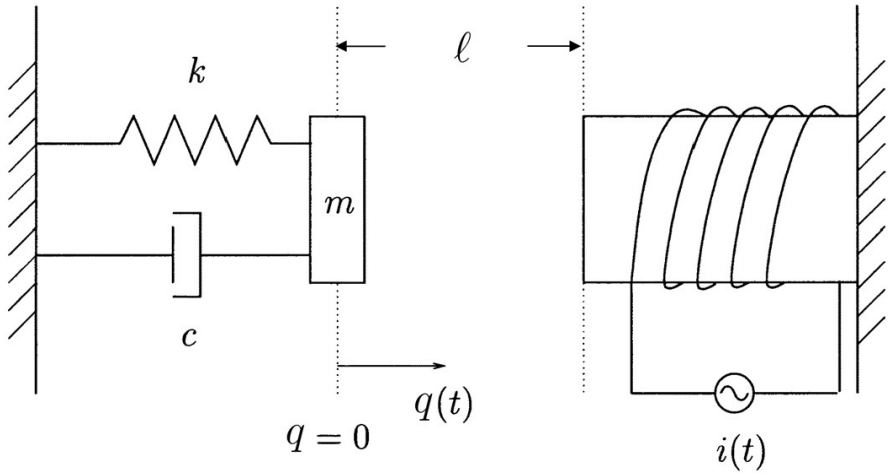

Figure 2.36: Schematic of the electromagnetically controlled oscillator.

equilibrium current $i_{\rm eq}$ satisfies

$$kq_{\rm eq} = \frac{i_{\rm eq}^2}{(\ell - q_{\rm eq})^2}. \tag{2.24}$$

Conversely, given a constant current $i_{\rm eq}$, (2.21) may have zero, one, or two equilibria depending on whether (2.24) has either zero, one, or two solutions.

Proposition 2.5.1. The following statements hold:

1. If $i_{\rm eq}^2 > \frac{4}{27}k\ell^3$, then (2.21) has no equilibria.

2. If $i_{\rm eq}^2 = \frac{4}{27}k\ell^3$, then (2.21) has a unique equilibrium, which is given by $q_{\rm eq} = \ell/3$.

3. If $0 < i_{\rm eq}^2 < \frac{4}{27}k\ell^3$, then (2.21) has two equilibria, namely, $q_{\rm eq_1} = \frac{2}{3}\ell(1 - \cos\frac{\alpha}{3})$ and $q_{\rm eq_2} = \frac{2}{3}\ell\left[1 + \cos\left(\frac{\alpha}{3} + \frac{\pi}{3}\right)\right]$), where $\alpha \triangleq \cos^{-1}\left(\frac{27i_{\rm eq}^2}{2k\ell^3} - 1\right)$.

Proof. Let $f_1(q_{\rm eq}) \triangleq kq_{\rm eq}$ and $f_2(q_{\rm eq}) \triangleq \frac{i_{\rm eq}^2}{(\ell - q_{\rm eq})^2}$. Then it follows that $f_1'(q_{\rm eq}) = k$ and $f_2'(q_{\rm eq}) = \frac{2kq}{\ell - q} \in (0, \infty)$. Furthermore, $f_1'(q_{\rm eq}) = f_2'(q_{\rm eq}) = k$ if and only if $q_{\rm eq} = \ell/3$. Therefore, $f_1(q_{\rm eq})$ has no intersection with $f_2(q_{\rm eq})$ if and only if $f_1(\ell/3) < f_2(\ell/3)$, one intersection point if and only if $f_1(\ell/3) = f_2(\ell/3)$, and two intersection points if and only if $f_1(\ell/3) > f_2(\ell/3)$. □

Proposition 2.5.2. Assume that $0 < i_{\text{eq}}^2 < \frac{4}{27}k\ell^3$. Then, $q_{\text{eq}_1} < \ell/3$ and $q_{\text{eq}_2} > \ell/3$.

Proof. Since $-1 < \left(\frac{27i_{\text{eq}}^2}{2k\ell^3} - 1\right) < 1$. It follows that $0 < \alpha < \pi$. Hence $\frac{\alpha}{3} \in (0, \frac{\pi}{3})$ and thus $\frac{\alpha}{3} + \frac{\pi}{3} \in (\frac{\pi}{3}, \frac{2\pi}{3})$. Furthermore, $\cos\frac{\alpha}{3} \in (\frac{1}{2}, 1)$ and $\cos\left(\frac{\alpha}{3} + \frac{\pi}{3}\right) \in (-\frac{1}{2}, \frac{1}{2})$. Therefore $q_{\text{eq}_1} = \frac{2}{3}\ell(1 - \cos\frac{\alpha}{3}) \in (0, \ell/3)$ and $q_{\text{eq}_2} = \frac{2}{3}\ell\left[1 + \cos\left(\frac{\alpha}{3} + \frac{\pi}{3}\right)\right] \in (\ell/3, \ell)$. □

Proposition 2.5.1 and Proposition 2.5.2 are illustrated in Figure 2.37.

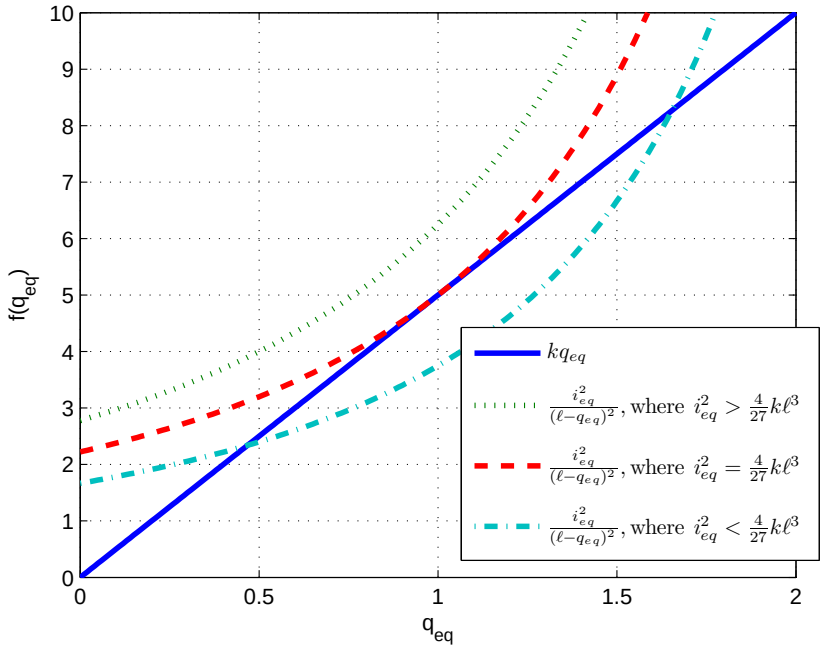

Figure 2.37: Forced equilibrium position q_{eq} corresponding to various values of i_{eq} for $m = 1$ kg, $\ell = 3$ m, and $k = 5$ N/m. The ECO has no equilibria if and only if $i_{\text{eq}}^2 > \frac{4}{27}k\ell^3$, one equilibrium at $q_{\text{eq}} = \ell/3 = 1$ m if and only if $i_{\text{eq}}^2 = \frac{4}{27}k\ell^3$, and two equilibria if and only if $0 < i_{\text{eq}}^2 < \frac{4}{27}k\ell^3$. In the last case, $q_{\text{eq}_1} < \ell/3$ is asymptotically stable, and $q_{\text{eq}_2} > \ell/3$ is unstable.

2.5.2 Linearization, Local Stability Analysis, and Discretization of the ECO

In this section, we linearize (2.21) around an equilibrium $q_{\rm eq}$, analyze the local stability, and discretize the linearized plant.

Linearizing (2.21) around $q = q_{\rm eq}$ yields

$$\begin{bmatrix} \dot{\xi} \\ \ddot{\xi} \end{bmatrix} = A_{\rm l} \begin{bmatrix} \xi \\ \dot{\xi} \end{bmatrix} + B_{\rm l}\delta i, \tag{2.25}$$

where

$$A_{\rm l} \triangleq \begin{bmatrix} 0 & 1 \\ -\frac{k}{m} + \frac{2i_{\rm eq}^2}{m(\ell - q_{\rm eq})^3} & -\frac{c}{m} \end{bmatrix}, \; B_{\rm l} \triangleq \begin{bmatrix} 0 \\ \frac{2i_{\rm eq}}{m(\ell - q_{\rm eq})^2} \end{bmatrix}.$$

Next, we define

$$\omega_{\rm n} \triangleq \sqrt{\frac{k}{m}}, \quad \zeta \triangleq \frac{c}{2\sqrt{mk}}, \tag{2.26}$$

where $\omega_{\rm n} > 0$ denotes the undamped natural frequency of vibration and $\zeta > 0$ denotes the damping ratio. Now $A_{\rm l}$ and $B_{\rm l}$ can be written as

$$A_{\rm l} = \begin{bmatrix} 0 & 1 \\ -\frac{\ell - 3q_{\rm eq}}{\ell - q_{\rm eq}}\omega_{\rm n}^2 & -2\zeta\omega_{\rm n} \end{bmatrix}, \; B_{\rm l} = \begin{bmatrix} 0 \\ \frac{2q_{\rm eq}\omega_{\rm n}^2}{i_{\rm eq}} \end{bmatrix}. \tag{2.27}$$

The linearized system (2.25) with $\delta i = 0$ is asymptotically stable if and only if $-\frac{\ell - 3q_{\rm eq}}{\ell - q_{\rm eq}}\omega_{\rm n}^2 < 0$, that is,

$$q_{\rm eq} < \ell/3. \tag{2.28}$$

Figure 2.38 shows the equilibrium current $i_{\rm eq}$ and the spectral abscissa of $A_{\rm l}$ for each

equilibrium of the ECO. Note that $i_{\rm eq}$ decreases as the mass moves farther into the stable region toward the left of $\ell/3$; $i_{\rm eq}$ attains its maximum value $i_{\rm eq} = \sqrt{\frac{4}{27}k\ell^3}$ at $q_{\rm eq} = \ell/3 = 1$ m; and $i_{\rm eq}$ decreases as the mass moves farther into the unstable region to the right of $\ell/3$. Meanwhile, note that the unstable equilibria become increasingly unstable as the mass moves farther to the right of $\ell/3$.

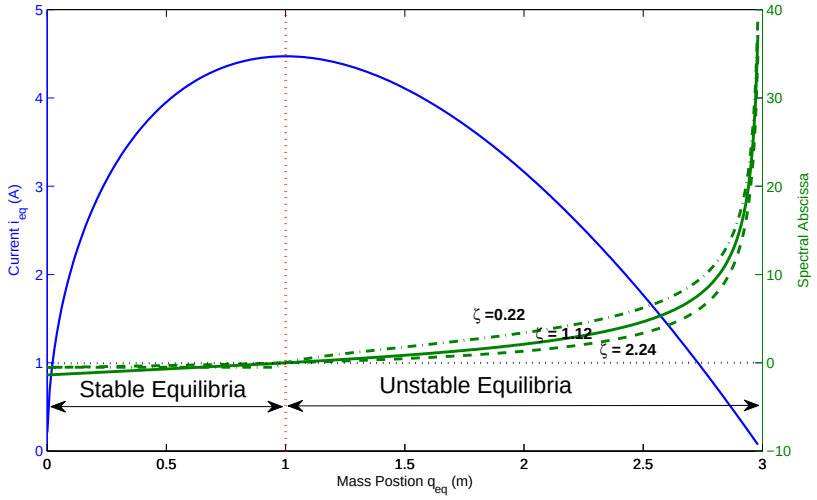

Figure 2.38: Equilibrium current $i_{\rm eq}$ and spectral abscissa of $A_{\rm l}$ corresponding to each equilibrium of the ECO for $m = 1$ kg, $\ell = 3$ m, $k = 5$ N/m, and $c = 1, 5, 10$ N-s/m respectively. Note that $i_{\rm eq}$ decreases as the mass moves farther into the stable region toward the left of $\ell/3$; $i_{\rm eq}$ attains its maximum value $i_{\rm eq} = \sqrt{\frac{4}{27}k\ell^3}$ at $q_{\rm eq} = \ell/3 = 1$; and $i_{\rm eq}$ decreases as the mass moves farther into the unstable region to the right of $\ell/3$. Meanwhile, the unstable equilibria become increasingly unstable as the mass moves farther to the right of $\ell/3$. Note that by decreasing the damping ratio ζ, the system becomes more unstable.

Next, assuming a zero-order-hold input operator with a sample time of $T_{\rm s}$, we obtain the discretized dynamics

$$x(k+1) = Ax(k) + Bu(k), \tag{2.29}$$

where $u(k) \triangleq \delta i(k)$. Defining $\gamma \triangleq \frac{\omega_{\rm n}}{2}\left|\zeta^2 - \frac{\ell - 3q_{\rm eq}}{\ell - q_{\rm eq}}\right|^{1/2}$, A and B are given by (2.10) and (2.11).

$$A = e^{A_{\rm l}T_{\rm s}} = \begin{cases} e^{-\zeta\omega_{\rm n}T_{\rm s}} \begin{bmatrix} \cos\gamma T_{\rm s} + \zeta\omega_{\rm n}\sin\gamma T_{\rm s} & \frac{1}{\gamma}\sin\gamma T_{\rm s} \\ -\frac{\ell-3q_{\rm eq}}{(\ell-q_{\rm eq})\gamma}\omega_{\rm n}^2\sin\gamma T_{\rm s} & \cos\gamma T_{\rm s} - \zeta\omega_{\rm n}\sin\gamma T_{\rm s} \end{bmatrix}, & \zeta^2 < \frac{\ell-3q_{\rm eq}}{\ell-q_{\rm eq}}, \\ e^{-\zeta\omega_{\rm n}T_{\rm s}} \begin{bmatrix} T_{\rm s} + \zeta\omega_{\rm n}T_{\rm s} & bT_{\rm s} \\ -\frac{\ell-3q_{\rm eq}}{\ell-q_{\rm eq}}\omega_{\rm n}^2 T_{\rm s} & T_{\rm s} - \zeta\omega_{\rm n}T_{\rm s} \end{bmatrix}, & \zeta^2 = \frac{\ell-3q_{\rm eq}}{\ell-q_{\rm eq}}, \\ e^{-\zeta\omega_{\rm n}T_{\rm s}} \begin{bmatrix} \cosh\gamma T_{\rm s} + \zeta\omega_{\rm n}\sinh\gamma T_{\rm s} & \frac{1}{\gamma}\sinh\gamma T_{\rm s} \\ -\frac{\ell-3q_{\rm eq}}{(\ell-q_{\rm eq})\gamma}\omega_{\rm n}^2\sinh\gamma T_{\rm s} & \cosh\gamma T_{\rm s} - \zeta\omega_{\rm n}\sinh\gamma T_{\rm s} \end{bmatrix}, & \zeta^2 > \frac{\ell-3q_{\rm eq}}{\ell-q_{\rm eq}}, \end{cases} \tag{2.10}$$

$$B = \left(\int_0^{T_{\rm s}} e^{A_{\rm l}\tau} {\rm d}\tau \right) B_{\rm l} = \begin{cases} A_{\rm l}^{-1}(A-I)B_{\rm l}, & q_{\rm eq} \neq \ell/3, \\ \frac{m}{c} \begin{bmatrix} 0 & \frac{m}{c} \\ 0 & -1 \end{bmatrix} (A-I)B_{\rm l} + \begin{bmatrix} \sqrt{3k/\ell}cT_{\rm s} \\ 0 \end{bmatrix}, & q_{\rm eq} = \ell/3. \end{cases} \tag{2.11}$$

2.5.3 Command-Following Problem for the ECO

We now consider the ECO command-following problem shown in Figure 2.39. We apply a feedforward/feedback controller to have the output y follow the command signal r. The goal is to develop an adaptive feedforward/feedback controller that minimizes the command-following error z in the presence of the command signal r with minimal modeling information about the dynamics of the ECO. For the feedforward path, the controller uses a measurement of the command r. For the feedback path, we apply RCAC to the ECO assuming that the state q is available for feedback.

To account for the nonlinearity of the ECO, the feedforward/feedback controller is constructed as follows. As shown in Figure 2.40, the RCAC controller uses one auxiliary nonlinearity. The auxiliary nonlinearity $\mathcal{N}_1$ modifies the RCAC controller output $u_{\rm c}$ to obtain the regressor input $u_{\rm r}$. The offset current $i_{\rm offset}$ is determined by the setpoint feedback rule described below.

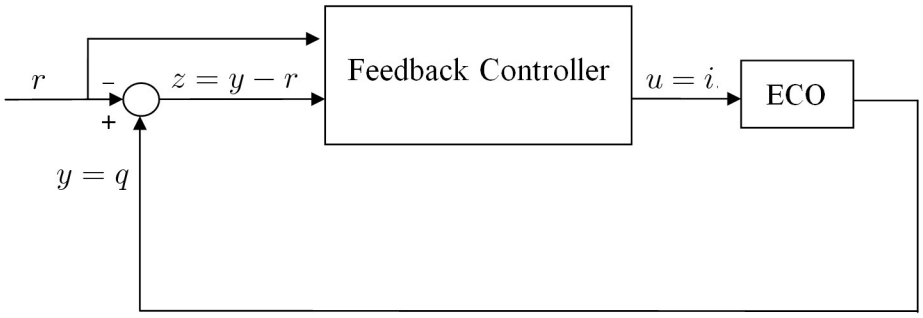

Figure 2.39: ECO command-following problem.

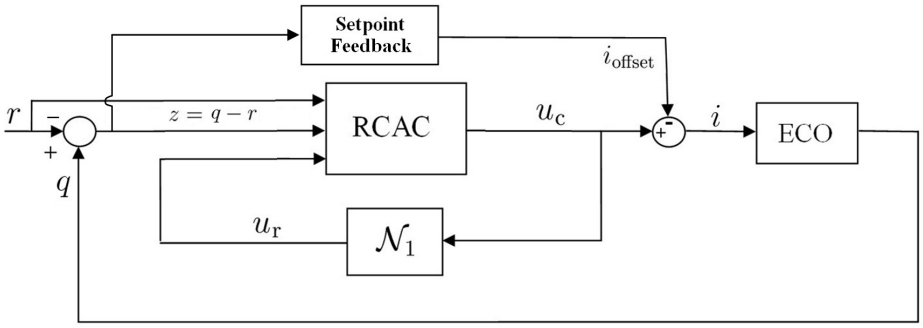

Figure 2.40: ECO command-following problem with the RCAC adaptive controller and auxiliary nonlinearity $\mathcal{N}_1$. The offset current i_{offset} is determined by the setpoint feedback rule.

Define the saturation function sat_a by

$$\text{sat}_a(x) = \begin{cases} -a, & x < -a, \\ x, & -a \leq x \leq a, \\ a, & x > a, \end{cases} \tag{2.12}$$

where $a > 0$ is the saturation level.

2.5.3.1 Offset Current i_{offset}

Let r be a nondecreasing sequence of step commands, that is, $r(k_1) \leq r(k_2)$ for all $k_1 < k_2$. Then $i_{\text{offset}}(k)$ is given by

$$i_{\text{offset}}(k) = \begin{cases} 0, & \text{if} \quad 0 < r(k) \leq \ell/3, \\ \rho e^{-\frac{\alpha}{|q(k)-r(k)|^\beta}}, & \text{if} \quad \ell/3 < r(k) < \ell, \end{cases} \tag{2.13}$$

where $\rho \geq 0$, $\alpha > 0$, $\beta > 0$, and $q(k)$ is the position of the mass at time step k.

As an example, consider $\rho = 1, \alpha = 1, \beta = 1$, and $r(k) = \ell/2$, where $\ell = 3$ m. Figure 2.41 shows the offset current i_{offset} corresponding to each mass position $q(k)$. Note that the offset current is nonzero except for $q(k) = r(k)$. The offset current increases as the distance between current mass position and commanded mass position increases.

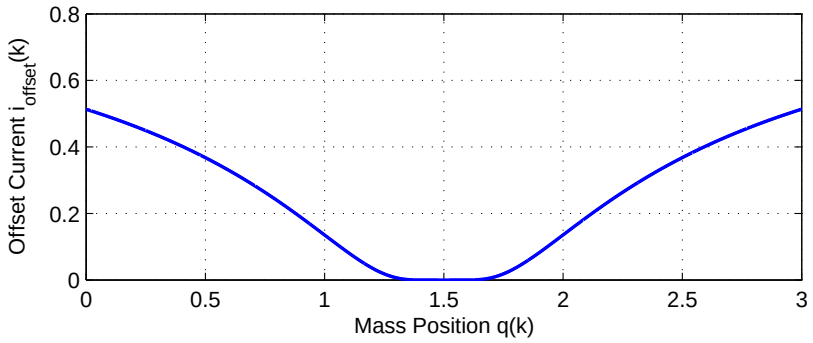

Figure 2.41: Offset current i_{offset} corresponding to each mass position $q(k)$ for the ECO for $r(k) = 1.5$ m, $\rho = 1, \alpha = 1$, and $\beta = 1$. Note that the offset current is nonzero except for $q(k) = r(k)$. The offset current increases as the distance between current mass position and commanded mass position increases.

2.5.4 Simulation Results

We now use RCAC with the auxiliary nonlinearity $\mathcal{N}_1$ and the offset current i_{offset} to control the position of the mass. In particular, we consider the command-following

problem with the step command $r = q_{\rm eq} \geq \ell/3$.

The adaptive controller requires an estimate of the first nonzero Markov parameter of the linearized plant (2.29). This Markov parameter is used to implement the retrospective optimization (5.18). RCAC generates the control signal $u_{\rm c}$, which is added to the offset current $i_{\rm offset}$.

For simulation we consider $m = 1$ kg, $k = 5$ N/m, $c = 5$ N-s/m, and $\ell = 3$ m with a sample time $T_{\rm s} = 0.01$ sec. Hence $\omega_{\rm n} = 2.2361$ rad/s and $\zeta = 1.1180$. First, numerical simulations are performed for the constant command input $q_{\rm eq} = \ell/3 = 1.0$ m. The first nonzero Markov parameter of (2.25) is $H_1(q_{\rm eq}) \stackrel{\triangle}{=} CB$, where B is defined in (2.11) and $C \stackrel{\triangle}{=} \left[\begin{array}{cc} 1 & 0 \end{array} \right]$. We choose $H_1(q_{\rm eq}) = H_1(1) = 1.0996 \times 10^{-4}$ m/A. Figure 3.51 shows the dependence of H_1 on the equilibria of the ECO. We initialize the control gains to zero, that is, $\theta(0) = 0$, and we choose the controller order $n_{\rm c} = 8$ and the covariance matrix $P(0) = 10^{-9} I_{3n_{\rm c}}$. Furthermore, since the linearized model is minimum phase, we choose the regularization $\eta = 0$. Finally, we set $\rho = 0$ so that $i_{\rm offset} = 0$, and we do not use a forgetting factor in the adaptive controller, that is, $\lambda = 1$. Figure 2.43 shows that the controller stabilizes the plant and follows the command input. Figure 2.44 shows the time history of the control input $u_{\rm c}$. It follows from Proposition 2.5.1 that the steady-state value of the current $i = u_{\rm c}$ is the maximum current such that (2.21) has an equilibrium.

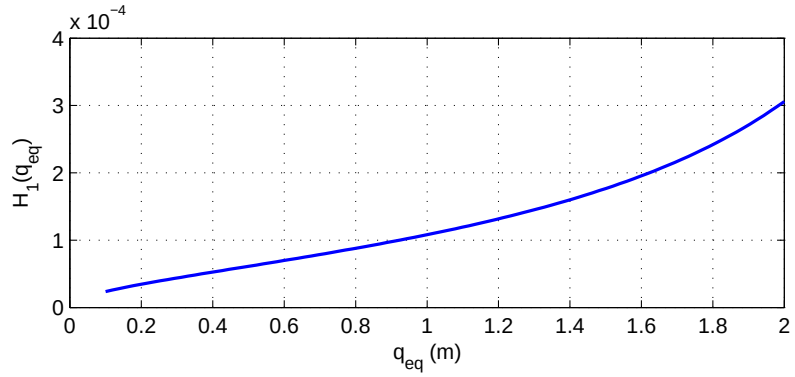

Figure 2.42: H_1 corresponds to each equilibrium of the ECO for $m = 1$ kg, $\ell = 3$ m, $c = 5$ N-s/m, and $k = 5$ N/m.

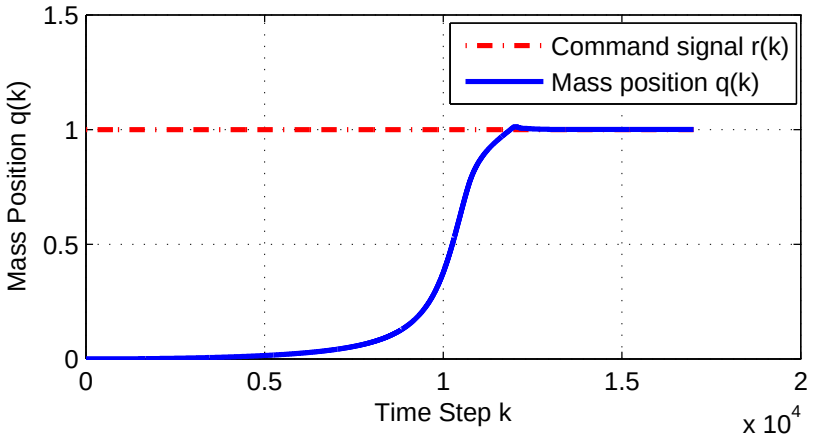

Figure 2.43: Position of the mass with the step command $r(k) = \mathbf{1}(k)$ for $m = 1$ kg, $\ell = 3$ m, $c = 5$ N-s/m, and $k = 5$ N/m. In this simulation, $\hat{H}_1(1) = H_1(1)$. Since $r(k) = \mathbf{1}(k) = \ell/3$, it follows that $i_{\text{offset}} = 0$.

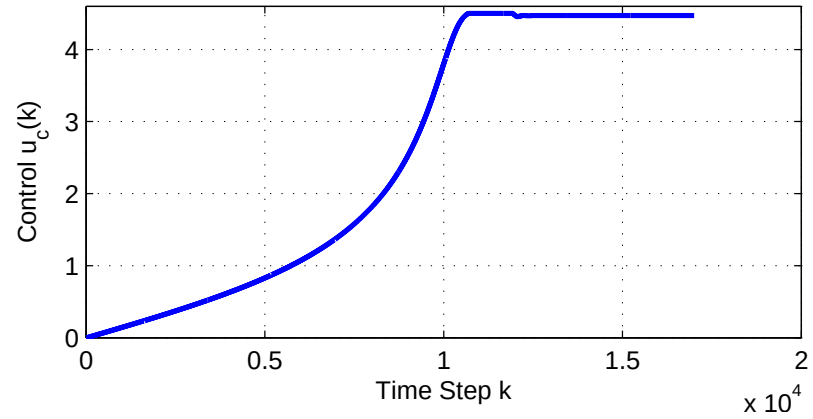

Figure 2.44: Time history of the control input u_c corresponding to the closed-loop response shown in Figure 2.43. In this case, $i_{\text{offset}} = 0$.

Next, we do not assume that $H_1(1)$ is known exactly. Figure 2.45 shows the position of the mass with various estimates $\hat{H}_1(1)$ of $H_1(1)$. The RCAC controller is able to stabilize the plant and follow the step command with erroneous estimates of $H_1(1)$. However, the best overall performance for both the transient response and the convergence time is obtained for $\hat{H}_1(1) = H_1(1)$.

Now, we implement the adaptive controller with a nondecreasing sequence of setpoint commands as shown in Figure 2.46. To do this, we set i_{offset} based on (2.41) when $r(k) > \ell/3$. In particular, we choose $\rho = 1$, $\alpha = 1, \beta = 1$, $\hat{H}_1(1) = H_1(1)$,

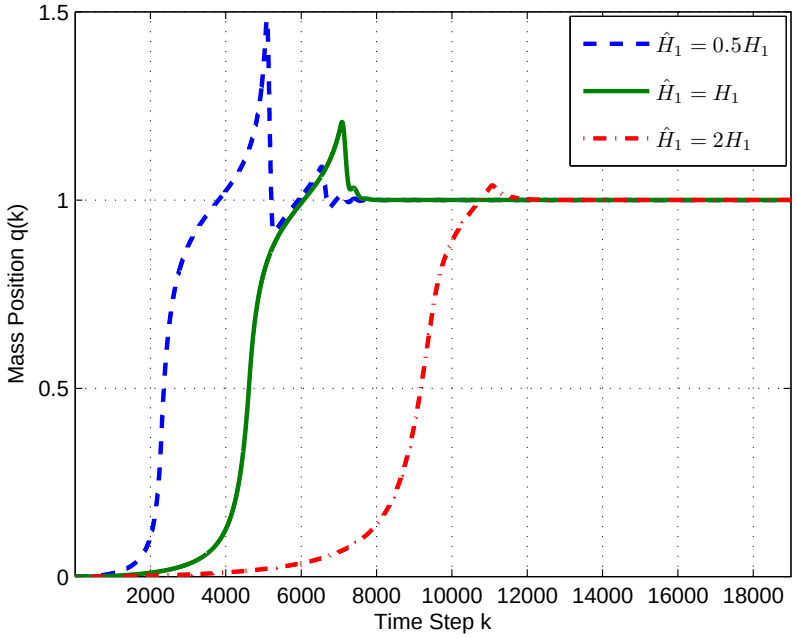

Figure 2.45: Position of the mass with the step command $r(k) = \mathbf{1}(k)$ with various estimates $\hat{H}_1(1)$ of $H_1(1)$ for $m = 1$ kg, $\ell = 3$ m, $c = 5$ N-s/m, and $k = 5$ N/m. The controller is able to stabilize the plant and follow the step commands in all cases. However, the accuracy of $\hat{H}_1(1)$ affects the transient response. In this case, $i_{\text{offset}} = 0$.

$n_c = 8$, and initialize the control gains to zero. Figure 2.46 shows that the control algorithm is able to stabilize the system up to $q_{\text{eq}} = 1.79$. Figure 2.47(a) shows the time history of the current offset i_{offset}, and Figure 2.47(b) shows the time history of the control input u_c from the RCAC.

Finally, we reduce the damping coefficient so that $c = 4$ N-s/m, and thus the ECO is underdamped with $\zeta = 0.8944$. Following the same procedure, and using the same parameters for initializing RCAC, Figure 2.48 shows that RCAC is able to stabilize the underdamped system up to $q_{\text{eq}} = 1.79$. Figure 2.49(a) shows the time history of the current offset i_{offset}, and Figure 2.49(b) shows the time history of the control input u_c from RCAC. Note that, in this case, the transient response for the open-loop underdamped ECO system is worse than the response in the open-loop overdamped case. Figure 2.50 shows the largest distance the mass can be moved by

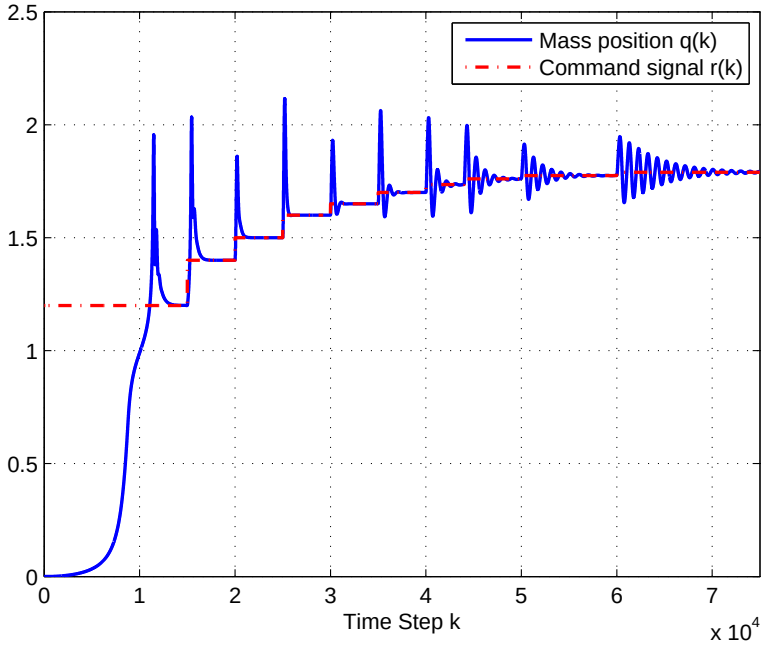

Figure 2.46: Position of the mass with a nondecreasing sequence of step commands for $m = 1$ kg, $\ell = 3$ m, $c = 5$ N-s/m, and $k = 5$ N/m, where $\zeta = 1.1180$. In order to stabilize the mass close to the electromagnet, the command signal is a nondecreasing sequence of step commands, which is shown as the red dash line. Note that all equilibria greater than $q_{\rm eq} = 1$ are open-loop unstable. In this simulation, we choose $\hat{H}_1 = H(1)$.

the feedforward/feedback controller versus the open-loop damping ratio of the ECO system. Note that, in all those cases, we choose $\hat{H}_1 = H(1)$.

Finally, to demonstrate the potential benefits of scheduling the Markov parameters as a function of $q_{\rm eq}$, we consider the same example shown in Figure 2.46. Since the Markov parameter increases as the mass moves farther into the unstable region (in Figure 3.51), we thus let $\hat{H}_1 = H(1)$ for $q_{\rm eq} \in (0, 1.7)$ and $\hat{H}_1 = 1.2H(1)$ for $q_{\rm eq} \geq 1.7$. Figure 2.51 shows that RCAC is able to stabilize the system up to $q_{\rm eq} = 1.815$.

2.5.5 Summary

In this example, we considered a command-following problem for the electromagnetically controller oscillator (ECO). RCAC was used with limited modeling infor-

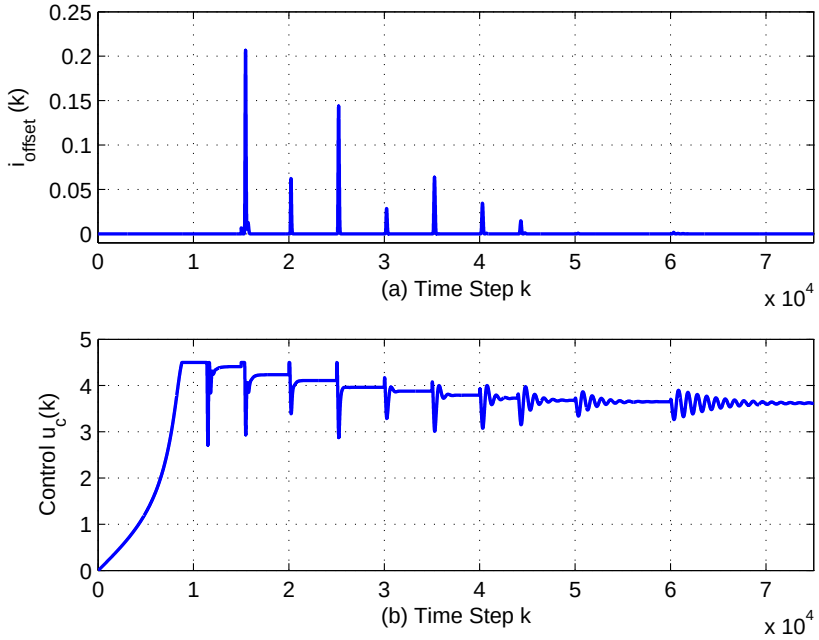

Figure 2.47: Current offset i_{offset} (a) and control input u_{c} (b) corresponding to the closed-loop response shown in Figure 2.46.

mation, namely, an estimate of the first nonzero Markov parameter of the linearized system. To handle the effect of the nonlinearities and the unstable region of the ECO, RCAC was augmented by an auxiliary nonlinearity. An equilibrium feedback path was also used to assist RCAC in reaching the desired unstable equilibrium. Future research will focus on the effect of noise and sample rate as well as the potential benefits of scheduling the Markov parameters as a function of q_{eq}.

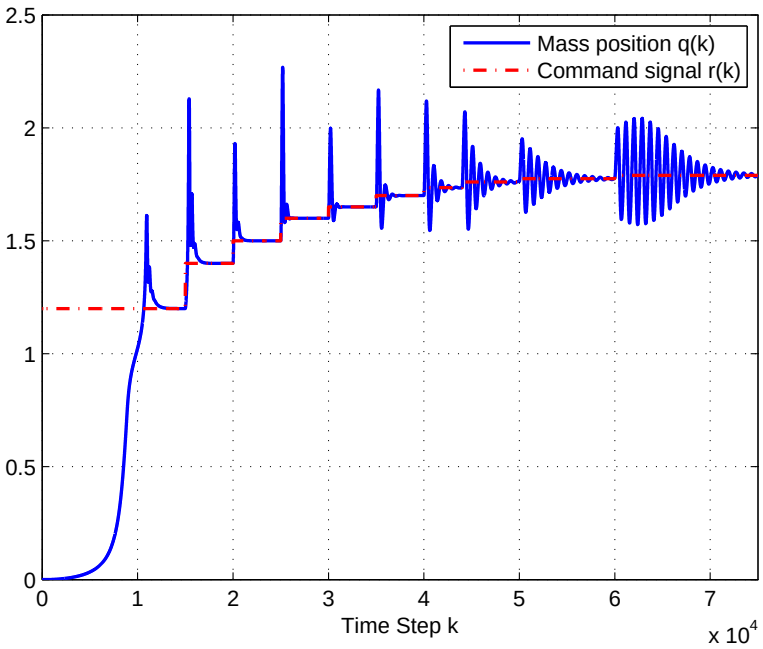

Figure 2.48: Position of the mass with a nondecreasing sequence of step commands for $m = 1$ kg, $\ell = 3$ m, $c = 4$ N-s/m, and $k = 5$ N/m, where $\zeta = 0.8944$. In order to stabilize the mass close to the electromagnet, the command signal is a nondecreasing sequence of step commands, which is shown as the red dash line. Note that we choose $\hat{H}_1 = H(1)$, and all equilibria greater than $q_{\text{eq}} = 1$ are open-loop unstable. In this case, which is underdamped, the transient response is worse than the response in Figure 2.46.

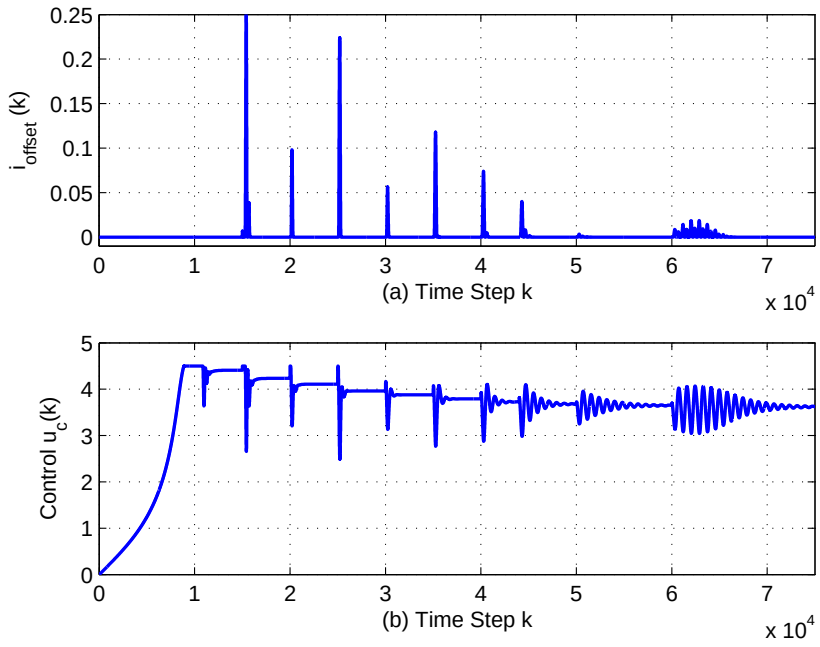

Figure 2.49: Current offset i_{offset} (a) and control input u_{c} (b) corresponding to the closed-loop response shown in Figure 2.48.

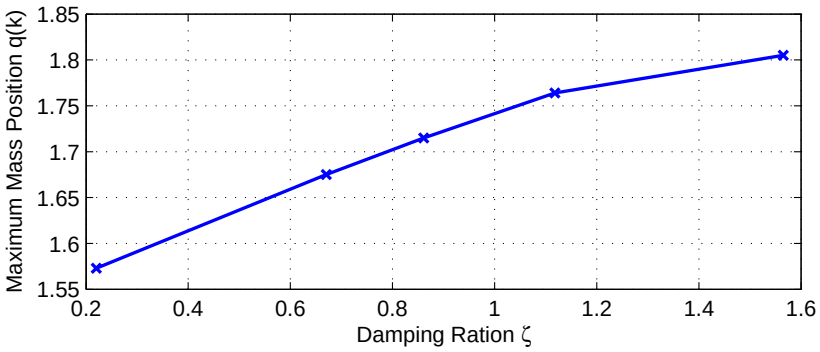

Figure 2.50: Largest distance that RCAC is able to move the mass for various open-loop damping ratios of the ECO. In all cases, we choose $\hat{H}_1 = H(1)$, that is, the Markov parameter for the ECO linearized at $q = 1$ for the simulation.

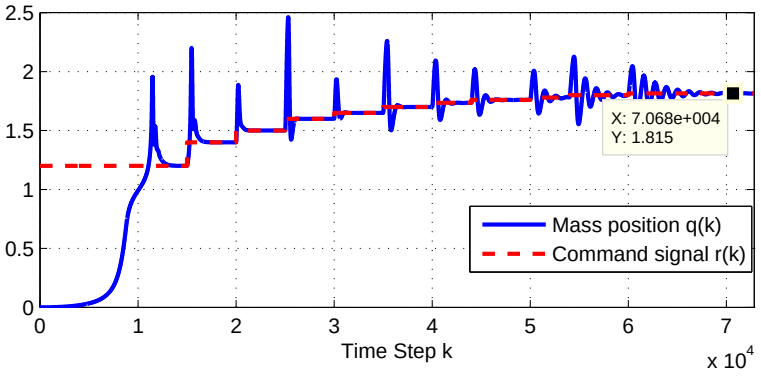

Figure 2.51: Position of the mass with a nondecreasing sequence of step commands for $m = 1$ kg, $\ell = 3$ m, $c = 5$ N-s/m, and $k = 5$ N/m, where $\zeta = 1.1180$. Note that all equilibria greater than $q_{\text{eq}} = 1$ are open-loop unstable. In this simulation, we let $\hat{H}_1 = H(1)$ for $q_{\text{eq}} \in (0, 1.7)$ and $\hat{H}_1 = 1.2H(1)$ for $q_{\text{eq}} \geq 1.7$. RCAC is able to stabilize the system up to $q_{\text{eq}} = 1.815$.

CHAPTER III

Retrospective Cost Adaptive Control with Convex Saturation Constraints

In this chapter, we apply retrospective cost adaptive control (RCAC) to command following in the presence of multivariable convex input saturation constraints. To account for the saturation constraint, we use convex optimization to minimize the quadratic retrospective cost function. The use of convex optimization bounds the magnitude of the retrospectively optimized input and thereby influences the controller update to satisfy the control bounds. This technique is applied to a multi-rotor helicopter with constraints on the total thrust magnitude and inclination of the rotor plane. The results of this chapter are published in [60].

3.1 Introduction

All real-world control systems must operate subject to constraints on the allowable control inputs. These constraints typically have the form of a saturation input nonlinearity [61]. Within classical control, the effects of saturation are addressed through anti-windup strategies [62, 63]. Within the context of modern multivariable control, techniques for dealing with saturation are addressed in [64, 65, 66, 67]. Saturation within the context of adaptive control is addressed in [68, 69, 70].

In the case of multiple control inputs, it is usually the case that individual control inputs are subject to independent saturation [71]. However, in many applications, a saturation constraint may affect multiple control inputs. This is the case, for example, if the control inputs are produced by common hardware, such as a single power supply, amplifier, or actuator.

In the present chapter we consider adaptive control for problems in which multiple control inputs may be subject to *dependent* saturation constraints. In particular, we are motivated by the problem of safely controlling the trajectory of a multi-rotor helicopter by constraining the total thrust magnitude and inclination in order to restrict the vehicle acceleration.

To address this problem, we revisit the problem of retrospective cost adaptive control (RCAC) under constraints [70]. RCAC can be used for adaptive command following and disturbance rejection for possibly nonminimum-phase systems under minimal modeling information [23, 25, 28, 26]. Unlike [71], the present chapter uses convex optimization to perform the retrospective input optimization [35]. The use of convex optimization bounds the magnitude of the retrospectively optimized input and thereby influences the controller update to satisfy the control bounds. We demonstrate this technique on illustrative numerical examples involving single and multiple inputs. We then apply this approach to trajectory control for a multi-rotor helicopter. We use the convex programming code [72] for the numerical optimization. The same technique was used within the context of RCAC in [73] to address the problem of unknown nonminimum-phase zeros.

The contents of the chapter are as follows. In Section 3.2, we describe the command-following problem with input saturation nonlinearities. In Section 3.3, we summarize the RCAC algorithm. Numerical simulation results are presented in Section 3.4, and conclusions are given in Section 3.5.

3.2 Problem Formulation

Consider the MIMO discrete-time Hammerstein system

$$x(k+1) = Ax(k) + B\mathrm{Sat}(u(k)) + D_1 w(k), \tag{3.1}$$

$$y(k) = Cx(k) + D_2 w(k), \tag{3.2}$$

$$z(k) = E_1 x(k) + E_0 w(k), \tag{3.3}$$

where, for all $k \geq 0$, $x(k) \in \mathbb{R}^n$, $y(k) \in \mathbb{R}^{l_y}$, $z(k) \in \mathbb{R}^{l_z}$, $w(k) \in \mathbb{R}^{l_w}$, and $u(k) \in \mathbb{R}^{l_u}$. The signal $u(k)$ is the commanded control input. However, due to saturation, the actual control input is given by $v(k) = \mathrm{Sat}(u(k))$, where the saturation input nonlinearity is $\mathrm{Sat} : \mathbb{R}^{l_u} \to \mathcal{U}$, and $\mathcal{U} \subseteq \mathbb{R}^{l_u}$ is the convex control constraint set. We assume that the function "Sat" is onto, that is, $\mathrm{Sat}(\mathbb{R}^{l_u}) = \mathcal{U}$. In particular, if $\mathcal{U}$ is rectangular, then

$$\mathrm{Sat}(u) = \begin{bmatrix} \mathrm{sat}_{a_1,b_1}(u_1) \\ \vdots \\ \mathrm{sat}_{a_{l_u},b_{l_u}}(u_{l_u}) \end{bmatrix}, \tag{3.4}$$

where $u = [u_1 \ \cdots \ u_{l_u}]^{\mathrm{T}} \in \mathcal{U} = [a_1, b_1] \times \cdots \times [a_{l_u}, b_{l_u}]$ and $\mathrm{sat} : \mathbb{R} \to [a, b]$ is defined as

$$\mathrm{sat}_{a,b}(u) = \begin{cases} a, & \text{if} \quad u < a, \\ u, & \text{if} \quad a \leq u \leq b, \\ b, & \text{if} \quad u > b. \end{cases} \tag{3.5}$$

The goal is to develop an adaptive output feedback controller that minimizes the command-following error z with minimal modeling information about the plant dynamics. Note that w can represent either a command signal to be followed, an

external disturbance to be rejected, or both. For example, if $D_1 = 0$ and $E_0 \neq 0$, then the objective is to have the output $E_1 x$ follow the command signal $-E_0 w$. On the other hand, if $D_1 \neq 0$ and $E_0 = 0$, then the objective is to reject the disturbance w from the performance variable $E_1 x$. The combined command-following and disturbance-rejection problem is considered when $D_1 = \left[\begin{array}{cc} D_{11} & 0 \end{array} \right]$, $E_0 = \left[\begin{array}{cc} 0 & E_{02} \end{array} \right]$, and $w(k) = \left[\begin{array}{cc} w_1^{\mathrm{T}}(k) & w_2^{\mathrm{T}}(k) \end{array} \right]^{\mathrm{T}}$, where the objective is to have $E_1 x$ follow $-E_0 w_2$ while rejecting the disturbance w_1. Finally, if D_1 and E_0 are zero matrices, then the objective is output stabilization, that is, convergence of z to zero.

3.3 Retrospective Cost Adaptive Control

In this section, we describe the constrained retrospective cost optimization algorithm.

3.3.1 ARMAX Modeling

Consider the ARMAX representation of (3.1)–(3.3) given by

$$z(k) = \sum_{i=1}^{n} -\alpha_i z(k-i) + \sum_{i=d}^{n} \beta_i \mathrm{Sat}(u(k-i)) + \sum_{i=0}^{n} \gamma_i w(k-i), \tag{3.6}$$

where $\alpha_1, \ldots, \alpha_n \in \mathbb{R}$, $\beta_1, \ldots, \beta_n \in \mathbb{R}^{l_z \times l_u}$, $\gamma_0, \ldots, \gamma_n \in \mathbb{R}^{l_z \times l_w}$, and d is the relative degree. Next, let $v(k) \stackrel{\triangle}{=} \mathrm{Sat}(u(k))$, and define the transfer function

$$G_{zv} \stackrel{\triangle}{=} E_1(\mathbf{z}I - A)^{-1}B = \sum_{i=d}^{\infty} \mathbf{z}^{-i} H_i = H_d \frac{\alpha(\mathbf{z})}{\beta(\mathbf{z})}, \tag{3.7}$$

where, for each positive integer i, the Markov parameter H_i of G_{zv} is defined by

$$H_i \stackrel{\triangle}{=} E_1 A^{i-1} B \in \mathbb{R}^{l_z \times l_u}. \tag{3.8}$$

Note that, if $d = 1$, then $H_1 = \beta_1$, whereas, if $d \geq 2$, then

$$\beta_1 = \cdots = \beta_{d-1} = H_1 = \cdots = H_{d-1} = 0 \tag{3.9}$$

and $H_d = \beta_d$. The polynomials $\alpha(\mathbf{z})$ and $\beta(\mathbf{z})$ have the form

$$\alpha(\mathbf{z}) = \mathbf{z}^{n-1} + \alpha_1 \mathbf{z}^{n-1} + \cdots + \alpha_{n-1}\mathbf{z} + \alpha_n, \tag{3.10}$$

$$\beta(\mathbf{z}) = \mathbf{z}^{n-d} + \beta_{d+1}\mathbf{z}^{n-d-1} + \cdots + \beta_{n-1}\mathbf{z} + \beta_n. \tag{3.11}$$

Next, define the *extended performance* $Z(k) \in \mathbb{R}^{pl_z}$ and *extended plant input* $V(k) \in \mathbb{R}^{q_c l_u}$ by

$$Z(k) \stackrel{\triangle}{=} \begin{bmatrix} z(k) \\ \vdots \\ z(k-p+1) \end{bmatrix}, \quad V(k) \stackrel{\triangle}{=} \begin{bmatrix} v(k-1) \\ \vdots \\ v(k-q_c) \end{bmatrix} = \begin{bmatrix} \mathrm{Sat}(u(k-1)) \\ \vdots \\ \mathrm{Sat}(u(k-q_c)) \end{bmatrix}, \tag{3.12}$$

where the data window size p is a positive integer, and $q_c \stackrel{\triangle}{=} n+p-1$. Therefore (5.6) can be expressed as

$$Z(k) = W_{zw}\phi_{zw}(k) + B_f V(k), \tag{3.13}$$

where

$$W_{zw} \stackrel{\triangle}{=} \begin{bmatrix} -\alpha_1 I_{l_z} & \cdots & -\alpha_n I_{l_z} & 0_{l_z\times l_z} & \cdots & 0_{l_z\times l_z} & \gamma_0 & \cdots & \gamma_n & 0_{l_z\times l_w} & \cdots & 0_{l_z\times l_w} \\ 0_{l_z\times l_z} & \ddots & & \ddots & \ddots & \vdots & 0_{l_z\times l_w} & \ddots & & \ddots & \ddots & \vdots \\ \vdots & \ddots & \ddots & & \ddots & 0_{l_z\times l_z} & \vdots & \ddots & \ddots & & \ddots & 0_{l_z\times l_w} \\ 0_{l_z\times l_z} & \cdots & 0_{l_z\times l_z} & -\alpha_1 I_{l_z} & \cdots & -\alpha_n I_{l_z} & 0_{l_z\times l_w} & \cdots & 0_{l_z\times l_w} & \gamma_0 & \cdots & \gamma_n \end{bmatrix} \in \mathbb{R}^{pl_z\times[q_c l_z+(q_c+1)l_w]}, \tag{3.14}$$

$$B_f \triangleq \begin{bmatrix} \beta_1 & \cdots & \beta_n & 0_{l_z \times l_u} & \cdots & 0_{l_z \times l_u} \\ 0_{l_z \times l_u} & \ddots & & \ddots & \ddots & \vdots \\ \vdots & \ddots & \ddots & & \ddots & 0_{l_z \times l_u} \\ 0_{l_z \times l_u} & \cdots & 0_{l_z \times l_u} & \beta_1 & \cdots & \beta_n \end{bmatrix} \in \mathbb{R}^{pl_z \times q_c l_u}, \tag{3.15}$$

and

$$\phi_{zw}(k) \triangleq \begin{bmatrix} z(k-1) \\ \vdots \\ z(k-p-n+1) \\ w(k) \\ \vdots \\ w(k-p-n+1) \end{bmatrix} \in \mathbb{R}^{q_c l_z + (q_c+1) l_w}. \tag{3.16}$$

Note that W_{zw} includes modeling information about the poles of G_{zv} and the exogenous signals, while B_f includes modeling information about the zeros of G_{zv}.

For the open-loop system (3.6), we make the following assumptions:

(A.1) The relative degree d is known.

(A.2) The first nonzero Markov parameter H_d is known.

(A.3) There exists an integer $\bar{n}$ such that $n < \bar{n}$ and $\bar{n}$ is known.

(A.4) If $\zeta \in \mathbb{C}$, $|\zeta| > 1$, and $\beta(\zeta) = 0$, then the spectral radius of A is less than 1.

(A.5) The performance variable $z(k)$ is measured and available for feedback.

(A.6) The function Sat is monotonically nondecreasing in each component in u with the remaining components of u fixed.

(A.7) The exogenous signal $w(k)$ is generated by

$$x_w(k+1) = A_w x_w(k), \tag{3.17}$$

$$w(k) = C_w x_w(k), \tag{3.18}$$

where $x_w \in \mathbb{R}^{l_w}$ and all of the eigenvalues of A_w are on the unit circle and do not coincide with the transmission zeros of G_{zv}.

(A.8) There exists an integer $\bar{n}_w$ such that $n_w < \bar{n}_w$ and $\bar{n}_w$ is known.

(A.9) The exogenous signal $w(k)$ is not measured.

(A.10) $\alpha(\mathbf{z}), \beta(\mathbf{z}), n$, and $x(0)$ are unknown.

The assumption (A.6) is motivated by [58, 59].

3.3.2 Controller Construction

The commanded control $u(k)$ is given by the exactly proper time-series controller

$$u(k) = \sum_{i=1}^{n_c} M_i(k) u(k-i) + \sum_{j=0}^{n_c} N_j(k) z(k-j), \tag{3.19}$$

where, for all $i = 1, \ldots, n_c$, $M_i(k) \in \mathbb{R}^{l_u \times l_u}$, and, for all $j = 0, \ldots, n_c$, $N_j(k) \in \mathbb{R}^{l_u \times l_z}$. We express (3.19) as

$$u(k) = \theta(k)\phi(k-1), \tag{3.20}$$

where

$$\theta(k) \triangleq \left[\begin{array}{cccccc} M_1(k) & \cdots & M_{n_c}(k) & N_0(k) & \cdots & N_{n_c}(k) \end{array} \right] \in \mathbb{R}^{l_u \times (n_c l_u + (n_c+1) l_z)} \tag{3.21}$$

and

$$\phi(k-1) \triangleq \begin{bmatrix} u(k-1) \\ \vdots \\ u(k-n_{\mathrm{c}}) \\ z(k) \\ \vdots \\ z(k-n_{\mathrm{c}}) \end{bmatrix} \in \mathbb{R}^{n_{\mathrm{c}}l_u+(n_{\mathrm{c}}+1)l_z}. \tag{3.22}$$

3.3.3 Retrospective Performance

Define the *retrospective performance* $\hat{Z}(k) \in \mathbb{R}^{pl_z}$ by

$$\hat{Z}(k) \triangleq W_{zw}\phi_{zw}(k) + B_f V(k) + \bar{B}_f[\hat{U}(k) - U(k)], \tag{3.23}$$

where

$$\bar{B}_f \triangleq \begin{bmatrix} 0_{l_z\times(d-1)l_u} & \bar{H}_d & \cdots & \bar{H}_m & 0_{l_z\times l_u} & \cdots & 0_{l_z\times l_u} & 0_{l_z\times l_u} & \cdots & 0_{l_z\times l_u} \\ 0_{l_z\times(d-1)l_u} & 0_{l_z\times l_u} & \ddots & & \ddots & \ddots & & \ddots & \ddots & \vdots \\ \vdots & \vdots & \ddots & \ddots & & \ddots & \ddots & & \ddots & \vdots \\ 0_{l_z\times(d-1)l_u} & 0_{l_z\times l_u} & \cdots & 0_{l_z\times l_u} & \bar{H}_d & \cdots & \bar{H}_m & 0_{l_z\times l_u} & \cdots & 0_{l_z\times l_u} \end{bmatrix} \in \mathbb{R}^{pl_z\times q_c l_u}, \tag{3.24}$$

is the *retrospective input matrix* with the model information of G_{zv}. Specifically, $\bar{H}_1, \ldots, \bar{H}_m$ in (3.24) are estimates of the Markov parameters of G_{zv}. Next, define the *extended commanded control* $U(k) \in \mathbb{R}^{q_c l_u}$ and the *retrospectively optimized extended*

control vector $\hat{U}(k) \in \mathbb{R}^{q_c l_u}$ by

$$U(k) \triangleq \begin{bmatrix} u(k-1) \\ \vdots \\ u(k-q_c) \end{bmatrix}, \quad \hat{U}(k) \triangleq \begin{bmatrix} \hat{u}_k(k-1) \\ \vdots \\ \hat{u}_k(k-q_c) \end{bmatrix}, \tag{3.25}$$

where $\hat{u}_k(k-i) \in \mathbb{R}^{l_u}$ is a recomputed control. Subtracting (3.13) from (3.23) yields

$$\hat{Z}(k) = Z(k) + \bar{B}_f[\hat{U}(k) - U(k)]. \tag{3.26}$$

Note that the retrospective performance $\hat{Z}(k)$ does not depend on W_{zw} or the exogenous signal w. For disturbance rejection, we do not assume that the disturbance is known; for command-following, the command w need not be measured. The model information matrix $\bar{B}_f$ is discussed in Section 3.3.5.

3.3.4 Retrospective Cost and RLS Controller Update Law

3.3.4.1 Retrospective Cost

We define the *retrospective cost function*

$$J(\hat{U}(k), k) \triangleq \hat{Z}^{\mathrm{T}}(k) R(k) \hat{Z}(k) + \eta(k) \hat{U}(k)^{\mathrm{T}} \hat{U}(k), \tag{3.27}$$

where, for all $k > 0$, $\eta(k) \geq 0$ is a scalar and $R(k) \in \mathbb{R}^{pl_z \times pl_z}$ is a positive-definite performance weighting. The goal is to determine retrospectively optimized controls $\hat{U}(k)$ that would have provided better performance than the controls $U(k)$ that were applied to the plant. The retrospectively optimized controls $\hat{U}(k)$ are subsequently used to update the controller. Using (3.26), (3.27) can be rewritten as

$$J(\hat{U}(k), k) = \hat{U}(k)^{\mathrm{T}} \mathcal{A}(k) \hat{U}(k) + \mathcal{B}(k) \hat{U}(k) + \mathcal{C}(k), \tag{3.28}$$

where

$$\mathcal{A}(k) \triangleq \bar{B}_f^{\mathrm{T}} R(k) \bar{B}_f + \eta(k) I_{q_c l_u},$$
$$\mathcal{B}(k) \triangleq 2\bar{B}_f^{\mathrm{T}} R(k)[Z(k) - \bar{B}_f U(k)],$$
$$\mathcal{C}(k) \triangleq Z^{\mathrm{T}}(k) R(k) Z(k) - 2Z^{\mathrm{T}}(k) R(k) \bar{B}_f U(k) + U(k)^{\mathrm{T}} \bar{B}_f^{\mathrm{T}} R(k) \bar{B}_f U(k).$$

Note that if either $\bar{B}_f$ has full rank or $\eta(k) > 0$, then $\mathcal{A}(k)$ is positive definite.

Next, we consider the problem of minimizing (3.27) subject to

$$\hat{U}(k) \in \mathcal{U} \times \cdots \times \mathcal{U}. \tag{3.29}$$

The following result follows from the Weierstrass theorem.

Lemma 3.3.1. *If $\mathcal{U}$ is compact, then* (3.27) *has at least one minimizer. If, in addition, $\mathcal{U}$ is convex, then* (3.27) *has a unique minimizer. In particular, if $\mathcal{U} = \mathbb{R}^{l_u}$, then the unique global minimizer of $J(\hat{U}(k), k)$ is*

$$\hat{U}(k) = -\frac{1}{2}\mathcal{A}^{-1}(k)\mathcal{B}(k). \tag{3.30}$$

3.3.4.2 Cumulative Cost and RLS Update

Define the *cumulative cost function*

$$J_{\mathrm{cum}}(\theta, k) \triangleq \sum_{i=d+1}^{k} \lambda^{k-i} \|\phi^{\mathrm{T}}(i-d-1)\theta(i-1) - \hat{u}_k(i-d)\|^2 + \lambda^k [\theta(k) - \theta(0)]^{\mathrm{T}} P_0^{-1} [\theta(k) - \theta(0)], \tag{3.31}$$

where $\|\cdot\|$ is the Euclidean norm, $P_0 \in \mathbb{R}^{l_u[n_c l_u + (n_c+1)l_z] \times [n_c l_u + (n_c+1)l_z]}$ is positive definite, and $\lambda \in (0, 1]$ is the forgetting factor. The next result follows from standard recursive least-squares (RLS) theory [74, 75].

Lemma 3.3.2. *For each $k \geq d$, the unique global minimizer of the cumulative retrospective cost function* (3.31) *is given by*

$$\theta(k) = \theta(k-1) + \frac{P(k-1)\phi(k-d)\varepsilon(k-1)}{\lambda + \phi^{\mathrm{T}}(k-d)P(k-1)\phi(k-d)}, \tag{3.32}$$

where

$$P(k) = \frac{1}{\lambda}\left[P(k-1) - \frac{P(k-1)\phi(k-d)\phi^{\mathrm{T}}(k-d)P(k-1)}{\lambda + \phi^{\mathrm{T}}(k-d)P(k-1)\phi(k-d)}\right], \tag{3.33}$$

$P(0) = P_0$, *and* $\varepsilon(k-1) \triangleq \phi^{\mathrm{T}}(k-d-1)\theta(k-1) - \hat{u}(k-d)$.

3.3.5 Model Information $\bar{B}_f$

For SISO, minimum-phase, asymptotically stable linear plants, using the first nonzero Markov parameter in $\bar{B}_f$ yields asymptotic convergence of z to zero [25, 30]. In this case, let $m = d$ and $\bar{H}_d = H_d$ in (3.24). Furthermore, if the open-loop linear plant is nonminimum-phase and the absolute values of all nonminimum-phase zeros are greater than the plant's spectral radius, then a sufficient number of Markov parameters can be used to approximate the nonminimum-phase zeros [25]. Alternatively, a phase-matching condition with $\eta > 0$ is given in [44, 76] to construct $\bar{B}_f$. For MIMO Lyapunov-stable linear plants, an extension of the phase-matching-based method is given in [77]. For unstable, nonminimum-phase plants, knowledge of the locations of the nonminimum-phase zeros is needed to construct $\bar{B}_f$. For details, see [25, 78].

In this chapter, we consider only the case where the zeros of G_{zv} are either minimum-phase or on the unit circle. Therefore, we set $p = 1$ and let

$$\bar{B}_f = \left[\begin{array}{ccc} 0_{1_z \times (d-1)l_u} & H_d & 0_{1_z \times (n-d)l_u} \end{array}\right] \in \mathbb{R}^{l_z \times n l_u}.$$

3.4 Numerical Examples

In this section, we present numerical examples to illustrate the response of RCAC for plants with input saturation based on constrained retrospective optimization under saturation. The numerical examples are constructed such that the objective is to minimize the performance $z = y - w$, with $\phi(k)$ given by (3.22). In all simulations, we choose $\lambda = 1$, and we initialize $\theta(0)$ to zero.

Example 3.4.1. *Step command following for a minimum-phase, asymptotically stable plant with saturation.* Consider the asymptotically stable, minimum-phase plant transfer function from v to y, given by

$$G_{zv}(\mathbf{z}) = \frac{0.04758}{\mathbf{z} - 0.9048}. \tag{3.34}$$

Our goal is to have the plant output y follow the step command $w(k) = 0.4$. First, consider the fixed-gain PI controller $u = G_{\mathrm{PI}}(\mathbf{z})z$, where

$$G_{\mathrm{PI}}(\mathbf{z}) \triangleq 8 + \frac{0.8}{\mathbf{z} - 1} = \frac{8\mathbf{z} - 7.2}{\mathbf{z} - 1}. \tag{3.35}$$

The controller (3.35) is implemented in feedback with the plant (3.34), where the input to the plant $v = \mathrm{sat}_{a,b}(u)$ is given by (3.5). We consider the unsaturated case, that is, $a = -\infty$ and $b = \infty$, and the saturated case, where $a = -1$ and $b = 1$. Figure 3.1 shows the time history of w, y, u, and v for the case without amplitude saturation as well as the case where $a = -1$ and $b = 1$. For the case without saturation, y follows the command with zero steady-state error. For the case with saturation, u exhibits integrator windup. In particular, the integrator windup results in the overshoot in y.

Next, consider the adaptive controller (3.19) with $a = -1$ and $b = 1$ in (3.29) is implemented in feedback with $n_c = 1$, $\eta = 0.1$, $P_0 = I$, and $\bar{B}_f = \begin{bmatrix} 0_{1\times d-1} & H_d \end{bmatrix} = 0.04758$. Note that, a, b, and $\bar{B}_f$ are the only required model information for the adap-

tive controller. We initialize RCAC as the PI controller in (3.35). Specifically, we let $\theta(0) = \begin{bmatrix} 8 & -7.2 & -1 \end{bmatrix}$. Figure 3.2 shows that y follows w with zero steady-state error and no overshoot. Note that the controller output u doesn't exceed the saturation $b = 1$, hence, u does not exhibit integrator windup. This compares favorably with the fixed gain proportional-integral controller used in Figure 3.1. ■

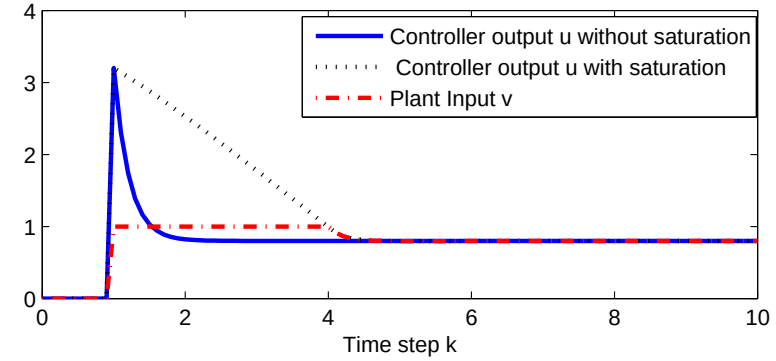

(a)

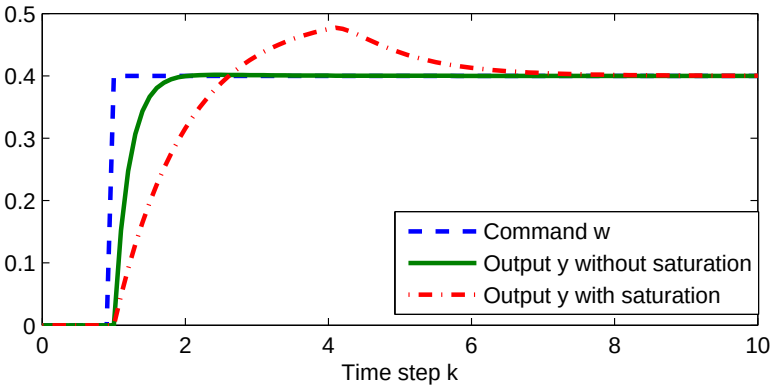

(b)

Figure 3.1: Example 3.4.1. *Step command following for a minmimum-phase, asymptotically stable plant with a proportional-integral controller.* The controller (3.35) is implemented in feedback with the plant (3.34), where the input to the plant $v = \text{sat}_{a,b}(u)$ is given by (3.5). We consider the unsaturated case, that is, $a = -\infty$ and $b = \infty$, and the saturated case, where $a = -1$ and $b = 1$. For the case without saturation, y follows the command with zero steady-state error. For the case with saturation, u exhibits integrator windup. In particular, the integrator windup results in the overshoot in y.

Example 3.4.2. *Square-wave command following for a minimum-phase, asymp-*

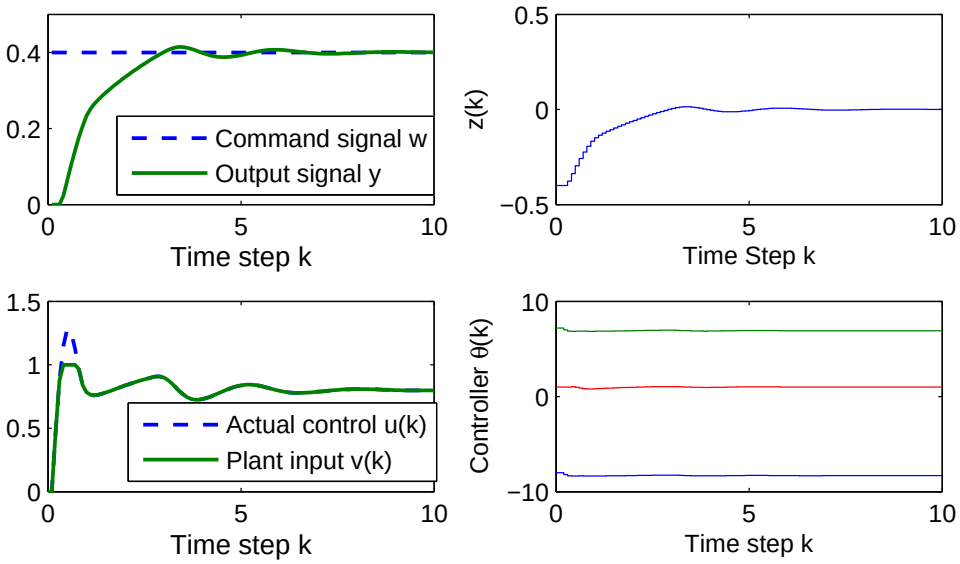

Figure 3.2: Example 3.4.1. *Step command following for a minmimum-phase, asymptotically stable plant with RCAC.* The adaptive controller (3.19) with $a = -1$ and $b = 1$ in (3.29) is implemented in feedback with $n_c = 1$, $\eta = 0.1$, $P_0 = I$, and $\bar{B}_f = 0.04758$. Note that, a, b, and $\bar{B}_f$ are the only required model information for the adaptive controller. We initialize RCAC as the PI controller in (3.35). For the case saturation $a = -1$ and $b = 1$, y follows w with zero steady-state error and no overshoot. Note that the controller output u doesn't exceed the saturation $b = 1$, hence, u does not exhibit integrator windup.

totically stable plant with saturation. Consider the asymptotically stable, minimum-phase plant

$$G_{zv}(\mathbf{z}) = \frac{(\mathbf{z} - 0.5)(\mathbf{z} - 0.9)}{(\mathbf{z} - 0.7)(\mathbf{z} - 0.5 - \jmath 0.5)(\mathbf{z} - 0.5 + \jmath 0.5)}. \tag{3.36}$$

The goal is to have the plant output y follow a square-wave command $w(k)$. The control saturation $v = \mathrm{Sat}(u) = \mathrm{sat}_{a,b}(u)$ is given by (3.5). We consider the unsaturated case, that is, $a = -\infty$ and $b = \infty$, together with four levels of saturation. For the plant (3.36), the saturation bounds $u_{\max} = 3$ and $u_{\min} = -3$ are sufficient to drive the performance z to zero. Next, we define the saturation levels, $b_{10\%} = 0.9u_{\max}$, $b_{20\%} = 0.8u_{\max}$, $b_{40\%} = 0.6u_{\max}$, $b_{80\%} = 0.2u_{\mathrm{ss,max}}$, $a_{10\%} = 0.9u_{\min}$, $a_{20\%} = 0.8u_{\min}$,

$a_{40\%} = 0.6u_{\min}$, and $a_{80\%} = 0.2u_{\min}$. In all four cases, the adaptive controller (3.19) with saturation is implemented in feedback with $n_c = 3$, $\eta = 0$, $P_0 = 10^{-2}I$, and $\bar{B}_f = \begin{bmatrix} 1 & 0 & 0 \end{bmatrix}$. Note that a, b, and $\bar{B}_f$ are the only model information required by the adaptive controller.

Figure 3.3 shows the time history of w, y, u, and v without saturation as well as with 10%, 20%, 40%, and 80% saturation. For the case without saturation, y follows the command w after each step. For the case with saturation, note that the adaptive controller is not able to follow the command because the saturation makes this impossible. However, the output y follows w without phase lag that is characteristic of integrator windup. ■

Example 3.4.3. *Triangle-wave command following for a minimum-phase, Lyapunov-stable plant with saturation.* Consider the Lyapunov-stable, minimum-phase plant

$$G_{zv}(\mathbf{z}) = \frac{1}{\mathbf{z} - 1}. \tag{3.37}$$

The goal is to have the plant output y follow a triangle-wave command. Following the procedure in Example 3.4.2, we choose $n_c = 3$, $\eta = 0$, $P_0 = 10^{-2}$, and $\bar{B}_f = 1$. Figure 3.4 shows the time history of w, y, u, and v for the case without saturation as well as with 10%, 20%, 40%, and 80% saturation. Without saturation, y follows the command w. Each time the slope of w changes sign, the control u experiences a transient. For the case with saturation, the adaptive controller is not able to follow the command because the saturation makes this impossible. ■

Example 3.4.4. *Square-wave command following for a nonminimum-phase, unstable plant with saturation.* Consider the unstable (double integrator) plant

$$G_{zv}(\mathbf{z}) = \frac{\mathbf{z} + 1}{(\mathbf{z} - 1)^2}. \tag{3.38}$$

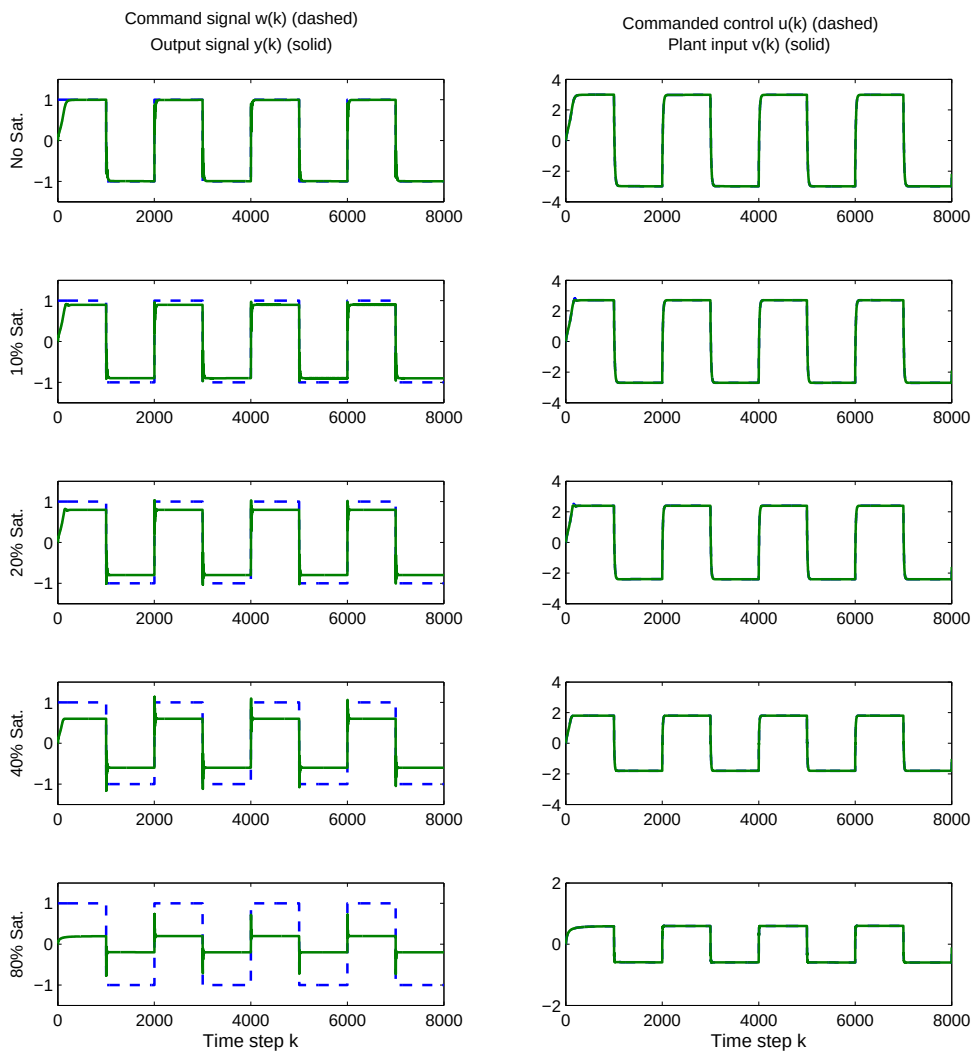

Figure 3.3: Example 3.4.2. *Square wave command following for a minimum-phase, asymptotically stable plant with saturation.* We consider no saturation as well as 10%, 20%, 40%, and 80% saturation. Without saturation, y follows the command w at each step. With saturation, note that the adaptive controller is not able to follow the command because the saturation makes this impossible. However, the output y follows w without the phase lag that is characteristic of integrator windup.

The command is a square wave. We consider the saturation control $v = \mathrm{Sat}(u) = \mathrm{sat}_{a,b}(u)$ with $a = -1$ and $b = 1$. The adaptive controller (3.19) with known saturation bounds in (3.29) is implemented in feedback with $n_c = 3$, $\eta = 0.01$, $P_0 = I$, and

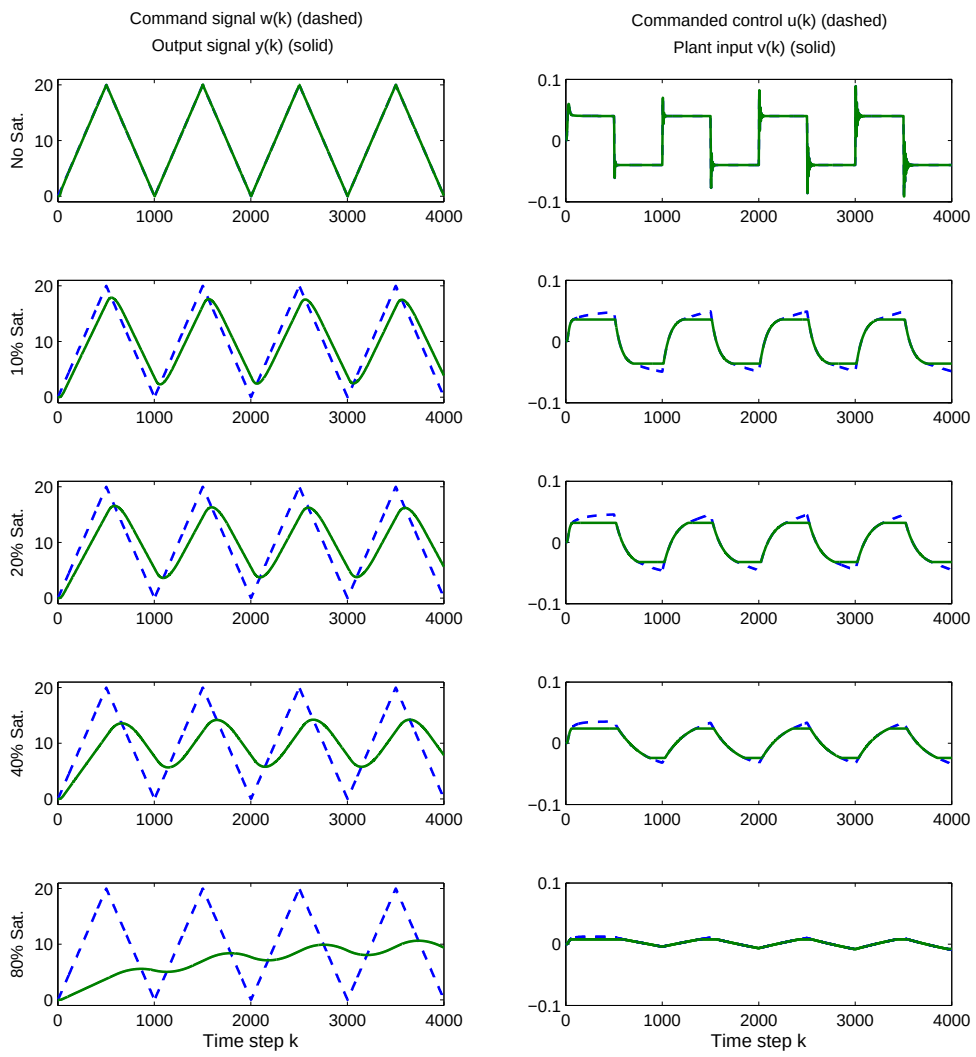

Figure 3.4: Example 3.4.3. *Triangle-wave command following for a minimum-phase, Lyapunov-stable plant with saturation.* We consider no saturation as well as with 10%, 20%, 40%, and 80% saturation. Without saturation, y follows the command w. Each time the slope of w changes sign, the control u experiences a transient, and the output $y(k)$ follows the command. With saturation, the adaptive controller is not able to follow the command because the saturation makes this impossible.

$\bar{B}_f = \begin{bmatrix} 1 & 0 \end{bmatrix}$. Figure 3.5 shows the time history of w, y, u, and v. Note that the response converges after the transient in the first period. ■

Example 3.4.5. *Command-following for an undamped mass-spring structure with*

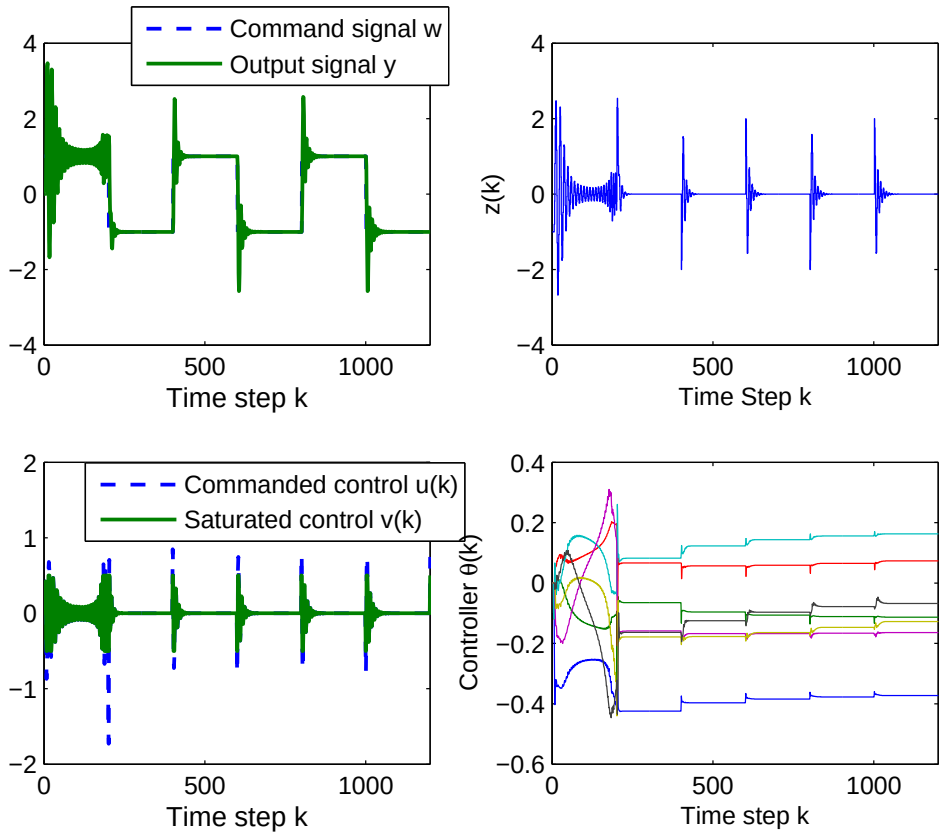

Figure 3.5: Example 3.4.4. *Square-wave command following for a double-integrator plant with saturation.* We consider $v = \mathrm{sat}_{-1,1}(u)$. The adaptive controller (3.19) is implemented in feedback with $n_c = 3$, $\eta = 0.01$, $P_0 = I$, and $\bar{B}_f = [1\ 0]$.

single-direction force actuation. Consider the mass-spring-damper structure shown in Figure 3.6 modeled by (3.39)

$$m\ddot{q} + kq = v, \tag{3.39}$$

where $m = 1$ kg and $k = 30$ N/m are the mass and stiffness, q and $\dot{q}$ are the position and velocity, respectively, of the mass, and $q(0) = 3$ m, $\dot{q}(0) = 5$ m/s. w is the command signal, and v is the saturated control given by

$$v = \mathrm{Sat}(u) = \mathrm{sat}_{0,50}(u) \tag{3.40}$$

The discrete-time transfer function is given by

$$G_{zv}(\mathbf{z}) = \frac{0.004(\mathbf{z}+1)}{\mathbf{z}^2 - 1.707\mathbf{z} + 1}. \tag{3.41}$$

The goal is to have the plant output y follow the step command $w(k) = 0$. We consider (3.5) with $v = \mathrm{sat}_{0,50}(u)$. Note that this problem is related to the classical problem of controllability using positive controls considered in [79, 80, 81]. However, Brammer's theorem given in [79, 80] assumes that $B = I$, which is not the case in this example.

The adaptive controller (3.19) with known saturation bounds is implemented in feedback with $n_c = 5$, $\eta = 0.0001$, $P_0 = 0.1I$, and $\bar{B}_f = \begin{bmatrix} 0.004 & 0 \end{bmatrix}$.

The goal is to bring the mass to $q = 0$ with single-direction force actuation. Figure 3.7 shows the response with $q(0) = 3$ m and $\dot{q}(0) = 5$ m/s. Note that, by constraining the retrospectively optimized control $\hat{u}(k)$, the commanded control $u(k)$ is nonnegative for all $k > 25$. ■

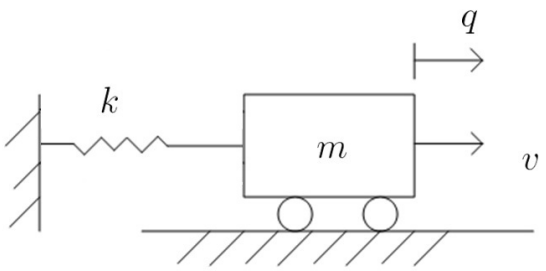

Figure 3.6: Example 3.4.5. Mass-spring structure with single-direction force actuation.

Example 3.4.6. *Command following for a multi-rotor helicopter.* The transla-

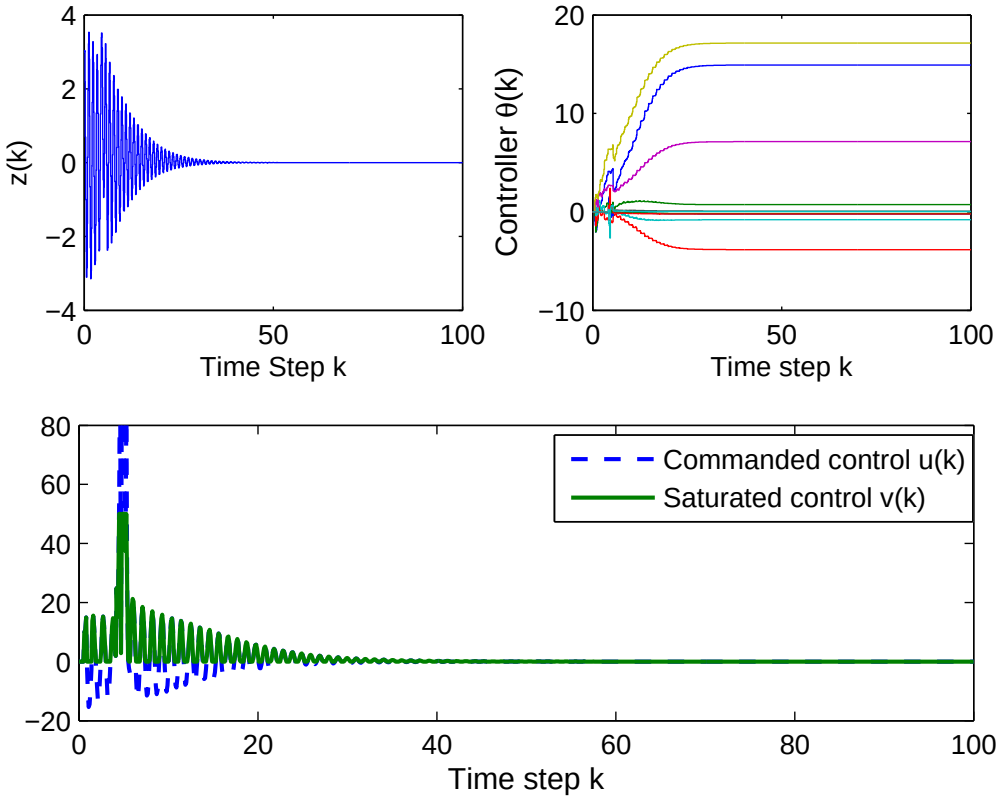

Figure 3.7: Example 3.4.5. *Command-following for an undamped mass-spring-damper structure with single-direction force actuation.* The adaptive controller (3.19) is implemented with $n_c = 5$, $\eta = 0.0001$, $P_0 = 0.1I$, and $\bar{B}_f = [0.004\ 0]$. The goal is to bring the mass to $q = 0$ with single-direction force actuation with $q(0) = 3$ m and $\dot{q}(0) = 5$ m/s.

tional motion of a multi-rotor helicopter is described by

$$\ddot{q} = \frac{1}{m}u + \begin{bmatrix} 0 \\ 0 \\ -g \end{bmatrix}, \tag{3.42}$$

where $q = \begin{bmatrix} q_1 & q_2 & q_3 \end{bmatrix}^{\mathrm{T}} \in \mathbb{R}^3$ denotes the position of the vehicle center of mass resolved in the Earth frame, where q_1 and q_2 denote horizontal displacements, while q_3 denotes the vertical displacement. The initial conditions are $q(0) = \begin{bmatrix} 0 & 0 & 0 \end{bmatrix}^{\mathrm{T}}$

and $\dot{q}(0) = \begin{bmatrix} 0 & 0 & 0 \end{bmatrix}^{\mathrm{T}}$. $u = \begin{bmatrix} u_1 & u_2 & u_3 \end{bmatrix}^{\mathrm{T}} \in \mathbb{R}^3$ is the control force, $g = 9.8$ m/s^2 is the gravitational acceleration, and $m = 0.5$ kg is the mass of the vehicle.

Define the inclination angle φ of u to be

$$\varphi \triangleq \cos^{-1} \frac{u_3}{\|u\|}, \tag{3.43}$$

where $\|u\|$ denotes the Euclidean norm of u. Let

$$w(t) = \begin{bmatrix} 2\cos(0.1t) \\ 2\sin(0.1)t \\ 0.3t + 1 \end{bmatrix} \in \mathbb{R}^3 \tag{3.44}$$

denote the position command, and define the tracking error $z \in \mathbb{R}^3$ by

$$z \triangleq q - w. \tag{3.45}$$

Let the positive real numbers $\varphi_{\max} = 20$ deg and $u_{\max} = 6$ N denote the maximum allowable values of φ and $\|u\|$, respectively. The control problem is thus to construct a feedback control law for u that minimizes $\|z\|$ subject to

$$\frac{\sqrt{u_1^2 + u_2^2}}{\|u\|} \leq \sin \varphi_{\max}, \tag{3.46}$$

$$u_3 \geq 0, \tag{3.47}$$

and

$$\|u\| \leq u_{\max}, \tag{3.48}$$

where (3.46)-(3.48) form the convex control constraint set $\mathcal{U}$ shown in Figure 3.8. The problem of minimizing the retrospective cost function on $\mathcal{U}$ can thus be rewritten as the following second-order cone programming (SOCP) problem:

$$\min J(\hat{U}(k), k) \tag{3.49}$$

subject to

$$\|P\hat{U}(k)\|_2 \leq Q\hat{U}(k) \quad \text{and} \quad \|\hat{U}(k)\|_2 \leq 6, \tag{3.50}$$

where $P \triangleq \begin{bmatrix} 1 & 0 & 0 \\ 0 & 1 & 0 \\ 0 & 0 & 0 \end{bmatrix}$ and $Q \triangleq \tan(\varphi_{\max}) \begin{bmatrix} 0 & 0 & 1 \end{bmatrix}^{\mathrm{T}}$. The nonlinear programming method SOCP in the CVX toolbox [72] is used to solve the optimization problem (3.49) and (3.50).

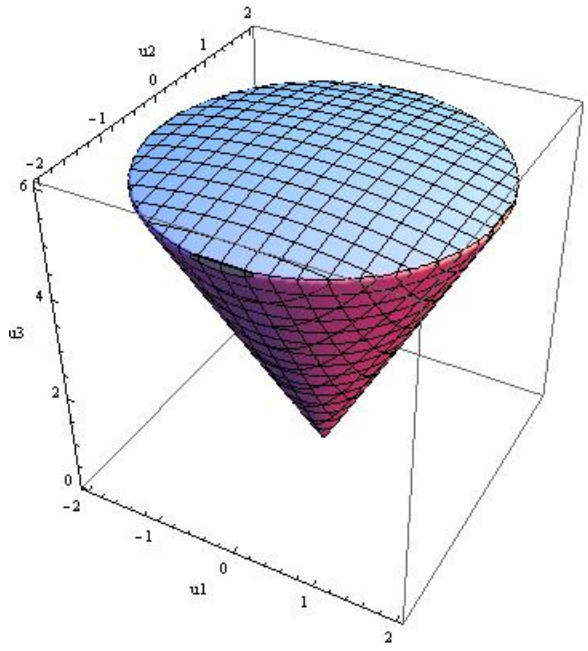

Figure 3.8: Example 3.4.6. The convex control constraint set $\mathcal{U}$ formed by (3.46)-(3.48).

Next, a state space representation of the multi-rotor helicopter is given by

$$\begin{bmatrix} \dot{q} \\ \ddot{q} \end{bmatrix} = \begin{bmatrix} 0_{3\times3} & I_{3\times3} \\ 0_{3\times3} & 0_{3\times3} \end{bmatrix} \begin{bmatrix} q \\ \dot{q} \end{bmatrix} + \begin{bmatrix} 0_{3\times3} \\ \frac{1}{m} I_{3\times3} \end{bmatrix} v + \begin{bmatrix} 0_{3\times1} \\ \begin{bmatrix} 0 \\ 0 \\ -g \end{bmatrix} \end{bmatrix}, \tag{3.51}$$

$$y = \begin{bmatrix} I_{3\times3} & 0_{3\times3} \end{bmatrix} \begin{bmatrix} q \\ \dot{q} \end{bmatrix}, \tag{3.52}$$

$$z = y - w, \tag{3.53}$$

where $v = \mathrm{Sat}(u) \in \mathcal{U}$ is the saturated control input given by

$$v = \begin{bmatrix} v_1 \\ v_2 \\ v_3 \end{bmatrix} = \mathrm{Sat}(u) = \begin{bmatrix} \mathrm{Sat}_1(u_1, u_2, u_3) \\ \mathrm{Sat}_2(u_1, u_2, u_3) \\ \mathrm{Sat}_3(u_3) \end{bmatrix}, \tag{3.54}$$

where

$$\mathrm{Sat}_1(u_1, u_2, u_3) \triangleq \begin{cases} u_1 & \text{if} \quad u_1 \leq \mathrm{Sat}_3(u_3) \tan\varphi_{\max} \cos\vartheta, \\ \mathrm{Sat}_3(u_3) \tan\varphi_{\max} \cos\vartheta & \text{otherwise}, \end{cases} \tag{3.55}$$

$$\mathrm{Sat}_2(u_1, u_2, u_3) \triangleq \begin{cases} u_2 & \text{if} \quad u_2 \leq \mathrm{Sat}_3(u_3) \tan\varphi_{\max} \sin\vartheta, \\ \mathrm{Sat}_3(u_3) \tan\varphi_{\max} \sin\vartheta & \text{otherwise}, \end{cases} \tag{3.56}$$

$$\mathrm{Sat}_3(u_3) \triangleq \mathrm{sat}_{0,6}(u_3), \tag{3.57}$$

and

$$\vartheta \triangleq \operatorname{atan2}(u_2, u_1) = 2 \arctan \frac{u_2}{\sqrt{u_1^2 + u_2^2} + u_1}. \tag{3.58}$$

Note that the function Sat in (3.54) satisfies (A.6). Next, we discretize (3.51)-(3.53) using zero-order-hold. The adaptive controller (3.19) with knowledge of the saturation (3.50) is implemented in feedback with $n_c = 8$, $\eta = 0$, $P_0 = 0.1I$, $d = 1$, $H_1 = I_{3\times 3}$, and we let $\bar{B}_f = \left[\begin{array}{cc} 0.01I_{3\times 3} & 0_{3\times 3} \end{array} \right]$.

Figure 3.9 shows the time history of y_1, y_2, and y_3 of the helicopter. The transient especially along y_3 direction is due to the fact that (3.51)-(3.53) is unstable, the discretized equivalent of (3.51)-(3.53) has nonminimum-phase zeros at -1, and the gravitational acceleration g is unmodeled. Furthermore, we initialize the adaptive controller at $\theta(0) = 0$. Note that the commanded control signal u does not exhibit integrator windup and remains bounded as shown in Figure 3.10, where the black dots represent the control constraint set $\mathcal{U}$, and the blue crosses represent the commanded control u. Note that the blue crosses outside the control constraint set $\mathcal{U}$ (black dots region) are caused by the transient behavior of RLS update in (3.32) and (3.33). Figure 3.11 shows the distance between the unsaturated commanded control $u(k)$ (blue crosses that are outside the control constraint set $\mathcal{U}$ in Figure 3.10) and the saturated control $v(k)$ at each time step. ■

3.5 Conclusions

Adaptive control based on constrained retrospective cost optimization was applied to command following for Hammerstein systems with multivariable convex input saturation. We numerically demonstrated that convex optimization applied to the retrospective cost can improve the tracking performance when following square-wave and triangle-wave commands in the presence of saturation. We also applied

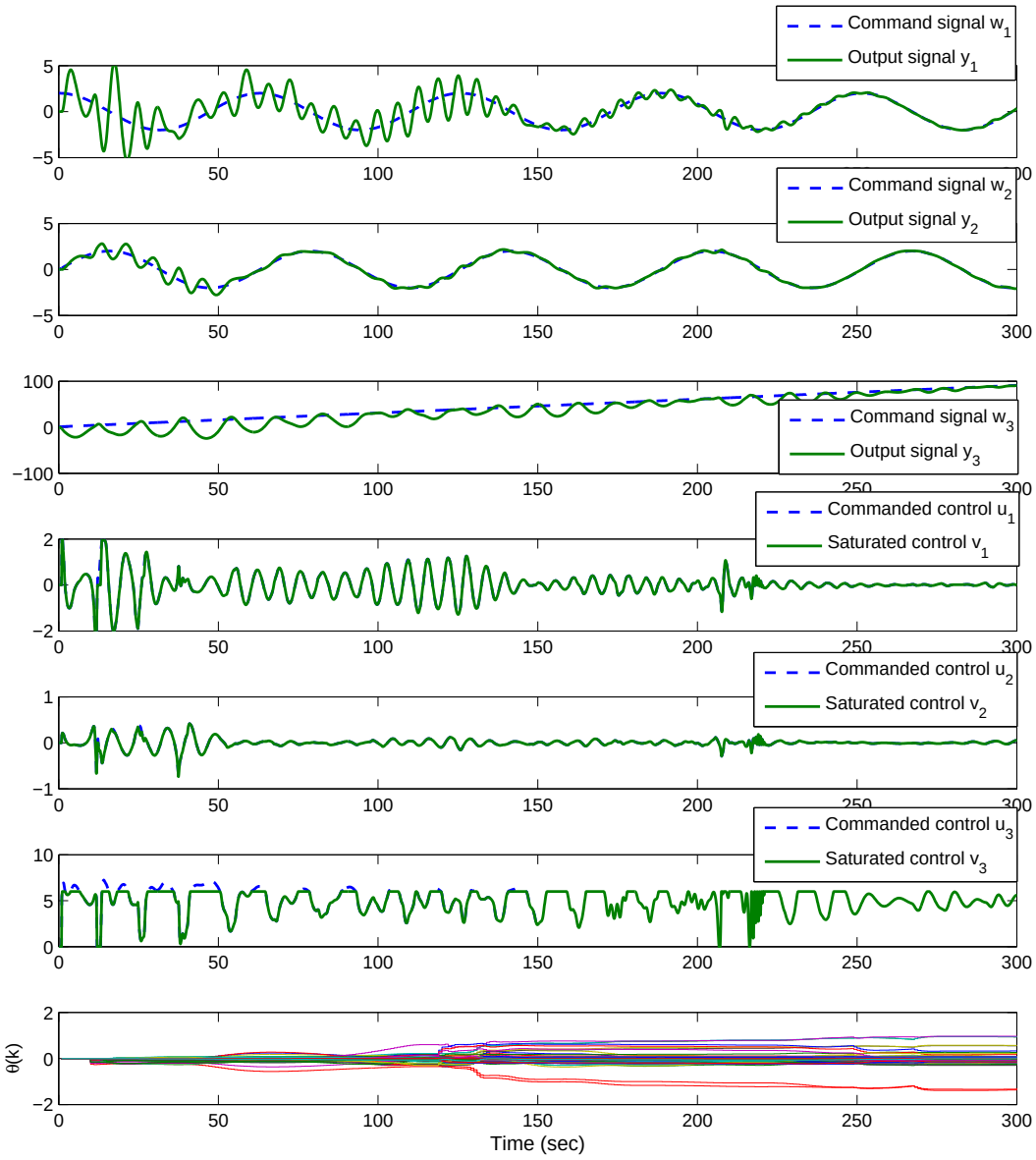

Figure 3.9: Example 3.4.6. *Command following for a multi-rotor helicopter.* The adaptive controller (3.19) with the saturation bounds in (3.50) is implemented in feedback with $n_c = 8$, $\eta = 0$, $P_0 = 0.1I$, $\bar{B}_f = [0.01I_{3\times3} \;\; 0_{3\times3}]$, and $\theta(0) = 0$. Note that the outputs of y_1, y_2, y_3 follow the commands w_1, w_2, and w_3 after the transient.

this technique to a multi-rotor helicopter command-following problem by formulating the multi-input constrained retrospective cost function as a second-order cone optimization (SOCP) problem. With this approach, RCAC is shown to adapt to these constraints. Future research will include a stability analysis of RCAC under input

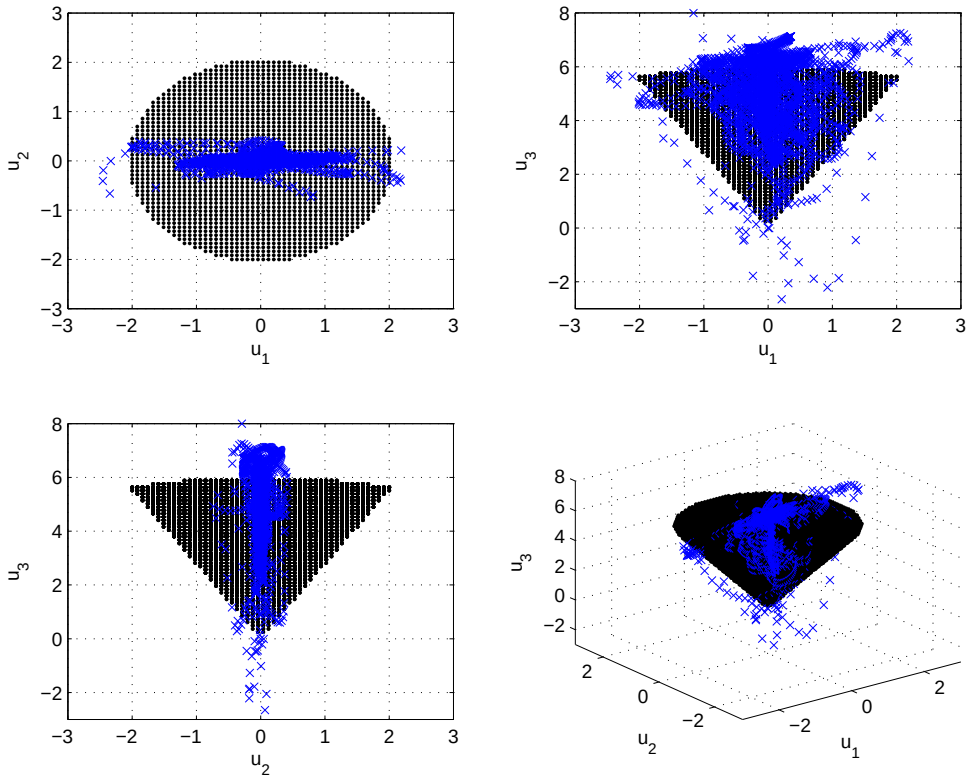

Figure 3.10: Example 3.4.6. The adaptive controller (3.19) with known saturation bounds in (3.50) is implemented in feedback with $n_c = 8$, $\eta = 0$, $P_0 = 0.1I$, $\bar{B}_f = [0.01I_{3\times3}\ 0_{3\times3}]$, and $\theta(0) = 0$. The black dots represent the constraint set in (3.46) and (3.48), and the blue dots represent the unsaturated controller output u. The blue crosses outside the boundary of the constraint (black dots region) are due to the transient behavior of RLS update in (3.32) and (3.33).

saturation.

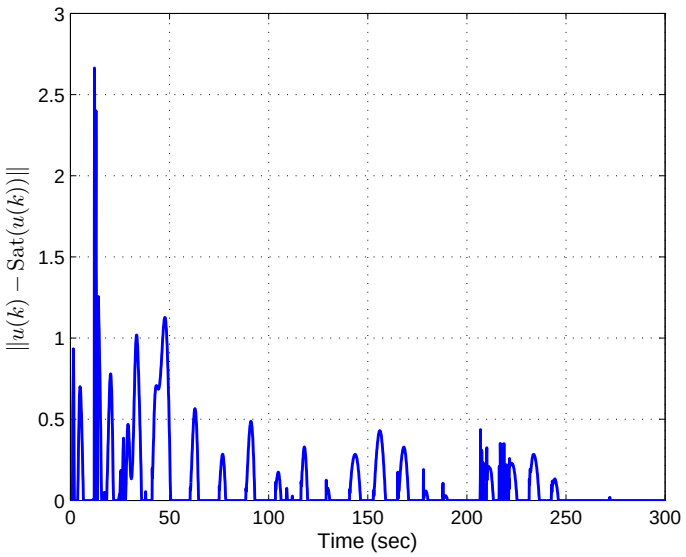

Figure 3.11: Example 3.4.6. At each time step, the distance between the unsaturated commanded control $u(k)$ (blue crosses that are outside the control constraint set $\mathcal{U}$ in Figure 3.10) and the saturated control $\mathrm{Sat}(u(k))$.

CHAPTER IV

Retrospective Cost Adaptive Control with Auxiliary Nonlinearities

In this chapter, we augment retrospective cost adaptive control (RCAC) with auxiliary nonlinearities to address a command-following problem for uncertain Hammerstein systems with possibly non-monotonic input nonlinearities. We assume that only one Markov parameter of the linear plant is known and that the input nonlinearity is uncertain. Auxiliary nonlinearities are used within RCAC to create a globally non-decreasing composite input nonlinearity. The required modeling information for the input nonlinearity includes the intervals of monotonicity as well as values of the nonlinearity that determine overlapping segments of the range of the nonlinearity within each interval of monotonicity. The results of this chapter are published in [58, 59, 82].

4.1 Introduction

A *Hammerstein system* consists of linear dynamics preceded by an input nonlinearity as considered in [83, 84, 85]. This nonlinearity may represent the properties of an actuator, such as saturation to reflect magnitude restrictions on the control input, deadzone to represent actuator stiction, or a signum function to represent on-off op-

eration. The ability to invert the input nonlinearity is often precluded in practice by the fact that the nonlinearity may be neither one-to-one nor onto, and it may also be uncertain.

If the input nonlinearity is uncertain, then adaptive control may be useful for learning the characteristics of the nonlinearity online and compensating for the distortion that it introduces. Adaptive inversion control of Hammerstein systems with uncertain input nonlinearities and linear dynamics is considered in [32, 33, 34]. In contrast, in the present chapter we make no attempt to identify or invert the input nonlinearity. In particular, we apply retrospective cost adaptive control (RCAC) along with auxiliary nonlinearities that account for the presence of the input nonlinearity.

RCAC is applicable to linear plants that are possibly MIMO, nonminimum phase (NMP), and unstable as shown in [24, 23, 25, 26, 27, 28, 29, 30]. RCAC relies on knowledge of Markov parameters and, for NMP open-loop-unstable plants, estimates of the NMP zeros. This information can be obtained from either analytical modeling or system identification, see [31]. As shown in [30], the Markov parameters provide an approach to matching the phase of the plant at the frequencies present in the command and disturbances. Alternative phase-matching techniques are given in [76].

The purpose of the auxiliary nonlinearities is to ensure that RCAC is applied to a Hammerstein system with a globally nondecreasing composite input nonlinearity. In particular, if the input nonlinearity is not nondecreasing, then an auxiliary blocking nonlinearity $\mathcal{N}_{\mathrm{b}}$, an auxiliary sorting nonlinearity $\mathcal{N}_{\mathrm{s}}$, and an auxiliary reflection nonlinearity $\mathcal{N}_{\mathrm{r}}$ are used to create a composite nonlinearity $\mathcal{N} \circ \mathcal{N}_{\mathrm{r}} \circ \mathcal{N}_{\mathrm{s}} \circ \mathcal{N}_{\mathrm{b}}$ that is nondecreasing, thus preserving the signs of the Markov parameters of the linearized system. An additional auxiliary saturation nonlinearity $\mathcal{N}_{\mathrm{sat}}$, which is used to tune the transient response of the closed-loop system, may depend on estimates of the range of the input nonlinearity and the gain of the linear dynamics.

In [32, 33, 34], the input nonlinearities are assumed to be piecewise linear. The present chapter does not impose this restriction. A preliminary version of some of the results in this chapter is given in [58].

The contents of the chapter are as follows. In Section 4.2, we describe the Hammerstein command-following problem. In Section 4.3, we summarize the RCAC algorithm. In Section 4.4, we apply an extension of RCAC using auxiliary nonlinearities to the Hammerstein command-following problem with non-monotonic input nonlinearities. Next, we present examples to illustrate the construction of the auxiliary nonlinearities. Numerical simulation results are presented in Section 4.5, 4.6, and 4.7. In section 4.5, we consider the case where the input nonlinearities are odd. In section 4.6, we propose two approaches for the case where input nonlinearities are even. In section 4.7, we present examples for the case where the input nonlinearities are neither odd or even. Conclusions are given in Section 4.8.

4.2 Hammerstein Command-following Problem

Consider the SISO discrete-time Hammerstein system

$$x(k+1) = Ax(k) + B\mathcal{N}(u(k)) + D_1 w(k), \tag{4.1}$$

$$y(k) = Cx(k), \tag{4.2}$$

where $x(k) \in \mathbb{R}^n$, $u(k)$, $y(k) \in \mathbb{R}$, $w(k) \in \mathbb{R}^d$, $\mathcal{N} : \mathbb{R} \to \mathbb{R}$, and $k \geq 0$. To avoid unnecessary complications, we assume that $\mathcal{N}$ is piecewise right continuous. We consider the Hammerstein command-following problem with the performance variable

$$z(k) = y(k) - r(k), \tag{4.3}$$

where $z(k) \in \mathbb{R}$ is the performance variable and $r(k) \in \mathbb{R}$ is the command. The goal is to develop an adaptive output feedback controller that minimizes the command-following error z using minimal modeling information about the dynamics, disturbance w, and input nonlinearity $\mathcal{N}$. We assume that measurements of $z(k)$ are available for feedback; however, measurements of $v(k) = \mathcal{N}(u(k))$ are not available. A block diagram for (4.1)-(4.3) is shown in Figure 4.1.

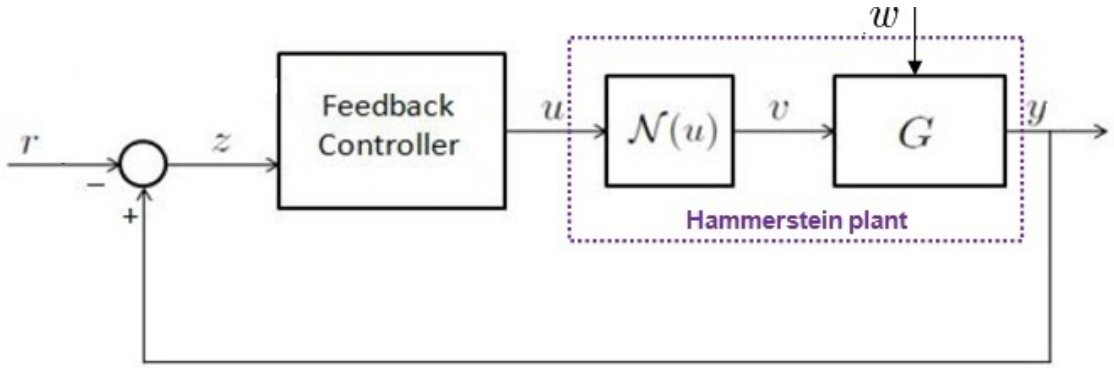

Figure 4.1: Adaptive command-following problem for a Hammerstein plant with input nonlinearity $\mathcal{N}$. We assume that measurements of $z(k)$ are available for feedback; however, measurements of $v(k) = \mathcal{N}(u(k))$ and $w(k)$ are not available.

4.3 Controller Construction

To formulate an adaptive control algorithm for (4.1)-(4.3), we use a strictly proper time-series controller with auxiliary nonlinearities $\mathcal{N}_{\text{sat}}$, $\mathcal{N}_{\text{b}}$, $\mathcal{N}_{\text{s}}$, and $\mathcal{N}_{\text{r}}$ to account for the presence of the input nonlinearity $\mathcal{N}$ in Figure 4.2. The construction of $\mathcal{N}_{\text{sat}}$, $\mathcal{N}_{\text{b}}$, $\mathcal{N}_{\text{s}}$, and $\mathcal{N}_{\text{r}}$ is described in Section 4.4. The RCAC controller of order n_{c} is given by

$$u_{\text{c}}(k) = \sum_{i=1}^{n_{\text{c}}} M_i(k) u_{\text{c}}(k-i) + \sum_{i=1}^{n_{\text{c}}} N_i(k) z(k-i), \tag{4.4}$$

where, for all $i = 1, \ldots, n_{\mathrm{c}}$, $M_i(k) \in \mathbb{R}$, and $N_i(k) \in \mathbb{R}$. The control (4.4) can be expressed as

$$u_{\mathrm{c}}(k) = \theta(k)\phi(k-1),$$

where

$$\theta(k) \triangleq \begin{bmatrix} M_1(k) & \cdots & M_{n_{\mathrm{c}}}(k) & N_1(k) & \cdots & N_{n_{\mathrm{c}}}(k) \end{bmatrix} \in \mathbb{R}^{l_u \times 2n_{\mathrm{c}}}$$

is the controller gain matrix, and the regressor vector $\phi(k)$ is given by

$$\phi(k-1) \triangleq [u_{\mathrm{c}}(k-1) \quad \cdots \quad u_{\mathrm{c}}(k-n_{\mathrm{c}}) \quad z(k-1) \quad \cdots \quad z(k-n_{\mathrm{c}})]^{\mathrm{T}} \in \mathbb{R}^{2n_{\mathrm{c}}}.$$

The transfer function matrix $G_{\mathrm{c},k}(\mathbf{q})$ from z to u_{c} at time step k can be represented by

$$G_{\mathrm{c},k}(\mathbf{q}) \triangleq \frac{N_1(k)\mathbf{q}^{n_{\mathrm{c}}-1} + N_2(k)\mathbf{q}^{n_{\mathrm{c}}-2} + \cdots + N_{n_{\mathrm{c}}}(k)}{\mathbf{q}^{n_{\mathrm{c}}} - \Big(M_1(k)\mathbf{q}^{n_{\mathrm{c}}-1} + \cdots + M_{n_{\mathrm{c}}-1}(k)\mathbf{q} + M_{n_{\mathrm{c}}}(k)\Big)},$$

where the forward shift operator $\mathbf{q}$ accounts for both the free and forced response of the system.

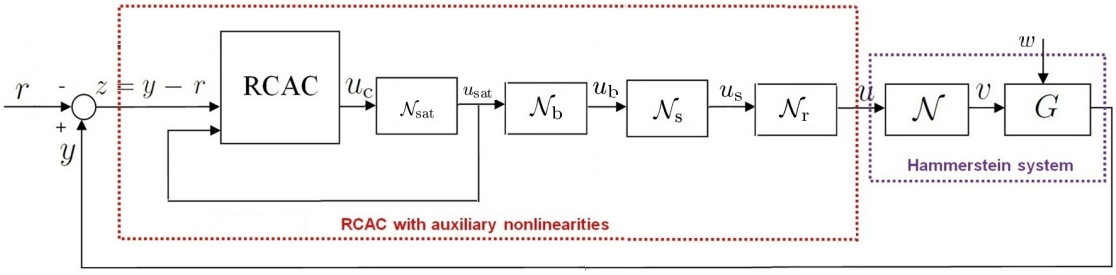

Figure 4.2: Hammerstein command-following problem with the RCAC adaptive controller and auxiliary nonlinearities $\mathcal{N}_{\mathrm{sat}}$, $\mathcal{N}_{\mathrm{b}}$, $\mathcal{N}_{\mathrm{s}}$, and $\mathcal{N}_{\mathrm{r}}$.

Next, for $i \geq 1$, define the Markov parameter

$$H_i \triangleq CA^{i-1}B.$$

For example, $H_1 = CB$ and $H_2 = CAB$. Let ℓ be a positive integer. Then, for all $k \geq \ell$, (4.1) can be written as

$$x(k) = A^{\ell}x(k-\ell) + \sum_{i=1}^{\ell} A^{i-1}B\mathcal{N}(\mathcal{N}_{\mathrm{b}}(\mathcal{N}_{\mathrm{s}}(\mathcal{N}_{\mathrm{r}}(\mathcal{N}_{\mathrm{sat}}(u_{\mathrm{c}}(k-i)))))) + \sum_{i=1}^{\ell} A^{i-1}D_1 w(k-i), \tag{4.5}$$

and thus

$$z(k) = CA^{\ell}x(k-\ell) + \sum_{i=1}^{\ell} CA^{i-1}D_1 w(k-i) - r(k) + \bar{H}\bar{U}(k-1), \tag{4.6}$$

where

$$\bar{H} \triangleq \left[\begin{array}{ccc} H_1 & \cdots & H_{\ell} \end{array} \right] \in \mathbb{R}^{1\times\ell}$$

and

$$\bar{U}(k-1) \triangleq \left[\begin{array}{c} \mathcal{N}(\mathcal{N}_{\mathrm{b}}(\mathcal{N}_{\mathrm{s}}(\mathcal{N}_{\mathrm{r}}(\mathcal{N}_{\mathrm{sat}}(u_{\mathrm{c}}(k-1)))))) \\ \vdots \\ \mathcal{N}(\mathcal{N}_{\mathrm{b}}(\mathcal{N}_{\mathrm{s}}(\mathcal{N}_{\mathrm{r}}(\mathcal{N}_{\mathrm{sat}}(u_{\mathrm{c}}(k-\ell)))))) \end{array} \right].$$

Next, we rearrange the columns of $\bar{H}$ and the components of $\bar{U}(k-1)$ and partition the resulting matrix and vector so that

$$\bar{H}\bar{U}(k-1) = \mathcal{H}'U'(k-1) + \mathcal{H}U(k-1), \tag{4.7}$$

where $\mathcal{H}' \in \mathbb{R}^{1\times(\ell-l_U)}$, $\mathcal{H} \in \mathbb{R}^{1\times l_U}$, $U'(k-1) \in \mathbb{R}^{\ell-l_U}$, and $U(k-1) \in \mathbb{R}^{l_U}$. Then, we

can rewrite (4.6) as

$$z(k) = \mathcal{S}(k) + \mathcal{H}U(k-1), \tag{4.8}$$

where

$$\mathcal{S}(k) \triangleq CA^{\ell}x(k-\ell) + \sum_{i=1}^{\ell} CA^{i-1}D_1 w(k-i) - r(k) + \mathcal{H}'U'(k-1). \tag{4.9}$$

Next, for $j = 1, \ldots, s$, we rewrite (4.8) with a delay of k_j time steps, where $0 \leq k_1 \leq k_2 \leq \cdots \leq k_s$, in the form

$$z_j(k-k_j) = \mathcal{S}_j(k-k_j) + \mathcal{H}_j U_j(k-k_j-1), \tag{4.10}$$

where (4.9) becomes

$$\mathcal{S}_j(k-k_j) \triangleq CA^{\ell}x(k-k_j-\ell) + \sum_{i=1}^{\ell} CA^{i-1}D_1 w(k-k_j-i) - r(k-k_j) + \mathcal{H}'_j U'_j(k-k_j-1)$$

and (4.7) becomes

$$\bar{H}\bar{U}(k-k_j-1) = \mathcal{H}'_j U'_j(k-k_j-1) + \mathcal{H}_j U_j(k-k_j-1),$$

where $\mathcal{H}'_j \in \mathbb{R}^{1\times(\ell-l_{U_j})}$, $\mathcal{H}_j \in \mathbb{R}^{1\times l_{U_j}}$, $U'_j(k-k_j-1) \in \mathbb{R}^{\ell-l_{U_j}}$, and $U_j(k-k_j-1) \in \mathbb{R}^{l_{U_j}}$. Now, by stacking $z(k-k_1), \ldots, z(k-k_s)$, we define the *extended performance*

$$Z(k) \triangleq \begin{bmatrix} z_1(k-k_1) \\ \vdots \\ z_s(k-k_s) \end{bmatrix} \in \mathbb{R}^s. \tag{4.11}$$

Therefore,

$$Z(k) = \tilde{\mathcal{S}}(k) + \tilde{\mathcal{H}}\tilde{U}(k-1), \tag{4.12}$$

where

$$\tilde{\mathcal{S}}(k) \triangleq \begin{bmatrix} \mathcal{S}_1(k-k_1) \\ \vdots \\ \mathcal{S}_s(k-k_s) \end{bmatrix} \in \mathbb{R}^s,$$

$\tilde{U}(k-1)$ has the form

$$\tilde{U}(k-1) \triangleq \begin{bmatrix} \mathcal{N}(\mathcal{N}_{\mathrm{b}}(\mathcal{N}_{\mathrm{s}}(\mathcal{N}_{\mathrm{r}}(\mathcal{N}_{\mathrm{sat}}(u_{\mathrm{c}}(k-q_1)))))) \\ \vdots \\ \mathcal{N}(\mathcal{N}_{\mathrm{b}}(\mathcal{N}_{\mathrm{s}}\mathcal{N}_{\mathrm{r}}(\mathcal{N}_{\mathrm{sat}}(u_{\mathrm{c}}(k-q_{l_{\tilde{U}}}))))) \end{bmatrix} \in \mathbb{R}^{l_{\tilde{U}}},$$

where, for $i = 1, \ldots, l_{\tilde{U}}$, $k_1 \leq q_i \leq k_s + \ell$, and $\tilde{\mathcal{H}} \in \mathbb{R}^{s \times l_{\tilde{U}}}$ is constructed according to the structure of $\tilde{U}(k-1)$. The vector $\tilde{U}(k-1)$ is formed by stacking $U_1(k-k_1-1), \ldots, U_s(k-k_s-1)$ and removing copies of repeated components.

Next, for $j = 1, \ldots, s$, we define the *retrospective performance*

$$\hat{z}_j(k-k_j) \triangleq \mathcal{S}_j(k-k_j) + \mathcal{H}_j\hat{U}_j(k-k_j-1), \tag{4.13}$$

where the past controls $U_j(k-k_j-1)$ in (4.10) are replaced by the retrospective controls $\hat{U}_j(k-k_j-1)$. In analogy with (4.11), the *extended retrospective performance*

for (4.13) is defined as

$$\hat{Z}(k) \triangleq \begin{bmatrix} \hat{z}_1(k-k_1) \\ \vdots \\ \hat{z}_s(k-k_s) \end{bmatrix} \in \mathbb{R}^s$$

and thus is given by

$$\hat{Z}(k) = \tilde{\mathcal{S}}(k) + \tilde{\mathcal{H}}\hat{\tilde{U}}(k-1), \tag{4.14}$$

where the components of $\hat{\tilde{U}}(k-1) \in \mathbb{R}^{l_{\tilde{U}}}$ are the components of $\hat{U}_1(k-k_1-1), \ldots, \hat{U}_s(k-k_s-1)$ ordered in the same way as the components of $\tilde{U}(k-1)$. Subtracting (4.12) from (4.14) yields

$$\hat{Z}(k) = Z(k) - \tilde{\mathcal{H}}\tilde{U}(k-1) + \tilde{\mathcal{H}}\hat{\tilde{U}}(k-1). \tag{4.15}$$

Finally, we define the *retrospective cost function*

$$J(\hat{\tilde{U}}(k-1), k) \triangleq \hat{Z}^{\mathrm{T}}(k)R(k)\hat{Z}(k), \tag{4.16}$$

where $R(k) \in \mathbb{R}^{s\times s}$ is a positive-definite performance weighting. The goal is to determine retrospectively optimized controls $\hat{\tilde{U}}(k-1)$ that would have provided better performance than the controls $U(k)$ that were applied to the system. The retrospectively optimized control values $\hat{\tilde{U}}(k-1)$ are subsequently used to update the controller.

Next, to ensure that (4.16) has a global minimizer, we consider the regularized cost

$$\bar{J}(\hat{\tilde{U}}(k-1), k) \triangleq \hat{Z}^{\mathrm{T}}(k)R(k)\hat{Z}(k) + \eta(k)\hat{\tilde{U}}^{\mathrm{T}}(k-1)\hat{\tilde{U}}(k-1), \tag{4.17}$$

where $\eta(k) \geq 0$. Substituting (4.15) into (4.17) yields

$$\bar{J}(\hat{\tilde{U}}(k-1),k) = \hat{\tilde{U}}(k-1)^{\mathrm{T}}\mathcal{A}(k)\hat{\tilde{U}}(k-1) + \mathcal{B}(k)\hat{\tilde{U}}(k-1) + \mathcal{C}(k),$$

where

$$\begin{aligned}
\mathcal{A}(k) &\triangleq \tilde{\mathcal{H}}^{\mathrm{T}}R(k)\tilde{\mathcal{H}} + \eta(k)I_{l_{\tilde{U}}},\\
\mathcal{B}(k) &\triangleq 2\tilde{\mathcal{H}}^{\mathrm{T}}R(k)[Z(k) - \tilde{\mathcal{H}}\tilde{U}(k-1)],\\
\mathcal{C}(k) &\triangleq Z^{\mathrm{T}}(k)R(k)Z(k) - 2Z^{\mathrm{T}}(k)R(k)\tilde{\mathcal{H}}\tilde{U}(k-1) + \tilde{U}^{\mathrm{T}}(k-1)\tilde{\mathcal{H}}^{\mathrm{T}}R(k)\tilde{\mathcal{H}}\tilde{U}(k-1).
\end{aligned}$$

If either $\tilde{\mathcal{H}}$ has full column rank or $\eta(k) > 0$, then $\mathcal{A}(k)$ is positive definite. In this case, $\bar{J}(\hat{\tilde{U}}(k-1),k)$ has the unique global minimizer

$$\hat{\tilde{U}}(k-1) = -\frac{1}{2}\mathcal{A}^{-1}(k)\mathcal{B}(k). \tag{4.18}$$

Next, let d be a positive integer such that $\hat{\tilde{U}}(k-1)$ contains $\hat{u}(k-d)$, and define the cumulative cost function

$$J_{\mathrm{R}}(\theta,k) \triangleq \sum_{i=d+1}^{k} \lambda^{k-i}\|\theta(k)\phi(i-d-1) - \hat{u}(i-d)\|^2 + \lambda^k(\theta(k)-\theta_0)P_0^{-1}(\theta(k)-\theta_0)^{\mathrm{T}}, \tag{4.19}$$

where $\|\cdot\|$ is the Euclidean norm, and $\lambda \in (0,1]$ is the forgetting factor. Minimizing (4.19) yields

$$\begin{aligned}
\theta(k) = \theta(k-1) &+ \beta(k)[\phi^{\mathrm{T}}(k-d)P(k-1)\phi(k-d-1) + \lambda]^{-1}P(k-1)\phi(k-d-1)\\
&\cdot [\theta(k-1)\phi(k-d-1) - \hat{u}(k-d)],
\end{aligned}$$

where $\beta(k)$ is either zero or one. The error covariance is updated by

$$P(k) = \beta(k)\lambda^{-1}P(k-1) + [1-\beta(k)]P(k-1) - \beta(k)\lambda^{-1}P(k-1)\phi(k-d-1)$$
$$\cdot [\phi^{\mathrm{T}}(k-d-1)P(k-1)\phi(k-d) + \lambda]^{-1} \cdot \phi^{\mathrm{T}}(k-d-1)P(k-1).$$

We initialize the error covariance matrix as $P(0) = \alpha I_{2n_{\mathrm{c}}}$, where $\alpha > 0$. Note that when $\beta(k) = 0$, $\theta(k) = \theta(k-1)$ and $P(k) = P(k-1)$. Therefore, setting $\beta(k) = 0$ switches off the controller adaptation, and thus freezes the control gains. When $\beta(k) = 1$, the controller is allowed to adapt. The parameter $\beta(k)$ is used only for numerical examples to illustrate the effect of adaptation.

4.4 Auxiliary Nonlinearities

In this section, we construct the auxiliary nonlinearities $\mathcal{N}_{\mathrm{sat}}, \mathcal{N}_{\mathrm{b}}, \mathcal{N}_{\mathrm{s}}$, and $\mathcal{N}_{\mathrm{r}}$ in Figure 4.2 along with the required model information. $\mathcal{N}_{\mathrm{sat}}$ modifies u_{c} to obtain the regressor input u_{sat}, while $\mathcal{N}_{\mathrm{b}}$, $\mathcal{N}_{\mathrm{s}}$, and $\mathcal{N}_{\mathrm{r}}$ modify u_{sat} to produce the Hammerstein plant input u. The auxiliary nonlinearities $\mathcal{N}_{\mathrm{b}}$, $\mathcal{N}_{\mathrm{s}}$, and $\mathcal{N}_{\mathrm{r}}$ are chosen such that the composite input nonlinearity $\mathcal{N} \circ \mathcal{N}_{\mathrm{r}} \circ \mathcal{N}_{\mathrm{s}} \circ \mathcal{N}_{\mathrm{b}}$ is globally nondecreasing. To avoid unnecessary complications, we assume that $\mathcal{N} \circ \mathcal{N}_{\mathrm{r}} \circ \mathcal{N}_{\mathrm{s}} \circ \mathcal{N}_{\mathrm{b}}$ is redefined at points of discontinuity to render it piecewise right continuous.

For the Hammerstein command-following problem, we assume that G is uncertain except for an estimate of a single nonzero Markov parameter. The input nonlinearity $\mathcal{N}$ is also uncertain, as described below.

4.4.1 Auxiliary Saturation Nonlinearity $\mathcal{N}_{\rm sat}$

The auxiliary saturation nonlinearity $\mathcal{N}_{\rm sat}$ is defined to be the saturation function $\mathrm{sat}_{p,q}$ given by

$$\mathcal{N}_{\rm sat}(u_{\rm c}) = \mathrm{sat}_{p,q}(u_{\rm c}) = \begin{cases} p, & \text{if} \quad u_{\rm c} < p, \\ u_{\rm c}, & \text{if} \quad p \leq u_{\rm c} \leq q, \\ q, & \text{if} \quad u_{\rm c} > q, \end{cases} \tag{4.20}$$

where the real numbers p and q are the lower and upper saturation levels, respectively. For minimum-phase plants, the auxiliary nonlinearity $\mathcal{N}_{\rm sat}$ is not needed, and thus, in this case, the saturation levels p and q are chosen to be large negative and positive numbers, respectively. For NMP plants, the saturation levels are used to tune the transient behavior. In addition, the saturation levels are chosen to provide a sufficiently large range of the control input to follow the command r. These values depend on the range of the input nonlinearity $\mathcal{N}$ as well as the gain of the linear system G at frequencies in the spectra of r and w.

4.4.2 Auxiliary Reflection Nonlinearity $\mathcal{N}_{\rm r}$

If the input nonlinearity $\mathcal{N}$ is not monotonic, then the auxiliary reflection nonlinearity $\mathcal{N}_{\rm r}$ is used to create a composite nonlinearity $\mathcal{N} \circ \mathcal{N}_{\rm r}$ that is piecewise nondecreasing. To construct $\mathcal{N}_{\rm r}$, we assume that the intervals of monotonicity of the input nonlinearity $\mathcal{N}$ are known, as described below.

In Section 4.4.3 and 4.4.4 below we restrict $\mathcal{N}_{\rm s}$ and $\mathcal{N}_{\rm b}$ so that $\mathcal{N}_{\rm s} : [p,q] \to [p,q]$ and $\mathcal{N}_{\rm b} : [p,q] \to [p,q]$. With this construction, we need to consider only $u_{\rm s} \in [p,q]$. Therefore, let $I_1, I_2, \ldots$ be the smallest number of intervals of monotonicity of $\mathcal{N}$ that are a partition of the interval $[p,q]$. If $\mathcal{N}$ is nondecreasing on I_i, then $\mathcal{N}_{\rm r}(u_{\rm s}) \stackrel{\triangle}{=} u_{\rm s}$ for all $u_{\rm s} \in I_i$. Alternatively, if $\mathcal{N}$ is nonincreasing on $I_i = [p_i, q_i)$, then $\mathcal{N}_{\rm r}(u_{\rm s}) \stackrel{\triangle}{=}$

$p_i + q_i - u_{\rm s} \in I_i$ for all $u_{\rm s} \in I_i$. Finally, if $\mathcal{N}$ is constant on I_i, then either choice can be used. Thus, $\mathcal{N}_{\rm r}$ is a piecewise-linear function that reflects $\mathcal{N}$ about $u_{\rm s} = \frac{p_i+q_i}{2}$ within each interval of monotonicity so that $\mathcal{N} \circ \mathcal{N}_{\rm r}$ is nondecreasing on I_i, and thus $\mathcal{N} \circ \mathcal{N}_{\rm r}$ is piecewise nondecreasing on I. Let $\mathcal{R}_I(f)$ denote the range of the function f with arguments in I.

Proposition 4.4.1. *Assume that $\mathcal{N}_{\rm r}$ is constructed by the above rule. Then the following statements hold:*

1. *$\mathcal{N} \circ \mathcal{N}_{\rm r}$ is piecewise nondecreasing on $[p, q]$.*

2. *$\mathcal{R}_I(\mathcal{N} \circ \mathcal{N}_{\rm r}) = \mathcal{R}_I(\mathcal{N})$.*

Proof. Let $I_i = (p_i, q_i)$. We first assume that $\mathcal{N}$ is nondecreasing on I_i. Since $\mathcal{N}_{\rm r}(u_{\rm s}) = u_{\rm s}$ for all $u_{\rm s} \in I_i$, it follows that $\mathcal{N} \circ \mathcal{N}_{\rm r}(u_{\rm s}) = \mathcal{N}(u_{\rm s})$ for all $u_{\rm s} \in I_i$. Hence $\mathcal{N} \circ \mathcal{N}_{\rm r}$ is nondecreasing on I_i and thus piecewise nondecreasing.

Alternatively, assume that $\mathcal{N}$ is nonincreasing on I_i. Let $u_{{\rm s},1}, u_{{\rm s},2} \in I_i$, where $u_{{\rm s},1} \leq u_{{\rm s},2}$. Then, $u_2 \stackrel{\triangle}{=} p_i + q_i - u_{{\rm s},2} \leq u_1 \stackrel{\triangle}{=} p_i + q_i - u_{{\rm s},1}$. Therefore, since $\mathcal{N}$ is nonincreasing on I_i, it follows that $\mathcal{N}(\mathcal{N}_{\rm r}(u_{{\rm s},1})) = \mathcal{N}(u_1) \leq \mathcal{N}(u_2) = \mathcal{N}(\mathcal{N}_{\rm r}(u_{{\rm s},2}))$. Thus, $\mathcal{N} \circ \mathcal{N}_{\rm r}$ is nondecreasing on I_i.

To prove *ii*), assume that $\mathcal{N}$ is nondecreasing on I_i. Since $\mathcal{N}_{\rm r}(u_{\rm s}) = u_{\rm s}$ for all $u_{\rm s} \in I_i$, it follows that $\mathcal{N}_{\rm r}(I_i) = I_i$, that is, $\mathcal{N}_{\rm r} : I_i \to I_i$ is onto. Alternatively, assume that $\mathcal{N}$ is nonincreasing on I_i so that $\mathcal{N}_{\rm r}(u_{\rm s}) = p_i + q_i - u_{\rm s}$. Note that $\mathcal{N}_{\rm r}(p_i) = q_i$, $\mathcal{N}_{\rm r}(q_i) = p_i$, and $\mathcal{N}_{\rm r}$ is continuous and decreasing on I_i. Therefore, $\mathcal{N}_{\rm r}(I_i) = I_i$, and thus $\mathcal{N}_{\rm r} : I_i \to I_i$ is onto. Hence, $\mathcal{R}_I(\mathcal{N} \circ \mathcal{N}_{\rm r}) = \mathcal{R}_I(\mathcal{N})$. □

Example 4.4.1. Consider the nonincreasing input nonlinearity $\mathcal{N}(u) = -{\rm sat}_{-1,1}(u-5)$ shown in Figure 4.3(a). Let $\mathcal{N}_{\rm r}(u_{\rm s}) = -u_{\rm s} + 10$ for all $u_{\rm s} \in [3, 7]$ according to Proposition 4.4.1. Figure 4.3(c) shows that the composite nonlinearity $\mathcal{N} \circ \mathcal{N}_{\rm r}$ is nondecreasing on $I \stackrel{\triangle}{=} [-2, 2]$. Note that $\mathcal{R}_I(\mathcal{N} \circ \mathcal{N}_{\rm r}) = \mathcal{R}_I(\mathcal{N}) = [-1, 1]$. ■

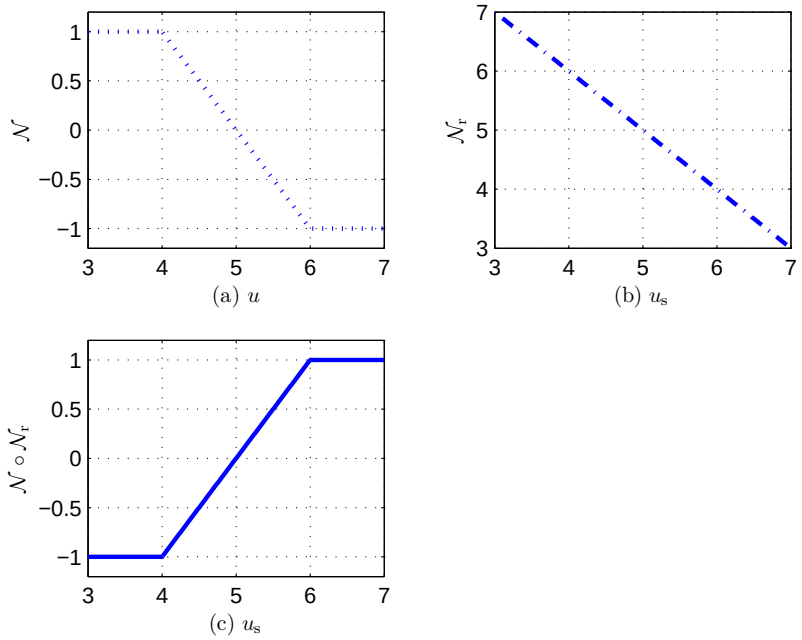

Figure 4.3: Example 4.4.1. (a) Input nonlinearity $\mathcal{N}(u) = -\mathrm{sat}_{-1,1}(u-5)$. (b) Auxiliary reflection nonlinearity $\mathcal{N}_\mathrm{r}(u_\mathrm{s}) = -u_\mathrm{s} + 10$ for $u_\mathrm{s} \in [3,7]$. (c) Composite nonlinearity $\mathcal{N} \circ \mathcal{N}_\mathrm{r}$. Note that $\mathcal{N} \circ \mathcal{N}_\mathrm{r}$ is nondecreasing on $I \stackrel{\triangle}{=} [3,7]$ and $\mathcal{R}_I(\mathcal{N} \circ \mathcal{N}_\mathrm{r}) = \mathcal{R}_I(\mathcal{N}) = [-1,1]$.

Example 4.4.2. Consider the non-monotonic input nonlinearity $\mathcal{N}(u) = |u-5|$ shown in Figure 4.4(a). Let $\mathcal{N}_\mathrm{r}(u_\mathrm{s}) = -u_\mathrm{s} + 6$ for all $u_\mathrm{s} \in [1,5)$ and $\mathcal{N}_\mathrm{r}(u_\mathrm{s}) = u_\mathrm{s}$ otherwise according to Proposition 4.4.1. Figure 4.4(c) shows that the composite nonlinearity $\mathcal{N} \circ \mathcal{N}_\mathrm{r}$ is piecewise nondecreasing but not globally nondecreasing on $I \stackrel{\triangle}{=} [1,9]$, and that $\mathcal{R}_I(\mathcal{N} \circ \mathcal{N}_\mathrm{r}) = \mathcal{R}_I(\mathcal{N}) = [0,4]$. ■

Example 4.4.3. Consider the non-monotonic input nonlinearity

$$\mathcal{N}(u) = \begin{cases} -\frac{1}{2}u, & \text{if } u \leq 0, \\ u-1, & \text{if } u > 0, \end{cases} \tag{4.21}$$

shown in Figure 4.5(a). Let $\mathcal{N}_\mathrm{r}(u_\mathrm{s}) = -u_\mathrm{s} - 2$ for all $u_\mathrm{s} \in [-2,0)$ and $\mathcal{N}_\mathrm{r}(u_\mathrm{s}) = u_\mathrm{s}$ otherwise according to Proposition 4.4.1. Figure 4.5(c) shows that the composite nonlinearity $\mathcal{N} \circ \mathcal{N}_\mathrm{r}$ is piecewise nondecreasing but not globally nondecreasing on

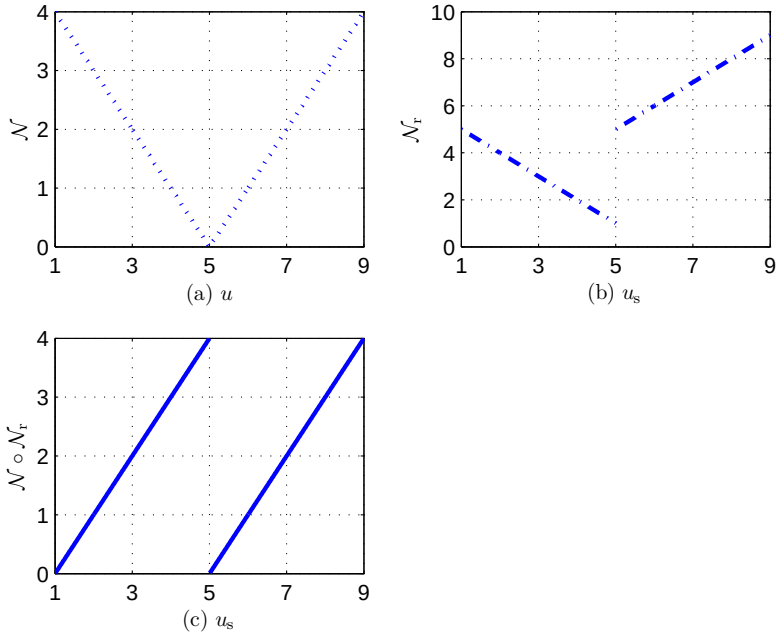

Figure 4.4: Example 4.4.2 (a) Non-monotonic input nonlinearity $\mathcal{N}(u) = -|u-5|$. (b) Auxiliary reflection nonlinearity $\mathcal{N}_{\rm r}(u_{\rm s}) = -u_{\rm s}+6$ for $u_{\rm s} \in [1,5)$ and $\mathcal{N}_{\rm r}(u_{\rm s}) = u_{\rm s}$ otherwise. (c) Composite nonlinearity $\mathcal{N} \circ \mathcal{N}_{\rm r}$. Note that $\mathcal{N} \circ \mathcal{N}_{\rm r}$ is piecewise nondecreasing but not globally nondecreasing on $I \stackrel{\triangle}{=} [1,9]$, and that $\mathcal{R}_I(\mathcal{N} \circ \mathcal{N}_{\rm r}) = \mathcal{R}_I(\mathcal{N}) = [0,4]$.

$I \stackrel{\triangle}{=} [-2,1]$, and that $\mathcal{R}_I(\mathcal{N} \circ \mathcal{N}_{\rm r}) = \mathcal{R}_I(\mathcal{N}) = [-1,1]$. ■

4.4.3 Auxiliary Sorting Nonlinearity $\mathcal{N}_{\rm s}$

As illustrated by Example 4.4.2 and Example 4.4.3, $\mathcal{N} \circ \mathcal{N}_{\rm r}$ is piecewise nondecreasing but not globally nondecreasing. In order to construct a composite input nonlinearity that is globally nondecreasing, we introduce the auxiliary sorting nonlinearity $\mathcal{N}_{\rm s}$ and auxiliary blocking nonlinearity $\mathcal{N}_{\rm b}$. The auxiliary sorting nonlinearity $\mathcal{N}_{\rm s}$ sorts portions of the piecewise nondecreasing nonlinearity $\mathcal{N} \circ \mathcal{N}_{\rm r}$ to create a composite nonlinearity $\mathcal{N} \circ \mathcal{N}_{\rm r} \circ \mathcal{N}_{\rm s}$ so that the composite nonlinearity $\mathcal{N} \circ \mathcal{N}_{\rm r} \circ \mathcal{N}_{\rm s} \circ \mathcal{N}_{\rm b}$ is globally nondecreasing. $\mathcal{N}_{\rm b}$ is discussed in Section 4.4.4. To construct $\mathcal{N}_{\rm s}$, we assume that the range of $\mathcal{N} \circ \mathcal{N}_{\rm r}$ within each interval of monotonicity is known. No further modeling information about $\mathcal{N}$ is needed.

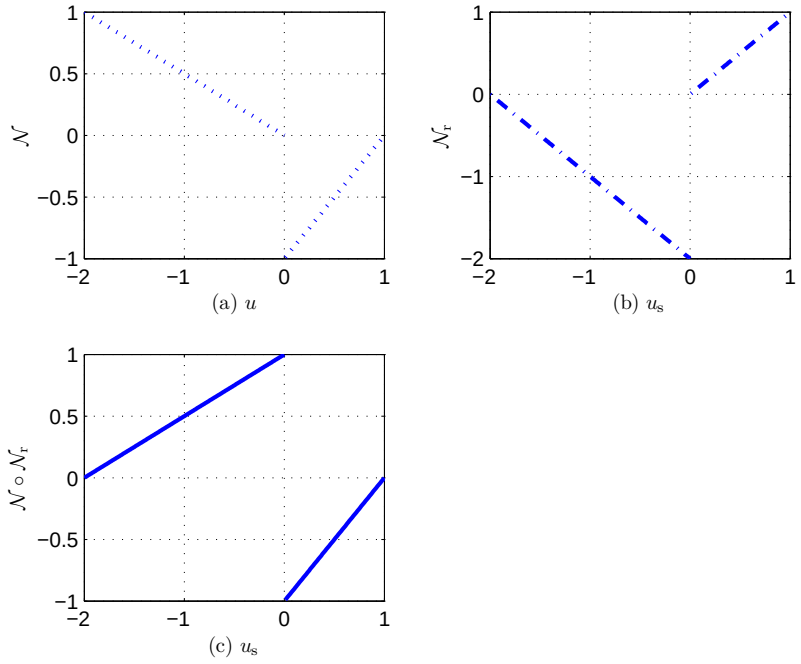

Figure 4.5: Example 4.4.3 (a) Non-monotonic input nonlinearity (4.21). (b) Auxiliary reflection nonlinearity $\mathcal{N}_\mathrm{r}(u_\mathrm{s}) = -u_\mathrm{s} - 2$ for $u_\mathrm{s} \in [-2, 0)$ and $\mathcal{N}_\mathrm{r}(u_\mathrm{s}) = u_\mathrm{s}$ otherwise. (c) Composite nonlinearity $\mathcal{N} \circ \mathcal{N}_\mathrm{r}$. Note that $\mathcal{N} \circ \mathcal{N}_\mathrm{r}$ is piecewise nondecreasing but not globally nondecreasing on $I \stackrel{\triangle}{=} [-2, 0]$, and that $\mathcal{R}_I(\mathcal{N} \circ \mathcal{N}_\mathrm{r}) = \mathcal{R}_I(\mathcal{N}) = [-1, 1]$.

Let $\mathcal{N}_\mathrm{s}$ be the piecewise right-continuous affine function defined as follows. Let $I_1 = [p_1, q_1), I_2 = [p_2, q_2), \ldots$ be the smallest number of intervals of monotonicity of $\mathcal{N}$ that are a partition of the interval $[p, q]$. If $\mathcal{R}_{I_i}(\mathcal{N} \circ \mathcal{N}_\mathrm{r}) \subset \mathcal{R}_{I_j}(\mathcal{N} \circ \mathcal{N}_\mathrm{r})$ for all $i \neq j$ or $(\mathcal{N} \circ \mathcal{N}_\mathrm{r})(q_i) \leq (\mathcal{N} \circ \mathcal{N}_\mathrm{r})(q_j)$, where $q_i < q_j$, then $\mathcal{N}_\mathrm{s}(u_\mathrm{b}) \stackrel{\triangle}{=} u_\mathrm{b}$ for all $u_\mathrm{b} \in I_i \cup I_j = [p_i, q_i) \cup [p_j, q_j)$, and thus $\mathcal{N}_\mathrm{s}$ is not needed. Alternatively, if $\mathcal{R}_{I_i}(\mathcal{N} \circ \mathcal{N}_\mathrm{r}) \nsubseteq \mathcal{R}_{I_j}(\mathcal{N} \circ \mathcal{N}_\mathrm{r})$ for all $i \neq j$ and $(\mathcal{N} \circ \mathcal{N}_\mathrm{r})(q_i) > (\mathcal{N} \circ \mathcal{N}_\mathrm{r})(q_j)$, where $q_i < q_j$, then $\mathcal{N}_\mathrm{s}(u_\mathrm{b}) \stackrel{\triangle}{=} \frac{1}{q_i - p_i}\left[(q_j - p_j)u_\mathrm{b} + p_j q_i - p_i q_j\right] \in I_j$ for all $u_\mathrm{b} \in I_i$ and $\mathcal{N}_\mathrm{s}(u_\mathrm{b}) \stackrel{\triangle}{=} \frac{1}{q_j - p_j}\left[(q_i - p_i)u_\mathrm{b} + p_i q_j - p_j q_i\right] \in I_i$ for all $u_\mathrm{b} \in I_j$.

Proposition 4.4.2. *Assume that $\mathcal{N}_\mathrm{s}$ is constructed by the above rule. Then the following statements hold:*

1. *$\mathcal{N} \circ \mathcal{N}_\mathrm{r} \circ \mathcal{N}_\mathrm{s}$ is piecewise nondecreasing on $[p, q]$.*

2. $\mathcal{R}_I(\mathcal{N} \circ \mathcal{N}_\mathrm{r} \circ \mathcal{N}_\mathrm{s}) = \mathcal{R}_I(\mathcal{N})$.

Proof. Let $I_i = (p_i, q_i)$ and $I_j = (p_j, q_j)$. We first assume that $\mathcal{R}_{I_i}(\mathcal{N} \circ \mathcal{N}_\mathrm{r}) \subset \mathcal{R}_{I_j}(\mathcal{N} \circ \mathcal{N}_\mathrm{r})$ for all $i \neq j$ or $\mathcal{N} \circ \mathcal{N}_\mathrm{r}(q_i) \leq \mathcal{N} \circ \mathcal{N}_\mathrm{r}(q_j)$, where $q_i < q_j$. Since $\mathcal{N}_\mathrm{s}(u_\mathrm{b}) = u_\mathrm{b}$ for all $u_\mathrm{b} \in I_i \cup I_j$, it follows from Proposition 4.4.1 *i*) that $\mathcal{N} \circ \mathcal{N}_\mathrm{r} \circ \mathcal{N}_\mathrm{s}$ is piecewise nondecreasing on $[p, q]$.

Alternatively, assume that $\mathcal{R}_{I_i}(\mathcal{N} \circ \mathcal{N}_\mathrm{r}) \nsubseteq \mathcal{R}_{I_j}(\mathcal{N} \circ \mathcal{N}_\mathrm{r})$ for all $i \neq j$ and $(\mathcal{N} \circ \mathcal{N}_\mathrm{r})(q_i) > (\mathcal{N} \circ \mathcal{N}_\mathrm{r})(q_j)$, where $q_i < q_j$. It follows from $\mathcal{N}_\mathrm{s}(u_\mathrm{b}) \stackrel{\triangle}{=} \frac{1}{q_i - p_i}\left[(q_j - p_j)u_\mathrm{b} + p_j q_i - p_i q_j\right] \in I_j$ for all $u_\mathrm{b} \in I_i$ and $\mathcal{N}_\mathrm{s}(u_\mathrm{b}) \stackrel{\triangle}{=} \frac{1}{q_j - p_j}\left[(q_i - p_i)u_\mathrm{b} + p_i q_j - p_j q_i\right] \in I_i$ for all $u_\mathrm{b} \in I_j$ that $\mathcal{N}_\mathrm{s} : I_i \to I_j$ and $\mathcal{N}_\mathrm{s} : I_j \to I_i$. Next, Let $u_{\mathrm{b},1}, u_{\mathrm{b},2} \in I_i$, where $u_{\mathrm{b},1} \leq u_{\mathrm{b},2}$. Then,

$$u_{s,1} \stackrel{\triangle}{=} \frac{1}{q_i - p_i}\left[(q_j - p_j)u_{\mathrm{b},1} + p_j q_i - p_i q_j\right] \in I_j \leq u_{s,2} \stackrel{\triangle}{=} \frac{1}{q_i - p_i}\left[(q_j - p_j)u_{\mathrm{b},2} + p_j q_i - p_i q_j\right] \in I_j.$$

Therefore, since $\mathcal{N} \circ \mathcal{N}_\mathrm{r}$ is nondecreasing on I_j, it follows that $(\mathcal{N} \circ \mathcal{N}_\mathrm{r} \circ \mathcal{N}_\mathrm{s})(u_{\mathrm{b},1}) = (\mathcal{N} \circ \mathcal{N}_\mathrm{r})(u_{\mathrm{s},1}) \leq (\mathcal{N} \circ \mathcal{N}_\mathrm{r})(u_{\mathrm{s},2}) = (\mathcal{N} \circ \mathcal{N}_\mathrm{r} \circ \mathcal{N}_\mathrm{s})(u_{\mathrm{b},2})$. Thus, $\mathcal{N} \circ \mathcal{N}_\mathrm{r} \circ \mathcal{N}_\mathrm{s}$ is nondecreasing on I_i. Similarly, the same argument shows that $\mathcal{N} \circ \mathcal{N}_\mathrm{r} \circ \mathcal{N}_\mathrm{s}$ is nondecreasing on I_i.

To prove *ii*), assume that $\mathcal{R}_{I_i}(\mathcal{N} \circ \mathcal{N}_\mathrm{r}) \subset \mathcal{R}_{I_j}(\mathcal{N} \circ \mathcal{N}_\mathrm{r})$ for all $i \neq j$ or $(\mathcal{N} \circ \mathcal{N}_\mathrm{r})(q_i) \leq (\mathcal{N} \circ \mathcal{N}_\mathrm{r})(q_j)$, where $q_i < q_j$. Since $\mathcal{N}_\mathrm{s}(u_\mathrm{b}) = u_\mathrm{b}$ for all $u_\mathrm{b} \in I_i \cup I_j$, it follows that $\mathcal{N}_\mathrm{s} : I_i \to I_i$ is onto. Alternatively, assume that $\mathcal{R}_{I_i}(\mathcal{N} \circ \mathcal{N}_\mathrm{r}) \nsubseteq \mathcal{R}_{I_j}(\mathcal{N} \circ \mathcal{N}_\mathrm{r})$ for all $i \neq j$ and $\mathcal{N} \circ \mathcal{N}_\mathrm{r}(q_i) > \mathcal{N} \circ \mathcal{N}_\mathrm{r}(q_j)$, where $q_i < q_j$. It follows from $\mathcal{N}_\mathrm{s}(u_\mathrm{b}) \stackrel{\triangle}{=} \frac{1}{q_i - p_i}\left[(q_j - p_j)u_\mathrm{b} + p_j q_i - p_i q_j\right] \in I_j$ for all $u_\mathrm{b} \in I_i$ and $\mathcal{N}_\mathrm{s}(u_\mathrm{b}) \stackrel{\triangle}{=} \frac{1}{q_j - p_j}\left[(q_i - p_i)u_\mathrm{b} + p_i q_j - p_j q_i\right] \in I_i$ for all $u_\mathrm{b} \in I_j$ that $\mathcal{N}_\mathrm{s} : I_i \to I_j$ and $\mathcal{N}_\mathrm{s} : I_j \to I_i$. Therefore, $\mathcal{N}_\mathrm{s} : I_i \to I_j$ and $\mathcal{N}_\mathrm{s} : I_j \to I_i$. Hence, $\mathcal{R}_I(\mathcal{N} \circ \mathcal{N}_\mathrm{r} \circ \mathcal{N}_\mathrm{s}) = \mathcal{R}_I(\mathcal{N} \circ \mathcal{N}_\mathrm{r}) = \mathcal{R}_I(\mathcal{N})$. □

Example 4.4.4. Consider the case where $\mathcal{R}_{[-2,0]}(\mathcal{N} \circ \mathcal{N}_\mathrm{r}) \cap \mathcal{R}_{[0,1]}(\mathcal{N} \circ \mathcal{N}_\mathrm{r}) = \varnothing$ as shown in Figure 4.6(a). We assume that values of $(\mathcal{N} \circ \mathcal{N}_\mathrm{r})(0)$ and $(\mathcal{N} \circ \mathcal{N}_\mathrm{r})(1)$ are known. In particular, $(\mathcal{N} \circ \mathcal{N}_\mathrm{r})(0) = 1 > (\mathcal{N} \circ \mathcal{N}_\mathrm{r})(1) = 0$. We thus choose $\mathcal{N}_\mathrm{s}(u_\mathrm{b}) = 0.5u_\mathrm{b} + 1$ for $u_\mathrm{b} \in [-2, 0)$ and $\mathcal{N}_\mathrm{s}(u_\mathrm{b}) = 2u_\mathrm{b} - 2$ for $u_\mathrm{b} \in [0, 1]$ as shown

in Figure 4.6(b). Note that $\mathcal{N} \circ \mathcal{N}_\mathrm{r}$ is piecewise nondecreasing on $[-2, 1]$. Figure 4.6(c) shows that the composite nonlinearity $\mathcal{N} \circ \mathcal{N}_\mathrm{r} \circ \mathcal{N}_\mathrm{s}$ is piecewise nondecreasing on $[-2, 1]$. ■

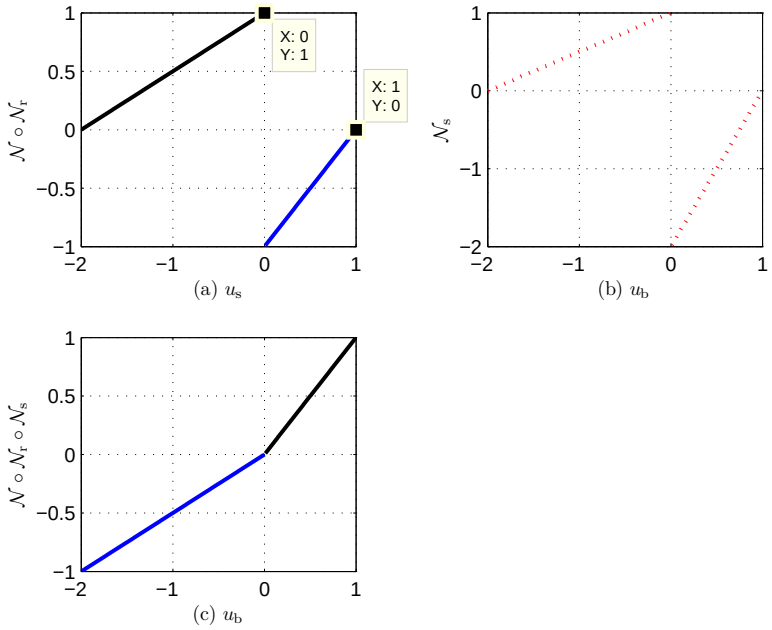

Figure 4.6: Example 4.4.4. In this example, $\mathcal{R}_{[-2,0]}(\mathcal{N} \circ \mathcal{N}_\mathrm{r}) \cap \mathcal{R}_{[0,1]}(\mathcal{N} \circ \mathcal{N}_\mathrm{r}) = \varnothing$. (a) Nondecreasing composite nonlinearity $\mathcal{N} \circ \mathcal{N}_\mathrm{r}$. Note that $(\mathcal{N} \circ \mathcal{N}_\mathrm{r})(0) = 1 > (\mathcal{N} \circ \mathcal{N}_\mathrm{r})(1) = 0$. (b) Auxiliary sorting nonlinearity $\mathcal{N}_\mathrm{s}(u_\mathrm{b}) = 0.5u_\mathrm{b} + 1$ for $u_\mathrm{b} \in [-2, 0)$ and $\mathcal{N}_\mathrm{s}(u_\mathrm{b}) = 2u_\mathrm{b} - 2$ for $u_\mathrm{b} \in [0, 1]$. (c) The composite nonlinearity $\mathcal{N} \circ \mathcal{N}_\mathrm{r} \circ \mathcal{N}_\mathrm{s}$.

Example 4.4.5. Consider the case where range of $\mathcal{N} \circ \mathcal{N}_\mathrm{r}$ on subintervals of its domain has partially overlapping intervals as shown in Figure 4.7(a), where neither $\mathcal{R}_{[-5,0]}(\mathcal{N} \circ \mathcal{N}_\mathrm{r})$ nor $\mathcal{R}_{[0,5]}(\mathcal{N} \circ \mathcal{N}_\mathrm{r})$ is contained in the other set. We assume that values of $(\mathcal{N} \circ \mathcal{N}_\mathrm{r})(0)$ and $(\mathcal{N} \circ \mathcal{N}_\mathrm{r})(5)$ are known. In particular, $(\mathcal{N} \circ \mathcal{N}_\mathrm{r})(0) = 4 > (\mathcal{N} \circ \mathcal{N}_\mathrm{r})(5) = 1$, we thus choose $\mathcal{N}_\mathrm{s}(u_\mathrm{b}) = u_\mathrm{b} + 5$ for $u_\mathrm{b} \in [-5, 0)$ and $\mathcal{N}_\mathrm{s}(u_\mathrm{b}) = u_\mathrm{b} - 5$ for $u_\mathrm{b} \in [0, 5]$ as shown in Figure 4.7(b). Note that $\mathcal{N} \circ \mathcal{N}_\mathrm{r} \circ \mathcal{N}_\mathrm{s}$ is piecewise nondecreasing on $[-5, 5]$, and Figure 4.7(c) shows that the composite nonlinearity $\mathcal{N} \circ \mathcal{N}_\mathrm{r} \circ \mathcal{N}_\mathrm{s}$ is piecewise nondecreasing on $[-5, 5]$. ■

Example 4.4.6. Consider the case where $\mathcal{R}_{[-5,0]}(\mathcal{N} \circ \mathcal{N}_\mathrm{r}) \subset \mathcal{R}_{[0,5]}(\mathcal{N} \circ \mathcal{N}_\mathrm{r})$ as

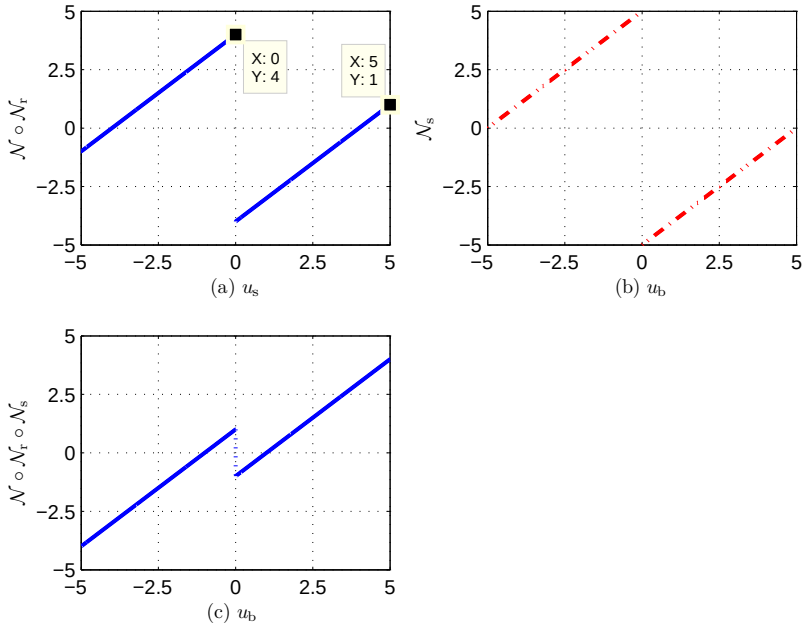

Figure 4.7: Example 4.4.5. In this example, range of $\mathcal{N} \circ \mathcal{N}_r$ on subintervals of its domain has partially overlapping intervals, where neither $\mathcal{R}_{[-5,0]}(\mathcal{N} \circ \mathcal{N}_r)$ nor $\mathcal{R}_{[0,5]}(\mathcal{N} \circ \mathcal{N}_r)$ is contained in the other set. Note that $(\mathcal{N} \circ \mathcal{N}_r)(0) = 4 > (\mathcal{N} \circ \mathcal{N}_r)(5) = 1$. (a) Piecewise nondecreasing composite nonlinearity $\mathcal{N} \circ \mathcal{N}_r$ with partially overlapping intervals. (b) Auxiliary sorting nonlinearity $\mathcal{N}_s(u_b) = u_b + 5$ for $u_b \in [-5, 0)$ and $\mathcal{N}_s(u_b) = u_b - 5$ for $u_b \in [0, 5]$. (c) The composite nonlinearity $\mathcal{N} \circ \mathcal{N}_r \circ \mathcal{N}_s$ is piecewise nondecreasing on $[-5, 5]$.

shown in Figure 4.8(a), and thus $\mathcal{N}_s$ is not needed. We choose $\mathcal{N}_s(u_b) = u_b$, and Figure 4.8(b) shows that $\mathcal{N} \circ \mathcal{N}_r \circ \mathcal{N}_s$ is piecewise nondecreasing on $[-5, 5]$. ■

4.4.4 Auxiliary Blocking Nonlinearity $\mathcal{N}_b$

As shown in Proposition 4.4.2 and illustrated by Example 4.4.5, $\mathcal{N} \circ \mathcal{N}_r \circ \mathcal{N}_s$ is piecewise nondecreasing. In order to construct a composite input nonlinearity that is globally nondecreasing, we introduce the auxiliary blocking nonlinearity $\mathcal{N}_b$. To construct $\mathcal{N}_b$, we assume that the range of $\mathcal{N} \circ \mathcal{N}_r \circ \mathcal{N}_s$ within each interval of monotonicity is known. If, in addition, these ranges are partially overlapping, then selected intermediate values of $\mathcal{N} \circ \mathcal{N}_r \circ \mathcal{N}_s$ must also be known. No further modeling

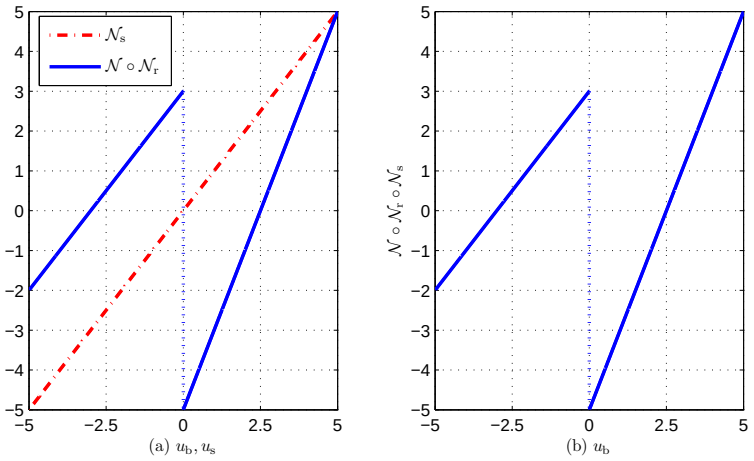

Figure 4.8: Example 4.4.6. In this example, $\mathcal{R}_{[-5,0]}(\mathcal{N} \circ \mathcal{N}_r) \subset \mathcal{R}_{[0,5]}(\mathcal{N} \circ \mathcal{N}_r)$. In this case, $\mathcal{N}_s$ is not needed. (a) Piecewise nondecreasing composite nonlinearity $\mathcal{N} \circ \mathcal{N}_r$, where $\mathcal{R}_{[-5,0]}(\mathcal{N} \circ \mathcal{N}_r) \subset \mathcal{R}_{[0,5]}(\mathcal{N} \circ \mathcal{N}_r)$ and the auxiliary sorting nonlinearity $\mathcal{N}_s(u_b) = u_b$ for $u_b \in [-5, 5]$. (b) The composite nonlinearity $\mathcal{N} \circ \mathcal{N}_r \circ \mathcal{N}_s$ is piecewise nondecreasing on $[-5, 5]$.

information about $\mathcal{N}$ is needed.

Let $\mathcal{N}_b$ be the piecewise right-continuous affine function defined as follows. Let $I_1, I_2, \ldots$ be the smallest number of intervals of monotonicity of $\mathcal{N}$ that are also a partition of the interval $[p, q]$. If $\mathcal{R}_{I_i}(\mathcal{N} \circ \mathcal{N}_r \circ \mathcal{N}_s) \cap \mathcal{R}_{I_j}(\mathcal{N} \circ \mathcal{N}_r \circ \mathcal{N}_s) = \varnothing$ for all $i \neq j$, then we choose $\mathcal{N}_b(u_{sat}) \stackrel{\triangle}{=} u_{sat}$ for all $u_{sat} \in I_j \cup I_j$. Alternatively, if $\mathcal{R}_{I_i}(\mathcal{N} \circ \mathcal{N}_r \circ \mathcal{N}_s) \cap \mathcal{R}_{I_j}(\mathcal{N} \circ \mathcal{N}_r \circ \mathcal{N}_s) \neq \varnothing$ and $\mathcal{R}_{I_i}(\mathcal{N} \circ \mathcal{N}_r \circ \mathcal{N}_s) \subsetneq \mathcal{R}_{I_j}(\mathcal{N} \circ \mathcal{N}_r \circ \mathcal{N}_s)$, we block the overlapping segments as shown by the following examples.

Example 4.4.7. Consider the case where $\mathcal{R}_{[-5,0]}(\mathcal{N} \circ \mathcal{N}_r \circ \mathcal{N}_s) \cap \mathcal{R}_{[0,5]}(\mathcal{N} \circ \mathcal{N}_r \circ \mathcal{N}_s) = \varnothing$ as shown in Figure 4.9(a). In this case, $\mathcal{N}_b$ is not needed, we thus choose $\mathcal{N}_b(u_{sat}) = u_{sat}$. Note that $\mathcal{N} \circ \mathcal{N}_r \circ \mathcal{N}_s$ is piecewise nondecreasing on $[-5, 5]$. Figure 4.9(b) shows that the composite nonlinearity $\mathcal{N} \circ \mathcal{N}_r \circ \mathcal{N}_s \circ \mathcal{N}_b$ is globally nondecreasing on $[-5, 5]$. ■

Example 4.4.8. Consider the case where range of $\mathcal{N} \circ \mathcal{N}_r \circ \mathcal{N}_s$ on subintervals of its domain has partially overlapping intervals, where neither $\mathcal{R}_{[-5,0]}(\mathcal{N} \circ \mathcal{N}_r \circ \mathcal{N}_s)$ nor $\mathcal{R}_{[0,5]}(\mathcal{N} \circ \mathcal{N}_r \circ \mathcal{N}_s)$ is contained in the other set. In particular, as shown in

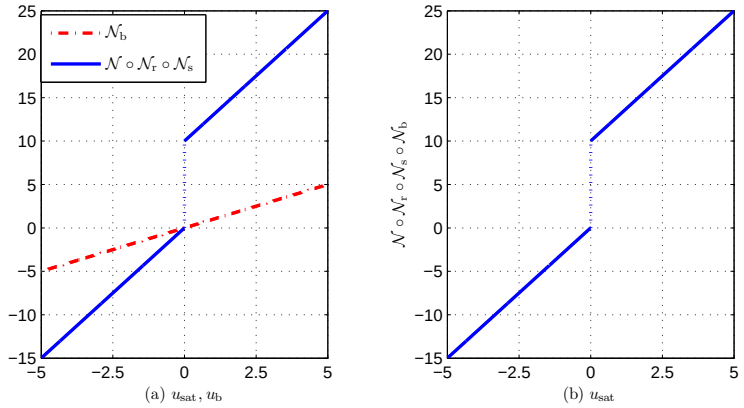

Figure 4.9: Example 4.4.7. In this example, $\mathcal{R}_{[-5,0]}(\mathcal{N} \circ \mathcal{N}_\mathrm{r} \circ \mathcal{N}_\mathrm{s}) \cap \mathcal{R}_{[0,5]}(\mathcal{N} \circ \mathcal{N}_\mathrm{r} \circ \mathcal{N}_\mathrm{s}) = \varnothing$. (a) Nondecreasing composite nonlinearity $\mathcal{N} \circ \mathcal{N}_\mathrm{r} \circ \mathcal{N}_\mathrm{s}$ and auxiliary blocking nonlinearity $\mathcal{N}_\mathrm{b}(u_\mathrm{sat}) = u_\mathrm{sat}$. (b) The composite nonlinearity $\mathcal{N} \circ \mathcal{N}_\mathrm{r} \circ \mathcal{N}_\mathrm{s} \circ \mathcal{N}_\mathrm{b}$ is globally nondecreasing on $[-5, 5]$.

Figure 4.10(a), $\mathcal{R}_{[-2,0]}(\mathcal{N} \circ \mathcal{N}_\mathrm{r} \circ \mathcal{N}_\mathrm{s}) = \mathcal{R}_{[0,2]}(\mathcal{N} \circ \mathcal{N}_\mathrm{r} \circ \mathcal{N}_\mathrm{s})$. In this case, we assume that intermediate values of $\mathcal{N} \circ \mathcal{N}_\mathrm{r} \circ \mathcal{N}_\mathrm{s}$ are known. In particular, knowledge of $(\mathcal{N} \circ \mathcal{N}_\mathrm{r} \circ \mathcal{N}_\mathrm{s})_{[-5,0]}(0) = 1$ is sufficient to construct $\mathcal{N}_\mathrm{b}$. We choose $\mathcal{N}_\mathrm{b}(u_\mathrm{sat}) = -2$ for $u_\mathrm{sat} \in [-2, 0)$ and $\mathcal{N}_\mathrm{b}(u_\mathrm{sat}) = u_\mathrm{sat}$ otherwise. Note that $\mathcal{N} \circ \mathcal{N}_\mathrm{r} \circ \mathcal{N}_\mathrm{s}$ is piecewise nondecreasing on $[-5, 5]$, and Figure 4.10(b) shows that the composite nonlinearity $\mathcal{N} \circ \mathcal{N}_\mathrm{r} \circ \mathcal{N}_\mathrm{s} \circ \mathcal{N}_\mathrm{b}$ is globally nondecreasing on $[-5, 5]$. ■

Example 4.4.9. Consider the case $\mathcal{R}_{[-5,0]}(\mathcal{N} \circ \mathcal{N}_\mathrm{r} \circ \mathcal{N}_\mathrm{s}) \subset \mathcal{R}_{[0,5]}(\mathcal{N} \circ \mathcal{N}_\mathrm{r} \circ \mathcal{N}_\mathrm{s})$ as shown in Figure 4.11(a). In particular, $\mathcal{R}_{[-5,0]}(\mathcal{N} \circ \mathcal{N}_\mathrm{r} \circ \mathcal{N}_\mathrm{s}) = [-2, 3]$ and $\mathcal{R}_{[0,5]}(\mathcal{N} \circ \mathcal{N}_\mathrm{r} \circ \mathcal{N}_\mathrm{s}) = [-5, 5]$. We let $\mathcal{N}_\mathrm{b}(u_\mathrm{sat}) = -5$ for all $u_\mathrm{sat} \in [-5, 0)$ and $\mathcal{N}_\mathrm{b}(u_\mathrm{sat}) = u_\mathrm{sat}$ for all $u_\mathrm{sat} \in [0, 5]$. Note that $\mathcal{N} \circ \mathcal{N}_\mathrm{r} \circ \mathcal{N}_\mathrm{s}$ is piecewise nondecreasing on $[-5, 5]$ and Figure 4.11(b) shows that the composite nonlinearity $\mathcal{N} \circ \mathcal{N}_\mathrm{r} \circ \mathcal{N}_\mathrm{s} \circ \mathcal{N}_\mathrm{b}$ is globally nondecreasing on $[-5, 5]$. ■

Proposition 4.4.3. *Assume that $\mathcal{N}_\mathrm{b}$ is constructed by the above rule. Then the following statements hold:*

1. *$\mathcal{N} \circ \mathcal{N}_\mathrm{r} \circ \mathcal{N}_\mathrm{s} \circ \mathcal{N}_\mathrm{b}$ is globally nondecreasing on $I \triangleq [p, q]$.*

2. *$\mathcal{R}_I(\mathcal{N} \circ \mathcal{N}_\mathrm{r} \circ \mathcal{N}_\mathrm{s} \circ \mathcal{N}_\mathrm{b}) = \mathcal{R}_I(\mathcal{N})$.*

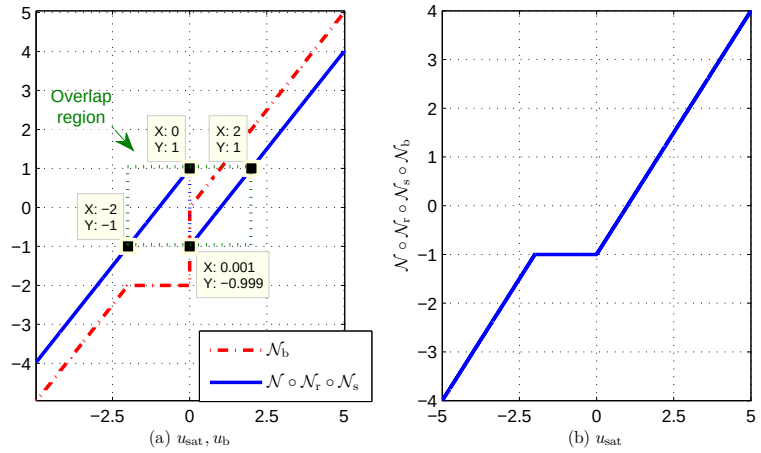

Figure 4.10: Example 4.4.8. In this example, range of $\mathcal{N} \circ \mathcal{N}_\mathrm{r} \circ \mathcal{N}_\mathrm{s}$ on subintervals of its domain has partially overlapping intervals, where neither $\mathcal{R}_{[-5,0]}(\mathcal{N} \circ \mathcal{N}_\mathrm{r} \circ \mathcal{N}_\mathrm{s})$ nor $\mathcal{R}_{[0,5]}(\mathcal{N} \circ \mathcal{N}_\mathrm{r} \circ \mathcal{N}_\mathrm{s})$ is contained in the other set. (a) Piecewise nondecreasing composite nonlinearity $\mathcal{N} \circ \mathcal{N}_\mathrm{r} \circ \mathcal{N}_\mathrm{s}$ with partially overlapping intervals, where $\mathcal{R}_{[-2,0]}(\mathcal{N} \circ \mathcal{N}_\mathrm{r} \circ \mathcal{N}_\mathrm{s}) = \mathcal{R}_{[0,2]}(\mathcal{N} \circ \mathcal{N}_\mathrm{r} \circ \mathcal{N}_\mathrm{s})$ and the auxiliary blocking nonlinearity $\mathcal{N}_\mathrm{b}(u_\mathrm{sat}) = u_\mathrm{sat}$. (b) The composite nonlinearity $\mathcal{N} \circ \mathcal{N}_\mathrm{r} \circ \mathcal{N}_\mathrm{s} \circ \mathcal{N}_\mathrm{b}$ is globally nondecreasing on $[-5, 5]$.

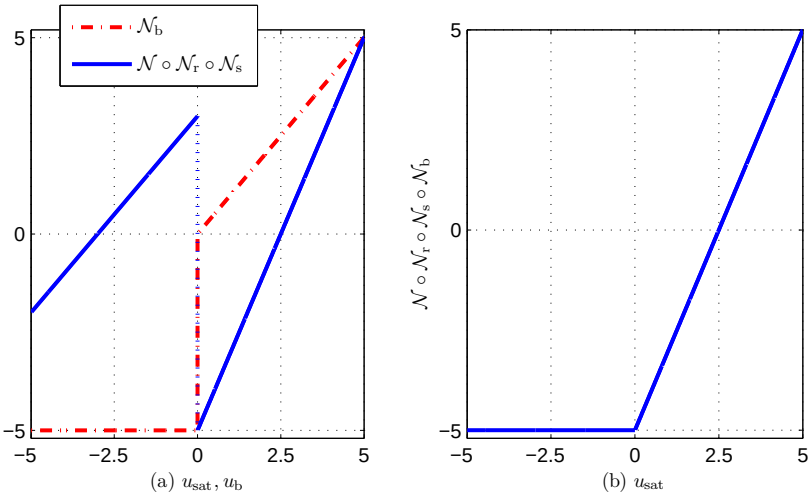

Figure 4.11: Example 4.4.9. In this example, $\mathcal{R}_{[-5,0]}(\mathcal{N} \circ \mathcal{N}_\mathrm{r} \circ \mathcal{N}_\mathrm{s}) \subset \mathcal{R}_{[0,5]}(\mathcal{N} \circ \mathcal{N}_\mathrm{r} \circ \mathcal{N}_\mathrm{s})$. (a) Piecewise nondecreasing composite nonlinearity $\mathcal{N} \circ \mathcal{N}_\mathrm{r} \circ \mathcal{N}_\mathrm{s}$, where $\mathcal{R}_{[-5,0]}(\mathcal{N} \circ \mathcal{N}_\mathrm{r} \circ \mathcal{N}_\mathrm{s}) \subset \mathcal{R}_{[0,5]}(\mathcal{N} \circ \mathcal{N}_\mathrm{r} \circ \mathcal{N}_\mathrm{s})$ and the auxiliary blocking nonlinearity $\mathcal{N}_\mathrm{b}(u_\mathrm{sat}) = -5$ for $u_\mathrm{sat} \in [-5, 0)$ and $\mathcal{N}_\mathrm{b}(u_\mathrm{sat}) = u_\mathrm{sat}$ for $u_\mathrm{sat} \in [0, 5]$. (b) The composite nonlinearity $\mathcal{N} \circ \mathcal{N}_\mathrm{r} \circ \mathcal{N}_\mathrm{s} \circ \mathcal{N}_\mathrm{b}$ is globally nondecreasing on $[-5, 5]$.

Proof. First, consider the case $\mathcal{R}_{I_i}(\mathcal{N} \circ \mathcal{N}_\mathrm{r} \circ \mathcal{N}_\mathrm{s}) \cap \mathcal{R}_{I_j}(\mathcal{N} \circ \mathcal{N}_\mathrm{r} \circ \mathcal{N}_\mathrm{s}) = \varnothing$ for all $i \neq j$. It follows from i) of Proposition 4.4.2 and $\mathcal{N}_\mathrm{b}(u_\mathrm{sat}) = u_\mathrm{sat}$ that $\mathcal{N} \circ \mathcal{N}_\mathrm{r} \circ \mathcal{N}_\mathrm{s} \circ \mathcal{N}_\mathrm{b}$ is

nondecreasing on I. Next, consider the case $\mathcal{R}_{I_i}(\mathcal{N}\circ\mathcal{N}_\mathrm{r}\circ\mathcal{N}_\mathrm{s})\cap\mathcal{R}_{I_j}(\mathcal{N}\circ\mathcal{N}_\mathrm{r}\circ\mathcal{N}_\mathrm{s})\neq\varnothing$, $(\mathcal{N}\circ\mathcal{N}_\mathrm{r}\circ\mathcal{N}_\mathrm{s}\circ\mathcal{N}_\mathrm{b})(u_\mathrm{sat})$ is constant for all $u_\mathrm{sat}\in\mathcal{R}_{I_i}(\mathcal{N}\circ\mathcal{N}_\mathrm{r}\circ\mathcal{N}_\mathrm{s})\cap\mathcal{R}_{I_j}(\mathcal{N}\circ\mathcal{N}_\mathrm{r}\circ\mathcal{N}_\mathrm{s})$. Therefore, $\mathcal{N}\circ\mathcal{N}_\mathrm{r}\circ\mathcal{N}_\mathrm{s}\circ\mathcal{N}_\mathrm{b}$ is nondecreasing.

To prove *ii*), let $I_1, I_2, \ldots$ be the smallest number of intervals of monotonicity of $\mathcal{N}$ that are a partition of the interval $[p,q]$. Since $\mathcal{R}_I(\mathcal{N}\circ\mathcal{N}_\mathrm{r}\circ\mathcal{N}_\mathrm{s})=\bigcup_{k=1}^{\infty}\mathcal{R}_{I_k}(\mathcal{N}\circ\mathcal{N}_\mathrm{r}\circ\mathcal{N}_\mathrm{s})$. Note that $\mathcal{N}_\mathrm{b}(u_\mathrm{sat})=u_\mathrm{sat}$ for all intervals I_i and I_j such that $\mathcal{R}_{I_i}(\mathcal{N}\circ\mathcal{N}_\mathrm{r}\circ\mathcal{N}_\mathrm{s})\cap\mathcal{R}_{I_j}(\mathcal{N}\circ\mathcal{N}_\mathrm{r}\circ\mathcal{N}_\mathrm{s})=\varnothing$. For the intervals where $\mathcal{R}_{I_i}(\mathcal{N}\circ\mathcal{N}_\mathrm{r}\circ\mathcal{N}_\mathrm{s})\cap\mathcal{R}_{I_j}(\mathcal{N}\circ\mathcal{N}_\mathrm{r}\circ\mathcal{N}_\mathrm{s})\neq\varnothing$. Let $\mathcal{N}_\mathrm{b}(u_\mathrm{sat})=\mu$, where $\mu\in\mathcal{R}_{I_i}(\mathcal{N}\circ\mathcal{N}_\mathrm{r}\circ\mathcal{N}_\mathrm{s})\cap\mathcal{R}_{I_j}(\mathcal{N}\circ\mathcal{N}_\mathrm{r}\circ\mathcal{N}_\mathrm{s})$. Therefore, $\mathcal{R}_I(\mathcal{N}\circ\mathcal{N}_\mathrm{r}\circ\mathcal{N}_\mathrm{s}\circ\mathcal{N}_\mathrm{b})=\mathcal{R}_I(\mathcal{N}\circ\mathcal{N}_\mathrm{r}\circ\mathcal{N}_\mathrm{s})$. It thus follows from Proposition 4.4.2 that $\mathcal{R}_I(\mathcal{N}\circ\mathcal{N}_\mathrm{r}\circ\mathcal{N}_\mathrm{s}\circ\mathcal{N}_\mathrm{b})=\mathcal{R}_I(\mathcal{N}\circ\mathcal{N}_\mathrm{r}\circ\mathcal{N}_\mathrm{s})=\mathcal{R}_I(\mathcal{N})$. □

4.4.5 Examples Illustrating the Construction of $\mathcal{N}_\mathrm{b}$, $\mathcal{N}_\mathrm{s}$, and $\mathcal{N}_\mathrm{r}$

Example 4.4.10. Consider the non-monotonic input nonlinearity

$$\mathcal{N}(u)=\begin{cases}10, & \text{if } u<2,\\ -3u+4, & \text{if } -2\le u<2,\\ u^2-6, & \text{if } u\ge 2,\end{cases} \tag{4.22}$$

which is shown in Figure 4.12(a). Let $\mathcal{N}_\mathrm{sat}(u_\mathrm{c})=\mathrm{sat}_{p,q}(u_\mathrm{c})$, where $p=-5$ and $q=5$. According to Propositions 4.4.1, 4.4.2, and 4.4.3, let

$$\mathcal{N}_\mathrm{r}(u_\mathrm{s})=\begin{cases}-u_\mathrm{s}, & \text{if } -2\le u_\mathrm{s}<2,\\ u_\mathrm{s}, & \text{if } u_\mathrm{s}\in[-5,-2)\cup(2,5),\end{cases} \tag{4.23}$$

$$\mathcal{N}_\mathrm{s}(u_\mathrm{b})=u_\mathrm{b}, \quad \text{if } u_\mathrm{b}\in[-5,5], \tag{4.24}$$

and

$$\mathcal{N}_{\rm b}(u_{\rm sat}) = \begin{cases} -2, & \text{if } -5 \le u_{\rm sat} < 2, \\ u_{\rm sat}, & \text{if } 2 \le u_{\rm sat} \le 5. \end{cases} \tag{4.25}$$

Figure 4.12(b) shows the auxiliary nonlinearities $\mathcal{N}_{\rm b}$, $\mathcal{N}_{\rm s}$, and $\mathcal{N}_{\rm r}$. Figures 4.12(c) and 4.12(d) show that the composite nonlinearity $\mathcal{N} \circ \mathcal{N}_{\rm r} \circ \mathcal{N}_{\rm s}$ is piecewise nondecreasing on $I \stackrel{\triangle}{=} [-5, 5]$ and the composite nonlinearity $\mathcal{N} \circ \mathcal{N}_{\rm r} \circ \mathcal{N}_{\rm s} \circ \mathcal{N}_{\rm b}$ is globally nondecreasing on I. Note that $\mathcal{R}_I(\mathcal{N} \circ \mathcal{N}_{\rm r} \circ \mathcal{N}_{\rm s} \circ \mathcal{N}_{\rm b}) = \mathcal{R}_I(\mathcal{N}) = [-2, 19]$. ■

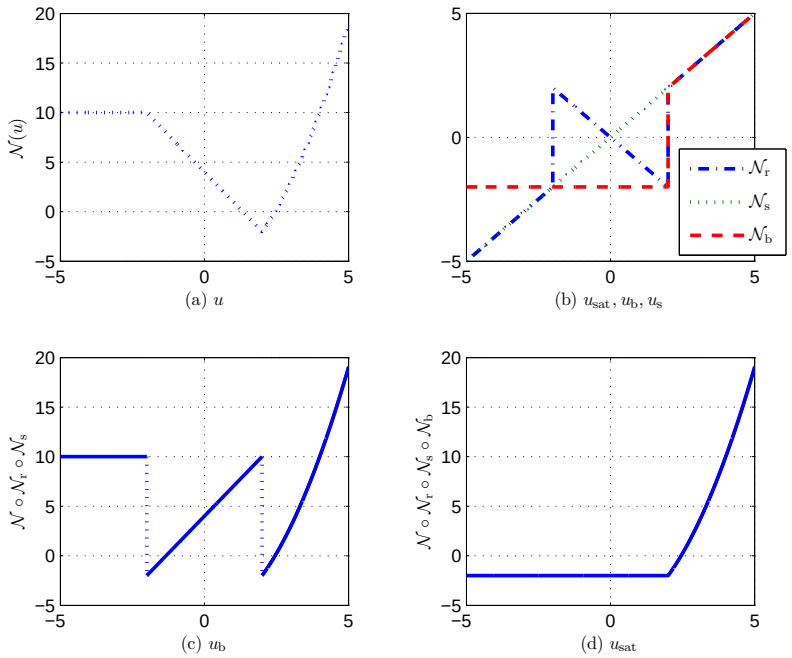

Figure 4.12: Example 4.4.10. (a) Input nonlinearity given by (4.22). (b) The auxiliary reflection nonlinearity $\mathcal{N}_{\rm r}$ given by (4.23) for $u_{\rm s} \in [-5, 5]$, the auxiliary sorting nonlinearity $\mathcal{N}_{\rm s}$ given by (4.24) for $u_{\rm b} \in [-5, 5]$, and the auxiliary blocking nonlinearity $\mathcal{N}_{\rm b}$ given by (4.25) for $u_{\rm sat} \in [-5, 5]$. (c) Composite nonlinearity $\mathcal{N} \circ \mathcal{N}_{\rm r} \circ \mathcal{N}_{\rm s}$. Note that $\mathcal{N} \circ \mathcal{N}_{\rm r} \circ \mathcal{N}_{\rm s}$ is piecewise nondecreasing on $[-5, 5]$. (d) Composite nonlinearity $\mathcal{N} \circ \mathcal{N}_{\rm r} \circ \mathcal{N}_{\rm s} \circ \mathcal{N}_{\rm b}$. Note that $\mathcal{N} \circ \mathcal{N}_{\rm r} \circ \mathcal{N}_{\rm s} \circ \mathcal{N}_{\rm b}$ is globally nondecreasing on $[-5, 5]$ and $\mathcal{R}_{[-5,5]}(\mathcal{N} \circ \mathcal{N}_{\rm r} \circ \mathcal{N}_{\rm s} \circ \mathcal{N}_{\rm b}) = \mathcal{R}_{[-5,5]}(\mathcal{N}) = [-2, 19]$.

Example 4.4.11. Consider the non-monotonic input nonlinearity

$$\mathcal{N}(u) = \begin{cases} -\text{sat}_{-0.5,0.5}u, & \text{if } u < 2, \\ 0.5u - 2, & \text{if } 2 \leq u < 4, \\ 0, & \text{if } u \geq 4, \end{cases} \tag{4.26}$$

which is shown in Figure 4.13(a). Let $\mathcal{N}_{\text{sat}}(u_{\text{c}}) = \text{sat}_{p,q}(u_{\text{c}})$, where $p = -2$ and $q = 6$. According to Propositions 4.4.1, 4.4.2, and 4.4.3, let

$$\mathcal{N}_{\text{r}}(u_{\text{s}}) = \begin{cases} -u_{\text{s}}, & \text{if } -2 \leq u_{\text{s}} < 2, \\ u_{\text{s}}, & \text{if } 2 \leq u_{\text{s}} \leq 6, \end{cases} \tag{4.27}$$

$$\mathcal{N}_{\text{s}}(u_{\text{b}}) = \begin{cases} u_{\text{b}} + 4, & \text{if } -2 \leq u_{\text{b}} < 2, \\ u_{\text{b}} - 4, & \text{if } 2 \leq u_{\text{b}} \leq 6, \end{cases} \tag{4.28}$$

and

$$\mathcal{N}_{\text{b}}(u_{\text{sat}}) = \begin{cases} 4, & \text{if } 2 \leq u_{\text{sat}} < 4, \\ u_{\text{sat}}, & \text{otherwise.} \end{cases} \tag{4.29}$$

Figure 4.13(b) shows the auxiliary nonlinearities $\mathcal{N}_{\text{r}}$ and $\mathcal{N}_{\text{s}}$. Figures 4.13(c) and 4.13(d) show that the composite nonlinearity $\mathcal{N} \circ \mathcal{N}_{\text{r}}$ and $\mathcal{N} \circ \mathcal{N}_{\text{r}} \circ \mathcal{N}_{\text{s}}$ are piecewise nondecreasing on $I \stackrel{\triangle}{=} [-2, 6]$. Figures 4.13(e) shows auxiliary blocking nonlinearities $\mathcal{N}_{\text{b}}$ and Figures 4.13(f) shows the composite nonlinearity $\mathcal{N} \circ \mathcal{N}_{\text{r}} \circ \mathcal{N}_{\text{s}} \circ \mathcal{N}_{\text{b}}$ is globally nondecreasing on I. Note that $\mathcal{R}_I(\mathcal{N} \circ \mathcal{N}_{\text{r}} \circ \mathcal{N}_{\text{s}} \circ \mathcal{N}_{\text{b}}) = \mathcal{R}_I(\mathcal{N} \circ \mathcal{N}_{\text{r}} \circ \mathcal{N}_{\text{s}}) = \mathcal{R}_I(\mathcal{N} \circ \mathcal{N}_{\text{r}}) = \mathcal{R}_I(\mathcal{N}) = [-1, 0.5]$. ■

Knowledge of the intervals of monotonicity of $\mathcal{N}$, the ranges of $\mathcal{N} \circ \mathcal{N}_{\text{r}}$ and $\mathcal{N} \circ \mathcal{N}_{\text{r}} \circ \mathcal{N}_{\text{s}}$ within each interval of monotonicity, and selected intermediate values of

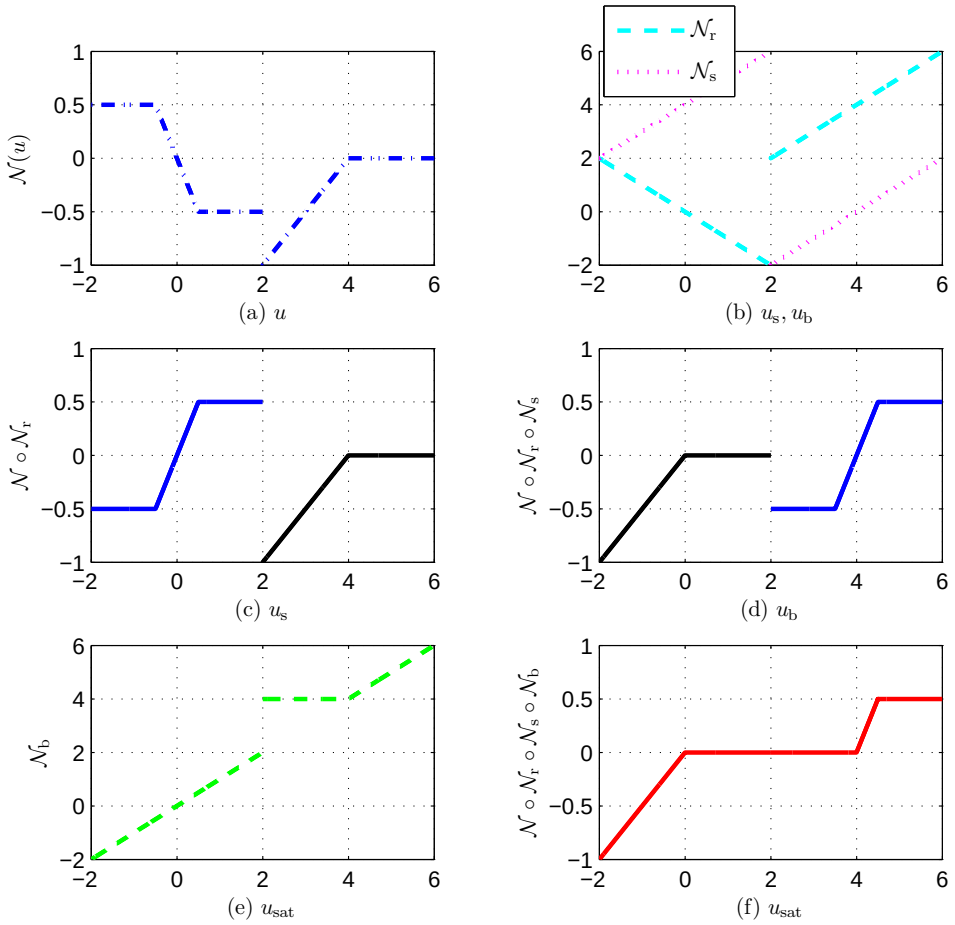

Figure 4.13: Example 4.4.11. (a) Input nonlinearity $\mathcal{N}(u)$ given by (4.26). (b) The auxiliary reflection nonlinearity $\mathcal{N}_\mathrm{r}$ given by (4.27) for $u_\mathrm{s} \in [-2, 6]$ and the auxiliary sorting nonlinearity $\mathcal{N}_\mathrm{s}$ given by (4.28) for $u_\mathrm{b} \in [-2, 6]$. (c) Composite nonlinearity $\mathcal{N} \circ \mathcal{N}_\mathrm{r}$. Note that $\mathcal{N} \circ \mathcal{N}_\mathrm{r}$ is piecewise nondecreasing on $[-2, 6]$. (d) Composite nonlinearity $\mathcal{N} \circ \mathcal{N}_\mathrm{r} \circ \mathcal{N}_\mathrm{s}$. Note that $\mathcal{N} \circ \mathcal{N}_\mathrm{r} \circ \mathcal{N}_\mathrm{s}$ is piecewise nondecreasing on $[-2, 6]$. (e) The auxiliary blocking nonlinearity $\mathcal{N}_\mathrm{b}$ given by (4.29) for $u_\mathrm{sat} \in [-2, 6]$. (f) Composite nonlinearity $\mathcal{N} \circ \mathcal{N}_\mathrm{r} \circ \mathcal{N}_\mathrm{s} \circ \mathcal{N}_\mathrm{b}$ is globally nondecreasing on $[-2, 6]$, and $\mathcal{R}_I(\mathcal{N} \circ \mathcal{N}_\mathrm{r} \circ \mathcal{N}_\mathrm{s} \circ \mathcal{N}_\mathrm{b}) = \mathcal{R}_I(\mathcal{N} \circ \mathcal{N}_\mathrm{r} \circ \mathcal{N}_\mathrm{b}) = \mathcal{R}_I(\mathcal{N} \circ \mathcal{N}_\mathrm{r}) = \mathcal{R}_I(\mathcal{N}) = [-1, 0.5]$.

$\mathcal{N} \circ \mathcal{N}_\mathrm{r} \circ \mathcal{N}_\mathrm{s}$ in the case of partially overlapping interval ranges is needed to modify the controller output u_sat so that $\mathcal{N} \circ \mathcal{N}_\mathrm{r} \circ \mathcal{N}_\mathrm{s} \circ \mathcal{N}_\mathrm{b}$ is globally nondecreasing. It thus follows that $\mathcal{N} \circ \mathcal{N}_\mathrm{r} \circ \mathcal{N}_\mathrm{s} \circ \mathcal{N}_\mathrm{b}$ preserves the signs of the Markov parameters of the linearized Hammerstein system.

4.5 Adaptive Control of Hammerstein Systems with Odd Input Nonlinearities

We now present numerical examples to illustrate the response of RCAC for Hammerstein systems with odd input nonlinearities. We consider a sequence of examples of increasing complexity, including minimum-phase, non-minimum-phase plants, asymptotically stable, and unstable cases. The odd input nonlinearities may be either monotonic or non-monotonic. For each example, we assume that d and H_d are known. In all simulations, the adaptive controller gain matrix $\theta(k)$ is initialized to zero. Unless otherwise stated, all examples assume $x(0) = 0$ and $\lambda = 1$.

Example 4.5.1. *(Minimum-phase, asymptotically stable plant, nonincreasing $\mathcal{N}$).* Consider the asymptotically stable, minimum-phase plant

$$G(\mathbf{z}) = \frac{1}{\mathbf{z} - 0.5} \tag{4.30}$$

with the cubic input nonlinearity

$$\mathcal{N}(u) = -u^3, \tag{4.31}$$

which is nonincreasing, one-to-one, and onto. Note that $d = 1$ and $H_d = 1$. We consider the sinusoidal command $r(k) = 5\sin(\Omega_1 k)$, where $\Omega_1 = \pi/5$ rad/sample. Since the linear plant is minimum phase, we choose $\mathcal{N}_{\text{sat}}(u_{\text{c}}) = \text{sat}_{p,q}(u_{\text{c}})$, where $p = -10^6$ and $q = 10^6$ in (4.20). As shown in Figure 4.14(a), $\mathcal{N}$ is decreasing for all $u \in \mathbb{R}$, we let $\mathcal{N}_{\text{b}} = u_{\text{sat}}$, $\mathcal{N}_{\text{s}} = u_{\text{b}}$, and $\mathcal{N}_{\text{r}} = -u_{\text{s}}$. Figure 4.14(a.iii) shows that the composite nonlinearity $\mathcal{N} \circ \mathcal{N}_{\text{r}} \circ \mathcal{N}_{\text{s}} \circ \mathcal{N}_{\text{b}}$ is nondecreasing. Note that knowledge of only the monotonicity of $\mathcal{N}$ is used to choose $\mathcal{N}_{\text{b}}$, $\mathcal{N}_{\text{s}}$, and $\mathcal{N}_{\text{r}}$. We let $n_{\text{c}} = 10$, $P_0 = 0.01 I_{2n_{\text{c}}}$, $\eta_0 = 0$, and $\tilde{\mathcal{H}} = H_1$. Figures 4.14(b.i) and (b.ii) show the time history of z, while Figure 4.14(b.iii) shows the input nonlinearity $\mathcal{N}$ and (b.iv) shows the time

history of u. Finally, Figure 4.14(b.v) shows the time history of θ and (b.vi) shows the frequency response of $G_{\mathrm{c},2000}(\mathbf{z})$. Note that $G_{\mathrm{c},2000}(\mathbf{z})$ has the form of an internal model controller with high gain at the command frequency Ω_1 and the harmonic $3\Omega_1$.

■

Consider the nonlinearity $\mathcal{N}(u) = u^n$, where n is odd, with the input signal $u(k) = \cos(\Omega k)$. Then the response $y(k) = \mathcal{N}(u(k))$ is given by

$$y(k) = \cos^n(\Omega k) = \frac{1}{2^{n-1}} \sum_{r=0}^{(n-1)/2} \binom{n}{r} \cos[(n-2r)\Omega k]. \tag{4.32}$$

Note that, if $\mathcal{N}$ is an odd polynomial, then $y(k)$ contains harmonics at only odd multiples of Ω. Furthermore, if $\mathcal{N}$ is an odd analytic function such as $\mathcal{N}(u) = \sin u$, then this observation applies to truncations of its Taylor expansion.

Example 4.5.2. *(Non-minimum-phase, asymptotically stable plant, nondecreasing $\mathcal{N}$).* We consider the asymptotically stable, NMP plant

$$G(\mathbf{z}) = \frac{\mathbf{z} - 1.5}{(\mathbf{z} - 0.8)(\mathbf{z} - 0.6)}, \tag{4.33}$$

with the saturation input nonlinearity

$$\mathcal{N}(u) = \begin{cases} -0.8, & \text{if } u < -0.8, \\ u, & \text{if } -0.8 \leq u \leq 0.8, \\ 0.8, & \text{if } u > 0.8, \end{cases} \tag{4.34}$$

which is nondecreasing and one-to-one but not onto. Note that $d = 1$ and $H_d = 1$. We consider the two-tone sinusoidal command $r(k) = 0.5\sin(\Omega_1 k) + 0.5\sin(\Omega_2 k)$, where $\Omega_1 = \pi/5$ rad/sample and $\Omega_2 = \pi/2$ rad/sample for the Hammerstein system with the input nonlinearity $\mathcal{N}$. As shown in Figure 4.15(a), since $\mathcal{N}$ is nondecreasing for all $u \in \mathbb{R}$, we choose $\mathcal{N}_{\mathrm{sat}}(u_{\mathrm{c}}) = \mathrm{sat}_{p,q}(u_{\mathrm{c}})$, where $p = -2$ and $q = 2$ in (4.20), and

let $\mathcal{N}_{\rm b} = u_{\rm sat}$, $\mathcal{N}_{\rm s} = u_{\rm b}$, and $\mathcal{N}_{\rm r} = u_{\rm s}$. Figure 4.15(a.iii) shows that the composite nonlinearity $\mathcal{N} \circ \mathcal{N}_{\rm r} \circ \mathcal{N}_{\rm s} \circ \mathcal{N}_{\rm b}$ is nondecreasing on $[-2, 2]$. We set $n_{\rm c} = 10$, $P_0 = 0.1 I_{2n_{\rm c}}$, $\eta_0 = 2$, and $\tilde{\mathcal{H}} = H_1$. The Hammerstein system runs open-loop for 100 time steps, and RCAC is turned on at $k = 100$. Figure 4.15(b) shows the time history of z. Figure 4.15(c) shows the frequency response of $G_{\rm c,1000}(\mathbf{z})$, which indicates that $G_{\rm c,1000}(\mathbf{z})$ has high gain at the command frequencies Ω_1 and Ω_2. ■

Example 4.5.3. *(Non-minimum-phase, asymptotically stable plant, nondecreasing $\mathcal{N}$).* To illustrate the choice of $\mathcal{N}_{\rm sat}$ for a NMP plant, consider (4.33) with the deadzone input nonlinearity

$$\mathcal{N}(u) = \begin{cases} u + 0.5, & \text{if } u < -0.5, \\ 0, & \text{if } -0.5 \leq u \leq 0.5, \\ u - 0.5, & \text{if } u > 0.5, \end{cases} \tag{4.35}$$

which is not one-to-one but onto. Note that $d = 1$ and $H_d = 1$. We consider the two-tone sinusoidal command $r(k) = \sin(\Omega_1 k) + 0.5 \sin(\Omega_2 k)$, where $\Omega_1 = \pi/4$ rad/sample, and $\Omega_2 = \pi/2$ rad/sample. As shown in Figure 4.16(a), since $\mathcal{N}(u)$ is nondecreasing for all $u \in \mathbb{R}$, we choose $\mathcal{N}_{\rm sat}(u_{\rm c}) = {\rm sat}_{p,q}(u_{\rm c})$, where $p = -a$, $q = a$, and let $\mathcal{N}_{\rm b} = u_{\rm sat}$, $\mathcal{N}_{\rm s} = u_{\rm b}$, and $\mathcal{N}_{\rm r} = u_{\rm s}$ on $\mathbb{R}$. Figure 4.16(a.iii) shows that the composite nonlinearity $\mathcal{N} \circ \mathcal{N}_{\rm r} \circ \mathcal{N}_{\rm s} \circ \mathcal{N}_{\rm b}$ is nondecreasing on $\mathbb{R}$. We set $n_{\rm c} = 10$, $P_0 = 0.1 I_{2n_{\rm c}}$, $\eta_0 = 0.2$, and $\tilde{\mathcal{H}} = H_1$, and we vary the saturation level a for the NMP plant (4.33). Figure 4.16(b.i) shows the time history of z with $a = 10$, where the transient behavior is poor. Figure 4.16(b.ii) shows the time history of z with $a = 2$, where the transient performance is improved and z reaches steady state in about 300 time steps. Finally, we further reduce the saturation level. Figure 4.16(b.iii) shows the time history of z with $a = 1$; in this case, RCAC cannot follow the command due to fact that $a = 1$ is not large enough to provide the control $u_{\rm c}$ needed to drive z to a small value. Figure

4.16(c) shows the time history of u for the case $a = 2$, and (d) shows the frequency response of $G_{\mathrm{c},1200}(\mathbf{z})$ with $a = 2$, which indicates that $G_{\mathrm{c},1200}(\mathbf{z})$ has high gain at the command frequencies Ω_1 and Ω_2. ■

Example 4.5.4. *(Minimum-phase, unstable plant, nondecreasing $\mathcal{N}$).* We consider the discretized unstable double integrator plant over sample period $h = 1/\sqrt{2}$

$$G(\mathbf{z}) = \frac{h^2(\mathbf{z}+1)}{2(\mathbf{z}-1)^2} \tag{4.36}$$

with the piecewise-constant input nonlinearity

$$\mathcal{N}(u) = \frac{1}{2}[\mathrm{sign}(u-0.2) + \mathrm{sign}(u+0.2)], \tag{4.37}$$

which can assume only the values -1, 0, and 1. Note that $d = 1$ and $H_d = 1$. We let the command $r(k)$ be zero, and consider stabilization using RCAC with the input relay nonlinearity given by (4.37). As shown in Figure 4.17(a), the relay nonlinearity is nondecreasing for all $u \in \mathbb{R}$, and we thus choose $\mathcal{N}_{\mathrm{sat}}(u_{\mathrm{c}}) = \mathrm{sat}_{p,q}(u_{\mathrm{c}})$, where $p = -3$, $q = 3$. We let $\mathcal{N}_{\mathrm{b}} = u_{\mathrm{sat}}$, $\mathcal{N}_{\mathrm{s}} = u_{\mathrm{b}}$, and $\mathcal{N}_{\mathrm{r}} = u_{\mathrm{s}}$. We choose $n_{\mathrm{c}} = 2$, $P_0 = I_{2n_{\mathrm{c}}}$, $\eta_0 = 0$, and $\tilde{\mathcal{H}} = H_1$. For $k \geq 1000$, the command is the step $r = -200$ as shown in Figure 4.17(b). Figure 4.17(c) shows the time history of z with the initial condition $x_0 = \begin{bmatrix} -5.2 & -1.1 \end{bmatrix}^{\mathrm{T}}$ and (d) shows the time history of u. ■

Example 4.5.5. *(Minimum-phase, asymptotically stable plant, non-monotonic $\mathcal{N}$).* Consider the asymptotically stable, minimum-phase plant

$$G(\mathbf{z}) = \frac{(\mathbf{z}-0.5)(\mathbf{z}-0.9)}{(\mathbf{z}-0.7)(\mathbf{z}-0.5-\jmath 0.5)(\mathbf{z}-0.5+\jmath 0.5)}, \tag{4.38}$$

with the non-monotonic input nonlinearity

$$\mathcal{N}(u) = \begin{cases} -0.5^{-(u+2)} - 3, & \text{if } u < -2, \\ \text{sign}(u)u^2, & \text{if } -2 \leq u \leq 2, \\ 0.5^{u-2} + 3, & \text{if } u > 2. \end{cases} \tag{4.39}$$

Note that $d = 1$ and $H_d = 1$. We consider the sinusoidal command $r(k) = \sin(\Omega_1 k)$, where $\Omega_1 = \pi/5$ rad/sample. Since the linear plant is minimum phase, we choose $\mathcal{N}_{\text{sat}}(u_{\text{c}}) = \text{sat}_{p,q}(u_{\text{c}})$, where $p = -5$ and $q = 5$ in (4.20). As shown in Figure 4.21(a), $\mathcal{N}$ is non-monotonic, we let $\mathcal{N}_{\text{r}}(u_{\text{s}}) = -u_{\text{s}} - 7$ for $u_{\text{s}} \in [-5, -2]$, $\mathcal{N}_{\text{r}}(u_{\text{s}}) = -u_{\text{s}} + 7$ for $u_{\text{s}} \in [2, 5]$, and $\mathcal{N}_{\text{r}}(u_{\text{s}}) = u_{\text{s}}$ otherwise, and choose $\mathcal{N}_{\text{s}} u_{\text{b}} = u_{\text{b}}$ so that the composite nonlinearity $\mathcal{N} \circ \mathcal{N}_{\text{r}} \circ \mathcal{N}_{\text{s}}$ is piecewise nondecreasing on $[-5, 5]$ as shown in Figure 4.21(a.ii). Knowledge of only the monotonicity of $\mathcal{N}$ is used to choose $\mathcal{N}_{\text{r}}$. To construct $\mathcal{N}_{\text{b}}$, note that the piecewise nondecreasing composite nonlinearity $\mathcal{N} \circ \mathcal{N}_{\text{r}} \circ \mathcal{N}_{\text{s}}$ satisfies $\mathcal{R}_{[-5,-2]}(\mathcal{N} \circ \mathcal{N}_{\text{r}} \circ \mathcal{N}_{\text{s}}) \cup \mathcal{R}_{[2,5]}(\mathcal{N} \circ \mathcal{N}_{\text{r}} \circ \mathcal{N}_{\text{s}}) \subset \mathcal{R}_{[-5,5]}(\mathcal{N} \circ \mathcal{N}_{\text{r}} \circ \mathcal{N}_{\text{s}})$, which is not partially overlapping. Therefore, no additional information about $\mathcal{N} \circ \mathcal{N}_{\text{r}} \circ \mathcal{N}_{\text{s}}$ is needed. We let $\mathcal{N}_{\text{b}}(u_{\text{sat}}) = -2$ for $u_{\text{sat}} \in [-5, -2]$, $\mathcal{N}_{\text{b}}(u_{\text{sat}}) = 2$ for $u_{\text{sat}} \in [2, 5]$ and $\mathcal{N}_{\text{b}}(u_{\text{sat}}) = u_{\text{sat}}$ otherwise. Figure 4.21(a.iii) shows that the composite nonlinearity $\mathcal{N} \circ \mathcal{N}_{\text{r}} \circ \mathcal{N}_{\text{s}} \circ \mathcal{N}_{\text{b}}$ is nondecreasing on $[-5, 5]$. We choose $n_{\text{c}} = 10$, $P_0 = I_{2n_{\text{c}}}$, $\eta_0 = 0.01$, and $\tilde{\mathcal{H}} = H_1$. Figure 4.21(b) shows the resulting time history of z, while Figure 4.21(c) shows the frequency response of $G_{\text{c},1200}(\mathbf{z})$ with $a = 2$. Note that $G_{\text{c},1200}(\mathbf{z})$ has high gain at the command frequency Ω_1 and the harmonic $3\Omega_1$. ■

4.6 Adaptive Control of Hammerstein Systems with Even Input Nonlinearities

We now present numerical examples to illustrate the response of RCAC for Hammerstein systems with even input nonlinearities. Consider the nonlinearity $\mathcal{N}(u) = u^n$, where n is even, with the input signal $u(k) = \cos(\Omega k)$. Then the response $y(k) = \mathcal{N}(u(k))$ is given by

$$y(k) = \cos^n(\Omega k) = \frac{1}{2^n}\binom{n}{n/2} + \frac{1}{2^{n-1}}\sum_{r=0}^{n/2-1}\binom{n}{r}\cos((n-2r)\Omega k). \tag{4.40}$$

Therefore, if $\mathcal{N}$ is an even polynomial, then $y(k)$ contains harmonics at only even multiples of Ω. In particular, $y(k)$ lacks spectral content at the command frequency. If $\mathcal{N}$ is an even analytic function, then this observation applies to truncations of its Taylor expansion.

To achieve command following in this case, we propose two approaches. First, we inject a pseudo-command into the controller, where the frequency of the pseudo-command is equal to half of the frequency of the command as shown in Figure 4.19. Therefore, the plant intermediate signal v contains a harmonic at the command frequency Ω if $\mathcal{N}$ is even. Note that the pseudo-command is not necessarily phase-matched with the command. Alternatively, we use auxiliary nonlinearities to construct a composite input nonlinearities that is not even.

4.6.1 Adaptive Control of Hammerstein Systems with Even Input Nonlinearities Using Pseudo-commands

Example 4.6.1. *(Minimum-phase, stable plant, even $\mathcal{N}$).* We consider the asymptotically stable, nonminimum-phase plant (4.38) with the quadratic input nonlinearity

$$\mathcal{N}(u) = u^2 - 2, \tag{4.41}$$

which is neither one-to-one nor onto and satisfies $\mathcal{N}(0) = -2$, see Figure 4.20(b). Note that $d = 1$ and $H_d = 1$. We consider the sinusoidal command $r(k) = \sin(\Omega_1 k)$, where $\Omega_1 = \pi/5$ rad/sample. We let $n_{\mathrm{c}} = 10$, $P_0 = I_{2n_{\mathrm{c}}}$, $\eta_0 = 0.01$, $\tilde{\mathcal{H}} = H_1$, and do not use a pseudo-command. Figure 4.20(a) shows the resulting time history of z. In this case, the adaptive controller fails to follow the command in the presence of the input nonlinearity. Figure 4.20(c) shows the frequency response of $G_{\mathrm{c},5000}(\mathbf{z})$, which has high gain at $2\Omega_1$, but not at the command frequency Ω_1. ■

Example 4.6.2. *(Minimum-phase, stable plant, even $\mathcal{N}$, and pseudo-command).* As in Example 4.6.1, we consider the asymptotically stable, nonminimum-phase plant (4.38) with the quadratic input nonlinearity (4.41) and the sinusoidal command $r(k) = \sin(\Omega_1 k + \phi)$, where $\Omega_1 = \pi/5$ rad/sample and $\phi = \pi/6$ rad. The pseudo-command frequency is $\Omega_{\mathrm{p}} = \Omega_1/2 = \pi/10$ rad/sample, and we let $n_{\mathrm{c}} = 10$, $P_0 = 0.01 I_{2n_{\mathrm{c}}}$, $\eta_0 = 0.01$, and $\tilde{\mathcal{H}} = H_1$. The Hammerstein system runs open-loop for 100 time steps, and RCAC is turned on at $k = 100$. Figure 4.21(a) shows the time history of z. Figure 4.21(b) shows the frequency response of $G_{\mathrm{c},3000}(\mathbf{z})$, which has high gain at the command frequency Ω_1. ■

4.6.2 Adaptive Control of Hammerstein Systems with Even Input Nonlinearities Using Auxiliary Nonlinearities

We now present numerical examples for RCAC controller with auxiliary nonlinearities under the condition that the input nonlinearity is even. The auxiliary nonlinearities are used such that the input nonlinearity $\mathcal{N} \circ \mathcal{N}_{\rm r} \circ \mathcal{N}_{\rm s} \circ \mathcal{N}_{\rm b}$ is globally nondecreasing and thus not even.

Example 4.6.3. We consider the asymptotically stable, nonminimum-phase plant

$$G(\mathbf{z}) = \frac{\mathbf{z} - 1.2}{\mathbf{z}^2 + 0.3\mathbf{z} - 0.1}, \tag{4.42}$$

with the quadratic input nonlinearity (4.41), which is neither one-to-one nor onto and satisfies $\mathcal{N}(0) = -2$. Note that $d = 1$ and $H_d = 1$. As shown in Figure 4.22(a.i), since $\mathcal{N}(u)$ is not monotonic and G is nonminimum-phase, we choose $\mathcal{N}_{\rm sat}(u_{\rm c}) = {\rm sat}_{p,q}(u_{\rm c})$, where $p = -4$ and $q = 4$ in (4.20), let $\mathcal{N}_{\rm r}(u_{\rm b}) = -u_{\rm b} - 4$ for $u_{\rm b} \in [-4, 0]$ and $\mathcal{N}_{\rm r}(u_{\rm b}) = u_{\rm b}$ otherwise, and select $\mathcal{N}_{\rm s}(u_{\rm b}) = u_{\rm b}$ so that the composite nonlinearity $\mathcal{N} \circ \mathcal{N}_{\rm r} \circ \mathcal{N}_{\rm s}$ is piecewise nondecreasing in Figure 4.22(a.ii). Knowledge of only the monotonicity of $\mathcal{N}$ is used to choose $\mathcal{N}_{\rm r}$. To construct $\mathcal{N}_{\rm b}$, note that the piecewise nondecreasing composite nonlinearity $\mathcal{N} \circ \mathcal{N}_{\rm r} \circ \mathcal{N}_{\rm s}$ satisfies $\mathcal{R}_{[-4,0)}(\mathcal{N} \circ \mathcal{N}_{\rm r} \circ \mathcal{N}_{\rm s}) \subset \mathcal{R}_{[0,4]}(\mathcal{N} \circ \mathcal{N}_{\rm r} \circ \mathcal{N}_{\rm s})$, which is not partially overlapping. Therefore, no additional information about $\mathcal{N} \circ \mathcal{N}_{\rm r} \circ \mathcal{N}_{\rm s}$ is needed. We let $\mathcal{N}_{\rm b}(u_{\rm sat}) = 0$ for $u_{\rm sat} \in [-4, 0)$ and $\mathcal{N}_{\rm b}(u_{\rm sat}) = u_{\rm sat}$ otherwise. Figure 4.22(a.iii) shows that the composite nonlinearity $\mathcal{N} \circ \mathcal{N}_{\rm r} \circ \mathcal{N}_{\rm s} \circ \mathcal{N}_{\rm b}$ is nondecreasing.

We consider the single-tone sinusoidal command $r(k) = \sin \Omega_1 k$, where $\Omega_1 = \pi/5$ rad/sample, and the disturbance $w(k) = 0.5 \sin(\frac{\pi}{2} k)$. We let $n_{\rm c} = 10$, $P_0 = 0.01 I_{2n_{\rm c}}$, $\eta_0 = 0.1$, and $\tilde{\mathcal{H}} = H_1$. Figure 4.22(b) shows the time history of z with the input nonlinearity and disturbance present and RCAC is able to follow the command. ■

Example 4.6.4. We consider the asymptotically stable, minimum-phase plant (4.30) with the non-monotonic input nonlinearity

$$\mathcal{N}(u) = \cos(2u), \tag{4.43}$$

which is neither one-to-one nor onto and satisfies $\mathcal{N}(0) = 1$. Note that $d = 1$ and $H_d = 1$. As shown in Figure 4.23(b), $\mathcal{N}(u)$ is increasing for all $u \in \bigcup_{n\in\mathbb{Z}} \left((n - \frac{1}{2})\pi, n\pi\right)$, and decreasing for all $u \in \bigcup_{n\in\mathbb{Z}} \left(n\pi, (n+\frac{1}{2})\pi\right)$. We thus choose $\mathcal{N}_{\rm sat}(u_{\rm c}) = {\rm sat}_{p,q}(u_{\rm c})$, where $p = -10^6$ and $q = 10^6$ in (4.20), let $\mathcal{N}_{\rm r}(u_{\rm s}) = u_{\rm s}$ in the intervals where $\mathcal{N}$ is increasing, and $\mathcal{N}_{\rm r}(u_{\rm s}) = -u_{\rm s}+(2n+1/2)\pi$ in the intervals where $\mathcal{N}$ is decreasing, and select $\mathcal{N}_{\rm s}(u_{\rm b}) = u_{\rm b}$. The composite nonlinearity $\mathcal{N}\circ\mathcal{N}_{\rm r}\circ\mathcal{N}_{\rm s}$ is piecewise nondecreasing in Figure 4.23(e). Knowledge of only the monotonicity intervals of $\mathcal{N}$ is used to choose $\mathcal{N}_{\rm r}$. To construct $\mathcal{N}_{\rm b}$, note that the piecewise nondecreasing composite nonlinearity $\mathcal{N} \circ \mathcal{N}_{\rm r} \circ \mathcal{N}_{\rm s}$ satisfies $\mathcal{R}_{I_i}(\mathcal{N} \circ \mathcal{N}_{\rm r} \circ \mathcal{N}_{\rm s}) \subset \mathcal{R}_{I_j}(\mathcal{N} \circ \mathcal{N}_{\rm r} \circ \mathcal{N}_{\rm s})$ for all $i \neq j$. Therefore, no additional information of $\mathcal{N} \circ \mathcal{N}_{\rm r} \circ \mathcal{N}_{\rm s}$ is needed. We let $\mathcal{N}_{\rm b}(u_{\rm sat}) = 0$ for $u_{\rm sat} < 0$, $\mathcal{N}_{\rm b}(u_{\rm sat}) = \pi/2$ for $u_{\rm sat} > \pi/2$ and $\mathcal{N}_{\rm b}(u_{\rm sat}) = u_{\rm sat}$ otherwise. Figure 4.23(f) shows that the composite nonlinearity $\mathcal{N} \circ \mathcal{N}_{\rm r} \circ \mathcal{N}_{\rm s} \circ \mathcal{N}_{\rm b}$ is nondecreasing.

We consider the single-tone sinusoidal command $r(k) = \sin \Omega_1 k$, where $\Omega_1 = \pi/5$ rad/sample. We let $n_{\rm c} = 10$, $P_0 = 0.1I_{2n_{\rm c}}$, $\eta_0 = 0$, and $\tilde{\mathcal{H}} = H_1$. Figure 4.23(a) shows the time history of the performance z with the input nonlinearity present and z approaches zero in about 500 time steps. Figure 4.23(b) shows the input nonlinearity $\mathcal{N}$, (c) and (d) show the auxiliary nonlinearity $\mathcal{N}_{\rm r}$ and $\mathcal{N}_{\rm b}$. ■

4.7 Hammerstein Systems with Arbitrary Input Nonlinearities

We now present numerical examples to illustrate the response of RCAC with auxiliary nonlinearities for the case where the input nonlinearities are neither odd

nor even.

Example 4.7.1. We consider the asymptotically stable, minimum-phase plant

$$G(\mathbf{z}) = \frac{1}{\mathbf{z} - 0.5}, \tag{4.44}$$

with the input nonlinearity

$$\mathcal{N}(u) = \begin{cases} u^3, & \text{if } u < -1, \\ -u - 2, & \text{if } -1 \leq u \leq 1, \\ 3u^2 - 6, & \text{if } u > 1. \end{cases} \tag{4.45}$$

The command is $r(k) = \sin(0.2\pi k)$. Note that $d = 1$ and $H_d = 1$. As shown in Figure 4.24 (a.i), the input nonlinearity $\mathcal{N}$ is one-to-one and onto and has the offset $\mathcal{N}(0) = -2$. Since $\mathcal{N}$ is non-monotonic and has partially overlapping intervals, and G is asymptotically stable, we choose $\mathcal{N}_{\text{sat}}(u_{\text{c}}) = \text{sat}_{p,q}(u_{\text{c}})$, where $p = -10^6$ and $q = 10^6$ in (4.20), let $\mathcal{N}_{\text{r}}(u_{\text{b}}) = -u_{\text{s}}$ for $u_{\text{s}} \in [-1, 1]$ and $\mathcal{N}_{\text{r}}(u_{\text{s}}) = u_{\text{s}}$ otherwise, and select $\mathcal{N}_{\text{s}}(u_{\text{b}}) = u_{\text{b}}$ so that the composite nonlinearity $\mathcal{N} \circ \mathcal{N}_{\text{r}} \circ \mathcal{N}_{\text{s}}$ is piecewise nondecreasing in Figure 4.24 (a.ii). Knowledge of only the monotonicity of $\mathcal{N}$ is used to choose $\mathcal{N}_{\text{r}}$. To construct $\mathcal{N}_{\text{b}}$, note that piecewise nondecreasing input nonlinearity $\mathcal{N} \circ \mathcal{N}_{\text{r}} \circ \mathcal{N}_{\text{s}}$ has partially overlapping intervals. Therefore, we assume that $(\mathcal{N} \circ \mathcal{N}_{\text{r}} \circ \mathcal{N}_{\text{s}})\,(1.29) = -1$ is known. We thus choose $\mathcal{N}_{\text{b}}(u_{\text{sat}}) = 1$ for $u_{\text{sat}} \in [-1, 1.29]$ and $\mathcal{N}_{\text{b}}(u_{\text{sat}}) = u_{\text{sat}}$ otherwise. Figure 4.24(a.iii) shows that the composite nonlinearity $\mathcal{N} \circ \mathcal{N}_{\text{r}} \circ \mathcal{N}_{\text{s}} \circ \mathcal{N}_{\text{b}}$ is nondecreasing. We let $n_{\text{c}} = 10$, $P_0 = 0.1 I_{2n_{\text{c}}}$, $\eta_0 = 0.1$, and $\tilde{\mathcal{H}} = H_1$. Figure 4.24(b) shows the resulting time history of z, while Figure 4.24(c) shows the time history of u. Finally, Figure 4.24(d) shows the frequency response of $G_{\text{c},2000}(\mathbf{z})$, which indicates that $G_{\text{c},2000}(\mathbf{z})$ has high gain at the command frequency 0.2π rad/sample. ■

Example 4.7.2. We consider the asymptotically stable, minimum-phase plant

$$G(\mathbf{z}) = \frac{z - 0.3}{(z - 0.6)(z - 0.8)}, \tag{4.46}$$

with the input nonlinearity (4.22). The command is $r(k) = \sin(0.2\pi k)$. Note that $d = 1$ and $H_d = 1$. As shown in Figure 4.25(a), the input nonlinearity $\mathcal{N}$ is neither one-to-one nor onto. Following the same procedures in Example 4.4.10, We thus choose $\mathcal{N}_{\rm b}$, $\mathcal{N}_{\rm s}$, and $\mathcal{N}_{\rm r}$ as in (4.23), (4.24), and (4.25). Figure 4.25(d) shows that the composite nonlinearity $\mathcal{N} \circ \mathcal{N}_{\rm r} \circ \mathcal{N}_{\rm s} \circ \mathcal{N}_{\rm b}$ is nondecreasing. We let $n_{\rm c} = 10$, $P_0 = 0.01 I_{2n_{\rm c}}$, $\eta_0 = 0.01$, and $\tilde{\mathcal{H}} = H_1$. Figure 4.25(e) shows the time history of the performance z with the input nonlinearity present and z approaches zero in about 1000 time steps and (f) shows the time history of u. Figure 4.25(g) shows the input nonlinearity $\mathcal{N}$ and (h) shows the time history of θ. ■

4.8 Conclusions

Retrospective cost adaptive control (RCAC) was applied to a command-following problem for Hammerstein systems. The input nonlinearities could be odd, even, or arbitrary, as well as monotonic or non-monotonic. RCAC was used with limited modeling information. In particular, RCAC uses knowledge of the first nonzero Markov parameter of the linear dynamics. To handle the effect of the non-monotonic nonlinearity, RCAC was augmented by auxiliary nonlinearities chosen based on the properties of the input nonlinearity. The auxiliary nonlinearities combine with the input nonlinearity to form a composite nonlinearity that is globally nondecreasing. Simulation results show that RCAC is able to follow the commands for the Hammerstein systems with an unknown disturbance when the composite input nonlinearity is globally nondecreasing.

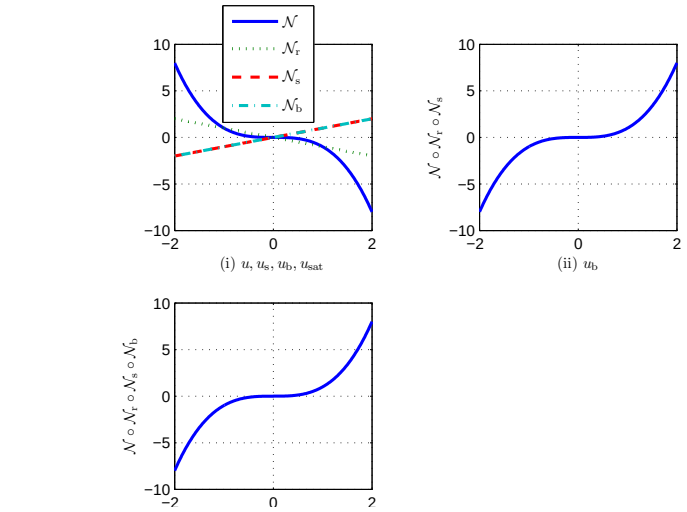

(a)

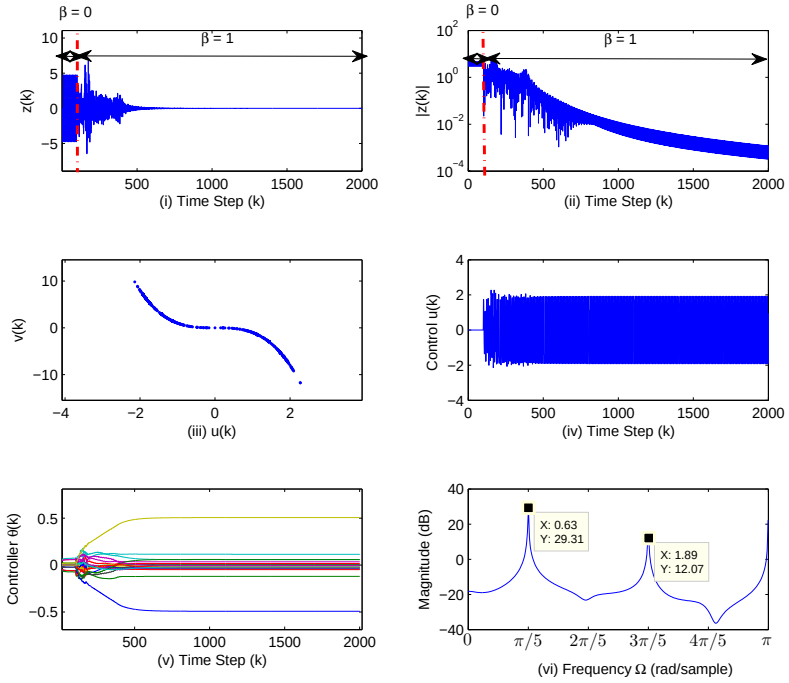

(b)

Figure 4.14: Example 4.5.1. (a.i) shows the nonlinear input nonlinearity $\mathcal{N}(u) = -u^3$ and the auxiliary nonlinearities $\mathcal{N}_\mathrm{b}$, $\mathcal{N}_\mathrm{s}$, and $\mathcal{N}_\mathrm{r}$. (a.ii) shows the nondecreasing input nonlinearity $\mathcal{N} \circ \mathcal{N}_\mathrm{r} \circ \mathcal{N}_\mathrm{s}$. (a.iii) shows that the composite nonlinearity $\mathcal{N} \circ \mathcal{N}_\mathrm{r} \circ \mathcal{N}_\mathrm{s} \circ \mathcal{N}_\mathrm{b}$ is nondecreasing. (b) shows the closed-loop response of the asymptotically stable minimum-phase plant G given by (4.30) with the sinusoidal command $r(k) = 5\sin(\Omega_1 k)$, where $\Omega_1 = \pi/5$ rad/sample. (b.iii) shows the input nonlinearity $\mathcal{N}$ for all $u \in \mathbb{R}$, and (b.iv) shows the time history of u. Finally, Figure 4.14(b.v) shows the time history of θ and (b.vi) shows the frequency response of $G_{\mathrm{c},2000}(\mathbf{z})$, which indicates that $G_{\mathrm{c},2000}(\mathbf{z})$ has high gain at the command frequency Ω_1 and the harmonic $3\Omega_1$.

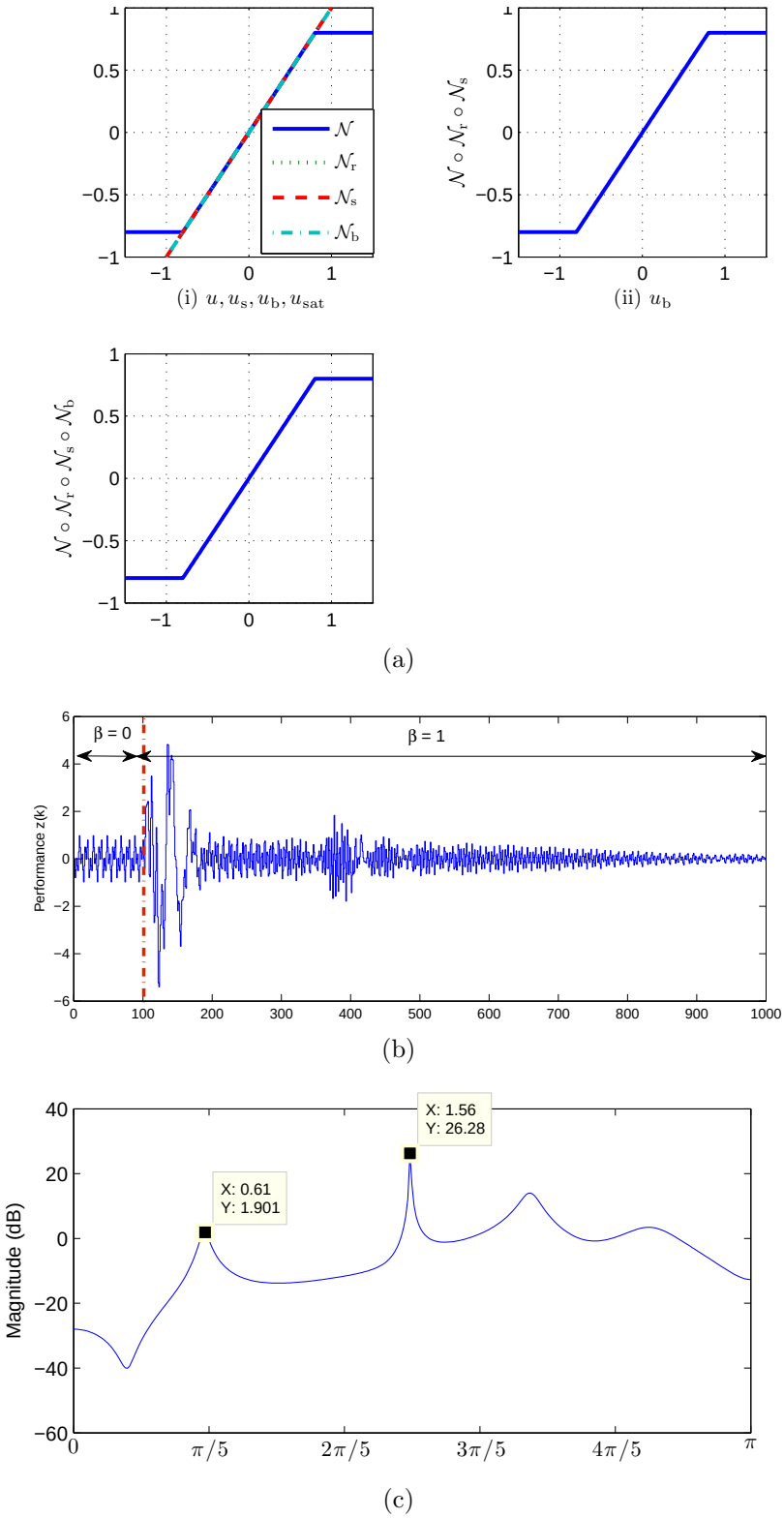

Figure 4.15: Example 4.5.2. (a) shows the saturation input nonlinearity $\mathcal{N}$ given by (4.34). (b) shows the closed-loop response of the asymptotically stable NMP plant G given by (4.33) with the two-tone sinusoidal command $r(k) = 0.5\sin(\Omega_1 k) + 0.5\sin(\Omega_2 k)$, $\Omega_1 = \pi/5$ rad/sample, and $\Omega_2 = \pi/2$ rad/sample. (c) shows the frequency response of $G_{\rm c,1000}(\mathbf{z})$, which indicates that $G_{\rm c,1000}(\mathbf{z})$ has high gain at the command frequencies Ω_1 and Ω_2.

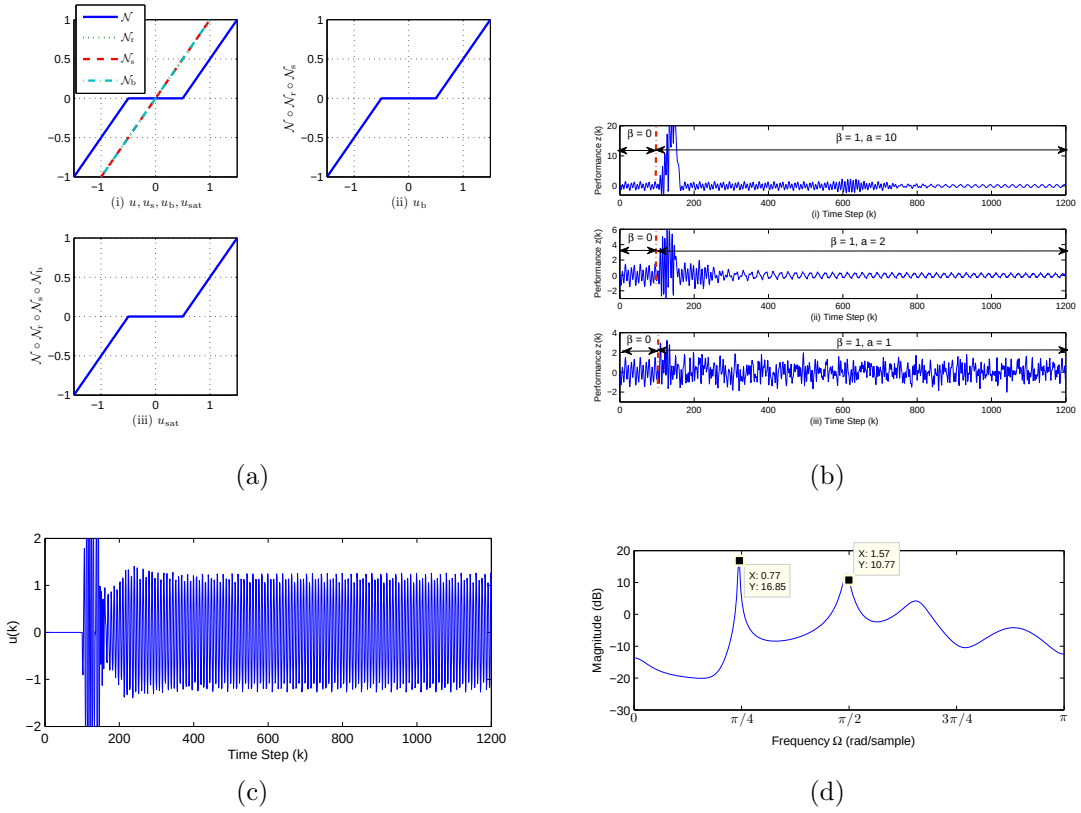

Figure 4.16: Example 4.5.3. (a) shows the deadzone input nonlinearity $\mathcal{N}(u)$ given by (4.35). (b) shows the closed-loop response of the asymptotically stable NMP plant G given by (4.33) with the two-tone sinusoidal command $r(k) = \sin(\Omega_1 k) + 0.5\sin(\Omega_2 k)$, where $\Omega_1 = \pi/4$ rad/sample and $\Omega_2 = \pi/10$ rad/sample. Figure 4.16(b.i) shows the time history of the performance z with $a = 10$, where the transient behavior is poor. Figure 4.16(b.ii) shows the time history of z with $a = 2$. Note that the transient performance is improved and z reaches steady state in about 300 time steps. Finally, Figure 4.16(b.iii) shows the time history of z with $a = 1$; in this case, RCAC cannot follow the command due to the fact that $a = 1$ is not large enough to provide the control u_c needed to drive z to a small value. (c) shows the time history of u for the case $a = 2$, and (d) shows the frequency response of $G_{c,1200}(\mathbf{z})$ with $a = 2$, which indicates that $G_{c,1200}(\mathbf{z})$ has high gain at the command frequencies Ω_1 and Ω_2.

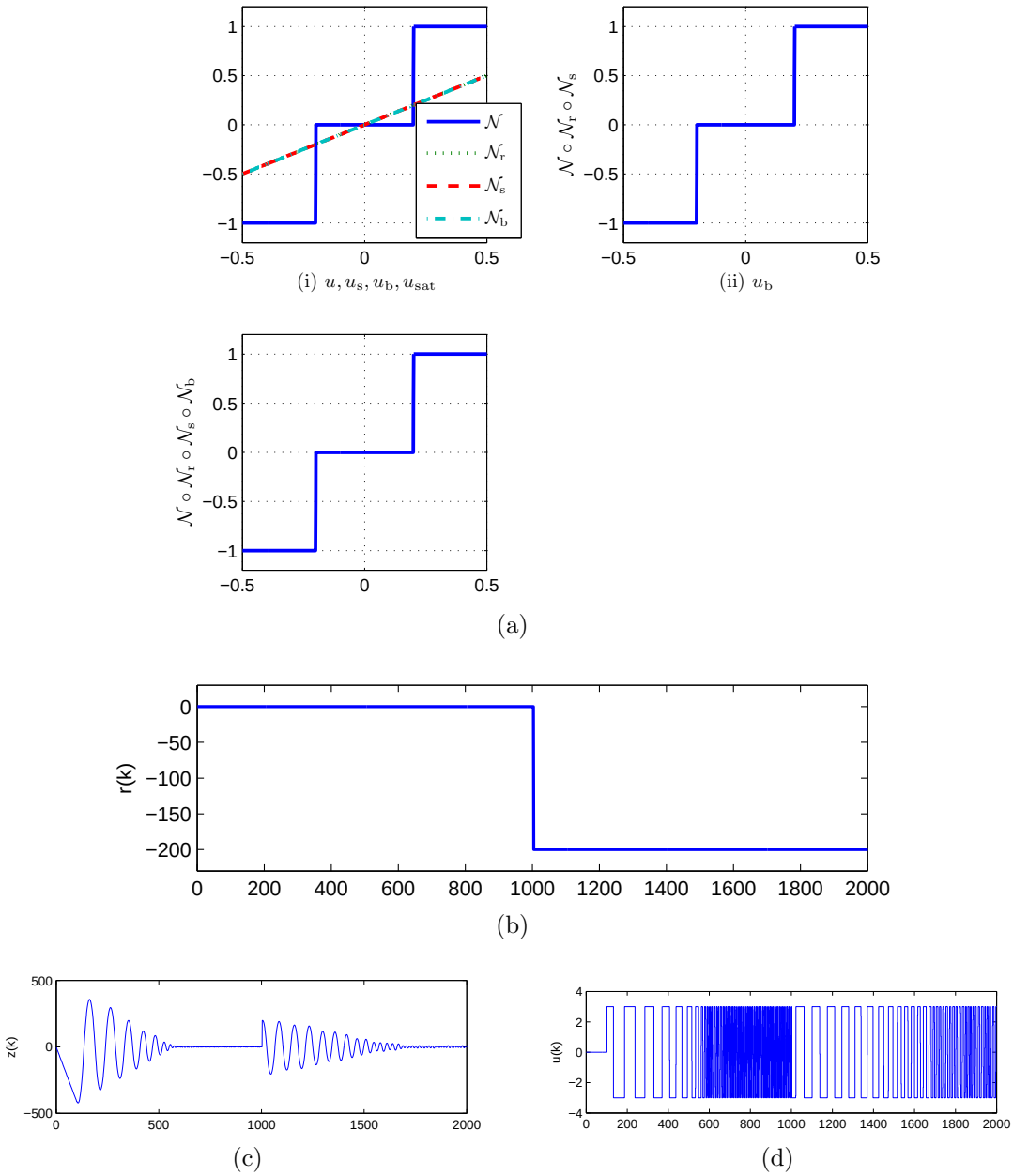

Figure 4.17: Example 4.5.4. Closed-loop response of the plant G given by (4.36) with the initial condition $x_0 = [-5.2 \quad -1.1]^{\rm T}$. The system runs open loop for 100 time steps, and the adaptive controller is turned on at $k = 100$ with the relay input nonlinearity given by (4.37) and $x(100) = [-415.2 \quad -411.1]^{\rm T}$. For $k \geq 1000$, the command is the step $r(k) = -200$ as shown in (b). (c) shows the time history of the performance z, and (d) shows the time history of u.

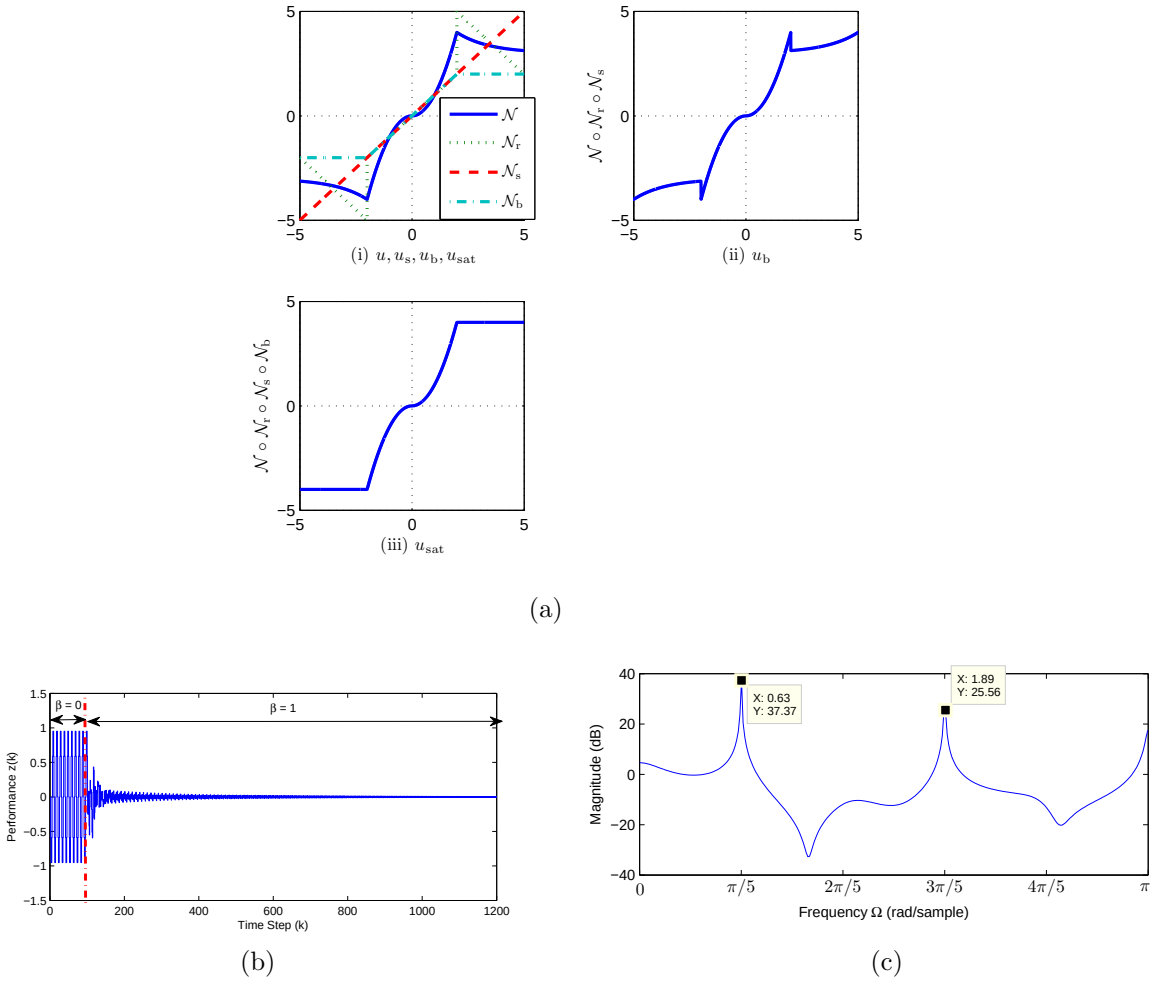

Figure 4.18: Example 4.5.5. (a.i) shows the input nonlinearity (4.39) and the auxiliary nonlinearities $\mathcal{N}_{\rm b}$ and $\mathcal{N}_{\rm r}$. (a.ii) shows the piecewise nondecreasing input nonlinearity $\mathcal{N} \circ \mathcal{N}_{\rm r}$. (a.iii) shows that the composite nonlinearity $\mathcal{N} \circ \mathcal{N}_{\rm r} \circ \mathcal{N}_{\rm b}$ is nondecreasing. (b) shows the closed-loop response of the stable minimum-phase plant G given by (4.38) with the sinusoidal command $r(k) = \sin(\Omega_1 k)$, where $\Omega_1 = \pi/5$ rad/sample. (c) shows the frequency response of $G_{\rm c,1200}(\mathbf{z})$, which indicates that $G_{\rm c,1200}(\mathbf{z})$ has high gain at the command frequency Ω_1 and the harmonic $3\Omega_1$.

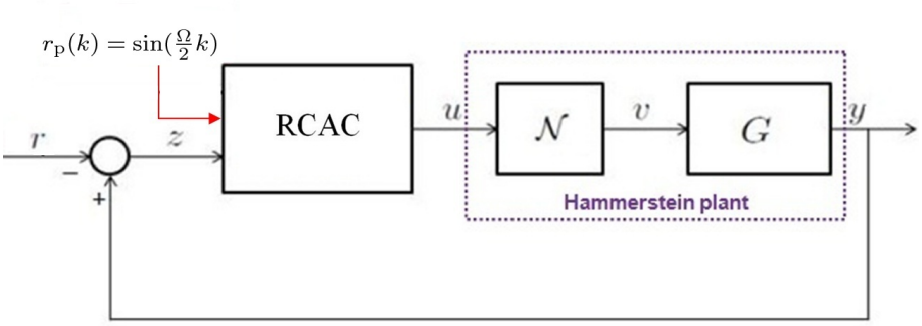

Figure 4.19: Adaptive command-following problem for a Hammerstein plant with an even input nonlinearity $\mathcal{N}$. The command signal r has frequency Ω and phase angle ϕ, while the pseudo-command is a sinusoid with frequency $\Omega/2$. The pseudo-command provides the harmonic content needed by RCAC due to the even nonlinearity, which produces harmonics at only DC and 2Ω.

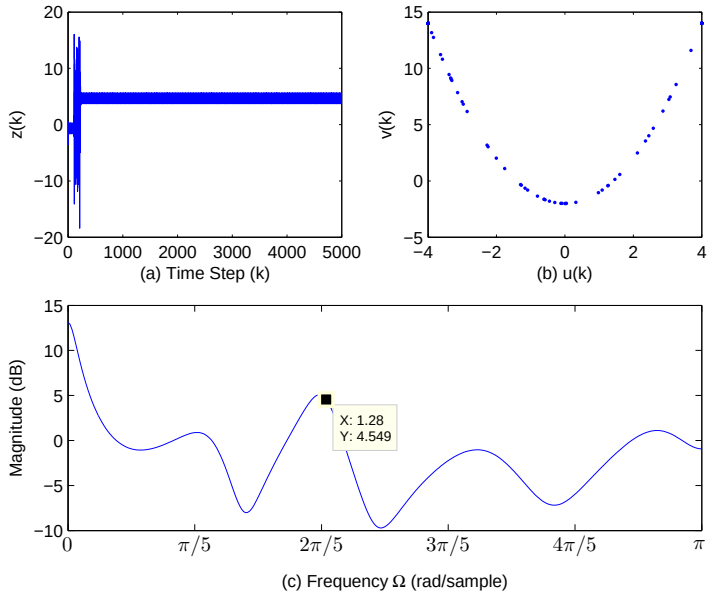

Figure 4.20: Example 4.6.1. (a) shows the resulting time history of the command-following performance z. In this case, the adaptive controller fails to follow the command in the presence of the quadratic input nonlinearity (4.41). Figure 4.20 (c) shows the frequency response of $G_{c,5000}(\mathbf{z})$, which indicates that $G_{c,5000}(\mathbf{z})$ has high gain at $2\Omega_1 = 2\pi/5$ rad/sample, but not at the command frequency $\Omega_1 = \pi/5$ rad/sample.

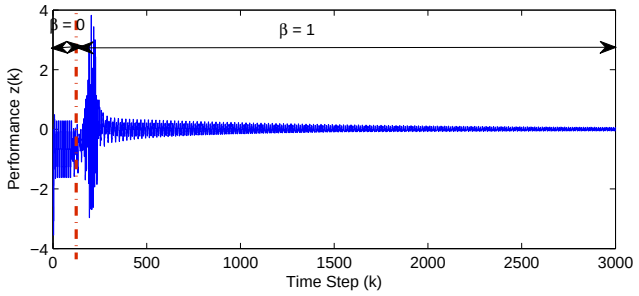

(a)

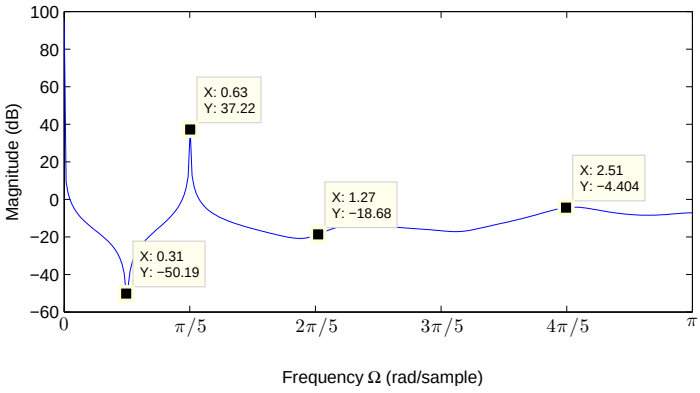

(b)

Figure 4.21: Example 4.6.2. Adaptive command-following problem for a Hammerstein plant with an even input nonlinearity (4.41). The command signal $r(k) = \sin(\Omega_1 k + \phi)$, where $\Omega_1 = \pi/5$ rad/sample and $\phi = \pi/6$ rad. The Hammerstein system runs open-loop for 100 time steps, and RCAC with the pseudo-command $r_{\mathrm{p}}(k) = \sin(\frac{\Omega_1}{2}k)$ is turned on at $k = 100$. Figure 4.6.2(a) shows the time history of z. Figure 4.6.2 (b) shows the frequency response of $G_{\mathrm{c},3000}(\mathbf{z})$, which indicates that $G_{\mathrm{c},3000}(\mathbf{z})$ has high gain at the command frequency $\Omega_1 = \pi/5$ rad/sample.

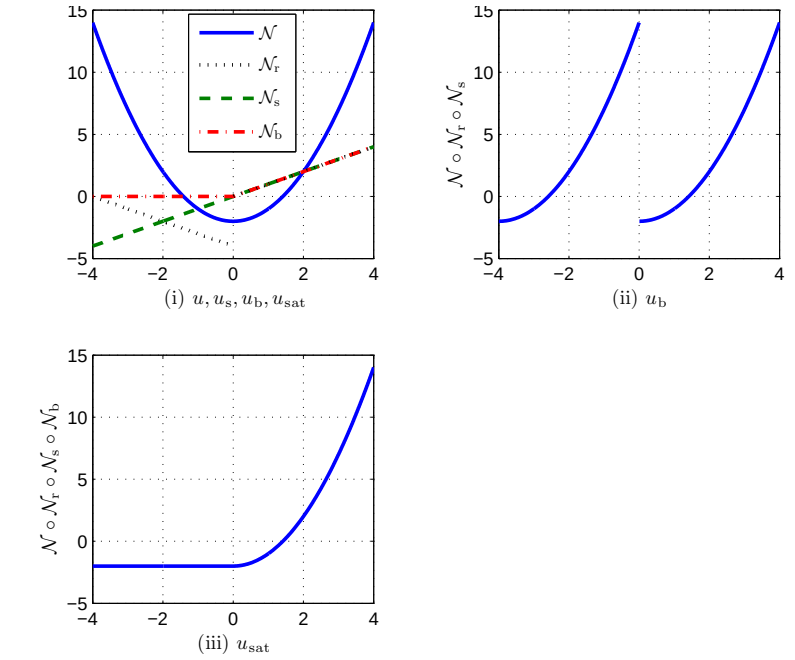

(a)

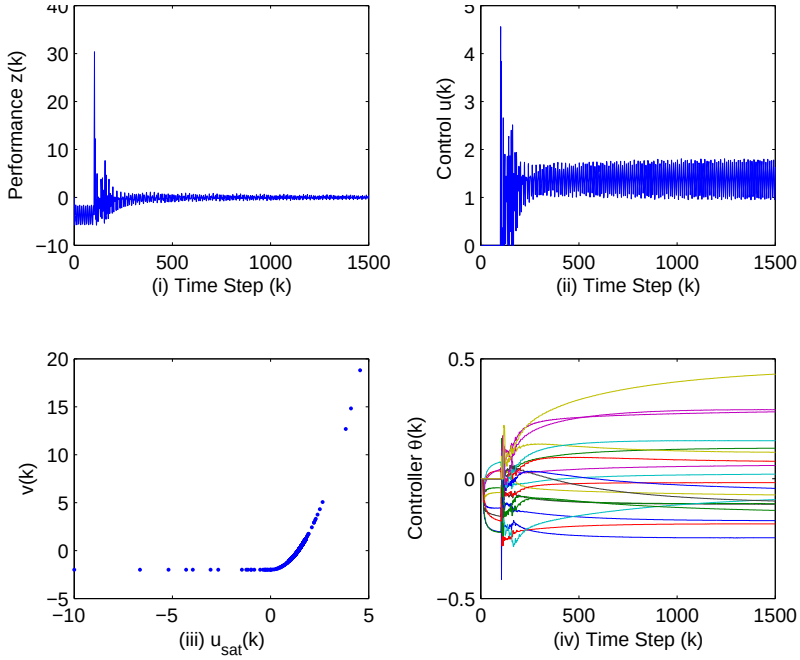

(b)

Figure 4.22: Example 4.6.3. (a.i) shows the quadratic input nonlinearity $\mathcal{N}(u) = u^2 - 2$ and the auxiliary nonlinearities $\mathcal{N}_\mathrm{b}$ and $\mathcal{N}_\mathrm{r}$. (a.ii) shows the piecewise nondecreasing input nonlinearity $\mathcal{R}_{[-4,0)}(\mathcal{N} \circ \mathcal{N}_\mathrm{r} \circ \mathcal{N}_\mathrm{s}) \subset \mathcal{R}_{[0,4]}(\mathcal{N} \circ \mathcal{N}_\mathrm{r} \circ \mathcal{N}_\mathrm{s})$, which is not partially overlapping. (a.iii) shows that the composite nonlinearity $\mathcal{N} \circ \mathcal{N}_\mathrm{r} \circ \mathcal{N}_\mathrm{s} \circ \mathcal{N}_\mathrm{b}$ is nondecreasing. (b) shows the closed-loop response of the stable minimum-phase plant G given by (4.30) with the sinusoidal command $r(k) = \sin(0.2\pi k)$ and disturbance $w(k) = 0.5\sin(\frac{\pi}{2}k)$.

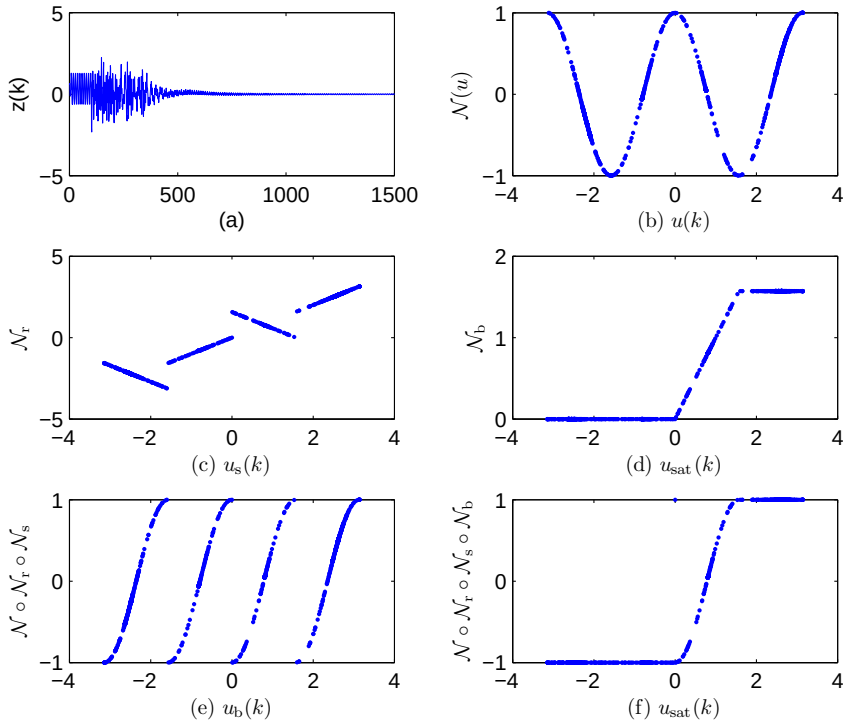

Figure 4.23: Example 4.6.4. (a) shows that RCAC follows the sinusoidal command for the Hammerstein system. (b) shows the input nonlinearity $\mathcal{N}$, (c) and (d) show the auxiliary nonlinearities $\mathcal{N}_\mathrm{r}$ and $\mathcal{N}_\mathrm{b}$, (e) shows that the composite nonlinearity $\mathcal{N} \circ \mathcal{N}_\mathrm{r} \circ \mathcal{N}_\mathrm{s}$ is piecewise increasing, and (f) shows that the composite nonlinearity $\mathcal{N} \circ \mathcal{N}_\mathrm{r} \circ \mathcal{N}_\mathrm{s} \circ \mathcal{N}_\mathrm{b}$ is nondecreasing.

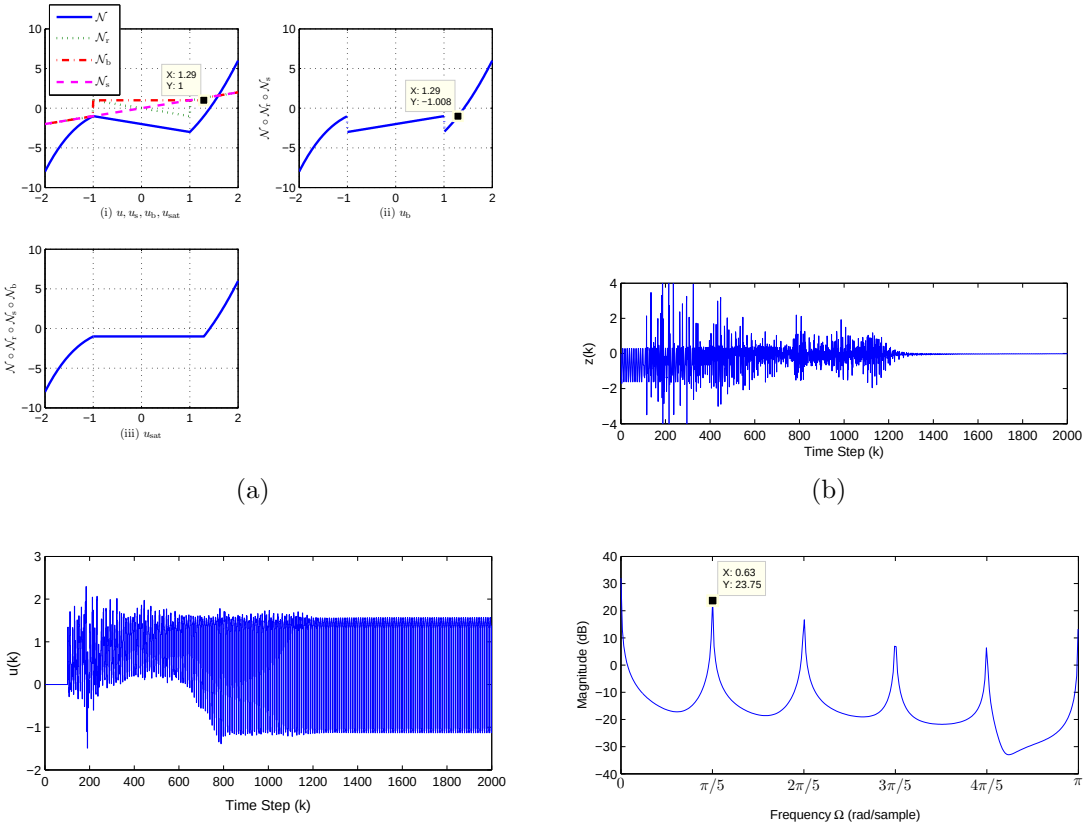

Figure 4.24: Example 4.7.1. (a.i) shows the input nonlinearity $\mathcal{N}(u)$ given by (4.45) and the auxiliary nonlinearities $\mathcal{N}_{\rm b}$ and $\mathcal{N}_{\rm r}$. (a.ii) shows the piecewise nondecreasing input nonlinearity $\mathcal{N} \circ \mathcal{N}_{\rm r} \circ \mathcal{N}_{\rm s}$ with partially overlapping intervals. (a.iii) shows that the composite nonlinearity $\mathcal{N} \circ \mathcal{N}_{\rm r} \circ \mathcal{N}_{\rm s} \circ \mathcal{N}_{\rm b}$ is nondecreasing. (b) shows the closed-loop response to the sinusoidal command $r(k) = \sin(0.2\pi k)$ of the stable minimum-phase plant G given by (4.44). (b) shows the resulting time history of z, and (c) shows the time history of u. Finally, (d) shows the frequency response of $G_{\mathrm{c},2000}(\mathbf{z})$, which indicates that $G_{\mathrm{c},2000}(\mathbf{z})$ has high gain at the command frequency $\Omega = \pi/5$ rad/sample.

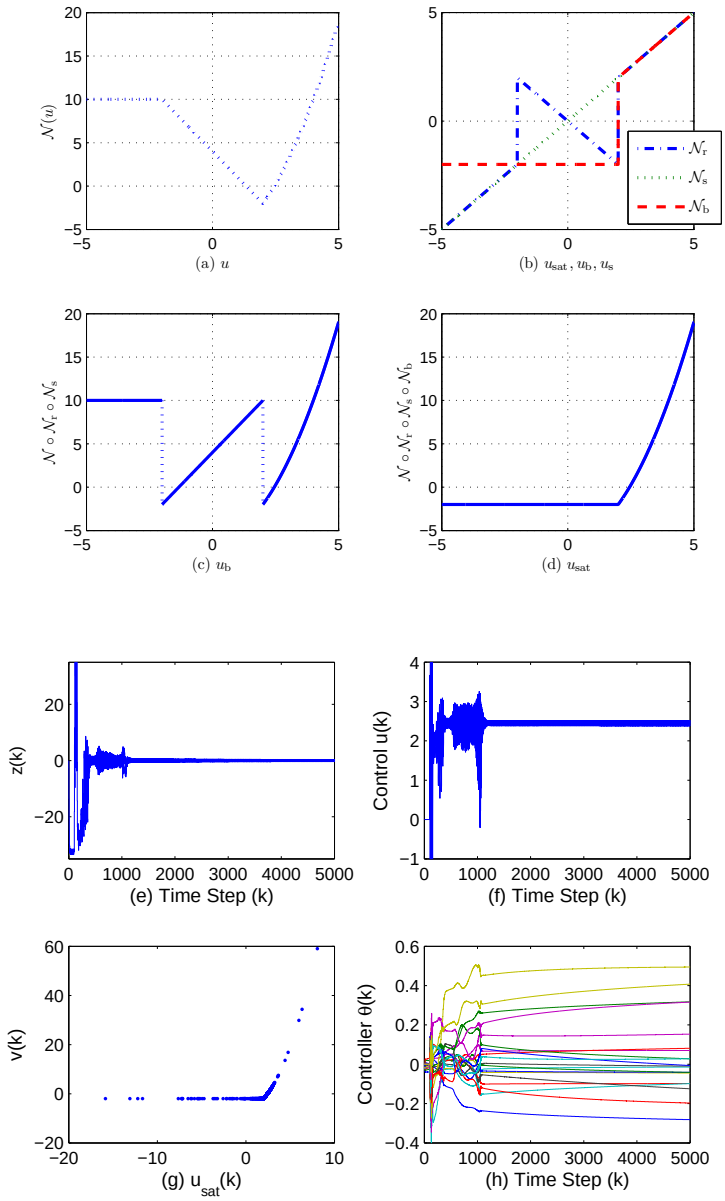

Figure 4.25: Example 4.7.2. (a) shows the non-monotonic input nonlinearity $\mathcal{N}(u)$ given by (4.22), and (b) shows the auxiliary nonlinearities $\mathcal{N}_{\rm b}$ and $\mathcal{N}_{\rm r}$. (c) shows that the composite nonlinearity $\mathcal{N} \circ \mathcal{N}_{\rm r} \circ \mathcal{N}_{\rm s}$ is piece-wise nondecreasing. (d) shows that the composite nonlinearity $\mathcal{N} \circ \mathcal{N}_{\rm r} \circ \mathcal{N}_{\rm s} \circ \mathcal{N}_{\rm b}$ is globally nondecreasing. (e) shows the closed-loop response to the sinusoidal command $r(k) = \sin(0.2\pi k)$ of the stable minimum-phase plant G given by (4.46). (f) shows the resulting time history of u, and (h) shows the time history of θ.

CHAPTER V

Retrospective Cost Adaptive NARMAX Control with Ersatz Nonlinearities

In this chapter, we generalize retrospective cost adaptive NARMAX control (RCANC) to a command-following problem for uncertain Hammerstein systems. In particular, RCANC with ersatz nonlinearities is applied to linear systems cascaded with input nonlinearities. We assume that one Markov parameter of the linear plant is known. RCANC also uses knowledge of the monotonicity properties of the input nonlinearity to select the ersatz nonlinearity. The goal is to determine whether RCANC can improve the command-following performance compared to the linear RCAC controller. The results of this chapter are published in [86, 87].

5.1 Introduction

While nonlinear control techniques have been extensively developed, the vast majority of modern methods assume the availability of full-state measurements. This is largely due to the fact that optimal control methods produce control laws that depend on full-state feedback as well as the fact that output-feedback control laws consisting of nonlinear observers combined with full-state feedback control laws may not be stabilizing. The lack of a widely applicable separation principle within a nonlinear

setting thus remains an impediment to nonlinear output-feedback control [88].

In the present chapter we focus on Hammerstein systems, which comprise a class of nonlinear systems consisting of an input nonlinearity cascaded with linear dynamics. These systems encompass plants that involve linear dynamics with, for example, saturation [70], deadzone, or on-off input nonlinearities. Identification of Hammerstein systems is widely studied [89, 90, 85], while control of Hammerstein systems includes the entire literature on control of linear systems with saturation [84] and actuator nonlinearities [91, 92].

For command-following problems, performance is degraded by the input nonlinearity in various ways. If the range of the input nonlinearity is insufficient for the plant output to follow the command, then the performance error is unavoidable; this is the case with saturation, which can also cause instability due to windup. On the other hand, if the range of the input nonlinearity is sufficiently large for the output to follow the command, performance degradation may result from the distortion introduced by the shape of the input nonlinearity. If the input nonlinearity is known, then this effect can be mitigated or removed by inversion; if the input nonlinearity is uncertain, or has a critical point, then adaptive inversion may be feasible [34].

In the present chapter we take an unconventional approach to nonlinear output feedback control of Hammerstein systems by using adaptive control to directly update the gains of a NARMAX controller. A NARMAX model is a discrete-time ARMAX system in which the past output and inputs appear as arguments of basis functions. These functions are chosen by the user, and the controller coefficients appear linearly. The constraint that the controller coefficients appear linearly implies that the basis function functions are fixed a priori and thus cannot be modified as part of the adaptation process. NARMAX models have been applied to nonlinear system identification [93, 94].

For adaptive NARMAX control, we apply retrospective cost adaptive control

(RCAC). RCAC has been developed in [95, 23, 25, 28, 30] and applied to Hammerstein systems in [58, 59] and NARMAX control in [86]. The present chapterextends and improves the results of [58, 59, 86] by modifying the adaptation mechanism to include a nonlinear adaptation mechanism. This modification ensures that the retrospective optimization accounts for the presence of the input nonlinearity. To account for the case in which the input nonlinearity is uncertain, we investigate the performance of RCNAC control in the case of uncertainty. In particular, we determine the minimal modeling information about the input nonlinearity that RCANC requires; once this information is known, an approximate input nonlinearity, called the ersatz nonlinearity, can be used by RCANC for adaptation.

5.2 Hammerstein Command-Following Problem

Consider the MIMO discrete-time Hammerstein system

$$x(k+1) = Ax(k) + B\mathcal{N}(u(k)) + D_1 w(k), \tag{5.1}$$

$$y(k) = Cx(k) + D_2 w(k), \tag{5.2}$$

$$z(k) = E_1 x(k) + E_0 w(k), \tag{5.3}$$

where $x(k) \in \mathbb{R}^n$, $y(k) \in \mathbb{R}^{l_y}$, $z(k) \in \mathbb{R}^{l_z}$, $w(k) \in \mathbb{R}^{l_w}$, $u(k) \in \mathbb{R}^{l_u}$, $\mathcal{N} : \mathbb{R}^{l_u} \to \mathbb{R}^{l_u}$, and $k \geq 0$. The goal is to develop an adaptive output feedback controller that minimizes the command-following error z with minimal modeling information about the dynamics, and input nonlinearity $\mathcal{N}$. We assume that measurements of $z(k)$ are available for feedback; however, measurements of $v(k) = \mathcal{N}(u(k))$ are not available. A block diagram for (5.1)-(5.3) is shown in Figure 5.1.

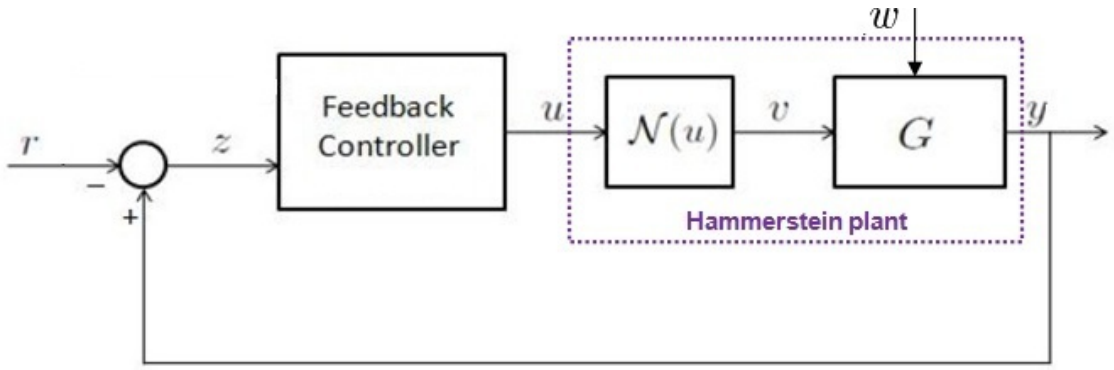

Figure 5.1: Adaptive command-following problem for a Hammerstein plant with input nonlinearity $\mathcal{N}$. We assume that measurements of $z(k)$ are available for feedback; however, measurements of $v(k) = \mathcal{N}(u(k))$ and $w(k)$ are not available.

5.3 Retrospective-Cost Adaptive NARMAX Control

5.3.1 ARMAX Modeling

Consider the ARMAX representation of (5.1)–(5.3) given by

$$z(k) = \sum_{i=1}^{n} -\alpha_i z(k-i) + \sum_{i=1}^{n} \beta_i \mathcal{N}(u(k-i)) + \sum_{i=0}^{n} \gamma_i w(k-i), \tag{5.4}$$

where $\alpha_1, \ldots, \alpha_n \in \mathbb{R}$, $\beta_1, \ldots, \beta_n \in \mathbb{R}^{l_z \times l_u}$, and $\gamma_0, \ldots, \gamma_n \in \mathbb{R}^{l_z \times l_w}$. Next, for each positive integer i, we define the ith Markov parameter of G_{zv} as

$$H_i \triangleq E_i A^{i-1} B \in \mathbb{R}^{l_z \times l_u}. \tag{5.5}$$

Note that if $i < d$, where d is the relative degree, then

$$\beta_1 = \cdots = \beta_{d-1} = H_1 = \cdots = H_{d-1} = 0,$$

and $H_d = \beta_d$.

Next, define the *extended performance* $Z(k) \in \mathbb{R}^{pl_z}$ and $U(k) \in \mathbb{R}^{q_c l_u}$ by

$$Z(k) \triangleq \begin{bmatrix} z(k) \\ \vdots \\ z(k-p+1) \end{bmatrix}, U(k) \triangleq \begin{bmatrix} u(k-1) \\ \vdots \\ u(k-q_c) \end{bmatrix}, \tag{5.6}$$

where the data window size p is a positive integer, and $q_c \triangleq n+p-1$. Therefore (5.6) can be expressed as

$$Z(k) = W_{zw}\phi_{zw}(k) + B_f\mathcal{N}(U(k)), \tag{5.7}$$

where

$$W_{zw} \triangleq \begin{bmatrix} -\alpha_1 I_{l_z} & \cdots & -\alpha_n I_{l_z} & 0_{l_z\times l_z} & \cdots & 0_{l_z\times l_z} & \gamma_0 & \cdots & \gamma_n & 0_{l_z\times l_w} & \cdots & 0_{l_z\times l_w} \\ 0_{l_z\times l_z} & \ddots & & \ddots & \ddots & \vdots & 0_{l_z\times l_w} & \ddots & & \ddots & \ddots & \vdots \\ \vdots & \ddots & \ddots & & \ddots & 0_{l_z\times l_z} & \vdots & \ddots & \ddots & & \ddots & 0_{l_z\times l_w} \\ 0_{l_z\times l_z} & \cdots & 0_{l_z\times l_z} & -\alpha_1 I_{l_z} & \cdots & -\alpha_n I_{l_z} & 0_{l_z\times l_w} & \cdots & 0_{l_z\times l_w} & \gamma_0 & \cdots & \gamma_n \end{bmatrix} \in \mathbb{R}^{pl_z\times[q_c l_z+(q_c+1)l_w]}, \tag{5.8}$$

$$B_f \triangleq \begin{bmatrix} \beta_1 & \cdots & \beta_n & 0_{l_z\times l_u} & \cdots & 0_{l_z\times l_u} \\ 0_{l_z\times l_u} & \ddots & & \ddots & \ddots & \vdots \\ \vdots & \ddots & \ddots & & \ddots & 0_{l_z\times l_u} \\ 0_{l_z\times l_u} & \cdots & 0_{l_z\times l_u} & \beta_1 & \cdots & \beta_n \end{bmatrix} \in \mathbb{R}^{pl_z\times q_c l_u}, \tag{5.9}$$

and

$$\phi_{zw}(k) \triangleq \begin{bmatrix} z(k-1) \\ \vdots \\ z(k-p-n+1) \\ w(k) \\ \vdots \\ w(k-p-n+1) \end{bmatrix} \in \mathbb{R}^{q_c l_z + (q_c+1) l_w}. \tag{5.10}$$

Note that W_{zw} and B_f are of block-Toeplitz structure. W_{zw} includes modeling information about the poles of the linear plant G and exogenous signals, that is, either the command signals to be followed or the disturbance to be rejected. B_f includes modeling information about the zeros of the linear plant G.

5.3.2 NARMAX Controller Construction

In this section, we assume a NARMAX structure for the adaptive controller, which uses a nonlinear difference equation to model the relation between the input z and output u of the controller. The nonlinear controller may include nonlinearities on the input to the controller (NARMAX/I), the output of the controller (NARMAX/O), or both (NARMAX/IO). The NARMAX controller structure is linear in the controller parameters, and linear regression is used to update the controller coefficients.

The control $u(k)$ is given by the strictly proper time-series controller of order n_c written as

$$u(k) = \sum_{j=1}^{s} \sum_{i=1}^{n_c} M_{ji}(k) f_j(u(k-i)) + \sum_{j=1}^{t} \sum_{i=1}^{n_c} N_{ji}(k) g_j(y(k-i)), \tag{5.11}$$

where, for all $j = 1, \ldots, s$, $i = 1, \ldots, n_c$, $s \in \mathbb{Z}^+$, $M_{ji}(k) \in \mathbb{R}^{l_u \times l_u}$, and for all $j = 1, \ldots, t$, $i = 1, \ldots, n_c$, $t \in \mathbb{Z}^+$, $N_{ji}(k) \in \mathbb{R}^{l_u \times l_y}$. The control (5.11) can be

expressed as

$$u(k) = \theta(k)\phi(k-1),$$

where

$$\theta(k) \triangleq \left[\begin{array}{cccccc} M_{11}(k) & \cdots & M_{sn_{\mathrm{c}}}(k) & N_{11}(k) & \cdots & N_{tn_{\mathrm{c}}}(k) \end{array} \right] \in \mathbb{R}^{l_u \times n_{\mathrm{c}}(sl_u + tl_y)}$$

and

$$\phi(k-1) \triangleq \left[\begin{array}{c} f_1(u(k-1)) \\ \vdots \\ f_s(u(k-n_{\mathrm{c}})) \\ g_1(y(k-1)) \\ \vdots \\ g_t(y(k-n_{\mathrm{c}})) \end{array} \right] \in \mathbb{R}^{n_{\mathrm{c}}(sl_u + tl_y)}. \tag{5.12}$$

To illustrate the NARMAX/O controller structure, let $f_1(u) = u$, $f_2(u) = u^2$, and $f_3(u) = u^3$. Then $\theta(k)$ and $\phi(k-1)$ can be expressed as

$$\theta(k) \triangleq \left[\begin{array}{cccccccccccc} M_1(k) & \cdots & M_{n_{\mathrm{c}}}(k) & M_{n_{\mathrm{c}}+1}(k) & \cdots & M_{2n_{\mathrm{c}}}(k) & M_{2n_{\mathrm{c}}+1}(k) & \cdots & M_{3n_{\mathrm{c}}}(k) & N_1(k) & \cdots & N_{n_{\mathrm{c}}}(k) \end{array} \right] \in \mathbb{R}^{l_u \times n_{\mathrm{c}}(3l_u + l_y)}$$

and

$$\phi(k-1) \triangleq \left[\begin{array}{cccccccccccc} u(k-1) & \cdots & u(k-n_{\mathrm{c}}) & u^2(k-1) & \cdots & u^2(k-n_{\mathrm{c}}) & u^3(k-1) & \cdots & u^3(k-n_{\mathrm{c}}) & y(k-1) & \cdots & y(k-n_{\mathrm{c}}) \end{array} \right]^{\mathrm{T}} \in \mathbb{R}^{n_{\mathrm{c}}(3l_u + l_y)}.$$

To illustrate the NARMAX/I controller structure, let $g_1(y) = y$ and $g_2(y) = y^2$. Then

$\theta(k)$ and $\phi(k-1)$ can be expressed as

$$\theta(k) \triangleq \begin{bmatrix} M_1(k) & \cdots & M_{n_c}(k) & N_1(k) & \cdots & N_{n_c}(k) & N_{n_c+1}(k) & \cdots & N_{2n_c}(k) \end{bmatrix} \in \mathbb{R}^{l_u \times n_c(l_u+2l_y)}$$

and

$$\phi(k-1) \triangleq \begin{bmatrix} u(k-1) & \cdots & u(k-n_c) & y(k-1) & \cdots & y(k-n_c) & y^2(k-1) & \cdots & y^2(k-n_c) \end{bmatrix}^{\mathrm{T}} \in \mathbb{R}^{n_c(l_u+2l_y)}.$$

5.3.3 Retrospective Performance

Define the *retrospective performance* $\hat{Z}(k) \in \mathbb{R}^{pl_z}$ by

$$\hat{Z}(k) \triangleq W_{zw}\phi_{zw}(k) + B_f\mathcal{N}(U(k)) + \bar{B}_f[\tilde{\mathcal{N}}(\hat{U}(k)) - \tilde{\mathcal{N}}(U(k))], \tag{5.13}$$

where $\bar{B}_f \in \mathbb{R}^{pl_z \times p_c l_u}$ is the retrospective input matrix, $\tilde{\mathcal{N}} : \mathbb{R} \to \mathbb{R}$ is the ersatz nonlinearity, $\tilde{\mathcal{N}}(\hat{U}(k))$ means componentwise evaluation, and $\hat{U}(k) \in \mathbb{R}^{q_c l_u}$ is the recomputed extended control vector, the components of $\hat{U}(k)$ are the recomputed control $\hat{u}(k-1)\ldots\hat{u}(k-q_c)$ ordered in the same way as the components in (5.6). Subtracting (5.7) from (5.13) yields

$$\hat{Z}(k) = Z(k) + \bar{B}_f[\tilde{\mathcal{N}}(\hat{U}(k)) - \tilde{\mathcal{N}}(U(k))]. \tag{5.14}$$

Note that the retrospective performance $\hat{Z}(k)$ does not depend on W_{zw} or the exogenous signal w. For the disturbance rejection problem, we do not need to assume that the disturbance is known; for the command-following problem, the command w can be unknown. Therefore, only limited model information is needed. The model information matrix $\bar{B}_f$ is discussed in Section 5.4, and the construction of ersatz nonlinearity $\tilde{\mathcal{N}}$ is discussed in Section 5.5.

5.3.4 Retrospective Cost and Recursive Least Square (RLS) Update Law

5.3.4.1 Retrospective Cost

We define the *retrospective cost function*

$$J(\tilde{\mathcal{N}}(\hat{U}(k)),k) \triangleq \hat{Z}^{\mathrm{T}}(k)R(k)\hat{Z}(k), \tag{5.15}$$

where $R(k) \in \mathbb{R}^{pl_z \times pl_z}$ is a positive-definite performance weighting. The goal is to determine retrospectively optimized controls $\hat{U}(k)$ that would have provided better performance than the controls $U(k)$ that were applied to the system. The retrospectively optimized control values $\hat{U}(k)$ are subsequently used to update the controller.

Next, to ensure that (5.15) has a global minimizer, we consider the regularized cost

$$\bar{J}(\tilde{\mathcal{N}}(\hat{U}(k)),k) \triangleq \hat{Z}^{\mathrm{T}}(k)R(k)\hat{Z}(k) + \eta(k)\tilde{\mathcal{N}}^{\mathrm{T}}(\hat{U}(k))\tilde{\mathcal{N}}(\hat{U}(k)), \tag{5.16}$$

where $\eta(k) \geq 0$. Substituting (5.7) into (5.16) yields

$$\bar{J}(\tilde{\mathcal{N}}(\hat{U}(k)),k) = \tilde{\mathcal{N}}^{\mathrm{T}}(\hat{U}(k))\mathcal{A}\tilde{\mathcal{N}}(\hat{U}(k)) + \mathcal{B}(k)\tilde{\mathcal{N}}(\hat{U}(k)) + \mathcal{C}(k),$$

where

$$\begin{aligned}
\mathcal{A}(k) &\triangleq \bar{B}_f^{\mathrm{T}}R(k)\bar{B}_f + \eta(k)I_{q_c l_u \times q_c l_u},\\
\mathcal{B}(k) &\triangleq 2\bar{B}_f^{\mathrm{T}}R(k)[Z(k) - \bar{B}_f\tilde{\mathcal{N}}(U(k))],\\
\mathcal{C}(k) &\triangleq Z^{\mathrm{T}}(k)R(k)Z(k) - 2Z^{\mathrm{T}}(k)R(k)\bar{B}_f\tilde{\mathcal{N}}(U(k)) + \tilde{\mathcal{N}}^{\mathrm{T}}(U(k))\bar{B}_f^{\mathrm{T}}R(k)\bar{B}_f\tilde{\mathcal{N}}(U(k)).
\end{aligned}$$

If either $\bar{B}_f$ has full column rank or $\eta(k) > 0$, then $\mathcal{A}(k)$ is positive definite. In this

case, $\bar{J}(\tilde{\mathcal{N}}(\hat{U}(k)), k)$ has the unique global minimizer

$$\tilde{\mathcal{N}}(\hat{U}(k)) = -\frac{1}{2}\mathcal{A}^{-1}(k)\mathcal{B}(k). \tag{5.17}$$

If $\tilde{\mathcal{N}}$ is not onto, then $\hat{U}(k)$ in (5.17) may not have a solution. Hence, we take

$$\hat{U}(k) = \operatorname{argmin} \left\| \tilde{\mathcal{N}}(\hat{U}(k)) + \frac{1}{2}\mathcal{A}^{-1}(k)\mathcal{B}(k) \right\|_2. \tag{5.18}$$

An arbitrary choice is made if the argmin in (5.18) is not unique.

5.3.4.2 Cumulative Cost and RLS Update

Let ρ be a positive integer such that $U(k)$ contains $u(k-\rho)$ and define the *cumulative cost function*

$$J_{\mathrm{cum}}(\theta, k) \triangleq \sum_{i=\rho+1}^{k} \lambda^{k-i} \|\phi^{\mathrm{T}}(i-\rho-1)\theta(k) - \hat{u}(i-\rho)\|^2 + \lambda^k (\theta(k)-\theta_0)^{\mathrm{T}} P_0^{-1} (\theta(k)-\theta_0), \tag{5.19}$$

where $\|\cdot\|$ is the Euclidean norm, $\lambda \in (0,1]$ is the forgetting factor, and $P_0 \in \mathbb{R}^{l_u n_c (s l_u + t l_y) \times l_u n_c (s l_u + t l_y)}$ is positive definite. Minimizing (5.19) yields

$$\begin{aligned}\theta^{\mathrm{T}}(k) = \theta^{\mathrm{T}}(k-1) &+ \beta(k) P(k-1)\phi(k-\rho-1) \cdot [\phi^{\mathrm{T}}(k-\rho) P(k-1)\phi(k-\rho-1) + \lambda]^{-1} \\ &\cdot [\phi^{\mathrm{T}}(k-\rho-1)\theta(k) - \hat{u}(k-\rho)],\end{aligned}$$

where $\beta(k)$ is either zero or one. The error covariance is updated by

$$\begin{aligned}P(k) = \beta(k)\lambda^{-1}P(k-1) &+ [1-\beta(k)]P(k-1) - \beta(k)\lambda^{-1}P(k-1)\phi(k-\rho-1) \\ &\cdot [\phi^{\mathrm{T}}(k-\rho-1)P(k-1)\phi(k-\rho) + \lambda]^{-1} \cdot \phi^{\mathrm{T}}(k-\rho-1)P(k-1).\end{aligned}$$

Note that when $\beta(k) = 0$, $\theta(k) = \theta(k-1)$ and $P(k) = P(k-1)$. Therefore, setting $\beta(k) = 0$ switches off the controller adaptation, and thus freezes the control gains. When $\beta(k) = 1$, the controller is allowed to adapt.

5.4 Model Information $\bar{B}_f$

For SISO, minimum-phase, asymptotically stable linear plants, using the first nonzero Markov parameter in $\bar{B}_f$ yields asymptotic convergence of z to zero [25, 30]. In this case, let $m = d$ and $\bar{H}_d = H_d$. Furthermore, if the open-loop linear plant is nonminimum-phase and the absolute values of all nonminimum-phase zeros are greater than the plant's spectral radius, then a sufficient number of Markov parameters can be used to approximate the nonminimum-phase zeros [25]. Alternatively, a phase-matching condition with $\eta > 0$ is given in [44, 76] to construct $\bar{B}_f$. For MIMO Lyapunov-stable linear plants, an extension of the phase-matching-based method is given in [77]. For unstable, nonminimum-phase plants, knowledge of the locations of the nonminimum-phase zeros is needed to construct $\bar{B}_f$. For details, see [25, 78].

In this chapter, we assume that the Hammerstein system is Lyapunov stable, and we choose $\bar{B}_f = \begin{bmatrix} 0_{1\times d-1} & H_d \end{bmatrix}$, that is, the first nonzero Markov parameter of G.

5.5 Construction of Ersatz Nonlinearity $\tilde{\mathcal{N}}$

In this section, we investigate the performance of various constructions for the ersatz nonlinearity $\tilde{\mathcal{N}}$. The objective is to determine the effect of model error in identifying $\mathcal{N}$. We consider the asymptotically stable, minimum-phase plant

$$G(z) = \frac{(z-0.5)(z-0.9)}{(z-0.7)(z-0.5-\jmath 0.5)(z-0.5+\jmath 0.5)}, \tag{5.20}$$

with the input nonlinearity

$$\mathcal{N}(u) = (u-2)^2 - 3. \tag{5.21}$$

We consider the sinusoidal command $r(k) = \sin(\Omega_1 k)$, where $\Omega_1 = \pi/5$ rad/sample. Let the controller structure be NARMAX/IO with $s = t = 6$ in (5.11). In particular, we choose $f_1(u) = u$, $f_2(u) = \exp(-(u+0.2)^2)$, $f_3(u) = \exp(-(u-0.2)^2)$, $f_4(u) = \exp(-(u+0.4)^2)$, $f_5(u) = \exp(-(u-0.4)^2)$, $f_6(u) = \exp(-u^2)$, and $g_1(y) = y$, $g_2(y) = \exp(-(y+0.2)^2)$, $g_3(y) = \exp(-(y-0.2)^2)$, $g_4(y) = \exp(-(y+0.4)^2)$, $g_5(y) = \exp(-(y-0.4)^2)$, $g_6(y) = \exp(-y^2)$ for the NARMAX/IO model. Furthermore, we let $n_\mathrm{c} = 10$, $P_0 = 10I_{12n_\mathrm{c}}$, $\eta_0 = 0$, and $\bar{B}_f = H_1 = 1$ as the required linear plant information.

We consider various choices of the ersatz nonlinearity $\tilde{\mathcal{N}}$ in order to elicit the required minimum model information of the input nonlinearity $\mathcal{N}$. First, we consider the ersatz nonlinearity $\tilde{\mathcal{N}}(u) = (u-2)^2$. The closed-loop response is shown in Figure 5.2. Note that the steady-state average performance $z_{\mathrm{ss,avg}} = 5.7154 \times 10^{-4}$. Note that RCANC compensates for the unknown bias in $\mathcal{N}$.

Next, we consider the ersatz nonlinearity $\tilde{\mathcal{N}}(u) = u^2$, and note that the intervals of monotonicity of $\tilde{\mathcal{N}}$ and $\mathcal{N}$ are different. As shown in Figure 5.3, RCANC is not able to follow the command.

Furthermore, consider the ersatz nonlinearity $\tilde{\mathcal{N}}(u) = 5(u-2)^2$. As shown in Figure 5.4, the steady-state average performance $z_{\mathrm{ss,avg}} = 9.0578 \times 10^{-4}$, and the performance degradation is 58.48%.

Last, consider the ersatz nonlinearity $\tilde{\mathcal{N}}(u) = |u-2|$, which matches the monotonicity but not the shape of $\mathcal{N}$. The closed-loop response is shown in Figure 5.5. Note that the steady-state average performance $z_{\mathrm{ss,avg}} = 0.0241$, which represents two orders of magnitude degradation.

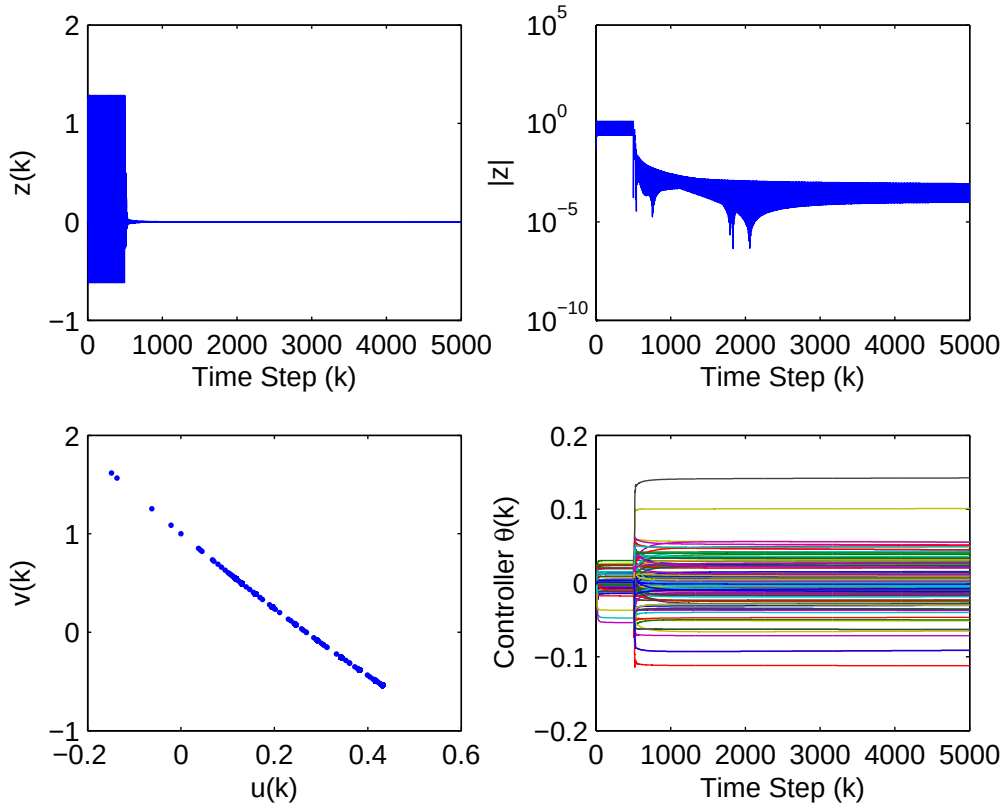

Figure 5.2: Response of the reference signal $r(k) = \sin(\pi/5k)$ with input nonlinearity $\mathcal{N}(u) = (u-2)^2 - 3$. We consider $\tilde{\mathcal{N}}(u) = (u-2)^2$ and the steady-state average performance $z_{\mathrm{ss,avg}} = 5.7154 \times 10^{-4}$. Note that RCANC compensates for the unknown bias in $\mathcal{N}$.

These examples suggest that the monotonicity intervals of $\mathcal{N}$ are needed to construct $\tilde{\mathcal{N}}$, and the more accurately $\tilde{\mathcal{N}}$ approximates $\mathcal{N}$, the better the performance is.

5.6 Effect of Basis Functions

We now present numerical examples to illustrate the response of the RCANC with different basis functions. We assume that first nonzero Markov parameter of G and the monotonicity of $\mathcal{N}$ are known. For convenience, each example is constructed such that the first nonzero Markov parameter $H_d = 1$, where d is the relative degree of

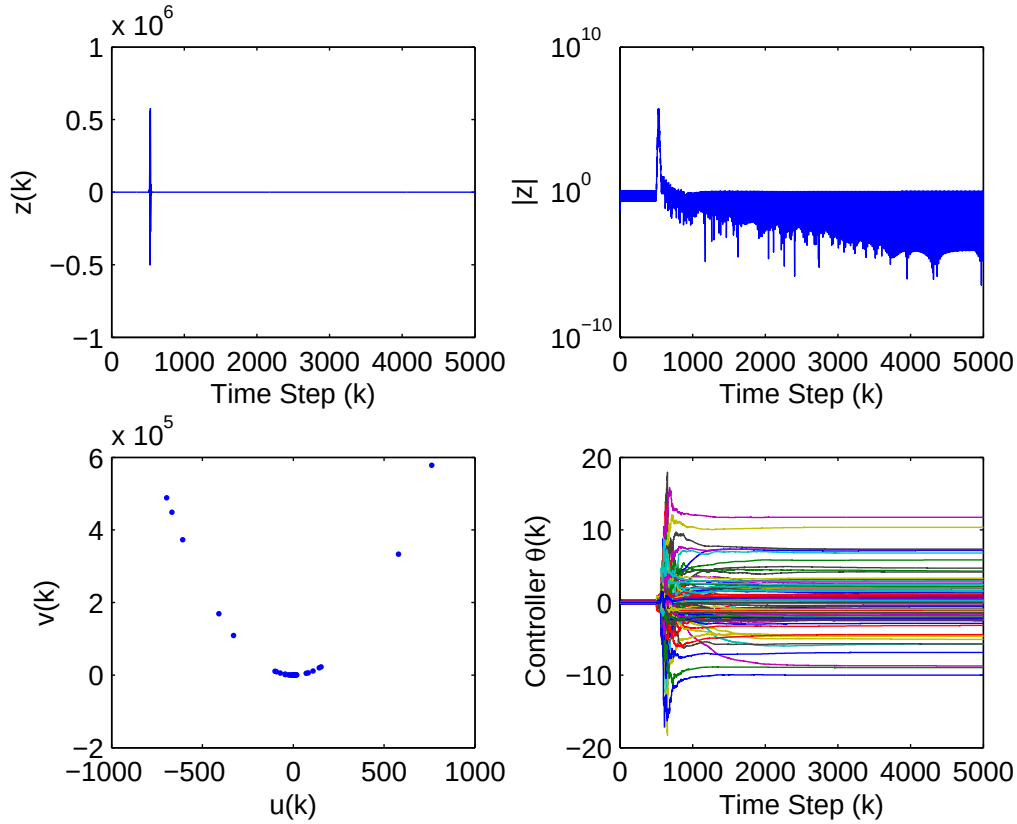

Figure 5.3: Response of the reference signal $r(k) = \sin(\pi/5k)$ with input nonlinearity $\mathcal{N}(u) = (u-2)^2 - 3$. We consider $\tilde{\mathcal{N}}(u) = u^2$ and note that the intervals of monotonicity of $\tilde{\mathcal{N}}$ and $\mathcal{N}$ are different. As shown in Fig 5.3, RCANC is not able to follow the command.

G. All examples assume $y = z$, with $\phi(k)$ given by (5.12), where f and g are chosen based on the choice of NARMAX structure. In all cases, we initialize the adaptive controller to be zero, that is, $\theta(0) = 0$. We let $\lambda = 1$ for all examples.

We consider the asymptotically stable, minimum-phase plant

$$G(z) = \frac{(z-0.5)}{z^2}, \tag{5.22}$$

with the input nonlinearity

$$\mathcal{N}(u) = (u-2)^2 - 3. \tag{5.23}$$

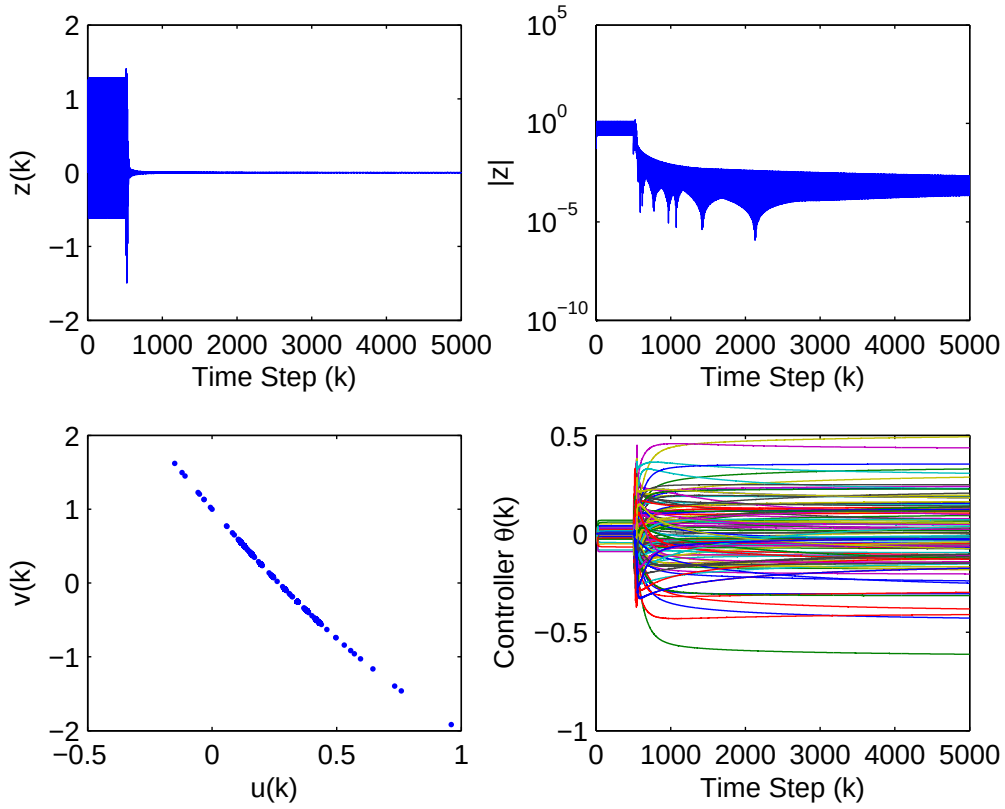

Figure 5.4: Response of the reference signal $r(k) = \sin(\pi/5k)$ with input nonlinearity $\mathcal{N}(u) = (u-2)^2 - 3$. We consider $\tilde{\mathcal{N}}(u) = 5(u-2)^2$ and the steady-state average performance $z_{\text{ss,avg}} = 9.0578 \times 10^{-4}$. Note that the performance degradation is 58.48%.

We consider the sinusoidal command $r(k) = \sin(\Omega_1 k)$, where $\Omega_1 = \pi/5$ rad/sample. We choose the ersatz nonlinearity $\tilde{\mathcal{N}}(u) = (u-2)^2$. Furthermore, we let $n_{\text{c}} = 10$, $P_0 = I_{(s+t)n_{\text{c}}}$, $\eta_0 = 0.011$, and select $\bar{B}_f = H_1 = 1$ as the required linear plant information.

First, we consider a linear controller structure, that is, $f(u) = u$ and $f(y) = y$. The closed-loop response is shown in Figure 5.6. In this case, the steady-state average performance $z_{\text{ss,avg}} = 0.0110$.

Next, we consider NARMAX controllers with four types of nonlinear functions, namely Fourier basis function, radial basis function [96], logistic basis function [96], and triangular basis function. In all simulations, we compute the closed-loop steady-

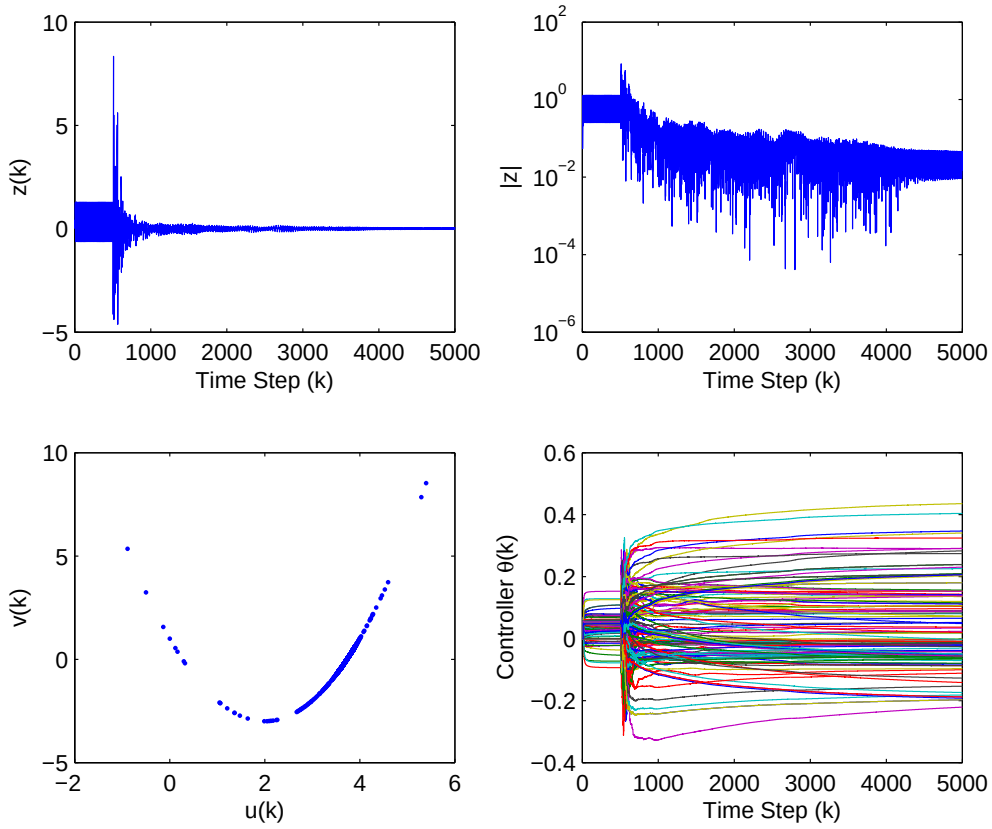

Figure 5.5: Response of the reference signal $r(k) = \sin(\pi/5k)$ with input nonlinearity $\mathcal{N}(u) = (u-2)^2 - 3$. Using $\tilde{\mathcal{N}}(u) = |u-2|$, the steady-state average performance $z_{\text{ss,avg}} = 0.0241$ and the performance degradation is of two orders of magnitude. In this case, the ersatz nonlinearity $\tilde{\mathcal{N}}$ matches the monotonicity but not the shape of $\mathcal{N}$.

state average performance $|z_{\text{ss,avg}}|$ as we increase the number of basis functions using NARMAX/O, NARMAX/I, and NARMAX/IO structures.

5.6.1 Fourier basis function

Consider sine and cosine functions of increasing frequency

$$f_i(u) = u, \sin(\frac{1}{4}u), \cos(\frac{1}{4}u), \sin(\frac{1}{2}u), \cos(\frac{1}{2}u), \sin u, \cos u, \ldots,$$
$$g_j(y) = y, \sin(\frac{1}{4}y), \cos(\frac{1}{4}y), \sin(\frac{1}{2}y), \cos(\frac{1}{2}y), \sin y, \cos y, \ldots,$$

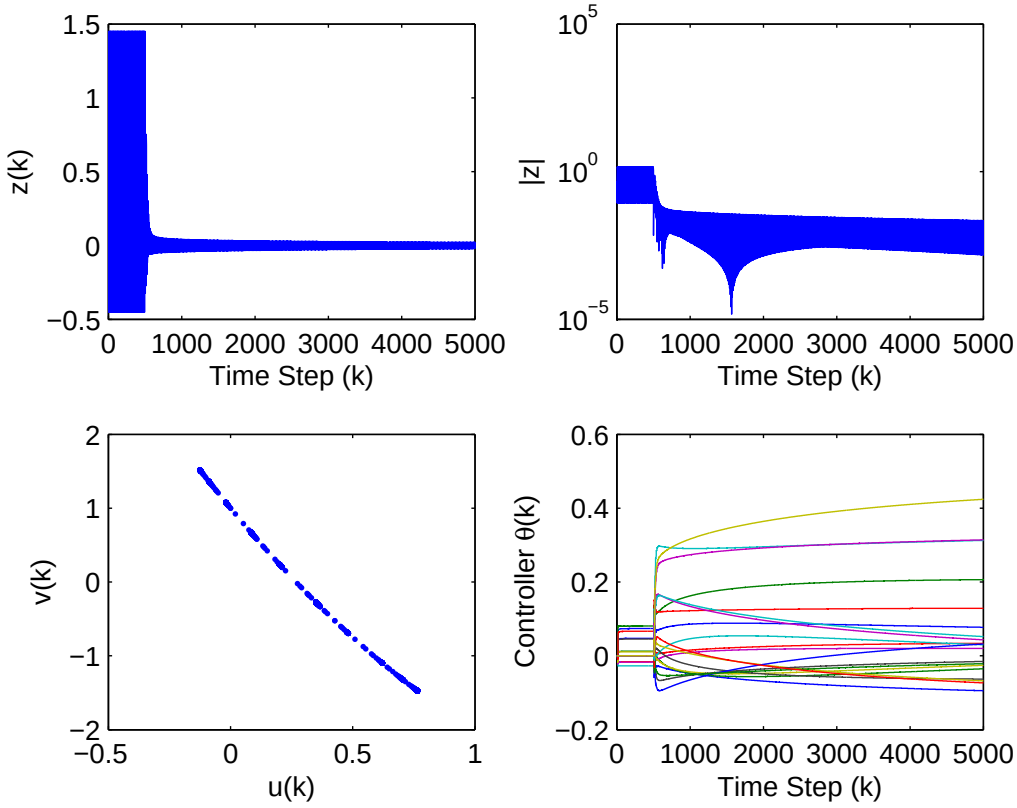

Figure 5.6: Response of reference signal $r(k) = \sin(\pi/5k)$ with input nonlinearity $\mathcal{N}(u) = (u-2)^2 - 3$. We consider $\tilde{\mathcal{N}}(u) = (u-2)^2$ with a linear controller structure and the steady-state average performance $|z_{\text{ss,avg}}| = 0.0110$.

For NARMAX/O controller structure, we let $g(y) = y$, that is, $t = 1$ in (5.11), and increase the number of basis functions in $f(u)$. Figure 5.7 shows the closed-loop steady-state average performance $|z_{\text{ss,avg}}|$ decreases as we increase the number of basis functions in $f(u)$ using the NARMAX/O structure. Following the same procedure, the closed-loop steady-state average performance $|z_{\text{ss,avg}}|$ for NARMAX/I and NARMAX/IO structures are shown in Figure 5.7. Note that overall NARMAX/O structure provides the best steady-state average performance $|z_{\text{ss,avg}}|$.

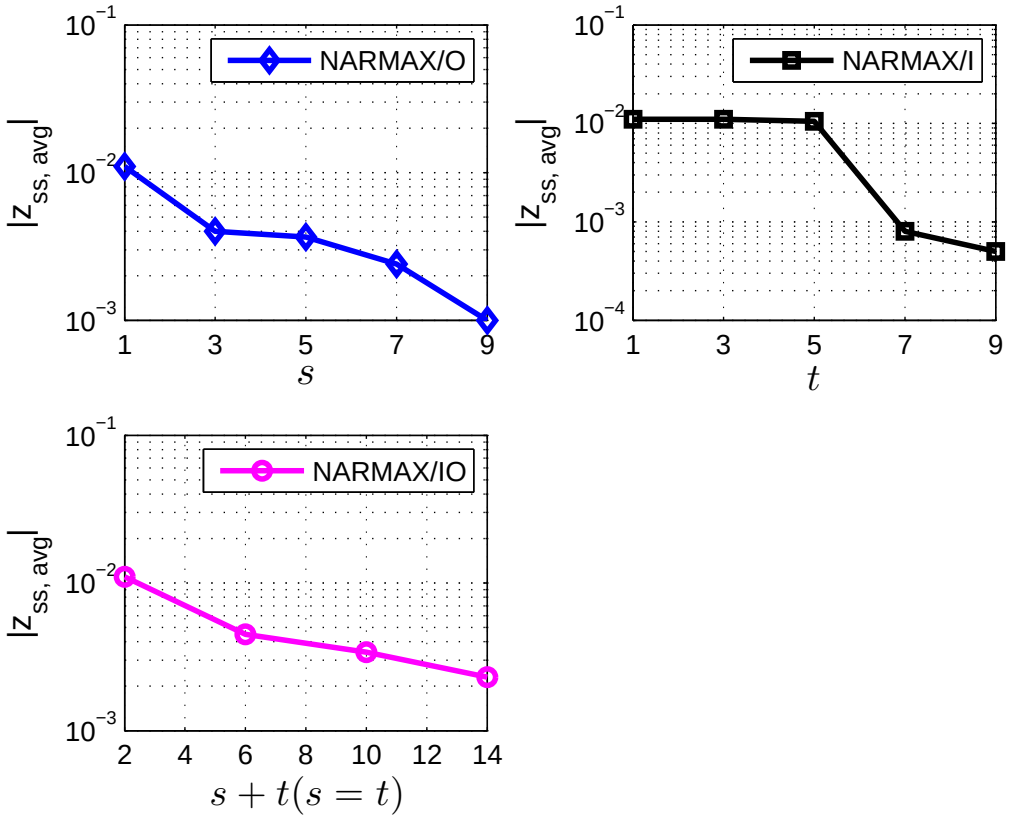

Figure 5.7: Closed-loop steady-state average performance $|z_{ss,avg}|$ with Fourier basis function for NARMAX/O, NARMAX/I and NARMAX/IO structure. $|z_{ss,avg}|$ decreases as we increase the number of basis functions for all three cases. Note that NARMAX/O structure provides the best steady-state average performance $|z_{ss,avg}|$.

5.6.2 Radial Basis Function

Consider the radial basis functions

$$f_i(u) = u, e^{-u^2}, e^{-(u-0.2)^2}, e^{-(u+0.2)^2}, e^{-(u-0.4)^2}, e^{-(u+0.4)^2}, \ldots,$$

$$g_j(y) = y, e^{-y^2}, e^{-(y-0.2)^2}, e^{-(y+0.2)^2}, e^{-(y-0.4)^2}, e^{-(y+0.4)^2}, \ldots,$$

Following the same procedures, the closed-loop steady-state average performance $|z_{ss,avg}|$ for NARMAX/O, NARMAX/I, and NARMAX/IO structures are shown in Figure 5.8. Note that overall NARMAXI/O structure provides the best steady-state

average performance $|z_{\text{ss,avg}}|$.

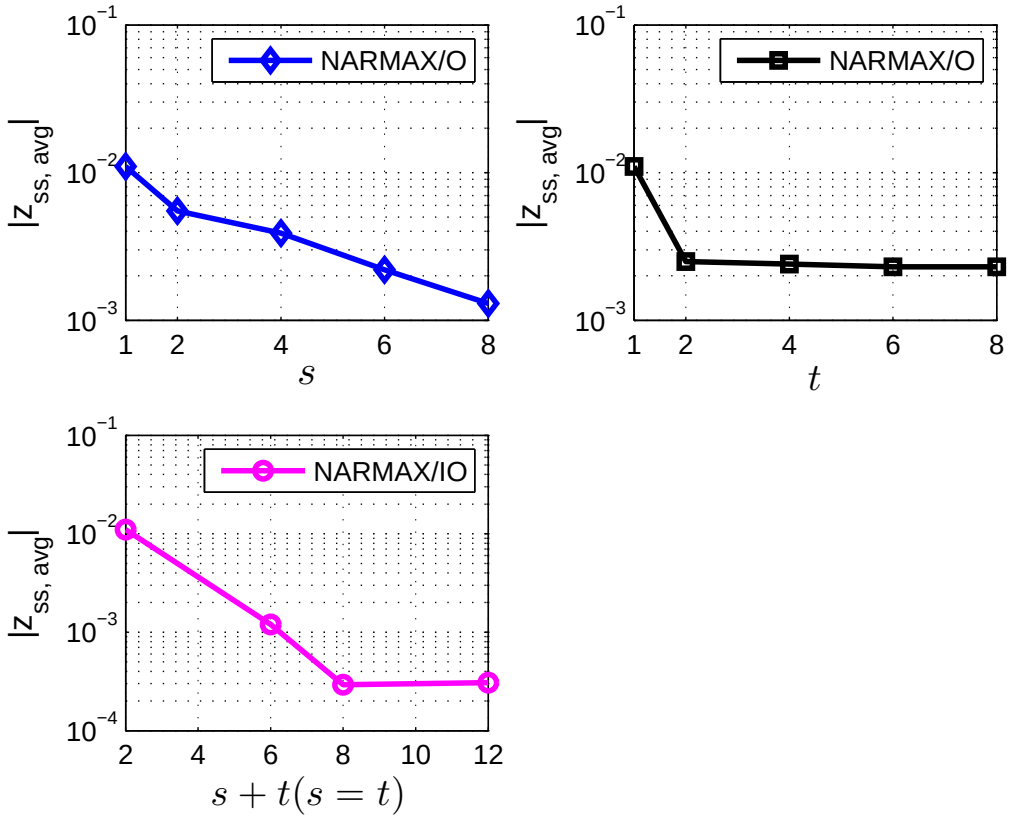

Figure 5.8: Closed-loop steady-state average performance $|z_{\text{ss,avg}}|$ with RBF for NARMAX/O, NARMAX/I and NARMAX/IO structure. $|z_{\text{ss,avg}}|$ decreases as we increase the number of basis functions for all the cases. Note that overall NARMAX/IO structure provides the best steady-state average performance $|z_{\text{ss,avg}}|$.

5.6.3 Logistic Basis Function

Consider the logistic basis functions

$$f_i(u) = u, \frac{1}{1+e^{-u}}, \frac{1}{1+e^{-(u-0.2)}}, \frac{1}{1+e^{-(u+0.2)}}, \frac{1}{1+e^{-(u-0.4)}}, \frac{1}{1+e^{-(u+0.4)}}, \ldots,$$
$$g_j(y) = y, \frac{1}{1+e^{-y}}, \frac{1}{1+e^{-(y-0.2)}}, \frac{1}{1+e^{-(y+0.2)}}, \frac{1}{1+e^{-(y-0.4)}}, \frac{1}{1+e^{-(y+0.4)}}, \ldots,$$

Following the same procedures, the closed-loop steady-state average performance $|z_{\text{ss,avg}}|$ for NARMAX/O, NARMAX/I, and NARMAX/IO structures are shown in Figure 5.9. Note that overall NARMAX/O structure provides the best steady-state average performance $|z_{\text{ss,avg}}|$.

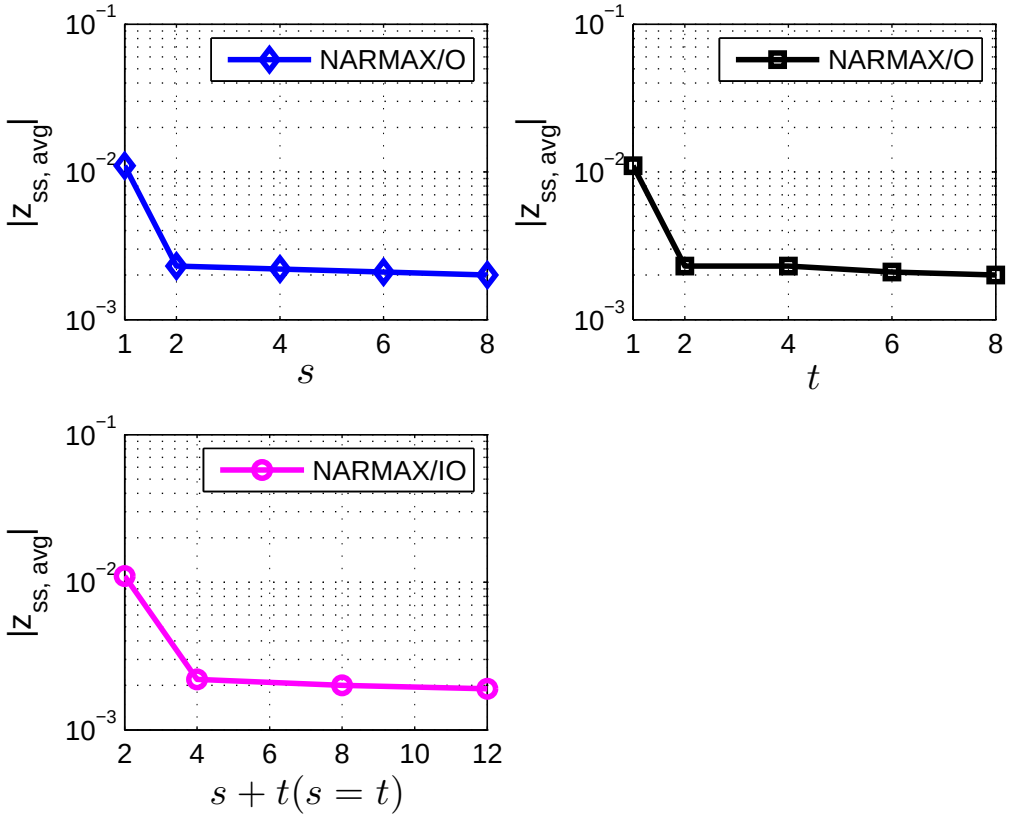

Figure 5.9: Closed-loop steady-state average performance $|z_{\text{ss,avg}}|$ with logistic basis function for NARMAX/O, NARMAX/I and NARMAX/IO structure. $|z_{\text{ss,avg}}|$ decreases as we increase the number of basis functions for all three cases. Note that NARMAX/O structure provides the best steady-state average performance $|z_{\text{ss,avg}}|$.

5.6.4 Triangular Basis Function

Consider the triangular basis functions

$$f_i(u) = u, 1 - \max(1 - |u|, 0), 1 - \max(1 - |u - 0.2|, 0), 1 - \max(1 - |u + 0.2|, 0), \ldots,$$
$$g_j(y) = y, 1 - \max(1 - |y|, 0), 1 - \max(1 - |y - 0.2|, 0), 1 - \max(1 - |y + 0.2|, 0), \ldots,$$

Following the same procedures, the closed-loop steady-state average performance $|z_{\mathrm{ss,avg}}|$ for NARMAX/O, NARMAX/I, and NARMAX/IO structures are shown in Figure 5.10. Note that overall NARMAX/O structure provides the best steady-state average performance $|z_{\mathrm{ss,avg}}|$.

5.6.5 Numerical Example Summary

RCANC can improve the command-following performance for the Hammerstein systems over the linear controller structure and the closed-loop steady-state average performance decreases as we increase the number of basis functions for all three controller structures. Simulation also demonstrates that NARMAX/O and MARMAX/IO provides better command-following performance compared with NARMAX/I. However, for NARAMX/IO, the number of parameters in θ is much larger than the number of parameters for NARMAX/O, which is more computational expansive. Therefore, the NARMAX/O controller structure is recommended for Hammerstein systems.

5.7 Conclusions

Retrospective cost adaptive NARMAX control (RCANC) was applied to command following for Hammerstein systems. RCANC was used with limited modeling information. In particular, RCANC uses knowledge of the first nonzero Markov parameter of the linear system and the monotonicity intervals of the input nonlinearity

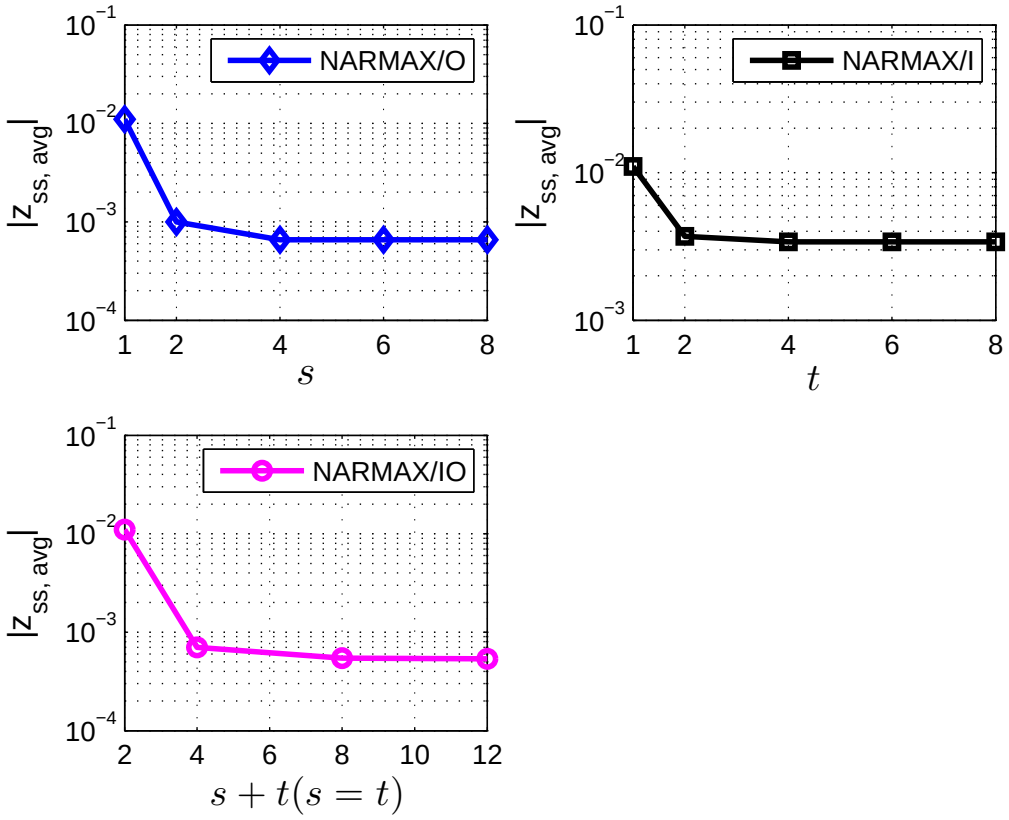

Figure 5.10: Closed-loop steady-state average performance $|z_{ss,avg}|$ with triangular basis function for NARMAX/O, NARMAX/I and NARMAX/IO structure. $|z_{ss,avg}|$ decreases as we increase the number of basis functions for all the cases. Note that overall NARMAX/O structure provides the best steady-state average performance $|z_{ss,avg}|$.

to construct the ersatz nonlinearity. To handle the effect of the input nonlinearity, we numerically demonstrated that RCANC can improve the command-following performance for the Hammerstein systems over the linear controller structure for compensating performance distortion caused by the input nonlinearity. Future research will focus on choosing the ersatz nonlinearity and basis functions for RCANC based on limited knowledge of Hammerstein nonlinearities.

CHAPTER VI

Concluding Remarks

This dissertation presented an extension in adaptive control for uncertain Hammerstein systems. Adaptive control is applicable to nonlinear systems that are expensive and difficult to model. In addition, adaptive control compensates for the unanticipated changes in the environment. Chapter II focus on applying adaptive control to various applications, whereas Chapter III-V modify retrospective-cost-based adaptive control to uncertain Hammerstein systems.

Chapter II presented nonlinear applications of linear retrospective cost adaptive control (RCAC) presented in [24, 30]. Four examples of input nonlinearities are considered. Specifically, we apply RCAC to command-following and disturbance-rejection problems for input nonlinearities of deadzone, hysteresis, diesel engine model, and uncertain electromagnetically controlled oscillator (ECO). Numerical examples demonstrate that RCAC was able to drive the Hammerstein system to follow the reference command in all those four examples.

Chapter III began the main topic of this dissertation. Adaptive control based on constrained retrospective cost optimization was applied to command following for Hammerstein systems with multivariable convex input saturation. We numerically demonstrated that convex optimization applied to the retrospective cost can improve the tracking performance when following squarewave and triangle-wave commands in

the presence of saturation. We also applied this technique to a multi-rotor helicopter command-following problem by formulating the multi-input constrained retrospective cost function as a second-order cone optimization (SOCP) problem. With this approach, RCAC is shown to adapt to these constraints.

Chapter IV considered the uncertain Hammerstein systems, where the input nonlinearities could be odd, even, or arbitrary, which may be monotonic or non-monotonic. To handle the effect of the non-monotonic nonlinearity, RCAC was augmented by auxiliary nonlinearities chosen based on the properties of the input nonlinearity. The auxiliary nonlinearities combine with the input nonlinearity to form a composite nonlinearity that is globally nondecreasing. Simulation results show that RCAC is able to follow the commands for the Hammerstein systems with an unknown disturbance when the composite input nonlinearity is globally nondecreasing.

Chapter V demonstrated that RCANC can improve the command-following performance for the Hammerstein systems over the linear controller structure for compensating performance distortion caused by the input nonlinearity. Numerical examples show that the closed-loop steady-state average performance decreases as we increase the number of basis functions in the nonlinear controller structures.

6.1 Extensions and Future Work

The results in this dissertation may be extended to uncertain Wiener systems. Future work includes understanding minimal model information for Wiener systems to compensate for output nonlinearities.

Moreover, we can explore the ideas of adaptive control based on constrained retrospective cost optimization in many applications. For example, the technique developed in Chapter III can be applied to the setpoint control of the uncertain electromagnetically controlled oscillator, where the control output current is constrained to be nonnegative, and the maximum current is also limited. Furthermore, the colli-

sions of the mass with the fixed electromagnet must be avoided. Further theoretical work including a stability analysis of RCAC based on constrained retrospective cost optimization under input saturation will be developed. In addition, the idea of convex optimization can be explored further for RCAC. For instance, for NMP system, constrained optimization for controller update can be formulated so as to prevent unstable pole-zero cancelation during the adaptation.

Last but not the least, for retrospective cost adaptive NARMAX control, future research will focus on the rule of choosing the ersatz nonlinearity and basis functions.

BIBLIOGRAPHY

BIBLIOGRAPHY

[1] P. Kokotovic, H. Khalil, and J. OReilly, *Singular Perturbation Methods in Control: Analysis and Design.* Academic Press, New York, 1986.

[2] H. P. Whitaker, J. Yamron, and A. Kezer, *Design of Model-Reference Adaptive Control Systems for Aircraft.* Massachusetts Institute of Technology, Instrumentation Laboratory, 1958.

[3] P. Osburn, *New Developments in the Design of Model Reference Adaptive Control Systems.* Institute of the Aerospace Sciences, 1961.

[4] R. E. Kalman, "Design of a self-optimising control system," *Trans. ASME*, vol. 80, pp. 468–478, 1958.

[5] R. Bellman, *Adaptive Control Processes: A Guided Tour.* Princeton university press Princeton, 1961, vol. 4.

[6] Y. Z. Tsypkin and S. Nikolic, *Adaptation and Learning in Automatic Systems.* Academic Press, Inc., 1971.

[7] B. Egardt and A. V. Balakrishnan, *Stability of Adaptive Controllers.* Springer Berlin, 1979, vol. 20.

[8] A. Morse, "Global stability of parameter-adaptive control systems," *Automatic Control, IEEE Transactions on*, vol. 25, no. 3, pp. 433–439, 1980.

[9] K. Narendra, Y.-H. Lin, and L. Valavani, "Stable adaptive controller design, part ii: Proof of stability," *Automatic Control, IEEE Transactions on*, vol. 25, no. 3, pp. 440–448, 1980.

[10] Y. D. Landau, *Adaptive Control: the Model Reference Approach.* IET, 1979.

[11] G. Goodwin, P. Ramadge, and P. Caines, "Discrete-time multivariable adaptive control," *Automatic Control, IEEE Transactions on*, vol. 25, no. 3, pp. 449–456, 1980.

[12] G. C. Goodwin and K. S. Sin, *Adaptive Filtering Prediction and Control.* Courier Dover Publications, 2013.

[13] C. J. Harris and S. Billings, *Self-tuning and Adaptive Control: Theory and Applications.* P. Peregrinus, 1981.

[14] H. Unbehauen, *Methods and Applications in Adaptive Control*. Springer Verlag, 1980, vol. 24.

[15] P. A. Ioannou and J. Sun, *Robust Adaptive Control*. Courier Dover Publications, 2012.

[16] B. D. Anderson, R. R. Bitmead, C. Johnson, P. V. Kokotovic, R. L. Kosut, I. M. Mareels, L. Praly, and B. D. Riedle, *Stability of Adaptive Systems: Passivity and Averaging Analysis*. MIT press Cambridge, MA, 1986.

[17] K. J. Åström and B. Wittenmark, *Adaptive Control*. Dover Publications, 2008.

[18] R. Bitmead, M. Gevers, and V. Wertz, *Adaptive Optimal Control: the Thinking Man's GPC*. Prentice Hall, 1990.

[19] C. Rohrs, L. Valavani, M. Athans, and G. Stein, "Robustness of continuous-time adaptive control algorithms in the presence of unmodeled dynamics," *Automatic Control, IEEE Transactions on*, vol. 30, no. 9, pp. 881–889, 1985.

[20] P. V. Kokotovic, *Foundations of Adaptive Control*. Springer-Verlag New York, Inc., 1991.

[21] R. Middleton and G. Goodwin, *Digital Control and Estimation: A Unified Approach*. Prentice Hall Press, 1990.

[22] K. S. Narendra and A. M. Annaswamy, *Stable Adaptive Systems*. Courier Dover Publications, 2005.

[23] J. B. Hoagg, M. A. Santillo, and D. S. Bernstein, "Discrete-time adaptive command following and disturbance rejection for minimum phase systems with unknown exogenous dynamics," *IEEE Trans. Autom. Contr.*, vol. 53, pp. 912–928, 2008.

[24] R. Venugopal and D. S. Bernstein, "Adaptive disturbance rejection using ARMARKOV system representations," *IEEE Trans. Contr. Sys. Tech.*, vol. 8, pp. 257–269, 2000.

[25] M. A. Santillo and D. S. Bernstein, "Adaptive control based on retrospective cost optimization," *AIAA J. Guid. Contr. Dyn.*, vol. 33, pp. 289–304, 2010.

[26] J. B. Hoagg and D. S. Bernstein, "Retrospective cost adaptive control for nonminimum-phase discrete-time systems part 1: The ideal controller and error system; part 2: The adaptive controller and stability analysis," in *Proc. IEEE Conf. Dec. Contr.*, Atlanta, GA, December 2010, pp. 893–904.

[27] ——, "Retrospective cost model reference adaptive control for nonminimum-phase discrete-time systems, part 1: The ideal controller and error system; part 2: The adaptive controller and stability analysis," in *Proc. Amer. Contr. Conf.*, San Francisco, CA, June 2011, pp. 2927–2938.

[28] ——, "Retrospective cost model reference adaptive control for nonminimum-phase systems," *AIAA J. Guid. Contr. Dyn.*, vol. 35, pp. 1767–1786, 2012.

[29] A. M. D'Amato, E. D. Sumer, and D. S. Bernstein, "Retrospective cost adaptive control for systems with unknown nonminimum-phase zeros," in *Proc. AIAA Guid. Nav. Contr. Conf.*, Portland, OR, August 2011, AIAA-2011-6203.

[30] ——, "Frequency-domain stability analysis of retrospective-cost adaptive control for systems with unknown nonminimum-phase zeros," in *Proc. IEEE Conf. Dec. Contr.*, Orlando, FL, December 2011, pp. 1098–1103.

[31] M. S. Fledderjohn, M. S. Holzel, H. Palanthandalam-Madapusi, R. J. Fuentes, and D. S. Bernstein, "A comparison of least squares algorithms for estimating markov parameters," in *Proc. Amer. Contr. Conf.*, Baltimore, MD, June 2010, pp. 3735–3740.

[32] M. C. Kung and B. F. Womack, "Discrete-time adaptive control of linear dynamic systems with a two-segment piecewise-linear asymmetric nonlinearity," *IEEE Trans. Autom. Contr.*, vol. 29, no. 2, pp. 170–172, 1984.

[33] ——, "Discrete-time adaptive control of linear systems with preload nonlinearity," *Automatica*, vol. 20, no. 4, pp. 477–479, 1984.

[34] G. Tao and P. V. Kokotović, *Adaptive Control of Systems with Actuator and Sensor Nonlinearities*. Wiley, 1996.

[35] A. M. D'Amato and D. S. Bernstein, "Adaptive forward-propagating input reconstruction for nonminimum-phase systems," in *Proc. Amer. Contr. Conf.*, Montreal, Canada, June 2012, pp. 598–603.

[36] M. A. Janaideh, J. Mao, S. Rakheja, W. Xie, and C. Y. Su, "Generalized Prandtl-Ishlinskii hysteresis model: Hysteresis modeling and its inverse for compensation in smart actuators," *Proc. IEEE Conf. Dec. Contr.*, pp. 5182–5187, December 2008.

[37] J. Yan, A. M. D'Amato, K. Butts, I. Kolmanovsky, and D. S. Bernstein, "Adaptive control of the air flow system in a diesel engine'," in *Proc. ASME Dynamic Systems and Control Conf.*, Fort Lauderdale, FL, October 2012.

[38] J. Yan, A. M. D'Amato, and D. S. Bernstein, "Setpoint control of the uncertain electromagnetically controlled oscillator," in *Proc. ASME Dynamic Systems and Control Conf.*, Fort Lauderdale, FL, October 2012.

[39] J. Mårtensson and H. Hjalmarsson, "Variance-error quantification for identified poles and zeros," *Automatica*, vol. 45, no. 11, pp. 2512–2525, 2009.

[40] Diesel engine. `http://en.wikipedia.org/wiki/Diesel_engine`.

[41] Deltaexpo. `http://www.deltaexpo.com/content/view/118/35/`.

[42] I. Kolmanovsky, P. Morall, M. Van Nieuwstadt, and A. Stefanopoulou, "Issues in modelling and control of intake flow in variable geometry turbocharged engines," *Chapman and Hall CRC research notes in mathematics*, pp. 436–445, 1999.

[43] J. A. Cook, J. Sun, J. H. Buckland, I. V. Kolmanovsky, H. Peng, and J. W. Grizzle, "Automotive powertrain control a survey," *Asian Journal of Control*, vol. 8, no. 3, pp. 237–260, 2006.

[44] E. D. Sumer, A. M. D'Amato, A. M. Morozov, J. B. Hoagg, and D. S. Bernstein, "Robustness of retrospective cost adaptive control to Markov-parameter uncertainty," in *Proc. IEEE Conf. Dec. Contr.*, Orlando, FL, December 2011, pp. 6085–6090.

[45] K. H. Lundberg, K. A. Lilienkamp, and G. Marsden, "Low-cost magnetic levitation project kits," *IEEE Contr. Sys. Mag.*, vol. 24, pp. 65–69, 2004.

[46] J. Hong, I. A. Cummings, P. D. Washabaugh, and D. S. Bernstein, "Stabilization of a mass and spring system with electromagnetic actuation," *Proc. Conf. Contr. Appl.*, pp. 189–194, October 1997.

[47] J. Hong, I. A. Cummings, D. S. Bernstein, and P. D. Washabaugh, "Stabilization of an electromagnetically controlled oscillator," *Proc. Amer. Contr. Conf.*, pp. 2775–2779, June 1998.

[48] H. S. Sane and D. S. Bernstein, "Robust nonlinear control of the electromagnetically controlled oscillator," *Proc. Amer. Contr. Conf.*, pp. 809–814, May 2002.

[49] R. H. Miller, I. Kolmanovsky, E. G. Gilbert, and P. D. Washabaugh, "Control of Constrained Nonlinear Systems: A Case Study," *IEEE Contr. Sys. Mag.*, vol. 19, pp. 23–32, 2000.

[50] H. Sane and D. S. Bernstein, "Asymptotic Disturbance Rejection for Hammerstein Positive Real Systems," *IEEE Trans. Contr. Sys. Tech.*, vol. 11, pp. 364–374, 2003.

[51] J. Su, H. Yang, P. Fay, W. Porod, and G. H. Bernstein, "A surface micromachined offset-drive method to extend the electrostatic travel rang," *Journal of Micromechanics and Microengineering*, vol. 20, pp. 1–10, 2010.

[52] S. D. Cairano, A. Bemporad, I. Kolmanovsky, and D. Hrovat, "Model predictive control of magnetically actuated mass spring dampers for automotive applications," *Int. J. Contr.*, vol. 80, no. 11, p. 17011716, 2007.

[53] J. Zhong, D. Cheng, and X. Hu, "Constructive stabilization for quadratic input nonlinear systems," *Automatica*, vol. 44, pp. 1996–2005, 2008.

[54] D. H. S. Maithripala, J. M. Berg, and W. P. Dayawansa, "A virtual velocity sensor for improved transient performance of electrostatically actuated mems," in *Proc. ASME Ing. Mech. Eng. Congress Expos.*, Washington, DC, November 2003, pp. 1–5, iMECE2003-42451.

[55] H. S. Sane, "Energy-based control for mems with one-sided actuation," in *Proc. Amer. Contr. Conf.*, Minneapolis, MN, June 2006, pp. 1209–1214.

[56] J. H. Lang and D. H. Staelin, "Electrostatically figured reflecting membrane antennas for satellites," *IEEE Trans. Autom. Contr.*, vol. 27, pp. 666–670, 1982.

[57] D. J. Mihora and P. J. Redmond, "Electrostatically formed antennas," *Journal of Spacecraft*, vol. 17, pp. 465–475, 1980.

[58] J. Yan, A. M. D'Amato, E. D. Sumer, J. B. Hoagg, and D. S. Bernstein, "Adaptive control of uncertain hammerstein systems using auxiliary nonlinearities," in *Proc. IEEE Conf. Dec. Contr.*, Maui, HI, December 2012, pp. 4811–4816.

[59] J. Yan and D. S. Bernstein, "Adaptive control of uncertain hammerstein systems with nonmonotonic input nonlinearities using auxiliary blocking nonlinearities," in *Proc. Amer. Contr. Conf.*, Washington, DC, June 2013.

[60] J. Yan, D. A. dos Santos, and D. S. Bernstein, "Adaptive control with convex saturation constraints," *IET Control Theory & Applications*, 2013, (submitted).

[61] D. S. Bernstein and A. N. Michel, "A chronological bibliography on saturating actuators," *Int. J. Robust and Nonlinear Control*, vol. 5, pp. 375–380, 1995.

[62] L. Zaccarian and A. R. Teel, *Modern Anti-windup Synthesis: Control Augmentation for Actuator Saturation*. Princeton University Press, 2011.

[63] P. Hippe, *Windup in Control: Its Effects and Their Prevention*. Springer, 2006.

[64] T. Hu and Z. Lin, *Control Systems with Actuator Saturation: Analysis and Design*. Birkhäuser, 2001.

[65] A. Glattfelder and W. Schaufelberger, *Control Systems with Input and Output Constraints*. Springer, 2003.

[66] T. Kapila and K. Grigoriadis, *Actuator Saturation Control*. CRC Press, 2002.

[67] S. Tarbouriech, G. Garcia, J. M. G. da Silva Jr., and I. Queinnec, *Stability and Stabilization of Linear Systems with Saturating Actuators*. Springer, 2011.

[68] A. M. Annaswamy and J.-E. Wong, "Adaptive control in the presence of saturation non-linearity," *Int. J. Adaptive Contr. Sig. Proc.*, vol. 11, pp. 3–19, 1998.

[69] J. Teo and J. P. How, "Anti-windup compensation for nonlinear systems via gradient projection: Application to adaptive control," in *Proc. IEEE Conf. Dec. Contr.*, Shanghai, China, December 2009, pp. 6910–6916.

[70] B. J. Coffer, J. B. Hoagg, and D. S. Bernstein, "Cumulative retrospective cost adaptive control of systems with amplitude and rate saturation," in *Proc. Amer. Contr. Conf.*, San Francisco, CA, June 2011, pp. 2344–2349.

[71] F. Tyan and D. S. Bernstein, "Global stabilization of systems containing a double integrator using a saturated linear controller," *Int. J. Robust Nonlinear Control*, vol. 9, no. 15, pp. 1143–1156, 1999.

[72] M. Grant and S. Boyd. (2013, March) CVX: Matlab software for disciplined convex programming, version 2.0. `http://cvxr.com/cvx/`.

[73] A. Morozov, A. M. D'Amato, J. B. Hoagg, and D. S. Bernstein, "Retrospective cost adaptive control for nonminimum-phase systems with uncertain nonminimum-phase zeros using convex optimization," in *Proc. Amer. Contr. Conf.*, San Francisco, CA, June 2011, pp. 1188–2293.

[74] K. J. Åström and B. Wittenmark, *Adaptive Control*. Addison-Wesley, 1995.

[75] G. C. Goodwin and K. S. Sin, *Adaptive Filtering, Prediction, and Control*. Prentice Hall, 1984.

[76] E. D. Sumer, M. H. Holzel, A. M. D'Amato, and D. S. Bernstein, "FIR-based phase matching for robust retrospective-cost adaptive control," in *Proc. Amer. Contr. Conf.*, Montreal, Canada, June 2012, pp. 2707–2712.

[77] E. D. Sumer and D. S. Bernstein, "Retrospective cost adaptive control with error-dependent regularization for mimo systems with unknown nonminimum-phase transmission zeros," in *Proc. AIAA Guid. Nav. Contr. Conf.*, Minneapolis, MN, August 2012, AIAA-2012-4070.

[78] J. B. Hoagg and D. S. Bernstein, "Cumulative retrospective cost adaptive control with rls-based optimization," in *Proc. Amer. Contr. Conf.*, Baltimore, MD, June 2010, pp. 4016–4021.

[79] R. F. Brammer, "Controllability in linear autonomous systems with positive controllers," *SIAM J. Control*, vol. 10, pp. 339–353, 1972.

[80] D. H. Jacobson, D. H. Margin, M. Pachter, and T. Geveci, *Extensions of Linear-Quadratic Control Theory*. Springer, 1980.

[81] H. Leyva, J. Sols-Daun, and R. Suárez, "Global CLF stabilization of systems with control inputs constrained to a hyperbox," *SIAM J. Control Optim.*, vol. 51, pp. 745–766, 2013.

[82] J. Yan and D. S. Bernstein, "Minimum modeling retrospective cost adaptive control of uncertain hammerstein systems using auxiliary nonlinearities," *Int. J. Contr.*, 2013, (Accepted pending minor revision).

[83] W. Haddad and V. Chellaboina, "Nonlinear control of hammerstein systems with passive nonlinear dynamics," *IEEE Trans. Autom. Contr.*, vol. 46, no. 10, pp. 1630–1634, 2001.

[84] L. Zaccarian and A. R. Teel, *Modern Anti-windup Synthesis: Control Augmentation for Actuator Saturation*. Princeton, 2011.

[85] F. Giri and E. W. Bai, *Block-Oriented Nonlinear System Identification*. Springer, 2010.

[86] J. Yan, A. M. D'Amato, and D. S. Bernstein, "Retrospective-cost adaptive control of uncertain hammerstein systems using a NARMAX controller structure," in *Proc. AIAA Guid. Nav. Contr. Conf.*, Minneapolis, MN, August 2012, AIAA-2012-4448-132.

[87] J. Yan and D. S. Bernstein, "Retrospective cost adaptive NARMAX control of hammerstein systems with ersatz nonlinearities," in *Proc. AIAA Guid. Nav. Contr. Conf.*, Boston, MA, August 2013.

[88] M. Arcak, "A global separation theorem for a new class of nonlinear observers," in *Proc. IEEE Conf. Dec. Contr.*, Las Vegas, NV, December 2002, pp. 676–681.

[89] R. Haber and L. Keviczky, *Nonlinear System Identification–Input-Output Modeling Approach*. Spinger, 1999, vol. 1.

[90] W. Greblicki and M. Pawlak, *Nonparametric System Identification*. Cambridge University Press, 2008.

[91] D. S. Bernstein and W. M. Haddad, "Nonlinear controllers for positive real systems with arbitrary input nonlinearities," *IEEE Trans. Autom. Contr.*, vol. 39, pp. 1513–1517, 1994.

[92] H. Sane and D. S. Bernstein, "Asymptotic Disturbance Rejection for Hammerstein Positive Real Systems," *IEEE Trans. Contr. Sys. Tech.*, vol. 11, pp. 364–374, 2003.

[93] S. Chen, S. A. Billings, C. F. N. Cowan, and P. M. Grant, "Practical Identication of NARMAX Models Using Radial Basis Function," *Int. J. Contr.*, vol. 52, no. 6, pp. 1327–1350, 1990.

[94] S. Chen and S. A. Billings, "Representation of nonlinear systems: the narmax model," *Int. J. Contr.*, vol. 49, no. 3, pp. 1013–1032, 1989.

[95] R. Venugopal and D. S. Bernstein, "Adaptive Disturbance Rejection Using ARMARKOV System Representations," *IEEE Trans. Contr. Sys. Tech.*, vol. 8, pp. 257–269, 2000.

[96] H. Karimabadi, T. B. Sipes, H. White, M. Marinucci, A. Dmitriev, J. K. Chao, J. Driscoll, and N. Balac, "Data mining in space physics: Minetool algorithm," *Journal of Geophysical Research: Space Physics*, vol. 112, 2007, dOI: 10.1029/2006JA012136.